



Doctoral Thesis

Multiomics Characterization of the Responses to diel and Seasonal Cycles in the Marine Picoeukaryote *Ostreococcus tauri*

Dissertation presented by Ana Belén Romero Losada to obtain the PhD Degree by Universidad de Sevilla.

Supervisors:

Prof. Francisco José Romero Campero

Prof. Mercedes García González

This work was supported by the research projects MINOTAUR (BIO2017-84066-R) and BLOOM (RTC-2017-6080-5) from the Spanish Ministry of Science and Innovation.



Dedicatoria . . .

word cloud

Contents

Index

Abstract.....	14
Introduction.....	18
Chronobiology.....	20
Circadian research.....	25
<i>Ostreococcus tauri</i>	29
Molecular Systems Biology.....	36
Materials and Methods.....	43
Organism and culture growth conditions.....	45
Organism and growth medium.....	45
Continuous culture conditions in photochemostats.....	45
Experimental design.....	47
Transcriptomic analysis.....	48
Sample Collection.....	48
Cell disruption.....	48
RNA extraction.....	48
RNA purification.....	48
RNA sequencing and processing.....	49
Proteomic analysis.....	49
Sample collection.....	49
Cell disruption.....	49
Proteins extraction.....	49
Proteins digestion.....	50
SWATH acquisition.....	50
Equipment and data acquisition method.....	50
Library construction.....	51
SWATH runs.....	51
Data processing.....	51
Cell cycle analysis.....	52
Sample collection and cell fixation method.....	52
Cell staining method.....	52
Data acquisition and processing.....	52
Analysis of photosynthetic activity.....	53
Sample collection.....	53
Data acquisition.....	53
Analytical determinations.....	53
Sample collection.....	53
Starch Content.....	53
Cell disruption.....	53
Starch solubilization and digestion.....	54
Spectrophotometric quantification.....	54
Carotenoid Content.....	55
Cell disruption.....	55
Carotenoids extraction.....	55
Carotenoids determination and quantification.....	56
Rhythmic patterns analysis.....	56
Rhythmic patterns detection.....	56

Rhythmic patterns comparison.....	57
Data and code availability.....	57
Hypothesis and Objetives.....	59
Results.....	63
Chapter 1. ALGAEFUN with MARACAS, microALGAE FUNctional enrichment tool for Mi- croAlgae RnA-seq and Chip-seq AnalysiS.....	65
Implementation.....	66
Integration of different microalgae databases.....	66
Development of functional annotation and genomic packages.....	69
MARACAS implementation: high-throughput sequencing data processing.....	70
ALGAEFUN implementation: functional annotation analysis.....	76
Case study 1: from RNA-seq raw sequencing data to biological processes and pathways.....	81
Case study 2: From ChIP-seq raw sequencing data to marked genes.....	83
Contribution of ALGAEFUN with MARACAS to the field.....	85
Chapter 2: Transcriptomic analysis of diel and seasonal cycles in <i>Ostreococcus tauri</i>	88
Transcriptomic characterization of diel expression profiles.....	90
Most genes in <i>Ostreococcus tauri</i> present diel expression profiles under both photoperiods	90
Under free running conditions rhythmicity is maintained in different proportions depending on the photoperiod of entrainment.....	91
Constant light and constant darkness as free-running conditions have different effects over the transcriptome of <i>Ostreococcus</i>	97
Transcriptomic characterization of seasonal effects over gene expression profiles.....	100
Seasonal changes induce changes in amplitude and phase over gene expression profiles.	100
Seasonal changes promote the emergence of 12 h period cycles.....	102
Seasonal cycles induces distinct temporal transcriptional programs organizing biological processes during diel cycles.....	105
Chapter 3: Proteomic analysis of seasonal variations in diel cycles in <i>Ostreococcus tauri</i>	111
Proteomic characterization of diel rhythmic abundance profiles.....	114
Phase offsets between genes and proteins involved in the same biological process are ad- justed by seasons.....	117
Chapter 4: diel and seasonal multi-omic integration with physiological data.....	121
Cell Division Cycle (CDC) of <i>Ostreococcus tauri</i> under diel and seasonal cycles.....	121
Temporal program of cell division cycle under summer and winter photoperiod.....	123
Integration of CDC program with transcriptomic and proteomic data.....	127
Diel and seasonal rhythm of photosynthesis in <i>Ostreococcus tauri</i>	132
Rhythmic oscillations of photosynthetic efficiency under summer and winter photoperiod	133
Integration of photosynthesis efficiency rhythmic profile with multi-omics data.....	135
Integration of starch content diel oscillations with multi-omic data.....	139
Other metabolic pathways of <i>Ostreococcus tauri</i> showing periodic oscillations under diel and seasonal cycles.....	142
Carotenoids biosynthesis in <i>Ostreococcus tauri</i> under diel and seasonal cycles.....	142
Integration of multi-omics data with oscillations described by carotenoids content in <i>Ost- reococcus tauri</i> under diel and seasonal cycles.....	143
Nitrate assimilation under diel and seasonal cycles in <i>Ostreococcus tauri</i>	149

Integration of key enzyme activities from nitrate assimilation pathway with multi-omic data.....	150
Conclusions.....	155
Bibliography.....	160

Abstract

Abstract text

Abstract text

Introduction

Chronobiology

Simple direct observations of our surroundings easily unveil many cyclic processes. We are so familiar with them that we are mainly unconscious about their drastic influences over our lives and bodies, in particular, and life on Earth, in general.

Four environmental cycles are the most apparent ones on Earth: tides (which repeat every 12 and half hours), lunar cycles (lasting 28.5 days), days (every 24 hours) and years (every 365.25 days). These cycles are also called circatidal, circalunar, circadian, or circannual (Numata et al., 2015). They arise from gravitational forces exerted by the Sun and the Moon over the Earth. Their key characteristic is full predictability. For example, it is possible to determine the exact time of a high tide months in advance. We constantly see how full moons are always followed by new moons, and everybody goes to bed certain that the sun will rise the next morning. The exact date and even time for the next solar equinox, the moment when Earth's rotational axis is perpendicular to the line linking the Sun and the Earth, is known and written in all calendars all over the world. Therefore, sequential and periodic seasonal changes are never a surprise.

Since these four cycles affect earth with an overwhelming precision, earthlings have evolved endogenous molecular systems, referred to as molecular clocks, that allow them to anticipate those cyclic changes. This has motivated the emergence of *chronobiology*, a young area of research that studies how these rhythmic environmental changes affect organisms responses and adaptions (Edmunds, 1983; Kuhlman et al., 2018).

Molecular clocks can be seen as central oscillators susceptible to be entrained by external environmental cyclic inputs (rhythmic environmental changes) that, in turn, generate rhythmic outputs controlling a myriad of biological processes. Chronobiologists have found biological rhythms regulated by the clock in a wide range of spatial scales, ranging from the molecular level (transcription, translation, protein degradation, metabolites biosynthesis, etc), to the cellular and tissue level (cell division, synaptic connections, apoptosis, etc.) or even at the level of whole organisms, populations and ecosystems (Edmunds, 1983; Merrow et al., 2005; Sharma et al., 2022).

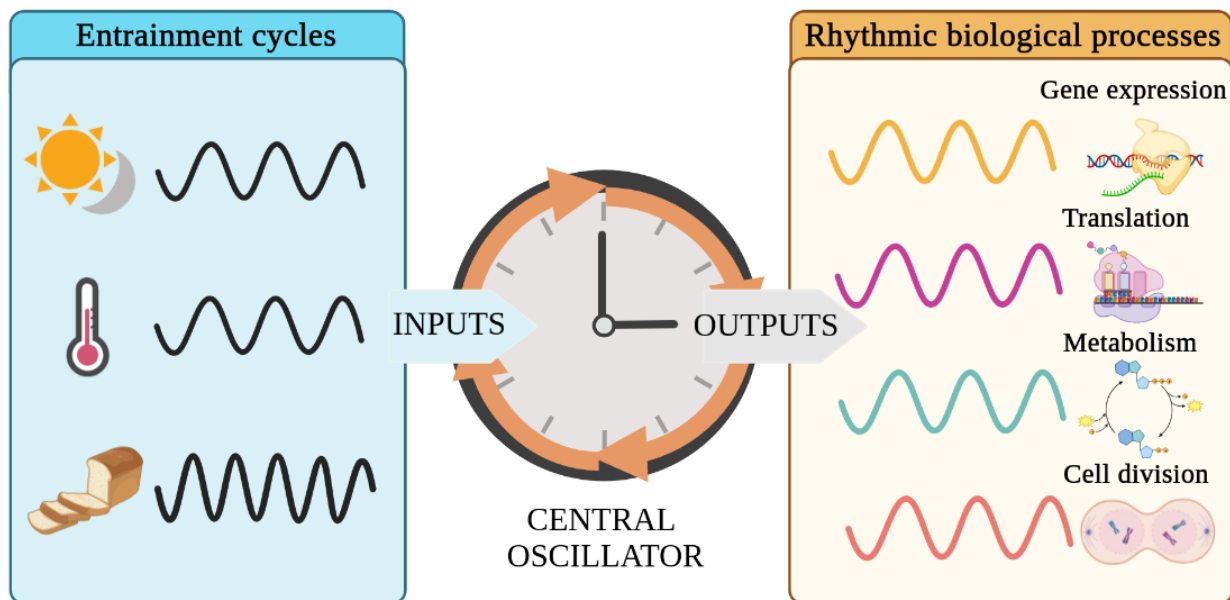


Figure 1: Diagram of the central oscillator known as clock. The clock acts as a central oscillator that is entrained by external cyclic inputs, such as as light/dark cycles or photoperiod, temperature changes and nutrients availability, generated by diel, seasonal, lunar or tidal cycles. As a response, the clock produce rhythmic outputs of biological processes that allow organisms to anticipate those environmental changes. Figure created using Biorender.

A distinctive and defining characteristic of clock-regulated biological rhythms is self-sustainability under constant non cycling environmental signals (Pittendrigh, 1960; Roenneberg & Merrow, 2005). Typically, when the response of an organism to rhythmic environmental changes (light/dark cycles, food availability, temperature changes, etc.) is studied (Fig. 2-A), multiple biological processes are found showing similar rhythmic profiles to the corresponding environmental signals (Fig. 2-B,C). Some of these processes would not maintain their rhythmicity under constant conditions indicating that their rhythmic profiles are direct responses to changes in the environment rather than being generated by endogenous oscillating systems or molecular clocks. Therefore, when environmental signals are constant, the profiles of such biological processes stop oscillating and remain constant as well (Fig. 2-B). However, a subset of biological processes would maintain a rhythmic profile under constant environmental conditions, revealing that their rhythmicity is self-sustained and, thus, regulated by endogenous oscillating systems acting as molecular clocks (Fig. 2-C).

Accordingly, chronobiology experiments are commonly designed as follows (Fig. 2-A). A temporal series consisting of consecutive days when the organism is exposed to a rhyth-

mic environmental condition (called *zeitgeber*, which is used as a synchronizer, literally a *time giver*) are followed by several consecutive days when the organism is exposed to constant non cycling conditions termed as *free-running* conditions (Kuhlman et al., 2018). Data are collected with a specific time interval, every few hours, minutes or seconds depending on the complexity of the data. Specifically, in the case of circadian experiments, as the ones performed in this thesis, the *zeitgeber* is the alternation of light-dark cycles and the free-running conditions consist of constant light and constant dark periods. Under this experimental design, circadian processes can be identified and distinguished from light/dark responding processes as those that maintain their oscillating profile under free running conditions.

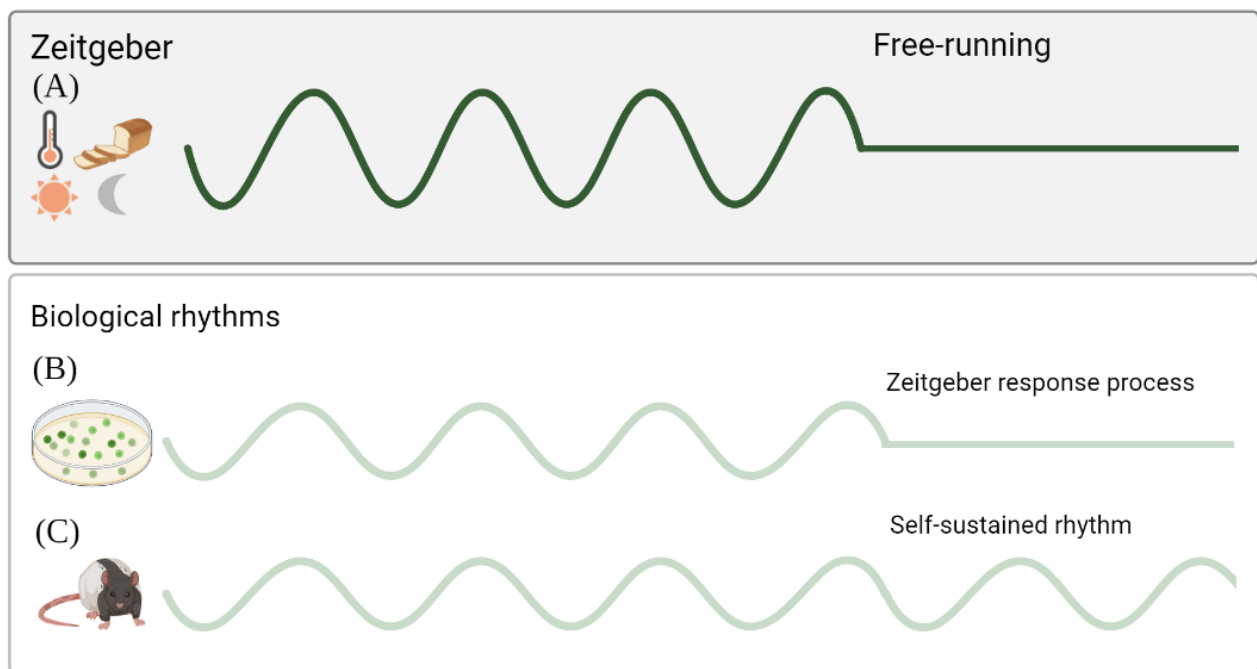


Figure 2: Different patterns of response to rhythmic environmental changes. (A) Under a *zeitgeber* (rhythmic environmental input such as light/dark, temperature and food availability) two kind of biological processes show rhythmic patterns: (B) the ones only responding to the *zeitgeber* that stop cycling under constant free running conditions; (C) the ones with self-sustained oscillations under free running conditions for which there is evidence of a regulation exerted by an endogenous clock that is still functional when the environmental condition stops cycling. Figure created using Biorender.

Following this experimental design, chronobiologists have described self-sustained biological rhythms reacting to the four different previously described environmental cycles acting as *zeitgebers*. In particular, some marine organisms has been shown to produce self-sustained circatidal rhythms when they are kept in laboratory tanks without its *zeitgeber*, in

this case, tidal rhythms (Rock et al., 2022). As an example, the marine diatom *Hantzschia amphioxys* descends to the sand at high tides and rises to the surface at low tides (Fauré-Fremiet, 1951). In contrast, self-sustained circalunar processes are yet more unknown (Andreatta & Tessmar-Raible, 2020). An eminent example is the larvae of the insect called Ant Lion, which builds small holes in the sand as traps for insects. Scientists found that the size of the traps changes showing a circalunar profile that is maintained under constant conditions (Youthed & Moran, 1969).

However, scientific studies about circadian or circannual rhythms are much more numerous, and they have been found in a wide range of organisms (Merrow et al., 2005; Pfeuty et al., 2012; Roenneberg & Merrow, 2005). In animals, circadian rhythms studies focus mainly on activity-rest cycles (Roenneberg et al., 2022; Zee & Abbott, 2020). Nevertheless, thousands of other parameters from ethology to gene expression also show circadian profiles. For example, the olfactory discrimination in mice is higher at night time, even at subjective nights during free running (Granados-Fuentes et al., 2006). Also fungi show circadian rhythmic phenomena, for instance, *Neurospora crassa* generates asexual spores according to a rhythm of 24 h that is maintained under constant darkness (Correa & Bell-Pedersen, 2002). Circadian rhythmic profiles in plants are found in leaf movement, growth rate, stomatal opening, as well as the expression of a wide range of genes (Merrow et al., 2005). In general, organisms in the green lineage react in many different ways to circadian cycles (Noordally & Millar, 2015), one of the most known ones is the 24 h cyclic movement in the water column adjusted to their metabolism requirements (Lebert et al., 1999).

Day length or photoperiod is a crucial signal for the circannual timing system. Seasonal changes of photoperiod have been strongly connected to reproduction. In fact, all animal reproductive systems are related to seasons, from gene expression profiles to anatomical structures. Hamsters kept in short day condition have 10-fold smaller testes than the ones kept in long day condition (Klante & Steinlechner, 1994; Nishiwaki-Ohkawa & Yoshimura, 2016). But also in plants, flowering and seed production are photoperiod-regulated (Brandoli et al., 2020; Serrano-Bueno et al., 2017).

Since light is the main source of energy for photosynthetic organisms, they are highly synchronized with cyclic environmental changes involving light such as circadian rhythms and photoperiods. Nevertheless, the chronobiology of microalgae is yet barely studied compared with other photosynthetic organisms despite representing one of the largest poly-

phyletic groups in the eukaryotic domain (Fig. 3). The genetics and molecular techniques used to identify clock components in other taxa have not been widely applied to microalgae yet (Noordally & Millar, 2015). This thesis aims to contribute to the chronobiology community by describing, for the first time, circadian rhythms emerging under different seasonal variations in diel cycles in the model marine planktonic microalga *Ostreococcus tauri*, considered the evolutionary eldest sister in the green lineage.

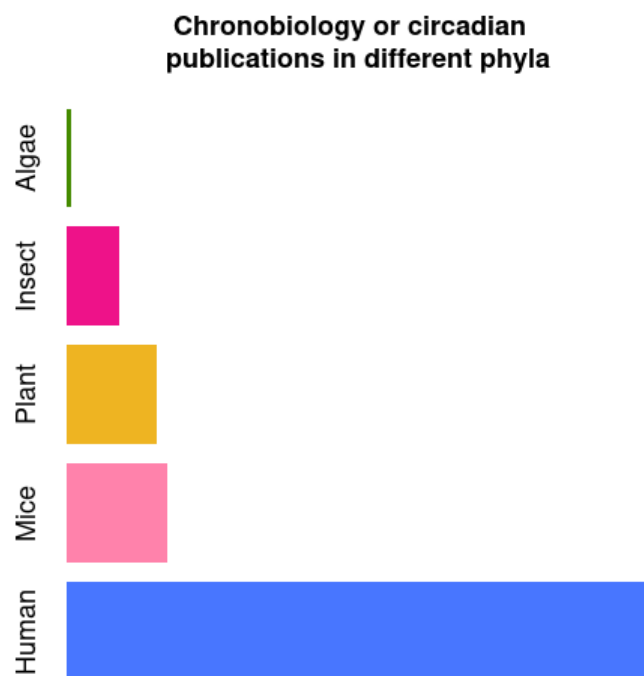


Figure 3: Number of publications found in PubMed using "chronobiology" or "circadian" keywords in their abstracts in July of 2023. For the algae group (using the generic term "algae", "microalgae" and "*Ostreococcus tauri*", "*Chlamydomonas reinhardtii*" and "*Polyedra*" as main model organisms of this group), only 493 publications were found. For the insect group (including the generic term "insect" and "*Drosophila melanogaster*" as main model organism), 5717 publications were found. For plants (including the generic term "plant" and "*Arabidopsis thaliana*" as main model organism), 9734 publications were found. For mice and human, 10771 and 62305 publications were found, respectively.

Circadian research

Our society is worldwide structured in a 24 h / 7 days system. People from different countries and cultures are experiencing jet-lags, shift work, exposure to artificial light and lack of outdoor activities. Circadian clock research is gaining relevance since this phenomena has a crucial impact on human health, behavior and quality of life (Mermet et al., 2017; Roenneberg et al., 2019, 2022; Roenneberg & Merrow, 2016). Understanding the physiology, genetics and epigenetics (Ripperger & Merrow, 2011) at a laboratory level using different model organisms besides mice such as plants, fungi and microalgae will greatly contribute to advance our comprehension of the mechanisms and functioning of circadian clocks in living organisms on Earth beyond humans.

The synchrony that exists between sunrise/twilight and organisms functioning have been so obvious for scientists that the underlying molecular mechanisms remained ignored and unexplored for centuries. The first observation indicating that daily rhythms were programmed took place in the 18th century. Jean Jacques d'Ortous De Mairan, a French astronomer, described in less than 350 words (nowadays, less than two tweets) how a mimosa plant inside a closet maintained its daily leaf movement (De Mairan, 1729). For some scientists, it was a clear proof that leaf movement was not controlled by the alternation of light and dark cycles indicating the existence of an endogenous oscillating system. De Mairan invited botanists to investigate his discovery to confirm that leaf movement was also maintained when temperature changes were absent (which inside its closet was difficult to ensure). However, it took 30 years to confirm his observations taking into account temperature for the first time (Duhamel du Monceau, 1759; Kuhlman et al., 2018; Merrow et al., 2005).

The history of circadian research was sparse in results with large gaps between discoveries during its early stages. For instance, the physiology of the endogenous nature of the clock in plants was not studied until 1832 (De Candolle, 1832), despite De Mairan's observations being reported in 1729. Similar phenomena in animals took another century to be identified (Richter, 1922), and 50 years more were needed to find them in humans (Kuhlman et al., 2018; McClung, 2006; Roenneberg & Merrow, 2005). Although circadian research and chronobiology were born in the 18th century, they only became relevant and coherent in the second half of 20th century. One of the breaking points in circadian research history was the international conference in Cold Spring Harbor in 1960, where 157

pioneering scientist in the field such as Colin Pittendrigh, Patricia Decourse and Franz Halberg met together for the first time (Evans, 1961). From all the data shared, Pittendrigh summarized the qualities of circadian clocks in 16 generic empirical features that he predicted to be true in all organisms (Pittendrigh, 1960).

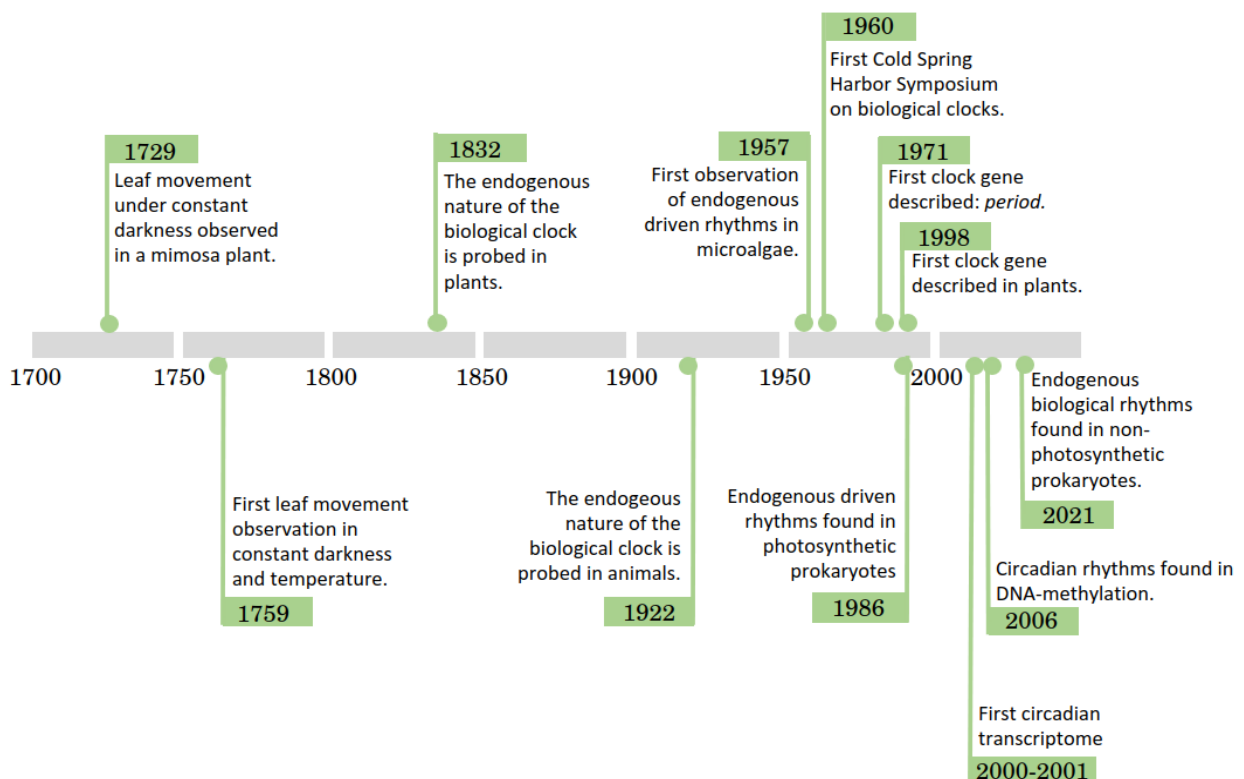


Figure 4: Timeline of circadian research. The main circadian discoveries have been listed in chronological order. (De Mairan, 1729; Duhamel du Monceau, 1759; De Candolle, 1832; Richter, 1922; Hastings & Sweeney, 1957; Evans, 1961; Konopka & Benzer, 1971; Mitsui et al., 1986; Somers et al., 1998; Akhtar et al., 2002; Eissenberg & Elgin, 2006; Eelderink-Chen et al., 2021; Kuhlman et al., 2018; Roenneberg & Merrow, 2005)

Nowadays, 62 years later, these empirical features are still useful in spite of the huge development in the field. Recent technological approaches have enabled a more controlled experimentation and data analysis in chronobiological studies. Chronobiologists have already identified circadian rhythms in organisms spanning almost the entire tree of life (Hastings & Sweeney 1957; Mitsui et al., 1986), even non-photosynthetic prokaryotes (Eelderink-Chen et al., 2021). Also the genetics behind the circadian clock have been broadly studied in a wide range of phyla, since the first clock gene was described in 1971 by Seymour Benzer and Ronald Konopka using mutant screening in *Drosophila melanogaster* (Konopka & Benzer, 1971; Takahashi, 2021) and the first clock gene in

plants in 1998 (Somers et al., 1998). This discoveries about individual genes directly involved in the circadian clock started the path for massive genetics approaches, obtaining in the early 2000s the first circadian transcriptome (Akhtar et al., 2002) followed by the discovery of DNA-methylations globally following circadian rhythms (Eissenberg & Elgin, 2006) (Fig. 4).

As it can be observed in the timeline, circadian rhythms discoveries are very diverse. Chronobiologists usually have strong roots in other fields such as anatomy, physiology, molecular biology, genetics, ecology, mathematics and/or computer science. The knowledge obtained from each field have been shared and integrated in order to obtain a precise characterization of circadian rhythms (Klante & Steinlechner, 1994; Merrow et al., 2005; Nishiwaki-Ohkawa & Yoshimura, 2016). In recent years, mathematics and computer science have strongly influenced the entire field of research by proposing a paradigm in which biological rhythms are studied as waves. Wave patterns repeat themselves periodically, maintaining several features that define their profiles. These features can be modelled as wave parameters and used to quantitatively compare different waves. Cosinusooidal parametrizations of the following form are commonly applied in circadian research to model rhythmic phenomena:

$$Y = m + \alpha \cos\left(\frac{2\pi}{\tau}(t - \varphi)\right)$$

where Y represents the measurements of the phenomena under study such as gene expression or protein abundance in this thesis; m is the mesor or wave mean value around which oscillations take place; α is the wave amplitude or range between the maximum and minimum wave values; τ is the wave period or the time length between successive repetition of the same wave pattern which is fixed to 24 h in circadian research and φ is the wave phase or time point when the maximum wave value is reached (Fig. 5).

These parameters can be estimated from experimental data applying methods such as non-linear least squares for different rhythmic phenomena and the statistical significance of the differences between them can be assessed (McClung, 2006; Parsons et al., 2020). A major drawback of the previous parametric models consists in their ability to detect only symmetric waves failing to identify more complex rhythmic patterns.

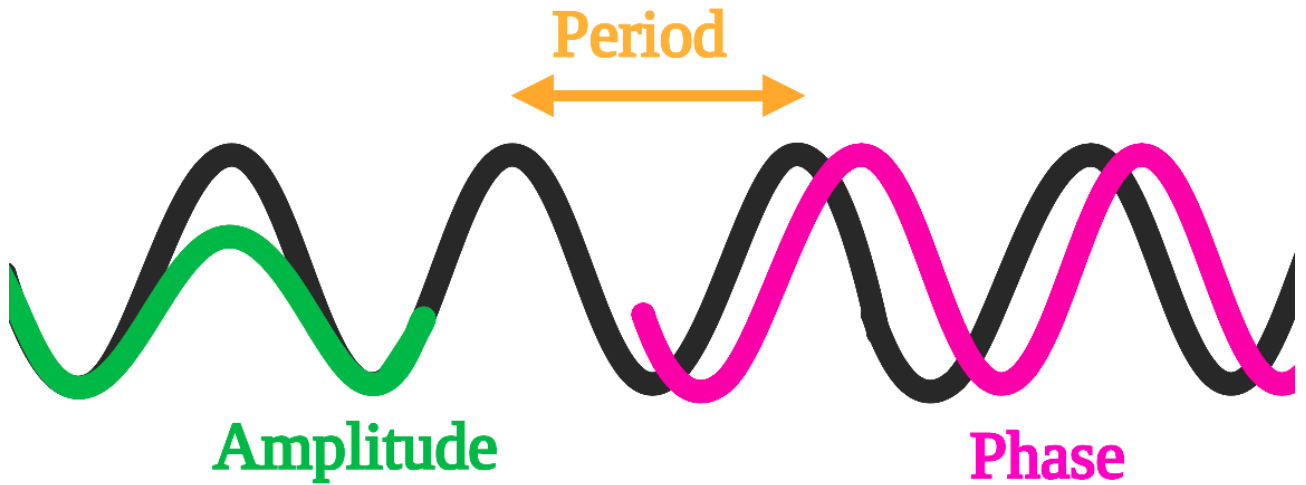


Figure 5: Graphical representation of cosinusoidal wave model parameters. Period is represented in orange and it corresponds to the time interval between consecutive repetitions of the wave pattern; amplitude is represented in green and it corresponds to the difference between the highest and lowest points the wave reaches; and phase is represented in pink and it corresponds to the time point where the wave reaches its maximum value

Therefore, non-parametric models have been proposed to complement these limitations detecting rhythmic patterns of arbitrary form. Robust non-parametric models have been developed based on rank tests for umbrella alternatives (Mack & Wolfe, 1981; Thaben & Westermark, 2014). Specifically, in this thesis these two complementary approaches, parametric and non-parametric, have been applied to obtain a deep characterization of circadian rhythms at three different molecular levels (transcriptome, proteome and physiology) in *Ostreococcus tauri* subjected to different seasonal variations of diel cycles.

Ostreococcus tauri

The green lineage (*Viridiplantae*), comprehends two of the most important groups of oxygen photosynthetic eukaryotes: green microalgae and their descendants, terrestrial plants.

Microalgae are a very diverse group of photosynthetic microorganisms of special interest due to their plastic physiology and their biotechnological applications. They can be found in different water-based habitats, from freshwater to oceans, as well and land ecosystems, including deserts. Microalgae grow under a broad range of temperature, salinity, pH and light intensity values. More than 5000 species of microalgae have been identified in the oceans accounting for the production of 50% of the oxygen necessary to sustain life on Earth (El Gamal, 2010). Microalgae play a central ecological role as primary producers of biomass establishing the base of aquatic trophic chains. They have also been of great interest for the scientific community due to the large and yet increasing number of their biotechnological applications. Specifically, microalgae have been described as a high yield source of carbon compounds and good candidates to mitigate CO₂ emissions. The fixation of CO₂ is coupled with growth and biosynthesis of compounds of biotechnological interests such as polysaccharides, lipids, vitamins and antioxidants. They are currently large-scale cultured to produce biostimulants in agriculture, health supplements, pharmaceuticals and cosmetics, as well as, successfully applied in wastewater treatment coupled with the fixation of atmospheric CO₂ (Abinandan et al., 2018; Borowitzka, 2013; H. Chen et al., 2019; García-Cubero et al., 2018).

Recently, the development of high-throughput sequencing is contributing to the clarification of the evolutionary history of the green lineage (Bachy et al., 2022; Becker & Marin, 2009; Benites et al., 2021; Leliaert et al., 2012; Merchant et al., 2007). These two main clades are, as previously mentioned, *Streptophyta*, including *Embryophyta* or land plants and *Charophyta* (land plant's closest algal ancestors or evolutionary eldest algal sisters); and *Chlorophyta*, comprising the core chlorophytes (*Chlorophyceae* and *Trebouxiophyceae*) and the evolutionary eldest sisters in this clade and the entire green lineage: *Prasinophyta*, which include *Mamiellales* (Bachy et al., 2022; Leliaert et al., 2012; Tragin & Vaultot, 2019) (Fig. 6).

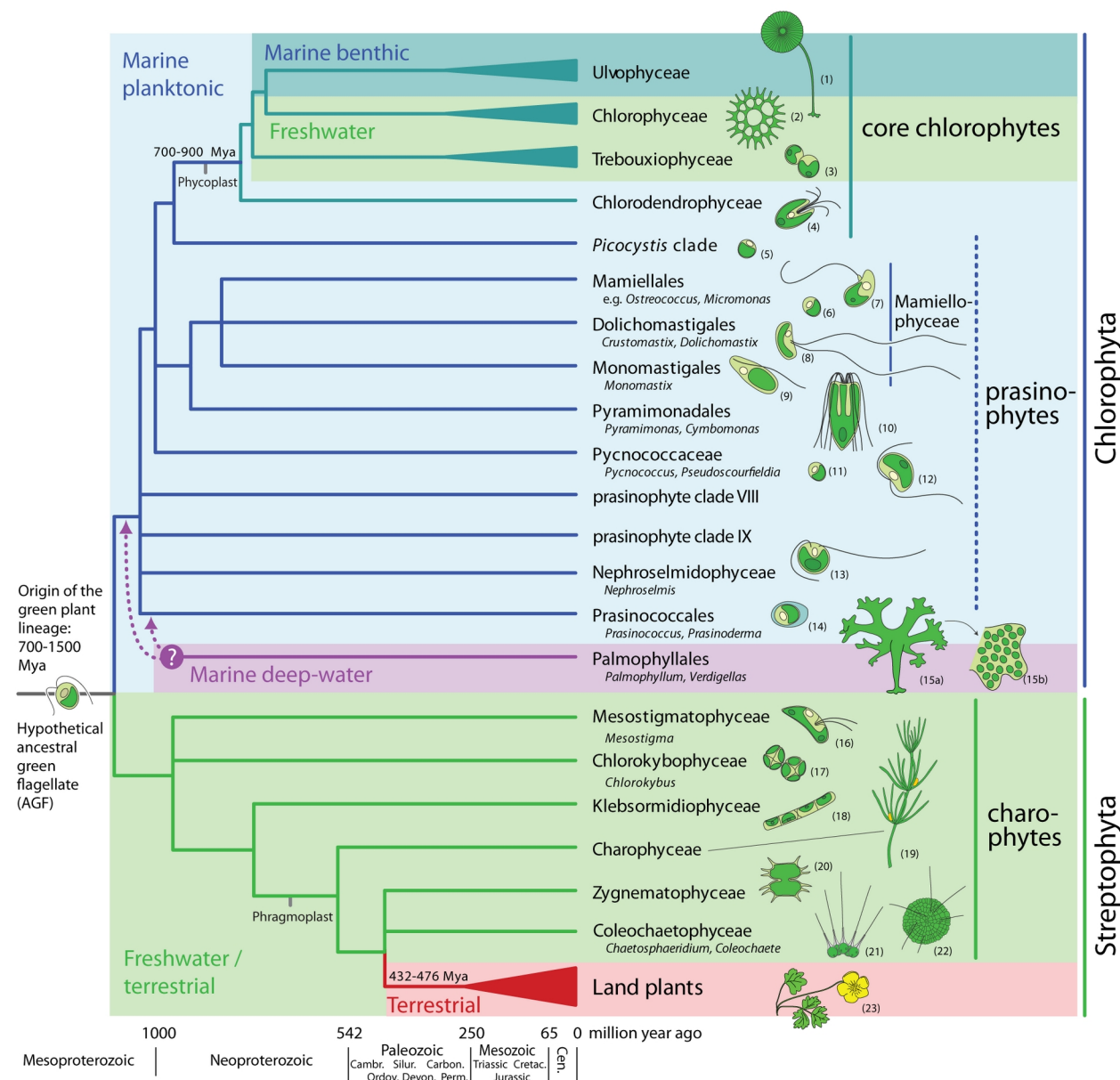


Figure 6: Phylogenetic relationships among the orders in the green lineage or Viridiplante. Figure obtained from (Leliaert et al., 2011). The tree topology is a composite on accepted relationships based on molecular phylogenetic evidence. Uncertain phylogenetic relationships are indicated by polytomies. The divergence times are rough approximations based on the fossil record and molecular clock estimates. Drawings illustrate representatives of each lineage: (1) Acetabularia, (2) Pedialstrum, (3) Chlorella, (4) Tetraselmis, (5) Picocystis, (6) Ostreococcus, (7) Micromonas, (8) Crustomastix, (9) Monomastix, (10) Pyramimonas, (11) Pycnococcus, (12) Pseudoscourfieldia, (13) Nephroselmis, (14) Prasinococcus, (15) Verdigellas (a: general habit, b: individual cells in a gelatinous matrix), (16) Mesostigma, (17) Chlorokybus, (18) Klebsormidium, (19) Chara, (20) Xanthidium, (21) Coleochaete, (22) Chaetosphaeridium, (23) Ranunculus.

Initial biodiversity studies on marine phytoplankton posited the domination of oceans by the so-called red lineage conformed by diatoms and dinoflagellates while the green lineage was thought to have less importance in marine ecosystems, being confined to freshwaters and terrestrial environments (Worden et al., 2004). These two lineages are early divergent from the endosymbiotic events that gave rise to chloroplasts. Whereas a single endosymbiotic event took place in *Viridiplantae*; two or even more endosymbiotic events are described in the red lineage (Leliaert et al., 2012).

However, in the last decade, metabarcoding studies have completed previous studies based solely on microscopic and traditional molecular techniques. These studies have unveiled the relevance of the green lineage in marine waters. Also, the cosmopolitan distribution of *Prasinophyta* has been described, especially for the order *Mamiellales* (Collado-Fabbri et al., 2011; Demir-Hilton et al., 2011; Leconte et al., 2020; Tragin & Vaulot, 2019; Worden et al., 2004).

In that taxonomic context, *Ostreococcus tauri* is classified as a green mamiellale microalgae (Fig. 6-7). Its contribution to the marine phytoplankton is crucial in a wide range of oceans and seas all over the world (Benites et al., 2021; Collado-Fabbri et al., 2011; Demir-Hilton et al., 2011). As examples of *Ostreococcus* cosmopolitan character, it is worth mentioning that different strains have caused blooms in the Atlantic and Pacific Oceans (O'Kelly et al., 2003; Worden et al., 2004) and that a specific *Ostreococcus* strain has been found to be the most prevalent *Mamiellale* in the Mediterranean Sea (Tragin & Vaulot, 2019). Beyond its ecologically important role (Chapman, 2013; Worden et al., 2004) and cosmopolitan presence in marine environments, *Ostreococcus tauri* key feature consists in being considered the world's smallest free-living eukaryote known to date (around 1 µm). Due to its small size, *Ostreococcus tauri* have been "invisible" to field researchers for a long time. It was first detected by flow cytometry as a rounded microalgae in a bloom that took place on the Mediterranean French lagoon, Étang de Thau, known for its semi-intensive farming of oysters. Hence, it was referred to as an "oysters coccus form the Thau lagoon" or *Ostreococcus tauri*. Its subcellular structure was resolved consisting of a nucleus, a single mitochondrion, a single chloroplast containing one starch granule and a very reduced or almost non-existent cytoplasmic compartment (Fig. 7) (Moreau, H, et al., 1995).

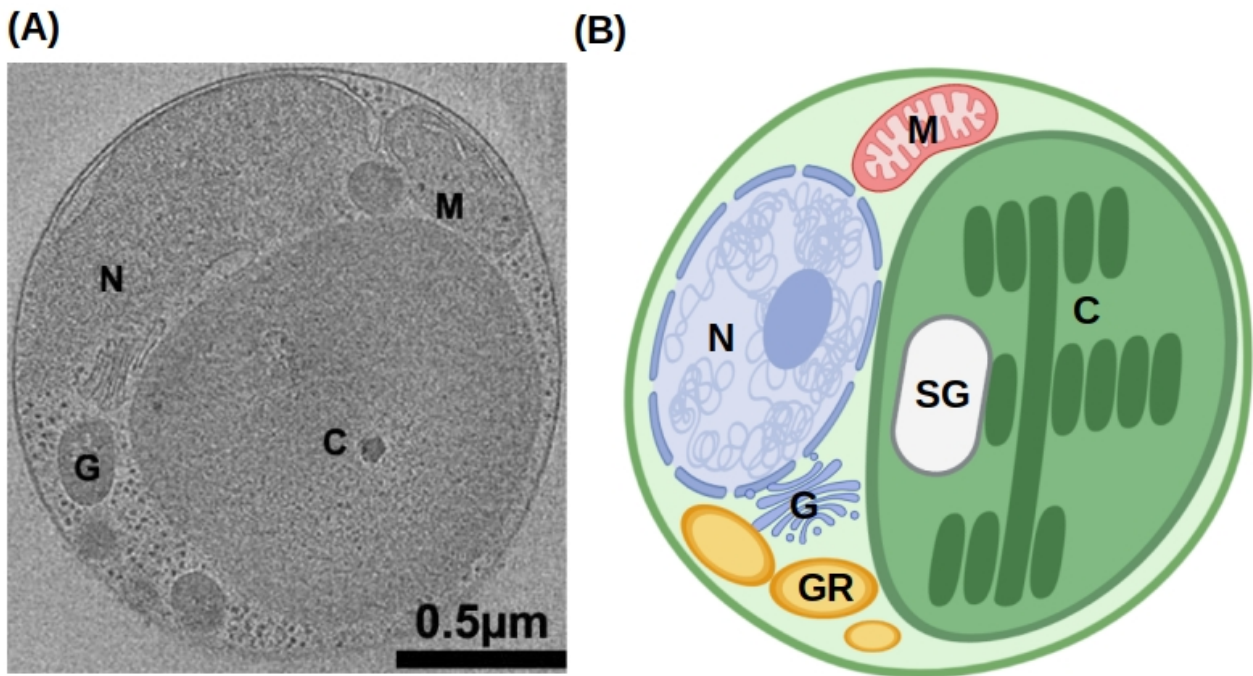


Figure 7: *Ostreococcus tauri*. (A) Tomographic 2D section from an *Ostreococcus tauri* cell from (Henderson et al., 2012). (B) An illustrated diagram of an *Ostreococcus tauri* cell (created using BioRender) based on the previous 2D segmentation. Labels: nucleus N, chloroplast C, Golgi body G, mitochondrion M, starch granule SG and granules GR.

At that time, genome sequencing studies to understand marine phytoplankton were mainly focused on prokaryotes (Berube et al., 2018; Palenik et al., 2003). *Ostreococcus tauri* genome was not sequenced for the first time until 2006 (Derelle et al., 2006). From that point on, an increasing number of picoeukaryotes genomes were sequenced, including a second version of *Ostreococcus tauri* genome (Blanc-Mathieu et al., 2014). These contributions allowed the identification of unique genomic features, showing that its simplicity goes beyond its reduced size and cell structure. Initially, no remarkable characteristic was identified in its 12.56 Mb genome arranged into 20 chromosomes when compared, for example, to *Saccharomyces*. Nevertheless, a unique feature is uncovered when the fascinating fact comes when the number of genes of these two organisms are compared. With a similar genome size, *Saccharomyces cerevisiae* has around 6275 protein coding genes, while *Ostreococcus tauri* has 8166 (Blanc-Mathieu et al., 2014; Derelle et al., 2006; Engel et al., 2014), making it the most gene dense free-living eukaryote known to date. This simplicity is also clear when genome size, number of genes and transcription factors in *Ostreococcus tauri* is compared to other photosynthetic species such as *Arabidopsis thaliana*

(*Embryophyta*), *Klebsormidium nitens* (*Charophyta*), *Chlamydomonas reinhardtii* (*Chlorophyta*) and *Phaeodactylum tricornutum* (*Heterokontophyta*) (Table 1).

Other key genomic characteristics in *Ostreococcus tauri* are its short intergenic regions and reduced gene family sizes comprising only a single gene copy or even merging different genes into a single one. These features contribute to its intense degree of genome compaction. With the only exception of a long internal duplication on chromosome 19, hypothesized to be of recent origin due to its lack of divergence. There are more special characteristics in chromosomes 19 and 2. They contain 77% of the transposable elements of the genome, have lower G+C content and a different codon usage (Blanc-Mathieu et al., 2014; Derelle et al., 2006).

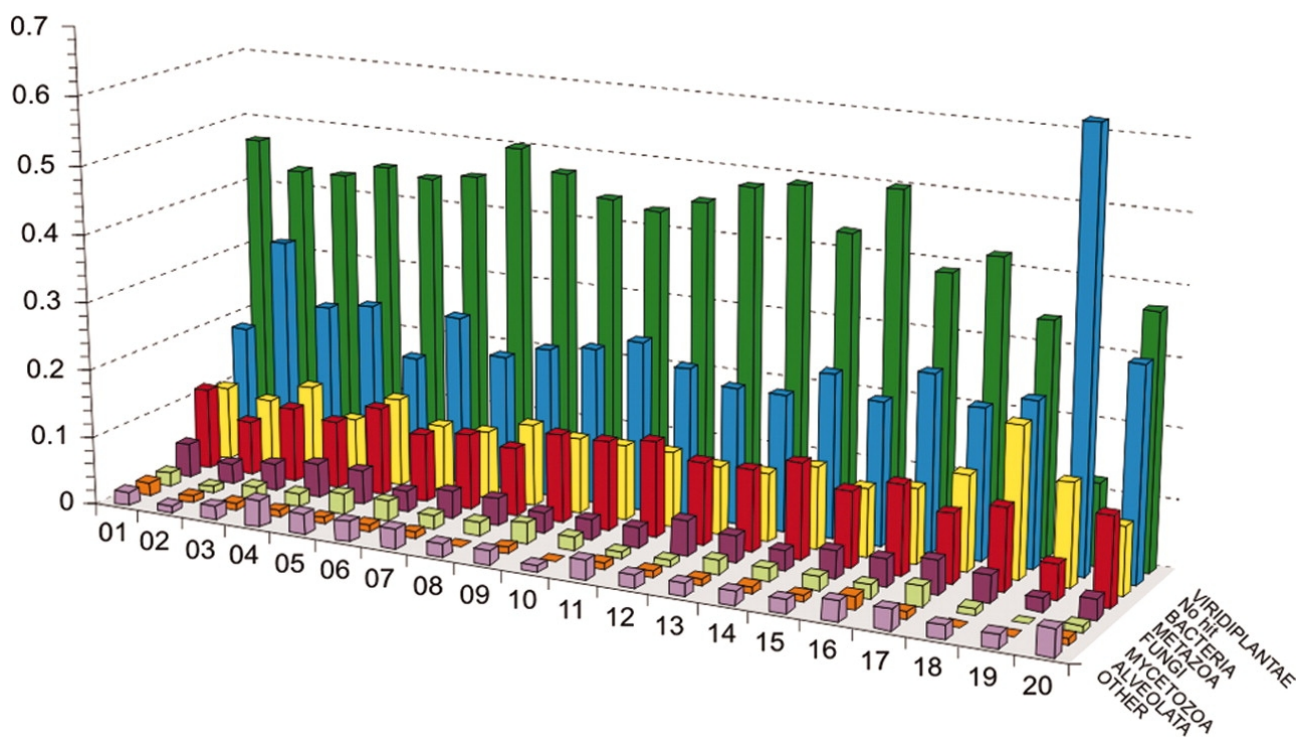


Figure 8: Taxon distribution of best hits for genes from each *Ostreococcus tauri* chromosome.

Figure from (Derelle et al., 2006). The number corresponding to each chromosome is represented in the x axis, the percentage of best hits is represented in y axis. Each color stands for: viridiplantae, green; no hit, blue; bacteria, yellow; metazoa, red; fungi, purple; mycetozoa, light yellow; alveolates, orange; others, light purple.

The first hypotheses about these chromosomes were that they had a different origin than the rest of the genome being the product of horizontal gene transfer events. Currently, only chromosome 19 is considered an “alien” chromosome since most of its protein coding genes are not related to the green lineage. However, chromosome 2 protein coding genes

are essential housekeeping genes not duplicated and related to the green lineage (Fig. 8). Alternatively, this chromosome has recently been considered as a sex-related or mating-type chromosome (Benites et al., 2021; Blanc-Mathieu et al., 2014) .

Although sex is now accepted as a ubiquitous and ancestral feature of eukaryotes (Sekimoto, 2017; Swanson et al., 2011), direct observation of sex is still missing in most unicellular eukaryotic lineages. The genomic regions, so-called mating-type, involved in sex have been characterized in other *Chlorophyta* (Sekimoto, 2017) and, recently, in *Ostreococcus tauri*, which appears to encode two highly divergent haplotypes. These *Mamiellales* mating-type candidate regions are likely to be the oldest mating-type loci described to date (Benites et al., 2021; Leconte et al., 2020).

Overall, *Ostreococcus tauri* is proposed as a novel model organism due to its structural and genomic features. In addition, inside the green lineage there is a lot of diversity and actually it is difficult to find a model organism that can represent the hole lineage (Cock & Coelho, 2011). *Ostreococcus tauri* taxonomical classification as the eldest sister in *Prasinophyta* makes it an ideal such organism potentially representing the green lineage eldest ancestor (Derelle et al., 2006; Leliaert et al., 2012). Therefore, *Ostreococcus tauri* molecular systems could be considered as representative of the fundamental systems in the green lineage and the knowledge gained from them could be somehow extrapolated to a wide range of photosynthetic organisms.

Also very relevant to this thesis, research in Molecular Systems Biology often faces challenges produced by the complexity of the model organisms used in the corresponding field and the high economical and computational costs associated to the generation and analysis of the necessary massive amounts of omics data (De Keersmaecker et al., 2006; Jamers et al., 2009; Joyce & Palsson, 2006; Weckwerth, 2011). In this respect, due its genomic simple features *Ostreococcus tauri* is an ideal model organism in Molecular Systems Biology when compared with other models in the green lineage such as *Arabidopsis thaliana* and *Chlamydomonas reinhardtii* (Table 1) (de los Reyes, Romero-Campero, Ruiz, Romero, & Valverde, 2017; Derelle et al., 2006; Krumholz et al., 2012; Le Bihan et al., 2011a; Lelandais et al., 2016). Indeed, in this thesis, *Ostreococcus tauri* has allowed us to generate, analyze and interpret massive multiomic and physiological data to characterize responses to seasonal variations of diel cycles in potentially fundamental systems in the green lineage.

Table 1: Genomic features of different green lineage model organisms. Their genome size and protein coding genes (Blaby et al., 2014; Blanc-Mathieu et al., 2014; Craig et al., 2021; Derelle et al., 2006; Hori et al., 2014; Lamesch et al., 2012; Swarbreck et al., 2008; M. Yang et al., 2018) are compared with their number of predicted transcription factors. (Rayko et al., 2010; Zheng et al., 2016)

	Genome size (Mb)	Number of protein coding genes.	Number of transcription factors.
<i>Arabidopsis thaliana</i>	135	27474	1779
<i>Klebsormidium nitens</i>	104	17055	286
<i>Chalmydononas reinhardtii</i>	110	14000	279
<i>Phaeodactylum tricornutum</i>	27.4	10567	212
<i>Ostreococcus tauri</i>	12.56	6275	102

Ostreococcus tauri allowed us to generate, analyze and interpret massive data from the complete system with less computational and experimental costs, so a holistic understanding of the chronobiology in this eukaryote was finally achieved.

Molecular Systems Biology

There is an ancient Indian fable that illustrate how a holistic view and ontological reasoning contributes to knowledge, it is called “Blind men and an elephant”. A poem of John Godfrey Saxe is one of the most famous written versions of it:

“ It was six men of Indostan
To learning much inclined,
Who went to see the Elephant
(Though all of them were blind),
That each by observation
Might satisfy his mind.

The Fourth reached out an eager hand,
And felt about the knee.
"What most this wondrous beast is like
Is mighty plain," quoth he;
"This clear enough the Elephant
Is very like a tree!"

The First approached the Elephant,
And happening to fall
Against his broad and sturdy side,
At once began to bawl:
"God bless me! but the Elephant
Is very like a wall!"

The Fifth, who chanced to touch the ear,
Said: "E'en the blindest man
Can tell what this resembles most;
Deny the fact who can
This marvel of an Elephant
Is very like a fan!"

The Second, feeling of the tusk,
Cried, "Ho! what have we here
So very round and smooth and sharp?
To me 'tis mighty clear
This wonder of an Elephant
Is very like a spear!"

The Sixth no sooner had begun
About the beast to grope,
Than, seizing on the swinging tailgeneraliza-
tions
That fell within his scope,
"I see," quoth he, "the Elephant
Is very like a rope!"

The Third approached the animal,
And happening to take
The squirming trunk within his hands,
Thus boldly up and spake:
"I see," quoth he, "the Elephant
Is very like a snake!"

And so these men of Indostan
Disputed loud and long,
Each in his own opinion
Exceeding stiff and strong,
Though each was partly in the right,
And all were in the wrong! (...)"

After touching different parts of the animal, one of the blind wise men concluded that the elephant was like a snake, he was touching only the trunk of the elephant. Another one concluded that it was like a fan since he was only touching the ear of the animal, and so on with the other blind wise men. Each one of them was confident about his individual findings and reaching an agreement between them was impossible. The subject of study was so massive that they individually were only able to collect information from very specific regions that were treated as independent and contradictory truths instead of considering them as complementary parts of a whole.

Until recently, studies producing holistic views of living organisms were impossible to carry out due to the lack of suitable technologies. The development of omics technologies together with advances in computational science and artificial intelligence have made possible such systemic approaches in biology (Ideker et al., 2001; Karahalil, 2016; Veenstra, 2021; Weckwerth, 2011).

In the last 50 years, sequencing methods have exponentially improved. First generation DNA sequencing methods were developed around 45 years ago shortly anticipating the development of one of the biggest international research projects in History, the Human Genome Project, which started about 20 years ago (Ideker et al., 2001; Veenstra, 2021). In this project an extremely ambitious goal was pursued, the sequencing of the whole human genome. However ambitious, its impact in Science was beyond expected transcending the initial purpose. Different groups cooperated all over the world to sequence the complete human genome which promoted the development of new sequencing methods in order to make the process easier and cheaper. These methods are now applicable to study the molecular systems codified in the genome of living organism spanning the entire tree of Life (Abascal et al., 2020).

During the Human Genome Project, 13 years were needed to sequence a single complete human genome and the overall costs were 2.7 billion dollars. Currently, with the emergence of Next Generation Sequencing (NGS) methods, around 100000 human genomes have been sequenced in the last 6 years. The Illumina HiSeq System generates around 500 gigabase sequences per second, dropping the cost of sequencing a complete human genome to \$1500 in only 10 years (Prendergast et al., 2020; Veenstra, 2021). Ultimately, these methods has changed how scientific projects are approached in biology.

These new approaches have been applied to sequence, identify and quantify complete transcriptomes, total mRNA transcripts from samples. This is generating unprecedented massive amounts of biological information. Although, transcriptomic studies are extremely informative they only focus on one layer of the complexity in biological systems leaving out the actual molecular components that perform most cellular functions, the proteins. This has promoted the development of methodologies based on High Performance Liquid Chromatography (HPLC) coupled to Mass Spectrometry (MS) aiming to the identification and quantification of the complete proteome, total set of proteins from biological samples. Moreover, in order to obtain a more complete picture of biomolecular systems, methods identifying and quantifying specific metabolites need to be explored developing targeted metabolomics. Finally, phenomics or the systematic acquisition of phenotypic data, using for example cell cytometry for the case of unicellular microorganisms, is necessary to link the most relevant molecular levels of complexity in living organisms with their physiology. Although, these molecular components are identified and quantified independently by different methods, genes, transcripts, proteins and metabolites highly interact with each other establishing different positive and negative regulatory loops underpinning cellular physiology. Based on these technologies and this view, researchers in Life Sciences are beginning to approach the study of living organisms and processes as systems with interacting modules comprising genes, transcripts, proteins and metabolites that constitute large biomolecular networks organized into cellular structures establishing the field of Molecular Systems Biology (Joyce & Palsson, 2006; Veenstra, 2021; Weckwerth, 2011).

While this holistic view of biological systems is gaining strength growing steadily during the first decades of the XXI century (Fig. 9), traditional reductionist methods focusing on individual molecular components, single genes, proteins and/or metabolites, are still the most popular ones in the study of specific organisms such as microalgae. Scientific projects in these research areas were limited by the time, economic resources and software tools needed to analyze and integrate massive amounts of biological data (Karahalil, 2016; Mazzocchi, 2012; Veenstra, 2021).

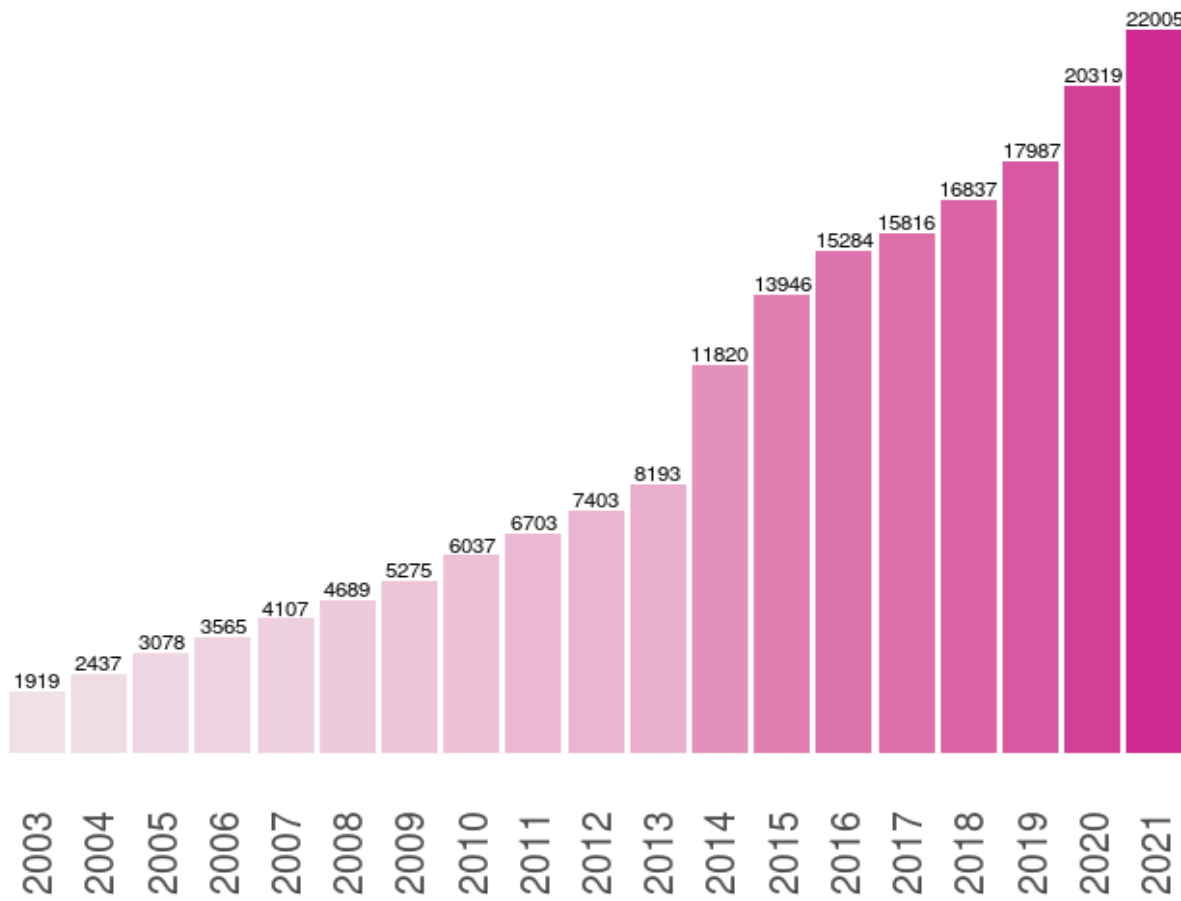


Figure 9: Publications on systems biology. Exponential increase in the number of publication using the term "systems biology" in PubMed since the year when the Genome Human Project was completed (2003). The number on the top of each bar corresponds to the exact number of publications of that year.

Nevertheless, on the one hand, the sequencing of an increasing number of microalgae genomes (Blanc et al., 2012; Bowler et al., 2008; Cheng et al., 2019; Derelle et al., 2006; Hori et al., 2014; Merchant et al., 2007; Morimoto et al., 2020; Prochnik et al., 2010) has allowed the application of omics technologies transcriptomics (de los Reyes, Romero-Campero, Ruiz, Romero, Valverde, et al., 2017; Ditz et al., 2021; Hoys et al., 2021; Serrano-Pérez et al., 2022), proteomics (Le Bihan et al., 2011b; Weckwerth, 2011) and metabolomics (Hoys et al., 2021; Serrano-Pérez et al., 2022; Weckwerth, 2011) in microalgae research. On the other hand, there was a lack of specific software tools for microalgae to analyze and interpret omics data. In order to contribute to resolve this deficiency in the microalgae research community, in the first steps of my doctoral thesis I developed the web-app ALGAEFUN with MARACAS, microALGAE FUNctional enrichment tool for Mi-

croAlgae RnA-seq and Chip-seq AnalysiS (Romero-Losada et al., 2022). These tools allow researchers without expertise in computational data analysis to process omic raw data to obtain list of relevant genes or genomic loci in their research and to perform functional enrichment analysis over them. This is contributing to the establishment of Microalgae Molecular Systems Biology. Following the main theme in Systems Biology the goal consists in improving our understanding of microalgae through the integration of partial characterizations obtained for their different biological components. Here the typical methodology in Molecular Systems Biology is adopted starting with the generation of massive amounts of omic data and its subsequent integrative analysis. The results obtained from computational analysis based on statistical and Artificial Intelligence methods must be validated by independent wet lab experiments revising these results if necessary. The final expected result is the development of predictive models enabling researchers in microalgae biotechnology to anticipate the physiological response of these organisms under specific conditions (Jamers et al., 2009; Veenstra, 2021; Weckwerth, 2011; Zurbriggen et al., 2012).

In this sense, this thesis aims at providing a molecular systems biology characterization of the responses in the prasinophyceae microalgae *Ostreococcus tauri* to seasonal variations in diel cycles. Accordingly, generation and integrative analysis of massive amounts of data from two different omics techniques, transcriptomics and proteomics, have been performed. Moreover, physiological measurements for cell cycle phases, photosynthetic activity, carotenoid and starch content, as a first approach towards phenomics, has been integrated into our analysis. Specifically, the transcriptomic method used in this thesis was RNA sequencing, RNA-seq, the up to date method used for this omic. The application of next-generation sequencing methods to study transcriptomes has produced the development of RNA-Seq analyses which has enabled researchers to identify and quantify a wide variety of different classes of RNAs without requiring transcript-specific probes which has almost driven microarrays to become obsolete previous method used in transcriptomic analyses), and not only to identify but also to quantify abundance of transcripts (Ditz et al., 2021; Veenstra, 2021; Z. Wang et al., 2009). Respectively, the proteomic technology applied in this thesis was SWATH-MS, Sequential Window Acquisition of all Theoretical fragment ion spectra Mass Spectrometry.

The field of proteomics have been directly connected with the development of mass spectrometry (MS) technology. During the first part of this century, there were two lines of de-

velopment working separately for what would be known as proteomics today: identification (2-D electrophoresis gel) and quantification (using isotope tags) of proteins. Nowadays, proteomic technologies have enable the development of proteins identification and quantification methods so the number of proteins that can be quantified/identified today is around several thousands (Shen et al., 2022; Veenstra, 2021). Precisely, SWATH-MS is a data independent acquisition (DIA) method in which liquid chromatography y coupled with two round of MS for protein identification and characterization, as well as label free relative quantification (M. X. Chen et al., 2021; Ludwig et al., 2018).

Molecular systems biology with its increasing amount of data generated and the biological complexity it has unveiled is demanding a new generation of qualified researchers proficient in computer science, mathematics/statistics and molecular biology. My main goal when developing this thesis is to join this generation of young researchers who are working to develop software applications, efficient data analysis algorithms and user-friendly app-tools to enable the progress of systems biology studies making it more accessible to the scientific community (Coletto-Alcudia & Vega-Rodríguez, 2020; Romero-Campero et al., 2016; Romero-Losada et al., 2022).

Materials and Methods

Organism and culture growth conditions.

Organism and growth medium.

The sequenced strain of *Ostreococcus tauri*, RCC4221, was used in this study. Cells were grown photoautotrophically on sterilized artificial sea water (ASW) (Kester et al., 1967) supplemented with nitrates, phosphates, trace metal and vitamins. Components and concentrations of the medium are described in Table 2.

Table 2: Components supplementing ASW as *Ostreococcus tauri* culture medium.

	Concentration in solution (g L ⁻¹)	Concentration in medium (mg L ⁻¹)
Solución I	400 NaNO ₃	222.2 NaNO ₃
Solución II	2.8 Na ₂ HPO ₄ 10 K ₂ HPO ₄	1.6 Na ₂ HPO ₄ 5.6 K ₂ HPO ₄
Solución III	5.4 NH ₄ Cl 10.4 Fe-EDTA 74.4 Na ₂ -EDTA $4.6 \cdot 10^{-2}$ ZnSO ₄ $2.8 \cdot 10^{-2}$ CoSO ₄ $1.6 \cdot 10^{-2}$ Na ₂ MoO ₄ · 2H ₂ O $5.0 \cdot 10^{-3}$ CuSO ₄ $3.4 \cdot 10^{-2}$ H ₂ SeO ₃ $3.6 \cdot 10^{-2}$ MnCl ₂ · 4H ₂ O	3.0 NH ₄ Cl 5.8 Fe-EDTA 41.3 Na ₂ -EDTA $2.6 \cdot 10^{-2}$ ZnSO ₄ $1.6 \cdot 10^{-2}$ CoSO ₄ $8.9 \cdot 10^{-2}$ Na ₂ MoO ₄ · 2H ₂ O $2.8 \cdot 10^{-3}$ CuSO ₄ $1.9 \cdot 10^{-2}$ H ₂ SeO ₃ $2.0 \cdot 10^{-2}$ MnCl ₂ · 4H ₂ O
Solución IV	0.2 Thiamin-HCl $1.5 \cdot 10^{-3}$ Biotin $1.5 \cdot 10^{-3}$ Cyanocobalamin	0.2 Thiamin-HCl $1.7 \cdot 10^{-3}$ Biotin $1.7 \cdot 10^{-3}$ Cyanocobalamin

Continuous culture conditions in photochemostats.

Continuous culture was performed in 2.0 L capacity (0.07m diameter, 0.50 m height) jacketed sterilized photochemostat (bubble columns) containing 1.8 L of cells suspension, continuously sparged with air (1L (L culture⁻¹) h⁻¹) (Fig. 10). Culture conditions (pH, dilution rate and illumination regime) were constantly measured and computationally controlled by

a LabJack. Temperature was maintained at 20°C, and pH at 7.5 by on demand injection of CO₂ into the air stream entering the culture.

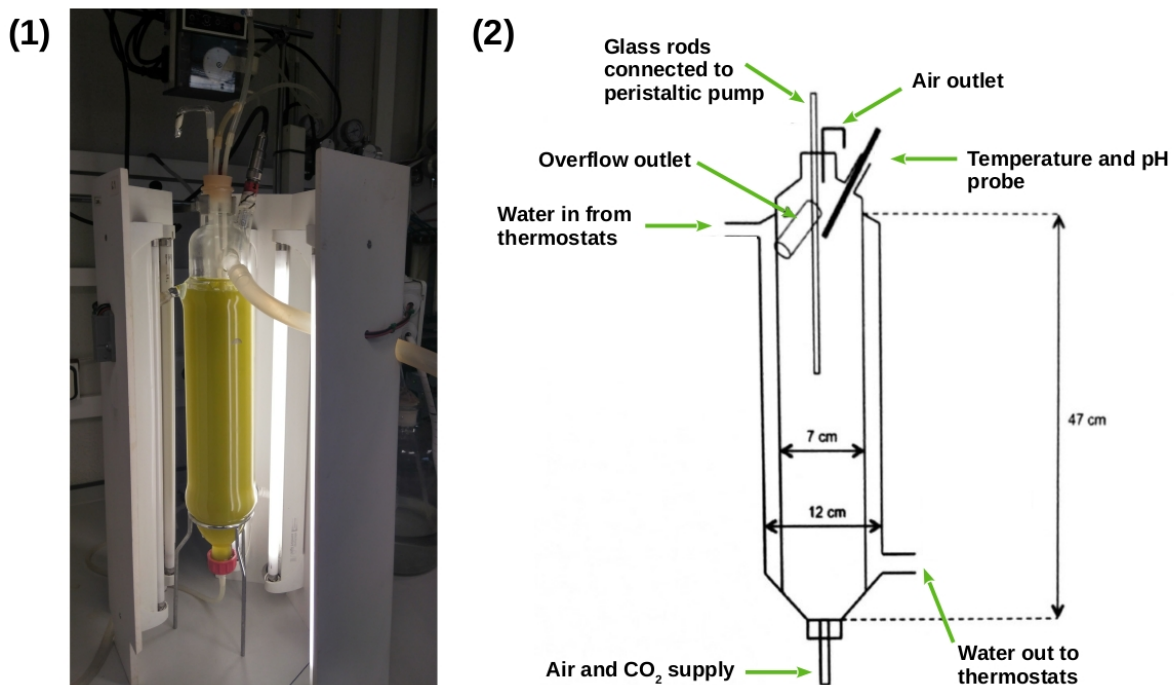


Figure 10: Growth system used for continuous cultures. (1) Picture of one of the photochemostats used. (2) Schematic detailed design of photochemostats.

Six Phillips PL-32W/840/4p white-light lamps, which provided a maximal incident irradiance of 1500 E m⁻² s⁻¹ on the reactor surface, were used as light inputs. Initially, the reactors were inoculated with batch-grown cells and operated on batch mode for about 3–4 d, with incident irradiance being progressively increased, until reaching stationary phase. Then, they were switched to operate on continuous mode, fresh medium being continuously fed during the light period at a flow rate of 45 mL h⁻¹ (dilution rate (D), 0.3 d⁻¹ under long day condition and 0.15 d⁻¹ under short day condition), with withdrawal of culture at the same rate. Once steady state conditions were achieved, samples were collected and analytical determinations were performed.

In addition, instead of a sudden transition from dark to light and from light to dark, our LabJack controlled system gradually increased light until an irradiance of 1500 µE m⁻² s⁻¹ is reached simulating the natural photoperiod (Fig. 11). Furthermore, they are surrounded by a wooden box and a completely opaque fabric to avoid any external light input.

Experimental design.

Our experiments are focused on two extreme photoperiods: summer long day condition (LD, 16h light : 8h dark) and winter short day condition (SD, 8h light : 16h dark). The experimental design (Fig. 10) consisted of three days under the specific photoperiod, LD or SD, followed by three days under free running conditions (constant light or constant dark). Cells were harvested at specific times during diel cycles, represented as zeitgeber time (ZT), where ZT0 corresponds to dawn, ZT4 to 4h after dawn and so on. Samples were taken every 4h (from ZT0 to ZT20) during the three days of alternating light/dark cycles. Therefore, a total of 6 samples for each day of sampling were generated. No samples were collected during the first day of free running condition to allow culture acclimation. Then, samples were collected every four hours starting at subjective dawn, during two days.

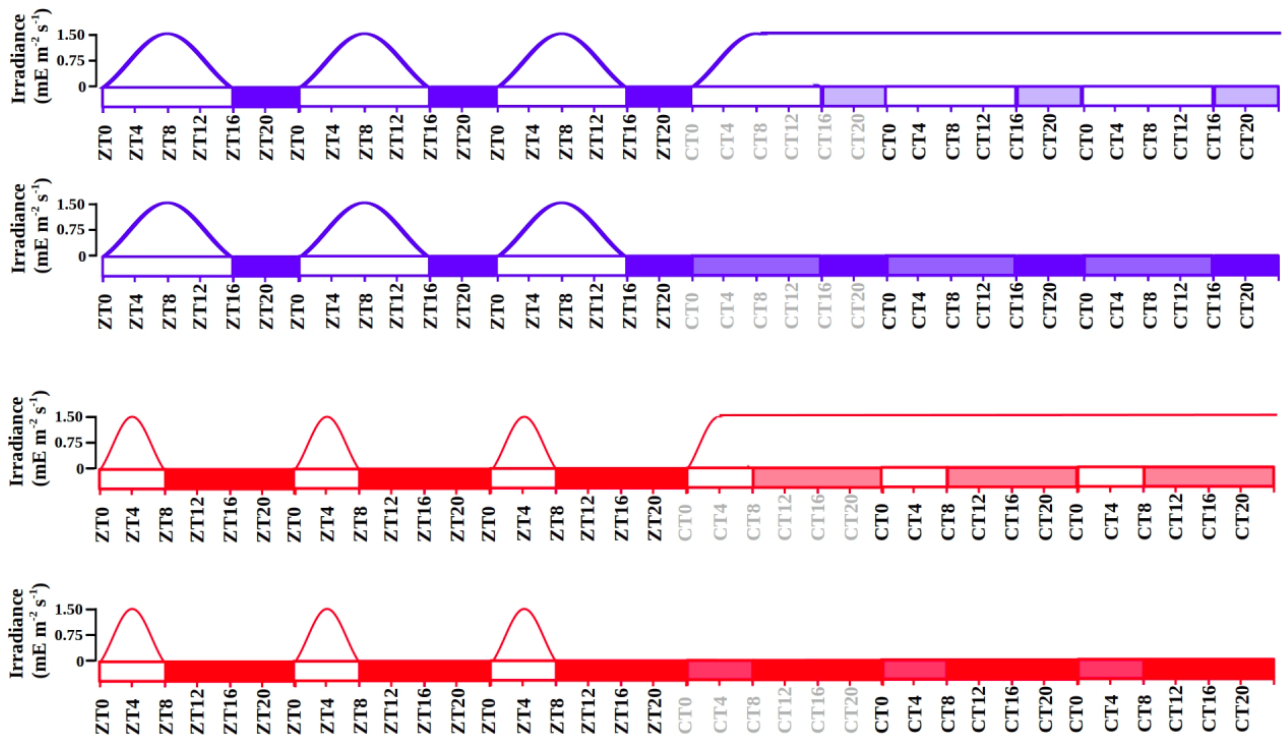


Figure 11: Schematic description of the experimental design. Gradually increased and decreased irradiance is represented during each light phase. Long day condition are represented in blue and short day condition in red. Photoperiods (light periods) correspond to white rectangles and skotoperiods (dark periods) to blue/red filled rectangles. Light blue and red filled rectangles are used to represent subjective photoperiods and skotoperiods under free running conditions. ZTN, Zeitgeber Time N, marks the time point N hours after dawn (lights on). CTN, Circadian Time N denotes the time point N hours after the subjective dawn.

Transcriptomic analysis

Sample Collection

From each chemostat, a volume of 50mL of cell suspension were harvested (4 min centrifugation at 5000 x g and 4°C) for each time point. Pellets were washed using Phosphate-buffered saline solution (PBS) and flash frozen with liquid Nitrogen before stored at -80°C.

Cell disruption

Frozen pellets were resuspended in 400 µL of disruption buffer (García-Domínguez & Florencio, 1997) and directly added to a 1,5 mL Eppendorf tube (RNase free and phenol-proof) containing 400 µL of phenol:chloroform 1:1 and 100 µL of acid washed glass beads (0.25–0.3 mm diameter; Braun, Melsungen, Germany). Mechanical disruption was performed by 30 min of repeated cycles of 60 s of vortexing and 60 s of incubating on ice.

RNA extraction

Extracts were centrifuged (4 °C) for 15 min at 13000 x g, producing three differentiated phases: an upper aqueous phase containing RNA, a white interphase containing DNA and a lower organic phase containing proteins, lipids and glass beads. The upper aqueous phase was collected, mixed with 400 µL of phenol:chloroform 1:1 and centrifuged for 5 min (4 °C at 13000 x g). This process was repeated three more times. In the last wash, only chloroform was used to avoid phenol contamination of the RNA samples. The supernatant was incubated overnight at -20 °C in a solution of 80 µL 10 M LiCl and 550 µL 100% EtOH for RNA precipitation. Finally, samples were centrifuged 10 min at 13000 x g 4 °C. Pellets were dried to avoid EtOH contamination.

RNA purification

RNA purification was performed using the Isolate II RNA Plant Kit (Bioline). Washing, DNase treatment and elution were carried out following the manufacturer instructions. The final RNA concentration and integrity were measured using a bioanalyzer 2100 (Agilent RNA 6000 Nano Kit).

RNA sequencing and processing

Library was prepared in accordance with the manufacturer's instructions and the sequencing was carried out on the Illumina NextSeq500 sequencer. Approximately, 10 million 75nt long single end reads were generated for each sample. The *Ostreococcus tauri* genome sequence and annotation v3.0 were used as reference genome (Blanc-Mathieu et al., 2014). Further computational analysis were carried out using the software tools developed in this thesis ALGAEFUN with MARACAS, microalgae FUNctional enrichment tool for MicroAlgae RnA-seq and Chip-seq AnalysiS (Romero-Losada et al., 2022).

Proteomic analysis

Sample collection

Sample collection for proteomic analysis followed the same procedure as the one previously described for RNA analysis.

Cell disruption

Directly onto frozen pellets, 1 mL of Trizol, 100 μ L of acid washed glass beads (0.25–0.3 mm diameter; Braun, Melsungen, Germany) and 40 μ L of Protein Inhibitor Cocktail PIC (25x) were applied, followed by 3 disruption cycles (60s agitation-60s incubation on ice) using a Mini-Beadbeater (BioSpec Products).

Proteins extraction

Proteins were extracted using TRIsure™ Reagent (Sigma-Aldrich), according to the manufacturer's instructions. The resulting proteins pellets were resuspended with 2 mL of 0.3 M guanidine solution in 95 % EtOH using 10 sonication cycles (30 s sonication - 30 s of incubating at 4 °C) in a Diagenode Bioruptor Pico Sonicator and then centrifuged at 4 °C during 5 min at 8000 x g. This washing process was repeated twice, followed by two additional washing using 90 % EtOH. The final pellets were resuspended in NH₄HCO₃ 50 mM / 0.2 % Rapigest (Waters) and total proteins were quantified using Qubit system.

Proteins digestion.

First, 50 µg of proteins were incubated with dithiothreitol (DTT 4.5 mM) for 30 min at 60 °C. Then, iodoacetamide was added to a final concentration of 10 mM and incubated for 30 min, under total darkness at room temperature. Treatment with trypsin was done overnight at 37 °C in a 1:40 trypsin:protein. Subsequently, formic acid was added and incubated at 37°C for 1h. Finally, 2% acetonitrile (v/v) were added to reach a concentration of the digested sample around 0.5 µg of protein/µl of solution.

SWATH acquisition

Equipment and data acquisition method.

Proteomic data acquisition was performed using a label free quantification platform that employs independent data acquisition (DIA) called SWATH-MS (Sequential Windowed Acquisition of all Theoretical Mass Spectra (SWATH-MS)(Ludwig et al., 2018) using a time-of-flight TOF triple quadrupole hybrid mass spectrometer MS (5600 plus, Sciex) equipped with a nano electrospray source coupled to a nanoHPLC Eksigent model 425. The Sciex software Analyst TF 1.7 was used for equipment control and data acquisition. Peptides were first loaded onto a trap column (Acclaim PepMap 100 C18, 5 µm, 100 Å, 100 µm id×20 mm, Thermo Fisher Scientific) under isocratical order in 0.1 % formic acid/2% acetonitrile (v/v) at a flow rate of 3 µL/min for 10 min. Subsequently, they were eluted on a reversed-phase analytical column, with the built-in emitter (New Objective PicoFrit column, 75 µm id×250 mm, packed with ReproSil-PUR 3 µm). In the case of the samples corresponding to the short day condition, the analytical column was Acclaim PepMap 100 C18, 3 µm, 100 Å, 75 µm id×250 mm, Thermo Fisher Scientific, coupled to a PicoTip emitter (F360-20-10-N-20_C12 from New Objective). Formic acid 0.1 % (v/v) was used as solvent A and 2% acetonitrile with formic acid 0.1 % (v/v) were used as solvent B. Peptides were eluted with a linear gradient of 5-35 % (v/v) of solvent B in 120 min at a flow rate of 300 nL/min. The source voltage was selected at 2600 V and the temperature was maintained at 100 °C. Gas 1 was selected at 20 PSI, gas 2 at zero, and curtain gas at 25 PSI.

For proteins identification, Data Independent Acquisition DIA method was used. It consisted of a TOF-MS with a scan window of 400-1250 m/z (accumulation time of 250 ms)

followed by 50 MS/MS with a scan window of 230-1500 m/z (accumulation time of 65 ms) and with a cycle time of 2574 s.

Library construction

Spectral libraries for LD and SD conditions were constructed by making one run with a mixture of the biological replicates corresponding to each time point. ProteinPilot v5.0.1 software (Sciex) was used to identify the proteins in the library. A pooled search of all runs was performed. The parameters of the Paragon method were: trypsin as enzyme and iodoacetamide as cysteine alkylating agent.

The *Ostreococcus tauri* annotated proteome v3.0 file from ORCAE (Sterck et al., 2012) linked to a Sciex Contaminants database were used in library construction. A false positive analysis (FDR) was performed and those with FDR ≤ 0.01 were considered.

SWATH runs

For each sample, the equivalent of 1 μ g of digested protein was injected into each run. Previously, the equipment was self-calibrated using a standard, MS synthetic peptide calibration kit from Sciex, to control sensitivity and chromatographic conditions. Protein identification and quantification were performed using SWATH runs with 60 ms of accumulation time and 3.7s of cycle time. Three technical replicates for each one of the three biological replicates were analysed resulting in 9 replicates per time point.

Data processing

The generated libraries (1% FDR) were analyzed using the Sciex software PeakView 2.2 with the microapp SWATH 2.0, together with the data obtained from the SWATH runs. Using this software, the chromatographic traces of the ions were extracted and dumped into the Marker view 1.2.1.1 program where the list of identified proteins with their corresponding areas were generated. The parameters for extraction of ions and areas were: 10 peptides per protein, 7 transitions of each peptide, threshold of confidence of the peptides set at 90 and FDR 1%. The software NormalizerDE (Willforss et al., 2019) was used to test several normalization methods in order to probe which one achieved the minimum replicate variation relative to Log2. Quantile normalization was selected as normalization method based on this comparison. Data were imputed with mean imputation method be-

tween the nine technical and biological replicates, which means that the missing value on a certain variable is replaced by the mean of the available cases.

Cell cycle analysis

Sample collection and cell fixation method

A volume of 1.5 mL of cell suspension was harvested for each time point. These samples were diluted 1:10 in PBS to ensure a suitable cell concentration for the assay. Two mL of these dilutions were centrifuged and cells in the pellets were fixed with 10 mL of 100% EtOH before stored at -20°C for, at least, 24h.

Cell staining method

After fixation, cell suspensions were centrifuged for 5 min at 3500 x g (room temperature) and resuspended in 1 mL of PBS, washed once with PBS and sonicated for 3 minutes in an Ultrasonic Cleaner (JSP, US21, ultrasonic power 50W), in order to eliminate cell clumps and aggregates before staining.

In the staining process, 2 μ L of the Vibrant Dye Cycle Green (V35004, Thermo Fisher) (10 μ M final stain concentration) were added to each sample and incubated 30 min (37°C) for selective DNA labeling. After incubation, cells were washed and transferred to flow cytometry tubes for cell cycle analysis.

Data acquisition and processing

Flow Cytometry acquisition were performed with a BD FACS Canto II (BD Biosciences) where stained DNA were excited by a 488nm laser and emission was collected in a 530/30 nm PMT. Flow rate was low and linear amplification were established for the acquisition.

Data were analyzed using FlowJo v.10.6.1 (Becton Dickinson & Company BD). Analysis was performed using one of the univariate cell cycle methods provided by FlowJo, specifically the Watson pragmatic algorithm (Watson et al., 1987) to adjust the data to the model.

Analysis of photosynthetic activity

Sample collection

Fresh culture was harvested at the different specific times of the day. The samples were diluted 1:1 with growing medium and incubated at 20 °C in total darkness during 10 min.

Data acquisition

In order to analyze photosynthetic parameters, Pulse-Amplitude-Modulation PAM fluorometry measurements were performed using a Waltz DUAL-PAM-100. After darkness incubation, the non-actinic modulated light (450 nm, 2.8 $\mu\text{E m}^{-2} \text{s}^{-1}$) was turned on, in order to measure F_o (fluorescence basal level). Then, to determine F_M (the maximum fluorescence level), a saturating red light pulse of 655nm and 5000 $\mu\text{E m}^{-2} \text{s}^{-1}$ was applied to the sample during 400 ms. The F_v/F_M , that corresponds to the maximum potential quantum efficiency of Photosystem II when all reaction centers were open, was calculated as:

$$\frac{F_v}{F_M} = \frac{(F_M - F_o)}{F_M}$$

Analytical determinations

Sample collection

At each time point, 50 mL of fresh culture was harvested and centrifuged at 7000 x g 10 min. Then pellets were washed with 1% ammonium formate (p/v) to eliminate salts from the growing medium and lyophilized.

Starch Content

Cell disruption

Approximately 2-3 mg of lyophilized biomass were added to hermetic tubes containing 1 mL of glass beads (0.25–0.3 mm diameter) and 2 mL of chloroform:methanol (2:1). Three disrupting cycles (60 s agitation - 60 s incubation on ice) were applied using Mini-Bead-beater (BioSpec Products). Then cellular extracts were separated from the beads and saved in new tubes. Cellular extracts were centrifuged for 4 min at 13000 x g and the su-

pernament was discarded. The addition of chloroform:methanol (2:1) and centrifugation steps were repeated until the pellets were white in order to ensure the elimination of pigments and lipids that could disturb the determination process. Finally, pigment free pellets were dried.

Starch solubilization and digestion

The proposed protocol for plants in (Rufty & Huber, 1983) was adapted to *Ostreococcus tauri*.

Starch granules in dry pellets were alkaline solubilized with 1mL of 0.2 M KOH and heated at 100 °C. After 30 min, samples were gradually cooled and pH was adjusted to 5.0 adding 300 µL of 1 M acetic acid.

To starch digestion, 7.4 U of α-amylase were added and incubated 30 min at 37 °C, breaking down starch in small linear and branched oligosaccharides. After that, 5 U of amyloglucosidase were added and incubated 1-2 h at 55 °C releasing glucose residues. Finally, in order to stop enzymatic reaction, the samples were incubated at 100 °C 2 min and centrifuged at 13000 x g for 10 min discarding pellet. Enzymes were prepared in 0.1 M of sodium acetate pH 4.5.

Spectrophotometric quantification

The quantification of released glucose residues from starch was achieved following (Rufty & Huber, 1983) protocol. The method combined two enzymatic activities: hexokinase, that phosphorylated glucose residues, and glucose-6-phosphate dehydrogenase (G6PDH) that reduced NAD⁺ oxidizing the phosphorylated glucose. NADH generated could be measured at 340 nm and correlated to glucose concentration in a ratio 1:1 (Fig. 12).

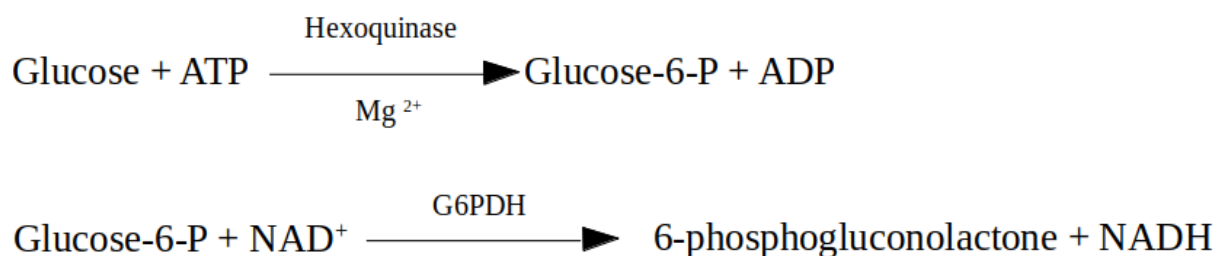


Figure 12: Enzymatic activities that link NADH production to glucose residues released from starch.

To achieve that measurement, quartz spectrophotometer cuvettes were used containing:

- 100 µL of the sample
- 500 µL of hexokinase buffer (100mM HEPES pH 7.7, 10 mM MgCl₂, 0.04% BSA p/v, 1mM DTT)
- 100 µL of ATP mix (containing 10mM ATP diluted in Hepes 100 mM ph 7.7)
- 100 µL of NAD+ mix (containing 4 mM NAD+ diluted in Hepes 100 mM ph 7.7)
- 2 µL of 2.5 U µL⁻¹ glucose-6-phosphate dehydrogenase
- 200 µL of destile water.

The absorbance of that mixture was measured at 340 nm followed by the addition of 5 µL of 1 U µL⁻¹ hexokinase enzyme and the incubation at 27 °C for 20 min. After that, a second measurement allowed to determine the amount of NADH produced during the reaction. NADH absorbance was related to the amount of glucose residues and consequently to the initial amount of starch in each the sample from calibration curves with commercial starch.

Carotenoid Content

Cell disruption

Four milligrams of lyophilized biomass were added to a hermetic tube containing 1 mL of glass beads (0.25–0.3 mm diameter) and 1 mL of pure acetone. Three disrupting cycles (60 s agitation – 60 s incubation on ice) were applied using Mini-Beadbeater (BioSpec Products).

Carotenoids extraction

Carotenoids extraction was achieved following the method proposed by (Del Campo et al., 2004). Darkness was maintain during the entire process to avoid pigments degradation.

After centrifugation for 4 min at 13000 x g, cellular extracts were collected and saved in new tubes. Again, 1 mL of pure acetone was added to wash glass beads, centrifuged and the supernatant was collected. This process was repeated until the supernatant turned col-

orless. Supernatants were pooled together in the same tube and acetone was evaporated using a stream of nitrogen gas. Finally, 350 µL of acetone were added for HPLC analysis.

Carotenoids determination and quantification

A Hitachi HPLC (Elite LaChrom), equipped with a photodiode-array detector (Hitachi L-2455) was used. Separation was performed on a Waters NovaPak C-18 (3.9×150 mm, 4 µm particle size, 60 Å pore size) column. Following the method proposed by (Böhme et al., 2002), the eluents used to create a gradient through the mobile phase were: eluent A (0.1 M ammonium acetate and 15:85 v/v H₂O-methanol) and eluent B (44:43:13 v/v methanol-acetonitrile-acetone). Temperature was maintained constant (20 °C) during the whole process and eluents flowed at 800 µL min⁻¹.

Different carotenoids were identified based on the retention times and absorption profiles of carotenoids patterns previously analyzed.

Rhythmic patterns analysis

Rhythmic patterns detection

The non parametric methods implemented in the R package RAIN (Thaben & Westermark, 2014) from Bioconductor were used to statistically identify rhythmic patterns in the different collected data. These rhythmic patterns were also independently identified using the co-sinusoidal parametrizations developed in the R package CircaCompare (Parsons et al., 2020).

Three complete diel cycles from both conditions (Long and short day) were used to detect rhythmic patterns in the different data of this study: expression levels of genes, abundance of proteins, maximum potential quantum efficiency of Photosystem II, cells in the different cell cycle phases and carotenoids and starch contents.

Rhythmic patterns with a single maximum point over a complete diel cycle were detected by setting the period parameter from RAIN to 24 hours. Similarly, more complex rhythmic patterns (the ones with two or even three maximum points per day) were detected changing the period parameter from RAIN to 12 and 8 hours respectively. A 0.05 p-value threshold was used in all scenarios.

In addition, the last two diel cycles and two consecutive days of continuous light or darkness were considered for the RAIN and CircaCompare analysis described above. In that way, RAIN and CircaCompare could statistically test if a similar pattern was maintained after changing the cycling light regime to free running conditions consisting in constant light or darkness preventing a bias towards any of the two conditions.

Rhythmic patterns comparison

The rhythmic patterns were fitted to a co-sinusoidal wave in order to be characterized and to enable comparison between them. The statistical significance of the differences in these waves parameters between different of rhythmic patterns was performed using the R package CircaCompare (Parsons et al., 2020) with a p-value threshold of 0.05. The significance of the global differences in the different rhythmic parameters was performed using the Mann-Whitney-Wilcoxon non parametric test implemented in the R function *wilcox.test*.

Data and code availability.

The RNA-seq transcriptomic data and the SWATH proteomic data generated and analysed in this thesis have been deposited in the Gene Expression Omnibus (NCBI) database and respectively and are freely available to the research community identified with the accession numbers GSE155535.

The codes for MARACAS (MicroAlgae RnA-seq and Chip-seq AnalysiS) pipeline and AlgaeFUN (microALGAE FUNctional enrichment tool) are freely available from the following Github repositories:

- <https://github.com/fran-romero-campero/MARACAS>
- <https://github.com/fran-romero-campero/AlgaeFUN>.

The actual R code developed in this thesis to perform all the analysis is available as an appendix generated from a Rmarkdown report, SANDAL (SeAsonal aNd diel cycles in Ostreoccocus), whose code is available from the Github repository:

<https://github.com/fran-romero-campero/SANDAL>

The code of the shiny app MINOTAUR, developed to facilitate the exploration of the results presented in this thesis is available from the Github repository:

<https://github.com/ABRomeroLosada/MINOTAUR>

Hypothesis and Objectives

Seasonal variations in diel cycles play a central role in the physiology and development of living organisms on Earth in general. Therefore, it is expected that seasonality highly affects microalgae physiology in particular. For example, seasonal oceanic massive microalgae blooms have been observed from outer space. Nevertheless, there is a lack of omics analysis in microalgae for these responses. Specifically, these studies were limited in *Ostreococcus tauri* to a single transcriptomic analysis based on microarrays and an independent single proteomic study. Both studies were performed over neutral day condition (12 h of light : 12 h of dark). Most of the *Ostreococcus* transcriptome has been reported as rhythmic, but *bona fide* circadian genes maintaining rhythmicity under different seasonal conditions and free-running conditions are not identified yet. Moreover, comparative analysis between rhythmic patterns at the transcriptomic, proteomic and physiological levels have not been performed and are expected to shed light on the responses of living organisms to seasonal variations in diel cycles.

The general objective in this thesis consist in carrying out a *multiomic characterization of the responses to photoperiodic seasonal variations in diel cycles in Ostreococcus tauri*. This is achieved pursuing the following specific objectives:

- 1 Development of software tools, computational pipelines and models to promote systems biology studies in microalgae in general and the exploration of the results in this thesis in particular.
- 2 Characterization of the transcriptomic responses to seasonal variations in diel cycles and free running conditions.
- 3 Characterization of the proteomic responses to seasonal variations in diel cycles and integration with the transcriptomic responses.
- 4 Characterization of responses of central physiological processes to seasonal variations in diel cycles and multiomics integration with transcriptomic and proteomic data.

Results

Chapter 1. ALGAEFUN with MARACAS, microALGAE FUNCtional enrichment tool for MicroAlgae RnA-seq and Chip-seq Analysis.

In order to characterize the molecular systems regulating microalgae physiology, high throughput sequencing technologies have been recently applied obtaining the genome sequences of a wide range of microalgae (Blanc et al., 2012; Bowler et al., 2008; Cheng et al., 2019; Corteggiani Carpinelli et al., 2014; Hori et al., 2014; Merchant et al., 2007; Moreau et al., 2012; Morimoto et al., 2020; Ottesen et al., 2013; Palenik et al., 2007; Polle et al., 2017; Roth et al., 2017; Worden et al., 2009). This has promoted the emergence of molecular systems biology studies and the use of different omics such as transcriptomics, based on RNA-seq data (Hoys et al., 2021; Serrano-Pérez et al., 2022), and cistromics, based on ChIP-seq data (Ngan et al., 2015; X. Zhao et al., 2021) in microalgae. Nonetheless, the progress of this type of studies on microalgae is limited by the lack of freely available and easy-to-use online tools to analyze and integrate omics data. Processing of the massive amount of high-throughput sequencing data and analysis of the resulting sets of genes and genomic loci obtained from molecular systems biology studies requires computational power, time, effort and expertise that some research groups on microalgae may lack. In addition, researchers must explore different data-bases separately, which makes the integration of the results and the generation of biological meaningful information difficult. Therefore, it is imperative the development of frameworks integrating microalgae genome sequences and annotations with tools for high-throughput sequencing data analysis and functional enrichment of gene and genomic loci sets.

In order to cover these needs for the microalgae research community and to promote studies in molecular systems biology we have developed the web portal ALGAEFUN with MARACAS (<https://greennetwork.us.es/AlgaeFUN/>) using the R package Shiny (<https://shiny.rstudio.com/>) other Bioconductor packages such as clusterProfiler (Wu et al., 2021; Yu et al., 2012) as well as annotation packages for microalgae developed in this thesis.

Our web portal consists of two different tools. First, MARACAS (MicroAlgae RnA-seq and Chip-seq Analysis) implements a fully automatic computational pipeline receiving as input

RNA-seq or ChIP-seq raw data from microalgae studies and producing set of differentially expressed genes or lists of genomic loci, respectively. These results can be further analyzed using our second tool, ALGAEFUN (microAlgae FUNctional enrichment tool). When receiving the results from an RNA-seq analysis, sets of genes are functionally annotated by performing Gene Ontology (GO) (Ashburner et al., 2000; Carbon et al., 2019) and metabolic pathways enrichment analysis (Kanehisa et al., 2016; Moriya et al., 2007; Ogata et al., 1999). When genomic loci from a ChIP-seq analysis are inputted, a set of potential target genes is generated together with the analysis of the distribution of the loci over gene features, as well as metagene plots representing the average mapping signal. This set of potential target genes can be further studied using the features for functional enrichment analysis in ALGAEFUN, as described above. The code for ALGAEFUN with MARACAS is publicly available at their respective GitHub repositories from the following links: <https://github.com/fran-romero-campero/ALGAEFUN> and <https://github.com/fran-romero-campero/MARACAS>.

Implementation

Integration of different microalgae databases.

ALGAEFUN with MARACAS supports 14 different microalgae species that cover an ample spectrum of their phylogeny (Fig.13): *Chlamydomonas reinhardtii* (Blaby et al., 2014; Merchant et al., 2007), *Volvox carteri* (Prochnik et al., 2010), *Chromochloris zofingiensis* (Roth et al., 2017), *Dunaliella salina* (Polle et al., 2017), *Haematococcus lacustris* (Morimoto et al., 2020) (Chlorophyceae), *Coccomyxa subellipsoidea* (Blanc et al., 2012) (Trebouxiophyceae), *Ostreococcus tauri* (Blanc-Mathieu et al., 2014; Palenik et al., 2007), *Bathycoccus prasinos* (Moreau et al., 2012), *Micromonas pusilla* CCMP1545 (Worden et al., 2009) (Mamiellophyceae), *Phaeodactylum tricornutum* (Bowler et al., 2008; M. Yang et al., 2018), *Nannochloropsis gaditana* (Corteggiani Carpinelli et al., 2014; Radakovits et al., 2012) (Stramenopiles), *Klebsormidium nitens* (Hori et al., 2014), *Mesotaenium endlicherianum* (Cheng et al., 2019) and *Spirogloea muscicola* (Cheng et al., 2019) (Charophyceae). Supported species include microalgae used in basic scientific research, as well as those used in biotechnology industry like *H. lacustris* (Hoys et al., 2021), *N. gaditana* (Ajjawi et al., 2017) or *P. tricornutum* (Cui et al., 2019; Pereira et al., 2021).

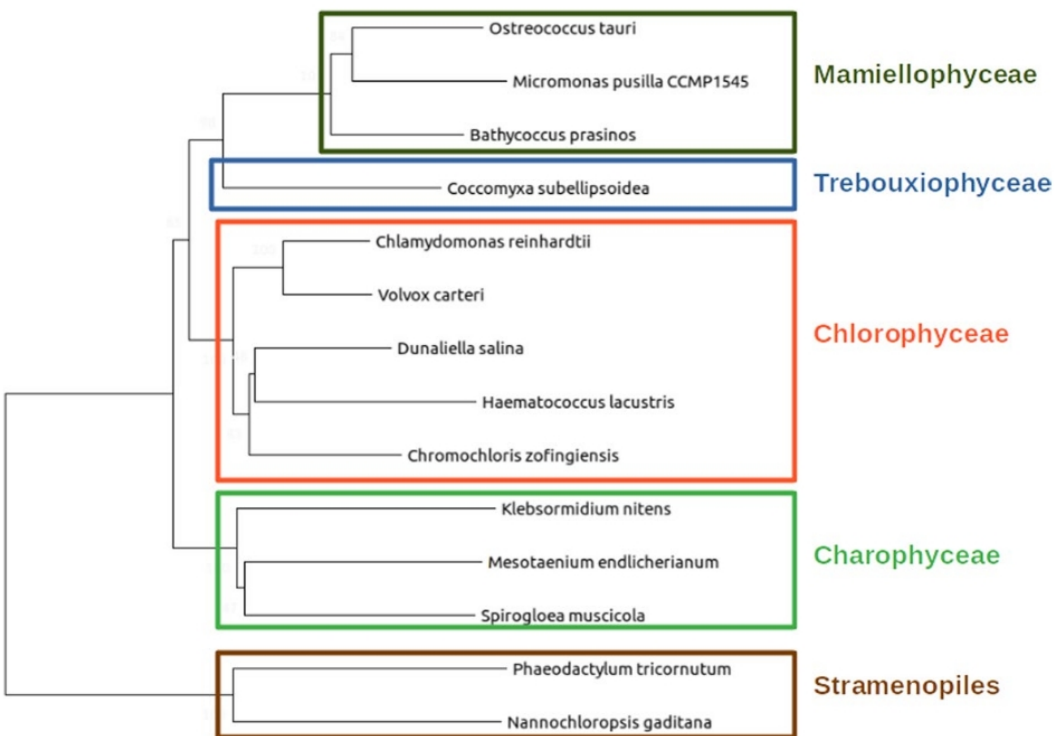


Figure 13: Phylogenetic relationship between the different microalgae species supported in AL-GAEFUN with MARACAS.

One of the goals of our tool is to integrate available genome sequences, functional annotations and genomic feature annotation files (Gene transfer files, GTF) for the already sequenced microalgae species in order to generate easily accessible resources. These data have been systematically collected from different freely available data bases, depending on the microalgae, Table 3. Specifically, for *N. gaditana* and *P. tricornutum*, we accessed Ensembl protist (Howe et al., 2021), a web based unicellular species genome browser storing gene annotation; *B. prasinus* is included in Orcae (Sterck et al., 2012) an online genome annotation resource built on the wiki philosophy; for *C. reinhardtii*, *V. carteri*, *C. zofingiensis*, *D. salina* and *C. subellipsoidea* the JointGenome Institute (JGI) / Phytozome (Goodstein et al., 2012), a web portal integrating omics for photosynthetic organisms was queried; for *M. endlicherianum* and *S. muscicola* a figshare associated to the corresponding publication was accessed; *M. pusilla*, *O. tauri*, *B. prasinus* and *K. nitens* genome sequence and annotation was downloaded from the JGI / PhycoCosm (Grigoriev et al., 2021), a comparative algal genomic resource; finally the genome of *H. lacustris* was available at NCBI genome database (https://www.ncbi.nlm.nih.gov/genome/67110?genome_assembly_id=839686).

Table 3: Resources used to collect genome sequences, functional and gene feature annotations for each supported microalgae.

Ensembl protists	PhycoCosm	Phytozome	Genomes NCBI datasets	Figshare associated to publication
<i>N. gaditana</i>	<i>B. prasinos</i>	<i>C. reinhardtii</i>	<i>H. lacustris</i>	<i>M. endlicherianum</i>
<i>P. tricornutum</i>	<i>K. nitens</i>	<i>V. carteri</i>		<i>S. muscicola</i>
	<i>M. pusilla</i>	<i>C. zofingiensis</i>		
	<i>O. tauri</i>	<i>D. salinas</i>		
		<i>C. subellipsoidea</i>		

Genome sequence and gene feature annotation files were downloaded in fasta and GTF format, respectively. When necessary, different chromosome and/or scaffold files were colligated programmatically to produce a single genome file. The GTF format in the gene feature annotation files consists of a data frame with nine columns. Each line corresponds to a specific gene feature. The first eight columns must contain information related to the gene feature (3' UTR, 5' UTR, gene, CDS or mRNA), chromosome start and end positions, the strand where it is positioned, and some other attributes in a well-defined format. The ninth column is not restricted to a specific format and can contain any type of information. Nonetheless, the mappers used in MARACAS assume that this last column follows the format taken by GTF files in the data-base Ensembl. In order to be able to use GTF files from other databases besides Ensembl, we developed an R script to translate any GTF file into the format followed by Ensembl and required by the read mapper HISAT2 (Kim et al., 2015).

Systematic functional annotation files consisting of Gene Ontology (GO) and KEGG (Kyoto Encyclopedia of Genes and Genome) Orthology (KO) terms were also downloaded for each microalga from the previously mentioned databases. Gene Ontology terms seek the development of a human-readable and machine-readable hierarchical vocabulary to relate genes with their molecular functions, biological processes in which they are involved and

the cellular components where they perform their function (Ashburner et al., 2000; Carbon et al., 2019). Complementary, KEGG Orthology terms associate genes to metabolic pathways and modules based on their orthologous relationships in sequenced genomes (Kanehisa et al., 2016; Moriya et al., 2007; Ogata et al., 1999). However, for microalgae species lacking these annotation systems, HMMER (biological sequence analysis using profile hidden Markov models) (Potter et al., 2018) was used to identify protein domains according to the PFAM (Protein Family) nomenclature (Mistry et al., 2021). PFAM terms were subsequently converted into GO terms using pfam2go (<http://current.geneontology.org/ontology/external2go/pfam2go>). KO terms were associated to genes applying KAAS (KEGG Automatic Annotation Server) (Moriya et al., 2007). Whenever possible, other systematic functional annotation format were also included: Protein Analysis Through Evolutionary Relationships (PANTHER) terms (Mi et al., 2021), that classifies, based of evolutionary families and subfamilies, gene products into classes capturing molecular function, biological process and metabolic pathways; Enzyme Commission numbers (EC numbers), that consists of a numerical classification identifier for enzymes, related to the biochemical reactions they perform; and Eukaryotic Orthologous Groups (KOG) terms, used to identify orthologue and parologue groups of proteins (Galperin et al., 2021).

Development of functional annotation and genomic packages.

In order to use all these annotation systems in ALGAEFUN two different types of R annotation packages were developed and were made freely available on our Github repository (<https://github.com/fran-romero-campero/AlgaeFUN/tree/master/packages>).

The systematic sources of functional annotation mentioned previously were gather together using the function makeOrgPackage from the Bioconductor R package AnnotationForge (Carlson & Pagès, 2019) which generated annotation packages for each microalga. These packages are instrumental when performing functional enrichment analysis over gene sets obtained from RNA-seq data analysis.

Gene featuring annotation of each microalgae from the previously downloaded and processed GTF files is stored in different packages applying the function makeTxDbFromGFF from the Bioconductor R package GenomicFeatures (Lawrence et al., 2013). These packages are central to carry out analysis over genomic loci obtained in ChIP-seq analysis.

Both functional annotation and gene feature packages of each microalga are freely available on our Github repository, in order to enable the research community in microalgae to use them and perform omics analysis independently from the tools available from ALGAE-FUN with MARACAS.

MARACAS implementation: high-throughput sequencing data processing.

The computational core of this tool consists of a parallel fully automatic computational pipeline or workflow synchronized through blackboards. This workflow is managed by the job scheduling system SLURM (Simple Linux Utility for Resource Management) and bash scripting. The inputs to our pipeline comprise the pre-computed index of the corresponding microalga reference genome, the previously processed gene feature annotation file in GTF format (both already included in MARACAS) and the raw sequencing data in fastq format from RNA-seq and ChIP-seq microalgae studies provided by the user. In turn, this workflow produces, as outputs, two lists of differentially expressed genes or DEGs (activated and repressed genes) when the fastq files correspond to a RNA-seq study; or a list of genomic loci or regions significantly occupied by the transcription factor or histone modification of interest in the case of a ChIP-seq study.

MARACAS requires the user to input specifications such as the microalga of interest, the names for control and experimental conditions, number of replicates and location of raw high-throughput sequencing files. In case of analyzing already published omic data, its accession number can be specified instead. Additionally, the user can set the statistical parameters to perform the corresponding analysis. Specifically, the fold-change and significance level cutoff thresholds for the identification of differentially expressed genes can be selected. In addition, user can choose as read mapper software either the short read mapper HISAT2 (Hierarchical Indexing for Spliced Alignment of Transcripts 2) or the pseudoalignment method implemented in kallisto. Whereas HISAT2 is an exact method requiring several hours for processing a typical sample (Kim et al., 2015; Pertea et al., 2016), kallisto produces near-optimal gene expression quantification in only a few minutes (Bray et al., 2016). Meanwhile, in the MARACAS ChIP-seq data analysis, pipeline is used the ultra-fast and memory-efficient short read mapper bowtie2 (Langmead & Salzberg, 2012). All this information is collected into a parameters file (Table 4 and Table 5), which is the main input received by the pipeline.

Table 4: Description of parameters file used as input in MARACAS for RNA-seq analyses.

Parameters file for RNA-seq analyses	
data_source	This parameter indicates the source of the data to be analyzed. It can take the value <i>FILES</i> when the fastq files are already located in a folder in the computer where MARACAS is installed or the value <i>DB</i> when the data has been already deposited in the GEO database.
cluster	Parameter specifying the execution mode. <i>SERVER</i> mode executes MARACAS with a sequential analysis of the different samples. Whereas <i>SLURM</i> mode executes MARACAS in a parallel manner, processing samples simultaneously in different computational nodes. In this last case, SLURM needs to be installed in user's computer cluster.
number_processors	Number of processors that can be used by MARACAS.
paired_end	It can take the values <i>FALSE</i> , when your data is single end, and <i>TRUE</i> , when your data is paired end.
working_directory	It indicates the location where the analysis folder will be generated.
microalgae	Name of the microalgae of interest.
read_mapper	This parameter specifies the software tool to perform read mapping. Two different options are provided: <i>HISAT2</i> and <i>Kallisto</i> .
main_folder	Name of the folder that will be created at the working directory to contain the outputs from the analysis.
number_of_samples	Total number of samples to be analyzed.
control_condition_name	Name of control condition.
experimental_condition_name	Name of experimental condition.
loc_sampleN	When <i>paired_end</i> : <i>FALSE</i> and <i>data_source</i> : <i>FILES</i> , this parameter indicates the path and file name of sampleN. N will take values from 1 to <i>number_of_samples</i> .
acc_sampleN	When <i>data_source</i> : <i>DB</i> , this parameter specifies accession number of fastq files in GEO.
loc_sample_leftN loc_sample_rightN	When <i>paired_end</i> : <i>TRUE</i> and <i>data_source</i> : <i>FILES</i> , this parameters indicates the path and file name of the fastq samples containing the left and right reads, respectively.
condition_sampleN	This parameters specifies which condition name of the ones chosen in <i>control_condition_name</i> or <i>experimental_condition_name</i> correspond to each sample.
fold_change q_value	These parameters specify the fold-change and q-value used to determine differential expressed genes in the experimental condition when compared to the control condition.

Table 5: Description of parameters file used as input in MARACAS for ChIP-seq analyses.

Parameters file for ChIP-seq analyses	
data_source	<i>FILES</i> or <i>DB</i> as it is explained in Table 4.
cluster	<i>SERVER</i> or <i>SLURM</i> as it is explained in Table 4.
number_processors	Number of processors that can be used by MARACAS.
paired_end	<i>FALSE</i> or <i>TRUE</i> as it is explained in Table 4.
working_directory	It indicates the location where the analysis folder will be generated.
microalgae	Name of the microalgae of interest.
main_folder	Name of the folder that will be created at the working directory to contain the outputs from the analysis.
number_of_replicates	Total number of samples to be analyzed.
included_control	It can receive <i>yes</i> if your experimental design includes a control condition such as input, mock or similar. Use <i>no</i> in negative cases.
mode	Use the values <i>transcription_factor</i> or <i>histone_modification</i> to specify if your ChIP-seq data was generated for a transcription factor or a histone modification study.
transcription_factor	When <i>mode: transcription_factor</i> this parameter specifies the name of the chosen transcription factor.
histone_modification	When <i>mode: histone_modification</i> this parameter specifies the name of the chosen histone modification.
loc_chip_replicate_N loc_control_replicate_N	When <i>paired_end: FALSE</i> and <i>data_source: FILES</i> , this parameter indicates the path and file name of ChIP sample and, in case of <i>included_control: yes</i> , the control sample. N will take values from 1 to <i>number_of_replicates</i> .
chip_replicate_N control_replicate_N	When <i>data_source: DB</i> , this parameter specifies accession number of ChIP sample in GEO. In case of <i>included_control: yes</i> , <i>control_replicate_N</i> will specify the one for control sample in GEO.
loc_chip_replicate_left_N loc_chip_replicate_right_N loc_control_replicate_left_N loc_control_replicate_right_N	When <i>paired_end: TRUE</i> and <i>data_source: FILES</i> , this parameter indicates the path and file name of the ChIP samples containing the left and right reads, respectively. If <i>included_control: yes</i> , they also indicate this information for control samples.

The first step in our workflow loads the parameters file and generates the working directory including one folder where the samples are downloaded or copied, another one where the results are generated and a third one, called “logs”. In this last folder, several text files are generated containing messages written by the different processes in the pipeline that are useful to keep track of the important events. More interestingly, a different type of text file, called blackboard, is created and the computational processes in our workflow are given read and write permissions for it. Files functioning as blackboards are used for indirect communication between the computational processes in the parallel pipeline in order to synchronize them. In the next step, the pipeline forks into two different modes to process either RNA-seq or ChIP-seq data.

The fork of our pipeline dedicated to RNA-seq analysis is represented in Fig. 14. Depending on the raw data source, the first step consists of either downloading and extracting the corresponding fastq files from a database or copying them to the specified working directory. Next, a quality control of these raw data is performed and short reads are mapped to the reference genome using HISAT2 or kallisto. When HISAT2 is used, this step generates BAM (Binary Alignment Maps) files that contain the mapped reads. The following steps take this mapping as input and perform transcripts assembly and expression quantification using STRINGTIE (Pertea et al., 2015, 2016). In this step, GTF files with the assembled transcripts and CTAB files (chemical table files) with the expression quantification values are generated for all samples. However, when kallisto is used, transcripts are mapped and quantified in the same step, so a TSV (tabular separated values) file containing the result of the quantification is generated (Bray et al., 2016). These processing steps are carried out in parallel, simultaneously for each sample, being synchronized using a blackboard file. These parallel processes write on the blackboard when a goal is reached (for example, BAM files are generated) in order to keep track of their progress. When all parallel processes reach their goals, the following sequential steps of the pipeline are executed. They consist of a differential expression analysis carried out using the Bioconductor R packages Ballgown (Frazee et al., 2015; Pertea et al., 2016) and Limma (Ritchie et al., 2015). Specifically, DEGs are selected using the statistics based on a moderated t-student. Finally, a differentially expression gene report is generated, containing text files with activated and repressed genes, principal component analysis visualization, and several informative graphs, such as scatter plots, volcano plots, box-plots and bar-plots.

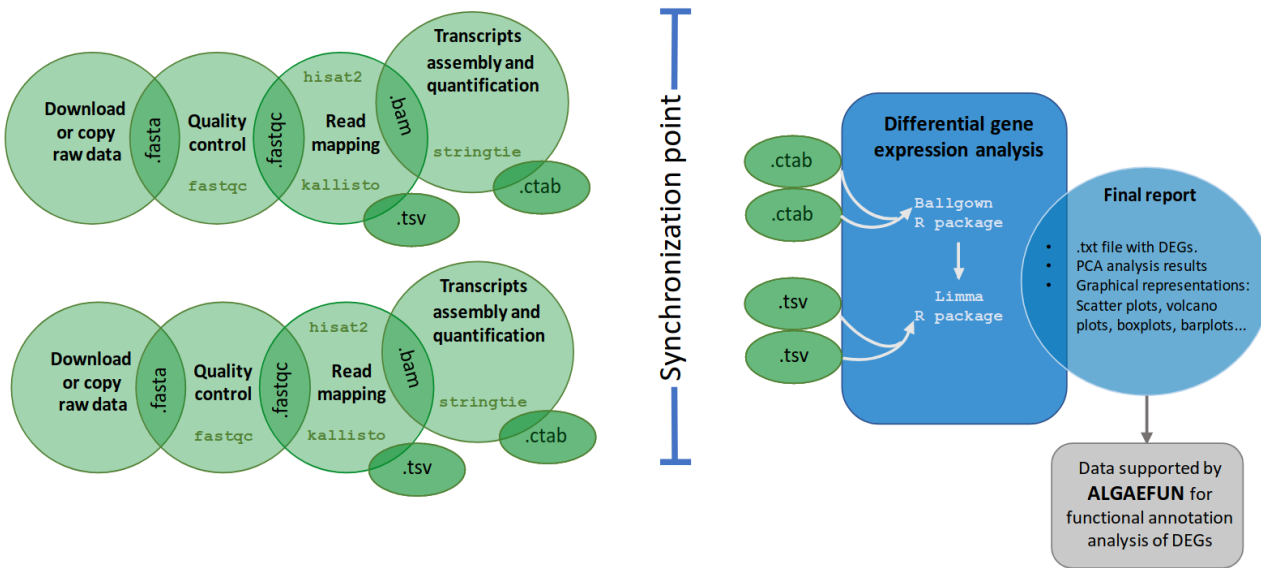


Figure 14: Workflow of the automatic pipeline for the analysis of RNA-seq data in MARACAS. The maracas-rna-seq pipeline receives as input a parameter file as described in Table 4. After data acquisition in fastq format, sequence quality analysis is performed using fastqc. Read mapping and gene expression quantification is then performed using HISAT2 and stringtie or kallisto depending on the user choice. A synchronization point ensuring the completion of all samples processing to quantify gene expression is necessary before identifying DEGs using the R packages ballgown and limma. Gene expression estimates measured as raw count, FPKM (Fragments per Kilobase of exon and Million of mapped reads) or TPM (Transcripts per Million) are stored in TSV files. Reports in html and pdf format are generated with details on sequence quality analysis, mapping process and normalization. Graphics for exploratory analysis such as principal components, box-plots, scatter-plots, volcano-plots and bar-plots of individual genes are also included. These reports include links to download gene expression estimates as well as lists of activated and repressed DEGs. The outputs of this pipeline are compatible with the input formats for ALGAEFUN in order to facilitate further functional enrichment analysis and visualization.

The second fork of our pipeline dedicated to ChIP-seq analysis (Fig. 15) shares with the above RNA-seq fork the first steps consisting of downloading or copying the fastq raw files for the ChIP samples (data corresponding to the chromatin immunoprecipitation condition) and control samples into the generated working directory and performing a quality control. Specifically, in this part of the workflow, short read mapping to the reference genome is executed using bowtie2 (Langmead & Salzberg, 2012) and the synchronization point requires that BAM files for every ChIP and control sample is generated. This synchronization point is also achieved using a blackboard. After synchronization, the last step takes as input all mappings in BAM format and performs peak calling using the software tool macs2

(Gaspar, 2018). This final step consists of the identification of genomic loci or regions significantly enriched with mapped reads, indicating the genomic occupation of the transcription factor or histone modification of interest. The output files of this pipeline consists of a BED (Browser Extensible Data) file, collecting the genomic loci or regions identified during the analysis, and a BW (BigWIG) file, containing the number of mapped reads or signal in each position of the genome.

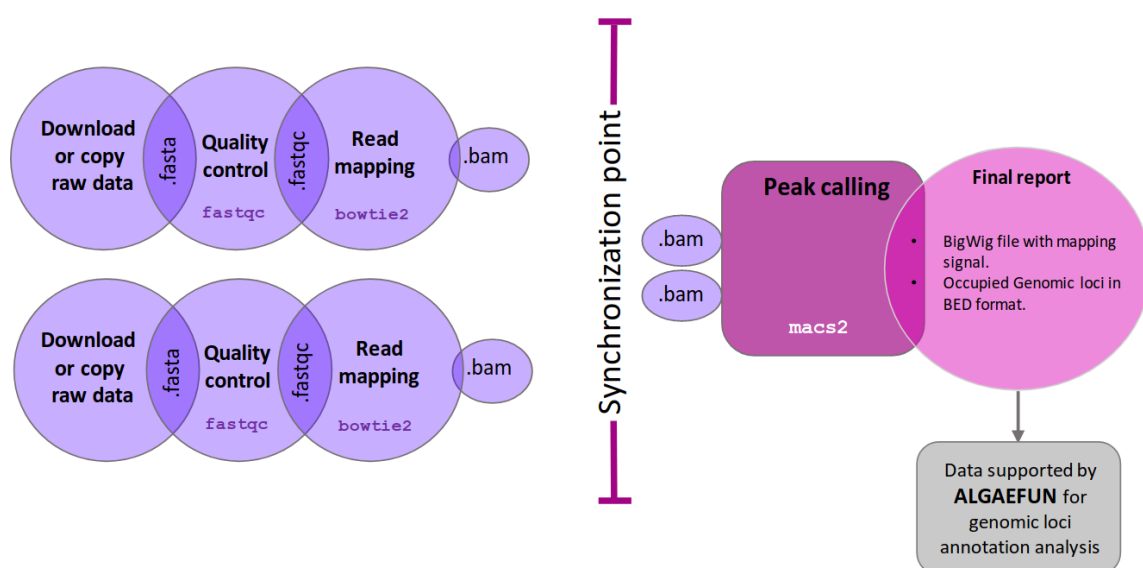


Figure 15: Workflow of the automatic pipeline for the analysis of ChIP-seq data in MARACAS. The maracas-chip-seq pipeline receives as input a parameter file as described in Table 5. After data acquisition in fastq format, sequence quality analysis is performed using fastqc. Read mapping to the reference genome is performed using bowtie2 and is stored in BAM format. A synchronization point ensuring the end of all replicates processing is necessary before carrying out peak calling with macs2. Reports in html and pdf format are generated with details on sequence quality analysis and mapping process. These reports include links to download the identified peaks in BED format and the genome wide mapping signal in bigwig format. These outputs are compatible with the input formats for ALGAEFUN in order to facilitate further annotation and visualization of the identified genomic loci significantly bound or occupied by the transcription factor or histone modification of interest.

ALGAEFUN implementation: functional annotation analysis.

The generated output from MARACAS, either sets of genes or genomic loci, can be functionally annotated using the next software tool in the portal, ALGAEFUN. Although this tool can also be used to functionally annotate genes sets or genomic loci generated independently from other tools.

The user interface of ALGAEFUN is shown in Fig. 16 and Fig. 17. Two different modes of operation, depending on the kind of input data to be analyzed, are implemented in ALGAEFUN.

The figure shows the ALGAEFUN web application interface. At the top is a navigation bar with a green cartoon alga icon. Below it is a main content area titled "ALGAEFUN with MARACAS" and "microALGAE FUNctional enrichment tool for MicroAlgae RnA-seq and Chip-seq Analysis". A detailed description of the tool's purpose and usage instructions follows. The interface is divided into four numbered sections:

- (1)** **Navigation bar:** A sidebar containing links to Home, Gene Set Functional Analysis (selected), Genomic Loci Functional Analysis, MARACAS, MicroAlgae RnA-seq and Chip-seq Analysis, Funtree, Phylogenomic Analysis of Genes in Viridiplantae, Tutorials, GitHub repository, and Citation and Contact.
- (2)** **Microalga selection dropdown:** A dropdown menu set to "Ostreococcus tauri".
- (3)** **Analysis parameters sidebar:** Includes:
 - "Choose your desirable analysis": Radio buttons for "GO terms enrichment" (selected), "KEGG pathways enrichment analysis", and "Both".
 - "Choose gene ontology": Radio buttons for "Biological process", "Cellular Component", and "Molecular Function".
 - "Which will be your chosen p-value?": Input field set to "0.05".
- (4)** **Main panel:** A large form for inputting genes and selecting background. It includes:
 - "Insert a set of genes" text input field.
 - "Example" and "Clear" buttons.
 - "Choose File with Gene Set To Upload" button, showing "No file selected".
 - A question "Would you rather use your own background set?" with radio buttons for "Yes" (selected) and "No".
 - A "Have fun!" button.

Figure 16: Microalgae Functional Annotation tool (ALGAEFUN) user interface for gene sets functional annotation. (1) Navigation bar for selecting the tool to use between the ones included in our web app; (2) Drop-down menu to select the microalga of interest; (3) Sidebar panel to select parameters for GO and/or KEGG pathway enrichment; (4) Main panel to input set of genes to analyze and select gene background.

In one of the modes, input data consists of sets of genes obtained, for instance, from an RNA-seq study. Here after selecting this analysis mode (Fig. 16-1), the user chooses the microalga of interest (Fig. 16-2) and the analysis to carry out, a GO term and/or KEGG pathway enrichment analysis at the selected significance level (Fig. 16-3). The set of genes to study can be inputted through a text box or uploaded from a file. Users can also choose between using their own background gene set or the entire microalga genome

(Fig. 16-4). In order to allow users to explore the functionalities of ALGAEFUN and to check the required gene id format, an example gene set for each microalga is included. This example can be accessed and inputted in the corresponding text box by clicking on the example button (Fig. 16-4). These examples were generated during the testing of MARACAS using previously published RNA-seq data sets and analysis and have in turn been used in the testing and validation of ALGAEFUN. The GO term and KEGG pathway enrichment analysis are carried out using the Bioconductor R package ClusterProfiler (Wu et al., 2021; Yu et al., 2012). This package implements statistical analysis and visualization of functional profiles for gene clusters or sets using the annotation packages developed for each microalga, integrating the systematic sources of functional annotation previously discussed. The outputs for the GO term and KEGG pathway enrichment analysis are presented in two different tabs. The first output in the GO enrichment tab consists of a table that summarizes the results from the GO enrichment analysis carried out over the input gene set. The user can find one row for each GO term and six columns that represent some relevant information about the enrichment. The first column shows the GO term identifier, followed by the second column where the user can find its description. Users can access more information about the GO term represented in a specific row by clicking on its identifier to be redirected to the web portal AmiGO (Carbon et al., 2009) where GO terms are described in detail. The third and fourth column represents the p-value and q-value, and the fifth one shows the enrichment value: $E = (m/n) / (M/N)$. The value "m" is the number of genes from the inputted gene set annotated with the corresponding GO term whereas "M" is the number of genes from the background annotated with the mentioned GO term. In a similar way, "n" is the number of genes with annotation from the gene set whereas "N" is the number of genes with annotation from the gene background. Finally, the last column shows the genes from the input set of genes annotated with each GO term. The user can click on them to get more information from the gene entry on the corresponding database from which the annotation was retrieved for the specific microalga under study. Furthermore, ALGAEFUN also generates several graphs that represent the GO term enrichment. Five visualization methods are used to illustrate the results:

- Acyclic graph: Each node stands for a GO term and their color indicates the level of significance (from grey, non-significant, to intense red, highly significant). An arrow

is drawn from GO term A to GO term B to represent that A is a more general GO term than B.

- Bar-plot: Each bar represents an enriched GO term whose length corresponds to the number of genes in the gene set annotated with the given GO term. Once again, the bar color shows the level of significance (from blue, less significant, to red, more significant).
- Dot-plot: Each dot represents an enriched GO term. The x-position of the dot corresponds to the ratio between the number of genes annotated with the corresponding GO term and the total number of annotated genes in the gene set. The dot color captures the level of significance (from blue, less significant, to red, more significant).
- Enrichment Map (emap-plot): Each node represents an enriched GO term and the size of each node is proportional to the number of genes annotated with the corresponding GO term in the inputted gene set. The node colors represent the level of significance (from less significant in blue to more significant in red). These nodes are connected by edges when the corresponding GO terms are semantically related.
- Gene-concept network (cnet-plot): The beige nodes represents GO terms and the grey nodes genes. An edge is drawn from a gene to a GO term when the gene is annotated with the corresponding GO term. The size of nodes representing GO terms is proportional to the number of genes annotated with the corresponding GO term.

The outputs shown on the KEGG pathway enrichment tab consist of:

- Table summarizing the result of the KEGG pathway enrichment analysis: Each row represents a pathway significantly enriched in the inputted gene set with respect to the selected gene background. The first column represents the KEGG pathway identifier and the user can click on it to read more information about the pathway. The second column contains its description. The third and fourth column present the p-value and q-value, and the fifth column displays the corresponding enrichment value E (m/n; M/N) as previously described. Finally, the last column shows the list of

genes from the inputted gene set assigned to the corresponding enriched pathway. KEGG pathways can be more informative than GO term since they are not general but specific to the corresponding organism of interest.

- KEGG pathway map: Users can choose a specific enriched pathway using a drop-down menu to generate the corresponding KEGG pathway map where genes from the inputted gene set are highlighted in red.
- Table summarizing the result of the KEGG module enrichment analysis: Each row represents a module significantly enriched in the gene set with respect to the selected gene universe or background. The columns in this table are organized in the same manner as the previously described. KEGG modules are distinct recurrent components of KEGG pathways in this respect they are more specific and can be more informative.

In the other mode, input data consists of genomic loci or regions obtained, for instance, from a Chip-seq study.

This analysis mode is selected from the side bar panel in Fig. 17-1. The microalga of interest can be selected using the drop-down menu from Fig. 17-2. Next, the distance around the transcriptional start site (TSS) that will be considered defining gene promoters must be specified. Gene features that will be considered when assigning gene targets to genomic loci or regions also need to be selected (Fig. 17-3). Genomic loci or regions to analyze can be inputted through a text box or uploading a file. Additionally, a BW file containing the number of mapped reads or signal in each position of the genome can be uploaded (Fig. 17-4). Similar to the previous mode, it is possible to explore the functionalities of this tool and check the required genomic loci or regions format, using an example included for each microalga by clicking on the example button (Fig. 17-4). These examples have been generated during the testing of MARACAS, using previously published ChIP-seq data sets and analysis, and have in turn been used in the testing and validation of ALGAEFUN. The functional annotation of the inputted genomic loci or regions is performed using the Bioconductor R packages ChIPseeker (Yu et al., 2015) and ChIPpeakAnno (L. J. Zhu, 2013). These package implements statistical analysis and visualization of genomic loci and re-

gions using the gene feature annotation packages generated for our tool. The outputs generated in this type of analysis consist of:

- A pie chart representing the distribution of the genomic loci or regions over the different type of gene features selected by the user such as the promoter, 3' UTR, 5'UTR, intron or exon.
- A table enumerating the target genes associated one generated when the data comes from a RNA-seq study. It represents each gene located in the enriched genomic loci and its different annotation terms. This set of genes can be downloaded and subsequently annotated functionally using ALGAEFUN.
- A visualization of the average level of signal around TSS and transcriptional end site (TES). For each individual gene, it generates a visualization of the signal and identification of DNA motifs recognized by transcription factors and regulators in microalgae.

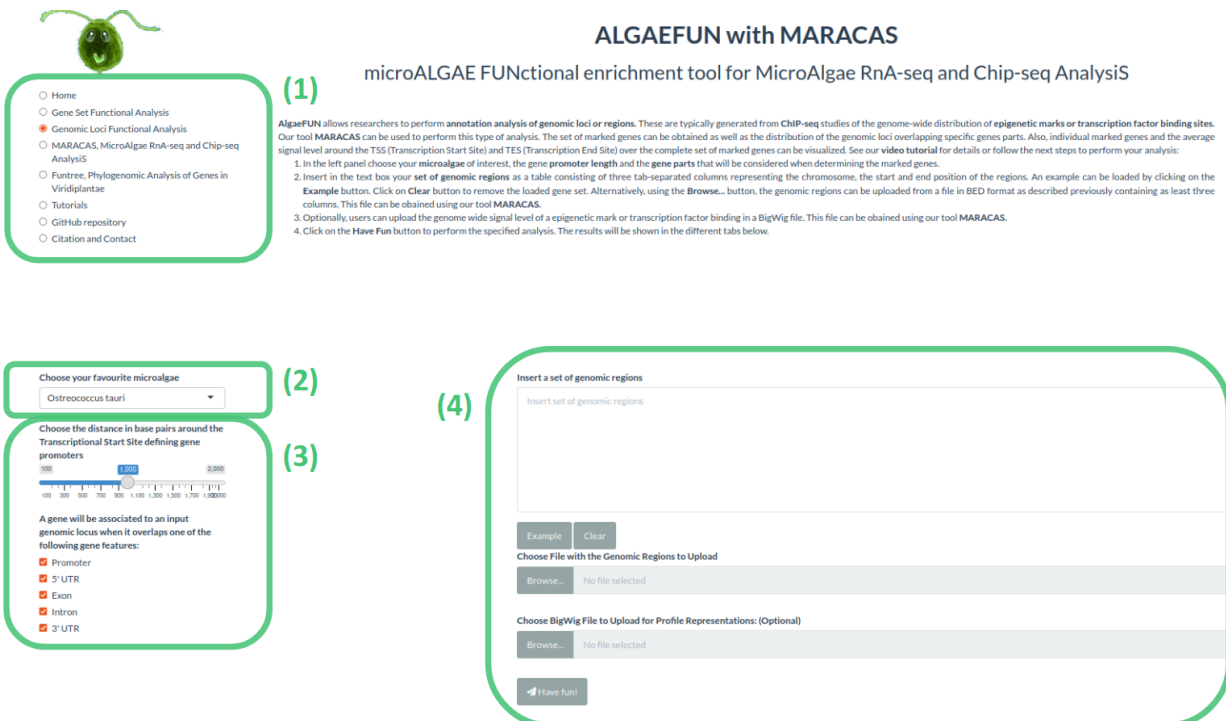


Figure 17: Microalgae Functional Annotation tool (ALGAEFUN) user interface for genomic loci annotation. (1) Navigation bar for selecting the tool to use; (2) Drop-down menu to select the microalga of interest; (3) Sidebar panel to select parameters for the identification of the promoter regions and the gene features or parts that will be considered to assign genes to genomic loci; (4) Main panel to input set of genomic loci and signal in bigWig format obtained from a ChIP-seq analysis.

Case study 1: from RNA-seq raw sequencing data to biological processes and pathways.

This case study is based on RNA-seq data generated in this thesis and illustrates the generation of relevant information suitable for publication. It consists of an RNA-seq study carried out using *Haematococcus*, a microalga of industrial interest for the bio-production of astaxanthin (Hoys et al., 2021). The analysis has been performed for vegetative *Haematococcus pluvialis* cells, grown both under N sufficiency and under moderate N limitation in order to unveil the transcriptomic program enhancing astaxanthin biosynthesis under N deprivation. This illustrates the type of information that ALGAEFUN with MARACAS is able to reveal from raw sequencing data.

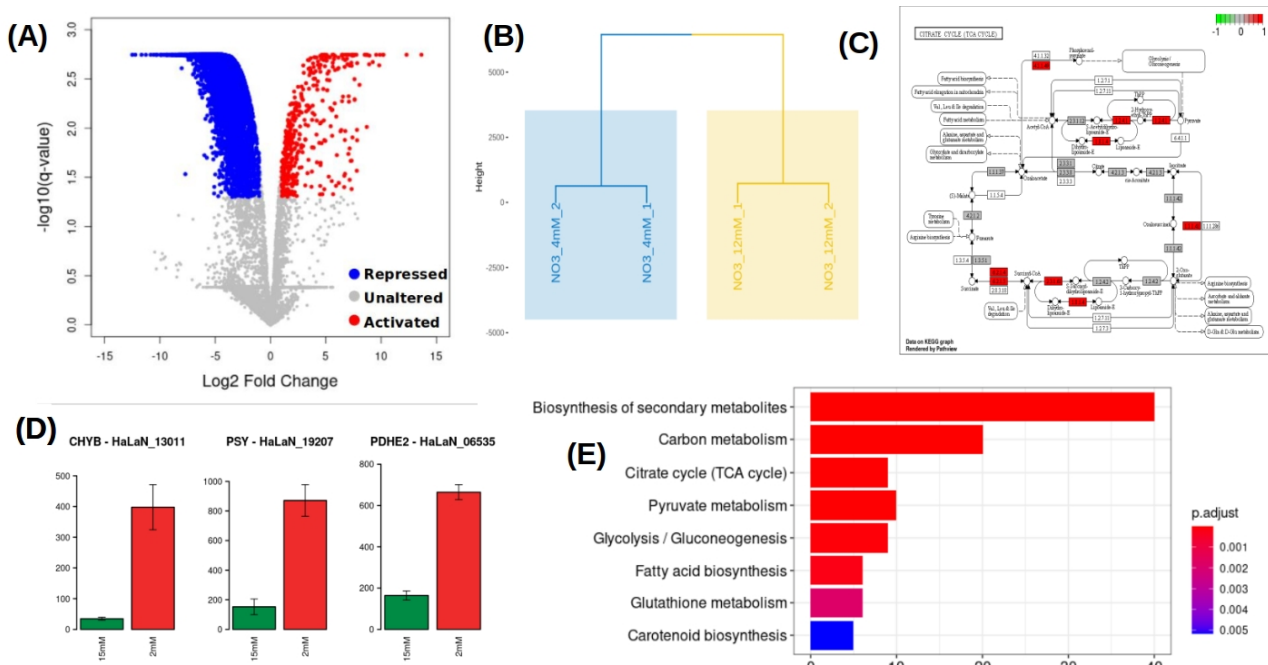


Figure 18: Results obtained from MARACAS final report and from ALGAEFUN analysis. (1) Volcano-plot generated by MARACAS showing the global effect over the transcriptome as well as the activated and repressed genes detected (in red and blue color, respectively); (2) Hierarchical clustering combined with PCA generated by MARACAS; (3) KEGG representation of one of the enriched pathways generated by ALGAEFUN, genes present in the list used as input are colored in red color; (4) Bar-plots representing individual gene expression levels of key enzymes, figure generated by MARACAS. Expression level of the selected gene under N sufficiency is represented in green color. Red color is used to represent moderate N deprivation condition; (5) Vertical bar-plot representing the enriched biological process in the set of genes used as input, figure generated by ALGAEFUN. Gradient from red to blue color is used to represent p-value.

The high-throughput sequencing raw data in fastq format was processed using MARACAS in order to obtain the set of differentially expressed genes using a criterion based on a fold-change value of 2 and a q-value of 0.05. The report produced by MARACAS confirmed that all samples are of high quality and notified no problem during read mapping to the reference genome with mapping rates greater than 86%. Scatter plots comparing gene expression between samples were also produced in the MARACAS report. High Pearson correlations greater than 98% were identified between replicates of the same condition. Accordingly, automatically hierarchical clustering combined with Principal Components Analysis (PCA) that leads to the identification of more stable clusters, due to the noise reduction achieved with PCA, was performed by MARACAS (Fig. 18-B). It identified two clearly separated clusters constituted by the control (N sufficiency) and experimental condition samples (moderate N deprivation). Volcano plots comparing moderate N limitation with N sufficiency transcriptomes were used in the report to represent the repressed genes and activated genes. Moderate N limitation has shown a strong repressing effect over the transcriptome with respect to N sufficient condition, identifying 414 activated and 5348 repressed genes (Fig. 18-A). These lists of genes can be then inputted into ALGAEFUN to determine significantly over-represented biological processes or pathways affected in the studied experimental conditions.

As described previously, ALGAEFUN can perform two different types of functional enrichment analysis when a set of genes from an RNA-seq analysis is used as input: GO terms and KEGG pathways enrichment. The GO terms analysis can identify, for example, specific biological processes enriched in the set of genes. Bar-plots are one of the available graphical representations of the GO enrichment results in ALGAEFUN (Figure 18-E), presenting the biological processes enriched in the activated set of genes obtained from the *Haematococcus* RNA-seq study under moderate N limitation experiment. Reduced availability of nitrogen activates processes like biosynthesis of secondary metabolites, TCA cycle or pyruvate metabolism at a transcriptomic level. GO term analysis provide a general overview of the functional annotation of gene sets since they constitute universal functional terms not specific to a particular organisms. Complementary, KEGG pathway enrichment is specific to the corresponding organism and can be more informative in some cases. It allows to identify the transcriptomic activated enzymes in enriched pathways (Fig. 18-C).

The genes involved in these processes can be further studied individually and their expression level in both conditions can be compared (Fig. 18-D).

ALGAEFUN with MARACAS analysis described differential expression of hundreds of genes affecting key pathways converging into astaxanthin biosynthesis and storage. The affected pathways were further studied at metabolic level and a massive cell reprogramming was verified for the cells growing under moderate N limitation. Furthermore, a major advance was made by discerning the underlying control mechanisms by finding differentially activated enzymes in the astaxanthin biosynthesis pathway. Moreover, the identification of significant DNA sequences in the promoters of these key enzymes was carried out and, for the first time, the family of transcription factors bHLH, was proposed as candidates for transcriptional regulators of these key enzymes in astaxanthin biosynthesis (Hoys et al., 2021).

Case study 2: From ChIP-seq raw sequencing data to marked genes.

As mentioned before, the development of ALGAEFUN with MARACAS has motivated our lab to generate transcriptomic as well as cistromic and epigenomic data. Although we have our own ChIP-seq data obtained during the study of epigenetic marks in *Ostreococcus tauri*, here we show, as an example of how the ALGAEFUN with MARACAS tool works, the re-analysis of raw data from a previously published epigenomic study in *Chlamydomonas*.

Histone modifications play a central role in gene expression control. The genome-wide distribution of the mark H3K4me3 associated to gene activation has been determined in *Chlamydomonas* (Ngan et al., 2015). After Chip-seq raw data was re-analyzed using MARACAS, as previously described, the 12,814 genomic loci identified as significantly occupied by H3K4me3 in the *Chlamydomonas* genome under standard growth conditions and the corresponding genome wide mapping signal file in BigWig format were uploaded in ALGAEFUN. The region of two kilobases around the TSS is considered as gene promoter and all the gene features are selected to determine the H3K4me3 marked genes. The outputs are presented in the graphical interface in different tabs. A downloadable table with the marked genes and their available annotation is generated. This gene list can, in turn, be analysed by ALGAEFUN to perform a GO term and/or pathways enrichment analysis. A total of 11,558 H3K4me3 marked genes are identified. Graphs representing the dis-

tribution of the genomic loci overlapping different gene features (Fig. 19-A) and the distribution of upstream and downstream signal around TSS and TES are also represented. In agreement with the previously published results, the 90.75% of the genomic loci occupied by H3K4me3 are located at gene promoters in *Chlamydomonas*.

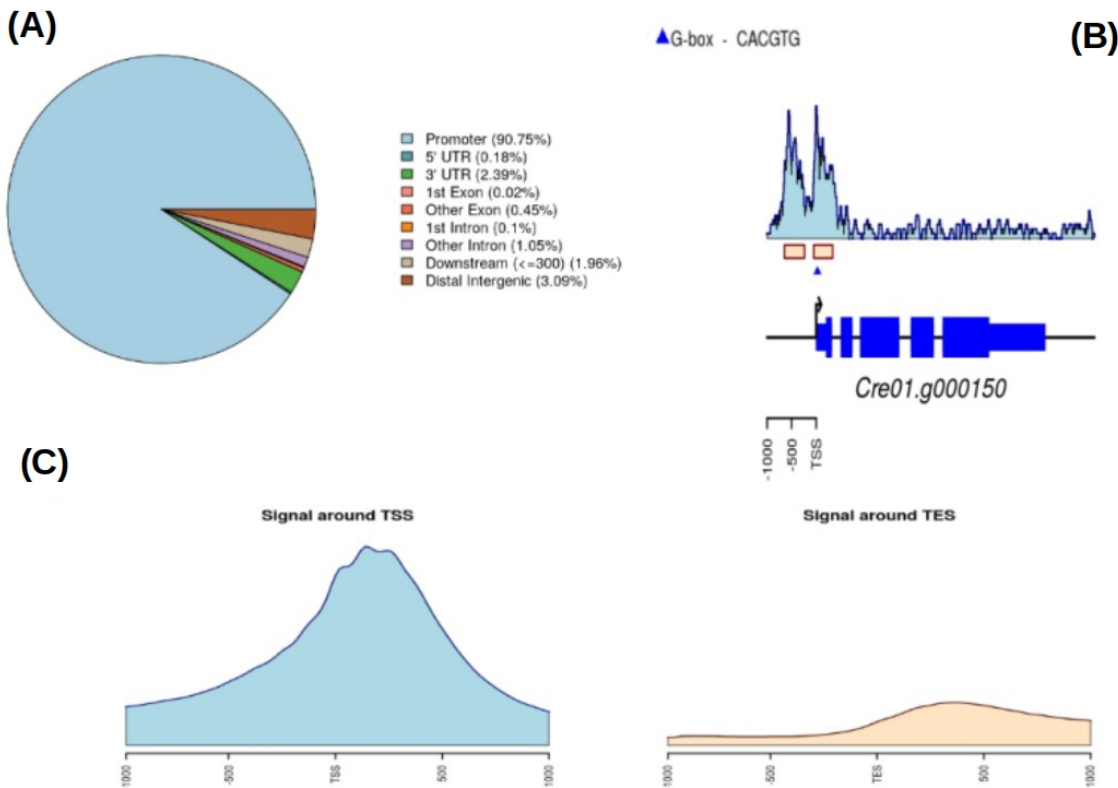


Figure 19: Summary of the outputs generated by ALGAEFUN when a genomic loci list is used as input. (A) Pie chart representing the distribution of peaks or genomic loci over the different type of gene features such as the promoter, 3' UTR, 5' UTR, intron or exon; (B) Visualization of the signal and identification of DNA motifs recognized by transcription factors and regulators in photosynthetic organisms for an individual gene; (C) Visualization of the average level of signal around Transcriptional Start Site (TSS) and Transcriptional End Site (TES) across all

As in this case study, when a BigWig file with the genome wide mapping signal is provided, specific marked genes can be selected to visualize the signal profile over their gene bodies and promoters. A gene example presenting two H3K4me3 peaks on its promoter is depicted to illustrate this functionality (Fig. 19-B). Moreover, DNA motifs recognized by specific transcription factors and regulators in photosynthetic organisms can be identified in the promoter of the selected gene. Finally, a visualization of the average level of signal around Transcriptional Start Site (TSS) and Transcriptional End Site (TES) across all

marked genes is generated (Fig. 19-C). For the case of H3K4me3 in *Chlamydomonas* further evidence is obtained, showing that this epigenetic mark specifically and exclusively locates at the TSS of marked genes and not at the TES.

Contribution of ALGAEFUN with MARACAS to the field.

ALGAEFUN with MARACAS constitutes one of the first steps that has been taken for the development of tools that would enable the microalgae research community to exploit high throughput next generation sequencing data by applying systems biology techniques. The first difference between ALGAEFUN with MARACAS with respect to already existing tools consists in the wide range of supported microalgae species (Fig. 13). For the model microalgae *Chlamydomonas reinhardtii*, researchers can find several online tools to functionally annotate set of genes, such as Algal Functional Annotation Tool (López et al., 2011) and ChlamyNET (Romero-Campero et al., 2016). Only the online tool AgriGO (Tian et al., 2017) offers the possibility of analysing a restrictive number of different microalgae species beyond *Chlamydomonas*. The second biggest difference between ALGAEFUN and other tools is the annotation systems they use. Most available functional enrichment tools can only perform functional annotation of gene sets based exclusively on GO enrichment analysis.

Table 6: Comparison between ALGAEFUN with MARACAS and other functional enrichment analysis tools

	Algal functional annotation tool	AgriGo	ChlamyNET	ALGAEFUN with MARACAS
Gene sets as input	YES	YES	YES	YES
Genomic loci as input	NO	NO	NO	YES
GO enrichment	YES	YES	YES	YES
KEGG pathways enrichment	YES	NO	NO	YES
Several microalgae	NO	YES	NO	YES
Statistical test	Hypergeometric tests	Fisher's exact test	Fisher's exact test	Hypergeometric tests

The identification of significantly enriched KEGG pathways in the inputted sets of genes is only supported by ALGAEFUN and Algal Functional Annotation Tool. A fundamental difference between ALGAEFUN and other tools consists of the statistical tests. Whereas AgriGO and ChlamyNET are based on Fisher's exact test, ALGAEFUN and Algal Func-

tional Annotation Tool compute statistical significance according to Hypergeometric tests. It has been shown that, in general, the hypergeometric test has more statistical power than Fisher's exact and χ^2 (Masseroli et al., 2004). Moreover, none of these tools can be used as a complete and integrated tool to process high-throughput sequencing raw data from RNA-seq or ChIP-seq experiments, or functionally annotate genomic loci obtained from a ChIP-seq analysis. In this respect, ALGAEFUN with MARACAS improves and implements several novel functionalities of similar already existing software tools (Table 6).

ALGAEFUN with MARACAS is a constantly growing tool that will include new microalgae whenever their sequenced genomes are available. Also it has settle the bases to build numerous tools by other members of our laboratory aiming at generating an enabling technology for the microalgae research community doing systems biology studies.

Chapter 2: Transcriptomic analysis of diel and seasonal cycles in *Ostreococcus tauri*

High-throughput transcriptome sequencing produced approximately 10 million short reads per sample (Appendix 1). This allowed us to accurately estimate gene expression levels measured as FPKM (Fragments Per Kilobase of exon per Million reads mapped) in the transcriptomes corresponding to each sample of the time series. Indeed, out of the 7668 genes currently annotated in the *Ostreococcus tauri* genome (Blanc-Mathieu et al., 2014; Palenik et al., 2007), only 3 genes were never expressed and 260 genes never exceeded an expression level of 10 FPKM. This shows that practically the entire *Ostreococcus tauri* genome is expressed under seasonal and diel cycles. A hierarchical clustering analysis performed over the 36 transcriptomes corresponding to the time points taken during three days under light/dark cycles showed homogeneity over the samples taken. The transcriptomes corresponding to the same time points during the three different days clustered together (Fig. 20-A). A cyclic circular organization of the transcriptomes was revealed over diel cycles constituted by three distinct clusters corresponding to midday (LD ZT4, SD ZT4 and LD ZT8), dusk (SD ZT8, LD ZT16 and LD ZT12) and night/dawn constituted by LD ZT0 and LD ZT20 on one hand and SD ZT12, SD ZT16, SD ZT20 and ZT0 on the other hand (Fig. 20-A). The transcriptomes at time points in the LD and SD nights constitute two distinct groups suggesting noticeable differences in the transcriptomic responses during the night under LD and SD conditions. It is also noteworthy the higher similarity between the dusk and night/dawn transcriptomes when compare to the midday one (Fig. 20-A).

In order to obtain a deeper understanding of the underlying structure in these data a principal components analysis was performed over the LD (Fig. 20-B) and SD (Fig. 20-C) transcriptomes. Under LD condition, the transcriptomes corresponding to the same time point in the three different days tightly cluster together, constituting a circular structure. Nonetheless, under SD condition, more variability is observed and transcriptomes form a structure resembling an ellipse. This could indicate that whereas in LD condition gene expression is globally cycling precisely with a similar period, a more complex behavior is expected under SD condition.

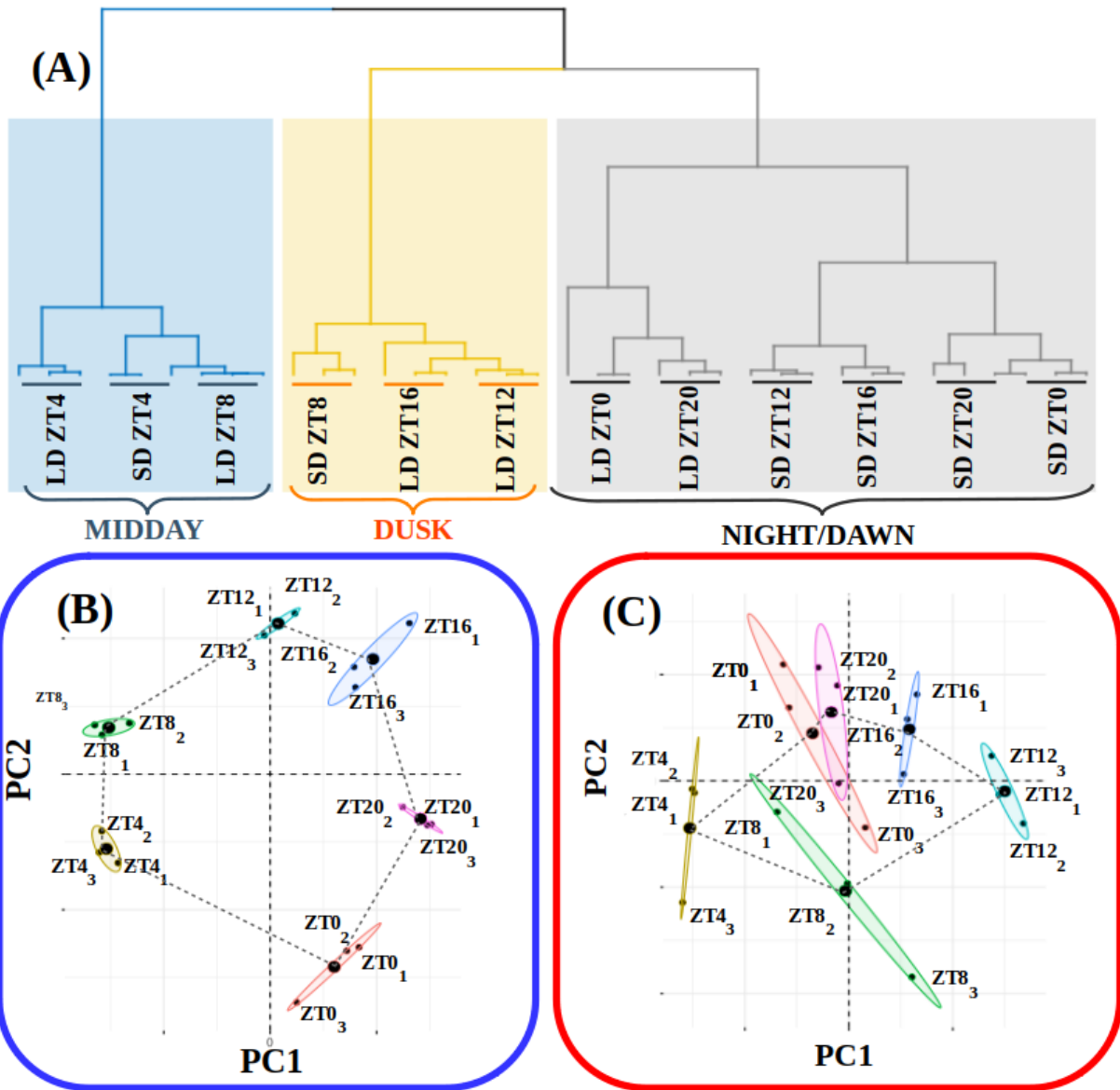


Figure 20: RNA reliability analysis. (A) Hierarchical clustering of the RNA-seq data corresponding to the 36 time points collected under alternating dark/light cycles simulating long and short day conditions. Three distinct clusters are observed corresponding to midday (blue rectangle), dusk (yellow rectangle) and night/dawn (grey rectangle); (B) Principal Component Analysis of the time point global transcriptomes under long day condition. Small dots correspond to the 2D projection of each time point global transcriptome. Big dots correspond to the average of the three replicates 2D projections for each time point. Ellipses mark the 95% confidence regions corresponding to each time point global transcriptome; (C) Principal Component Analysis of the time point global transcriptomes under short day condition. Points and ellipses are used as described before.

In addition, it is remarkable the high similarity between the transcriptomes corresponding to ZT0 and ZT20 under SD condition that is not that obvious under LD condition. This would suggest that the transcriptomic response at the end of a SD night is already prepar-

ing all molecular systems for the incoming light availability at dawn, whereas this anticipation is not so evidently observed under LD condition. In overall, these results support that the experimental design grants a high level of synchronization in the data, allowing to proceed to the identification and comparison of genes exhibiting rhythmic expression patterns under LD and SD conditions.

Transcriptomic characterization of diel expression profiles

Most genes in Ostreococcus tauri present diel expression profiles under both photoperiods

Applying bioconductor R package RAIN (Rhythmicity Analysis Incorporating Non-parametric Methods) (Thaben & Westermark, 2014), genes exhibiting diel (rhythmic profile with a 24 h period) expression patterns under both seasonal conditions have been identified. Specifically, more than 6000 genes comprising approximately 80% of the entire *Ostreococcus* genome present diel periodic rhythmic expression patterns. Seasonal variations in photoperiod did not affect transcriptome rhythmicity, as the sets of rhythmic genes under LD and SD entrainment were almost coincident (Fig. 21-A). This result is in agreement with previous studies in *Ostreococcus tauri* (Monnier et al., 2010) under neutral day photoperiod (12h of light and 12 h or darkness) and other chlorophyte microalgae such as *Chlamydomonas reinhardtii* (Zones et al., 2015). These results indicate that transcriptome rhythmicity in chlorophyte phytoplankton is much higher than the ones found in other organisms such as *Arabidopsis thaliana* 30-50% (Bläsing et al., 2005), *Solanum tuberosum* 18-45% (Hoopes et al., 2022), *Drosophila melanogaster* 24% (Ma et al., 2021) or *Mus musculus* 3-10% (Miller et al., 2007).

The 20% of the genome of *Ostreococcus* that is apparently identified as non-rhythmic, present three time lower expression levels than rhythmic genes. This difference was significant according to a p-value of 1.45×10^{-4} computed using Mann-Whitney-Wilcoxon test (Fig. 21-B). Since the rhythmicity analysis method used requires high levels of expression to perform optimally (Laloum & Robinson-Rechavi, 2020), it is possible part of these 20% of the genome is also rhythmic. In addition, some of these non-rhythmic genes are associated with stress responses (Appendix 2), so they could potentially become rhythmic once the stress signals are present and their expression level is increased, possibly resulting in a fully rhythmic transcriptome.

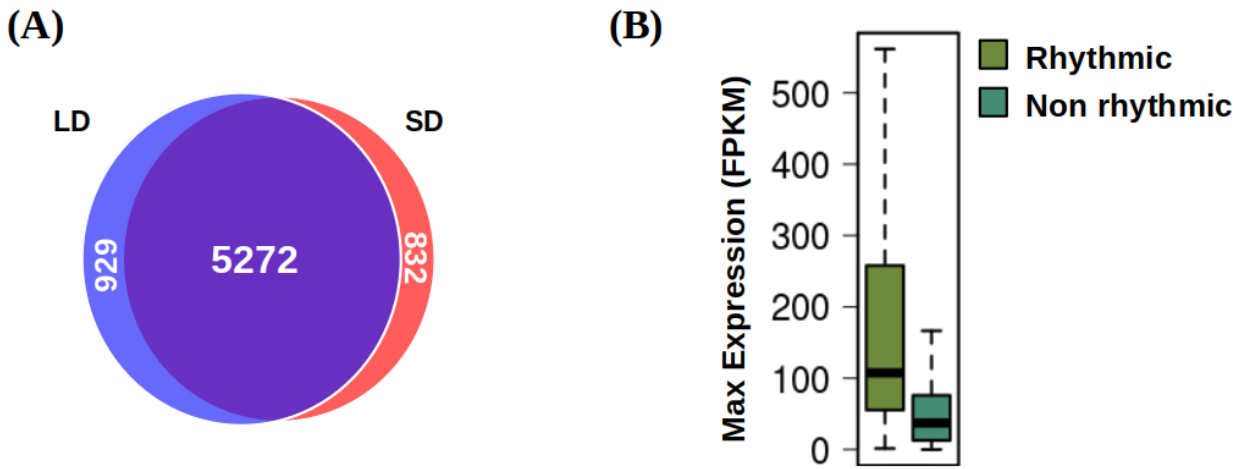


Figure 21: Diel rhythmic expression patterns detected in the transcriptome of *Ostreococcus tauri* under both photoperiods. (A) Venn diagram comparing rhythmic genes under LD condition (light blue circle) and SD condition (light red circle); (B) Boxplot representing the maximum expression level of rhythmic genes (light green) and non-rhythmic genes (dark green). Gene expression levels are measured as FPKM (Fragments Per Kilobase of transcript per Million fragments mapped).

Under free running conditions rhythmicity is maintained in different proportions depending on the photoperiod of entrainment

As it was described previously in the introduction, *bona fide* circadian processes are self-sustained and maintain their rhythmicity even when their specific zeitgeber, or synchronizing environmental signal, becomes constant. Following this definition, *bona fide* circadian genes can be identified and distinguished from light or dark responding ones from data generated under free-running conditions consisting in constant light (LL) and/or constant dark (DD). Specifically, approximately 21% of the transcriptome (1470 and 1567 genes in LD and SD, respectively) was completely reliant on light/dark cycles to maintain rhythmicity since these genes lost their rhythms under both LL and DD, independently from the photoperiod of entrainment (Table 7, Appendix 3 and Appendix 4).

In contrast, the transcriptome proportion maintaining its oscillations exclusively under LL or DD was found to be dependent on the previous photoperiod of entrainment. Whereas 1160 genes (15% of the entire genome) with a previous LD entrainment maintained their rhythmicity only under constant light (LL) condition (Fig. 22-A, Table 7, Appendix 5), only 495 (6,4% of the entire genome) were rhythmic under LL after SD entrainment (Fig. 22-B, Ta-

ble 7, Appendix 6). The detrimental effect of DD over transcriptome rhythmicity was smaller than LL, with almost 22% (1667 genes) maintaining oscillations after LD entrainment (Fig. 22-A, Table 7, Appendix 7) and 39% (2975 genes) after SD entrainment (Fig. 22-B, Table 7, Appendix 8). This results suggest that dark is the main zeitgeber for the rhythmic expression of a substantial number of genes. Specially evident for rhythmic gene expression under SD condition which was found to be very dependent on the presence of a dark period.

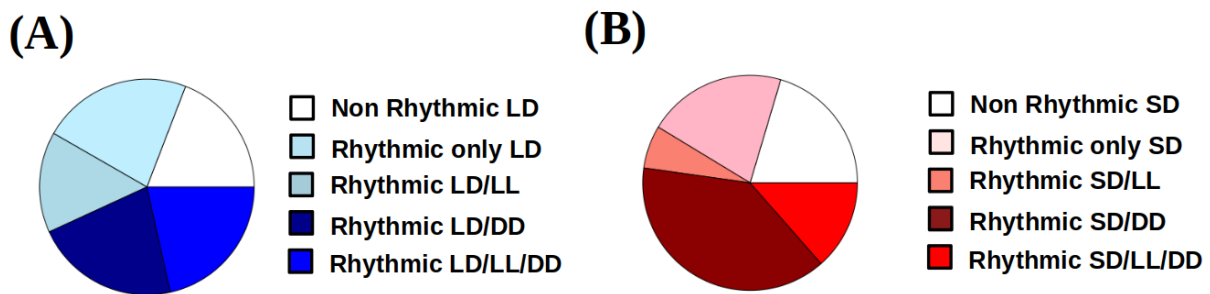


Figure 22: Rhythmicity maintenance under free-running conditions: (A) Pie plot representing with blue colors different rhythmic gene sets under LD condition. From bottom to top: circadian genes exhibiting rhythmicity under LD, under constant light (LL) and constant dark (DD); genes maintaining their rhythmicity only under LD and DD; genes maintaining their rhythmicity only under LD and LL; genes maintaining their rhythmicity only LD and non-rhythmic genes; (B) Pie plot representing with red colors different rhythmic gene sets under SD condition. From bottom to top: circadian genes exhibiting rhythmicity under SD, under constant light (LL) and constant dark (DD); genes maintaining their rhythmicity only under SD and DD;genes maintaining their rhythmicity only under SD and LL; genes maintaining their rhythmicity only under SD and non-rhythmic genes. The different sets of genes and their annotation can be found in Appendix 2-10.

Table 7: Number of genes maintaining their rhythmic expression profiles depending on the photoperiod of entrainment and free-running conditions applied. The different sets of genes and their annotation can be found in Appendix 2-10.

	LD	SD
Non-rhythmic genes	1470	1567
Genes that become non-rhythmic under free-running conditions	1737	1609
Genes that only maintain their rhythmicity under LL	1160	495
Genes that only maintain their rhythmicity under DD	1667	2975
Genes that maintain their rhythmicity under LL and DD	1650	1037

Regulatory mechanisms are often composed of large networks influenced by a wide range of inputs. Circadian clocks are strongly influenced by external environmental signals but there exists a complex interplay between the clock and cell physiology as well (Mazzoccoli et al., 2020; Morris et al., 2020). In line with that observation, genes maintaining their rhythmic expression profiles only under LL or DD could be regulated by the circadian clock, but also influenced by other regulatory mechanisms.

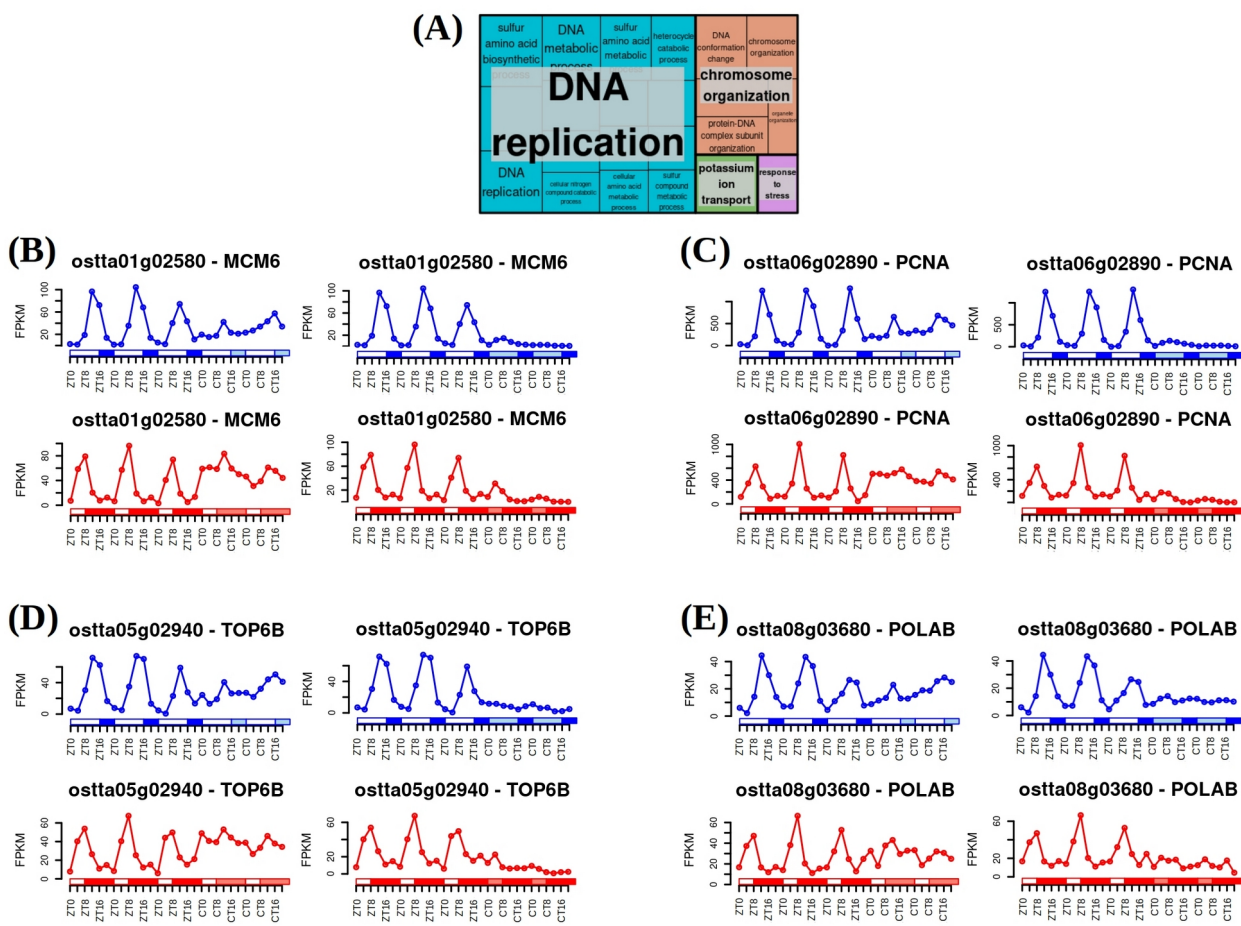


Figure 23: Biological processes significantly enriched in the genes exhibiting rhythmicity under alternating light/dark cycles and constant light. (A) Treemap summarizing the significantly enriched biological processes. Semantically similar biological processes are grouped into the same colored rectangle. The most representative biological process is shown for each rectangle; (B), (C), (D) and (E) Gene expression profiles under LD / LL (top left), LD / DD (top right), SD / LL (bottom left) and SD / DD (bottom right) condition for Minichromosome Maintenance 6 (MCM6), Proliferating Cell Nuclear Antigen (PCNA), Topoisomerase 6 subunit B (TOP6B) and DNA Polymerase Alpha subunit B (POLAB).

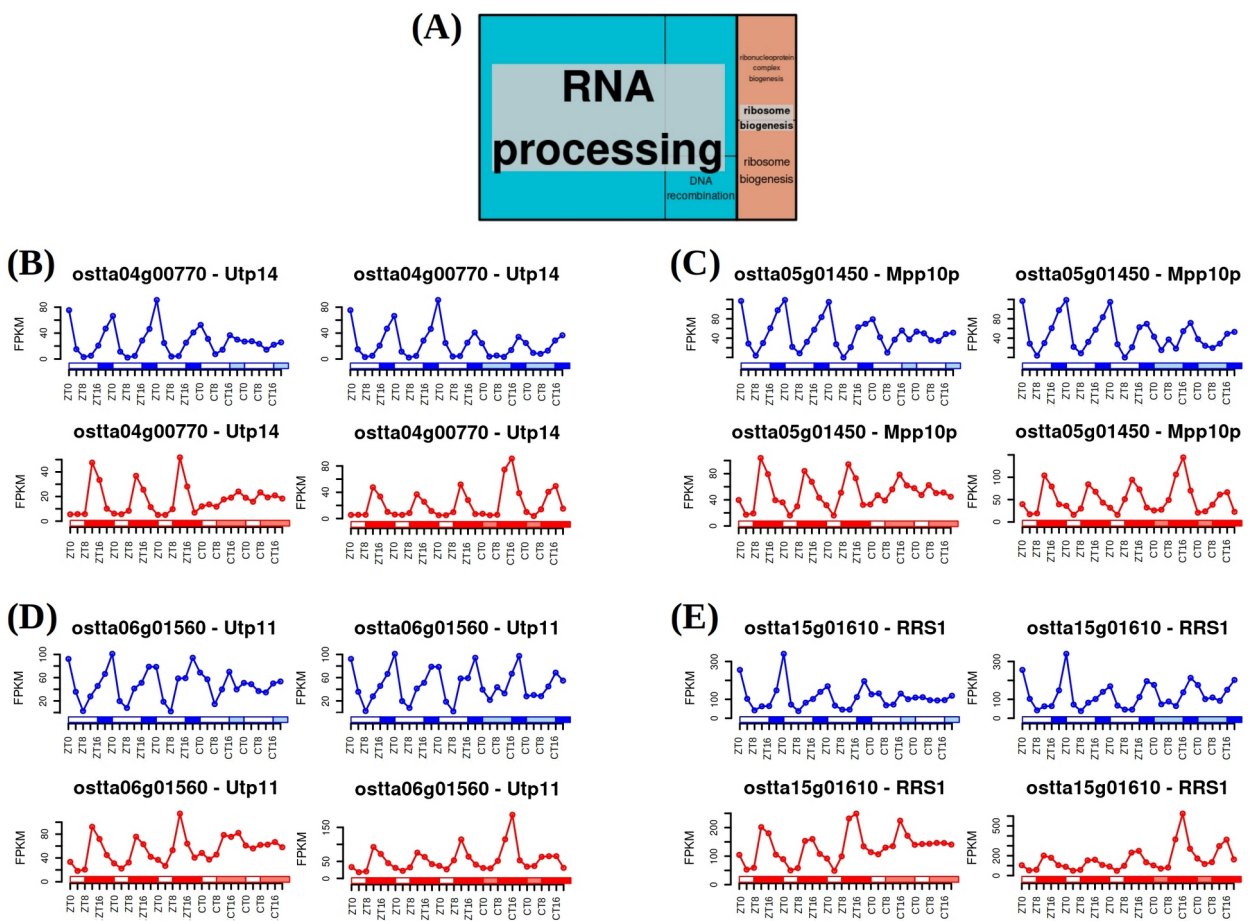


Figure 24: Biological processes significantly enriched in the genes exhibiting rhythmicity under alternating light/dark cycles and constant dark. (A) Treemap summarizing the significantly enriched biological processes. Semantically similar biological processes are grouped into the same colored rectangle. The most representative biological process is shown for each rectangle; (B), (C), (D) and (E) Gene expression profiles under LD / LL (top left), LD / DD (top right), SD / LL (bottom left) and SD / DD (bottom right) condition for U3 small nucleolar RNA-associated protein 14 (Utp14), M-phase phosphoprotein 10 (Mpp10p), U3 small nucleolar RNA-associated protein 11 (Utp11) and ribosome biogenesis regulator 1 (RRS1).

The oscillating genes under LL, both after LD and SD entrainment, were found to be significantly involved in DNA replication and Chromosome organization (Fig. 23). It agrees with previous cell cycle studies in microalgae like *Euglena* (Kato & Nam, 2021), *Chlamydomonas* (Donnan & John, 1983; Zones et al., 2015) and *Ostreococcus* (Moulager et al., 2007, 2010), where cell cycle seem to have a strong circadian clock regulation, but G1 phase is light-dependent due to the need of light to grow in photosynthetic organisms. This two affirmation suggest a complex regulatory mechanism supporting rhythmic patterns in the cell cycle of microalgae. These results provides evidence that, for these processes, a

light input is needed in order to respond to a circadian regulation and, thus, maintain their rhythmicity.

In addition, the RNA processing and ribosome biogenesis were found to be significantly enriched biological processes among the rhythmic genes under DD, both after LD and SD entrainment (Fig. 24). These processes are commonly programmed at transcriptomic level to take place during the night, so translation of proteins can be achieved during the day (Merchant et al., 2017). It could suggest that a dark input is needed in order to respond to a synchronized circadian regulation of those genes since their activation take place during skotoperiods. However, in contrast to the genes involved in DNA replication and chromosome organization (Fig. 23-B,C,D,E) which expression level is strongly reduced without the light input, RNA processing and ribosome biogenesis genes (Fig. 24-B,C,D,E) don't seem to be inactivated by the absence of dark but simply desynchronized.

We consider *bona fide* circadian genes those presenting rhythmicity under both LD and SD as well as maintaining their rhythmic expression profiles under both LL and DD free-running conditions. A clear dependence on the previous entrainment regime was observed with 1647 and 1034 genes keeping rhythmicity under both free running conditions after LD and SD entrainment respectively (Table 7, Appendix 9-10). These two sets overlapped partially identifying 350 *bona fide* circadian genes corresponding to 4.6% of the *Ostreococcus* transcriptome (Fig. 25-A, Appendix 11).

In previous work, RuBisCO activase (RCA) and RuBisCO small subunit (RBCS) mRNA were quantified in *Arabidopsis* under a light dark cycle, constant light and constant darkness conditions (Pilgrim & McClung, 1993). Their results are in agreement with our transcriptomic data in *Ostreococcus*, where the gene expression profile of RuBisCO activase (ostta04g02510, RCA) under the different conditions exemplifies how *bona fide* circadian genes maintain their rhythmicity (Fig. 25-B). In fact, functional enrichment analysis revealed that these genes were significantly involved in photosynthesis, chloroplast organization and pigment metabolic process (Fig. 25-C). Some of those processes are known to present a circadian physiological activity in plants and microalgae like *Euglena*, but there is a lack of confirmation at the transcriptomic level in most cases like the one provided in this work for *Ostreococcus* (Cumming & Wagner, 1968; Noordally & Millar, 2015; Panter et al., 2019).

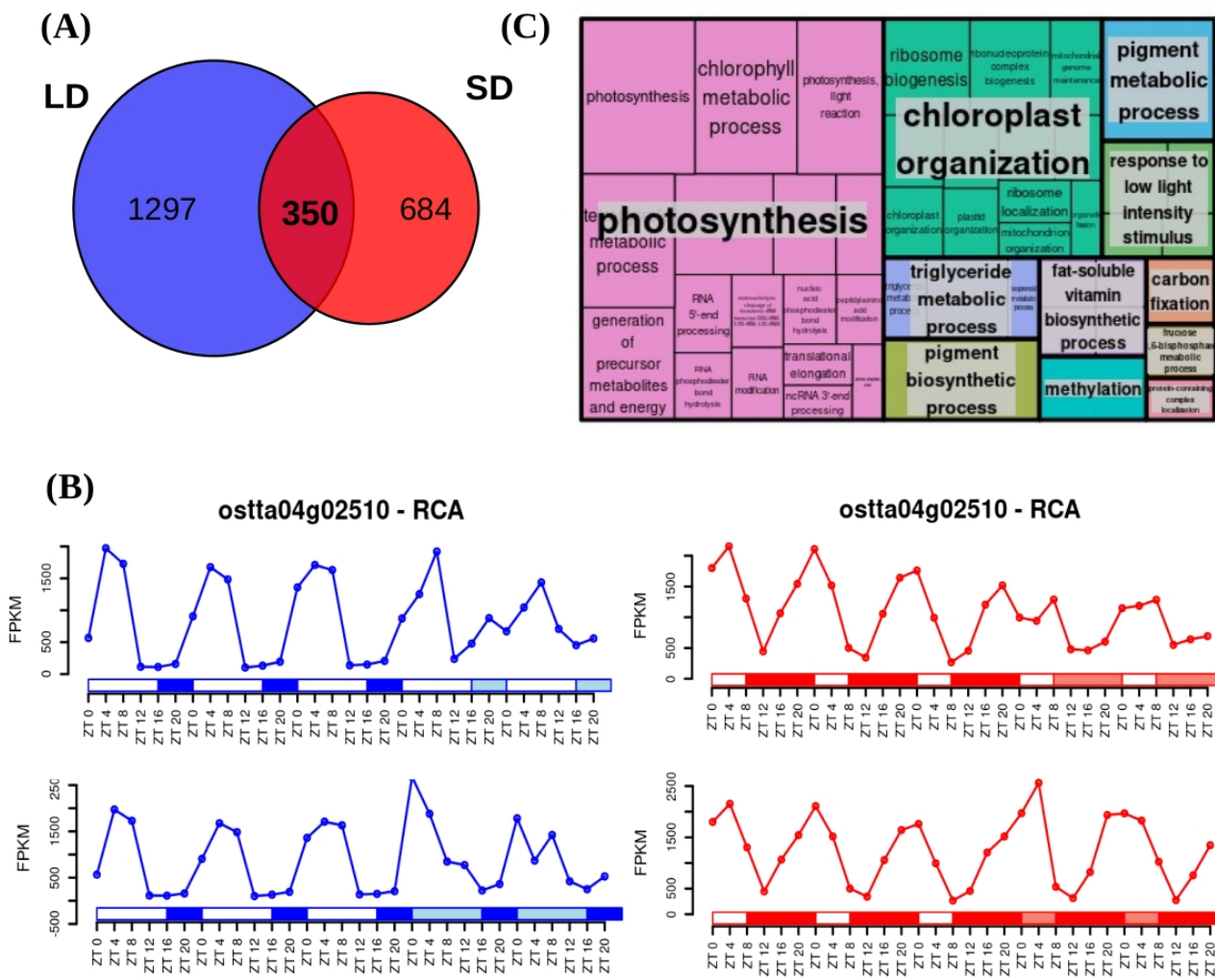


Figure 25: Identification of bona fide circadian genes and their functional enrichment analysis:
(A) Venn diagram comparing circadian genes identified after LD entrainment (blue circle) and after SD entrainment (red circle); **(B)** Gene expression profiles under LD, SD, LL and DD of RuBisCO Activase (RCA); **(C)** Treemap summarizing the biological processes significantly enriched over the bona fide circadian genes. Semantically similar biological processes are grouped together into the same colored rectangles. The most representative biological process is shown for each rectangle.

Constant light and constant darkness as free-running conditions have different effects over the transcriptome of Ostreococcus

The effect of the transition to constant light (LL) or dark (DD) on rhythmic gene expression patterns was performed using the co-sinusoidal parametric method implemented in the R package *circacompare*.

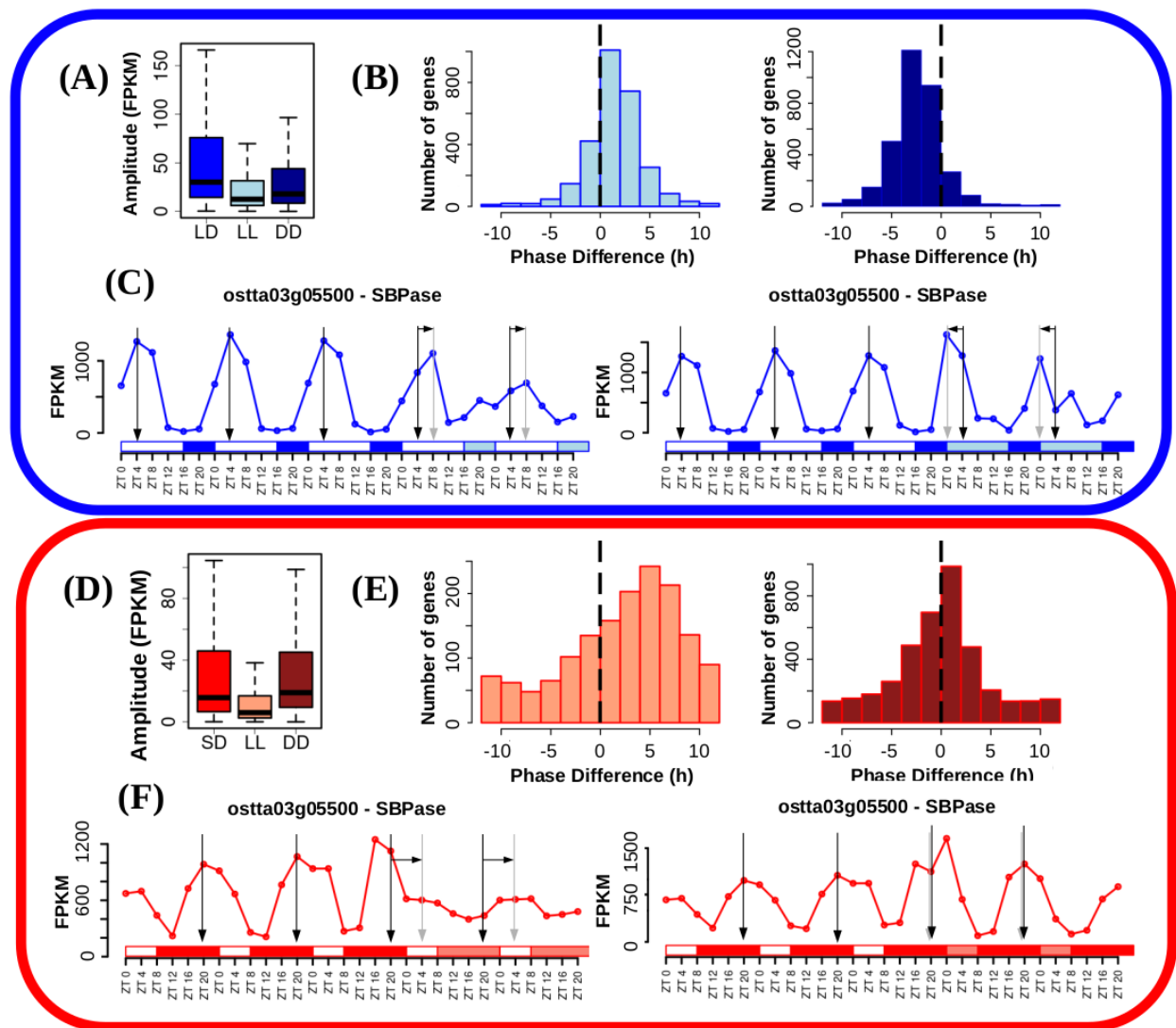


Figure 26: Free running conditions effects over gene expression profiles. (A,D) Boxplot representing rhythmic genes amplitude reached under LD or SD condition (blue top and red bottom, respectively), when cultures were kept under free running condition consisting of constant light (light blue/red) and when cultures were kept under free running condition consisting of constant dark (dark blue/red); (B,E) Histograms showing the distribution of the number of genes exhibiting positive and negative phase shifts under LL (light blue/red, left) and DD (dark blue/red, right) free running condition when compared to LD (top) or SD (bottom). Vertical dashed lines mark no shift; (C-F) Gene expression profiles under LD (top) and SD (bottom) followed by LL (left) and DD (right) of Sedoheptulose-bisphosphatase (SBPase). Vertical black arrows mark LD/SD phases, vertical grey arrows mark LL and DD phases and horizontal black arrows represent phase shifts.

In the LD entrained cultures, significant reductions in amplitude were detected when transferred to both LL and DD, being more drastic under LL according to p-values of 4.23×10^{-140} and 1.09×10^{-60} respectively (Fig. 26-A). Specifically, 97.68% of the genes maintaining their rhythmicity under free-running conditions presented a decrease in amplitude when transferred to LL and 79.43% when transferred to DD after LD entrainment. Moreover, the reduction in amplitude is significantly stronger under LL than under DD with a p-value of 6.71×10^{-28} . In contrast, in SD entrained cultures, amplitude reduction was only present when transferred to LL with a p-value of 5.94×10^{-65} . This effect is more drastic than the one observed after LD entrainment and it is present on 87.9% of rhythmic genes. Nonetheless, a slight but significant amplitude increase was found when transfer to DD after SD entrainment, according to a p-value of 2.5×10^{-8} (Fig. 26-D).

Free-running conditions also affected rhythmic gene expression patterns phases. Independently from the previous entrainment regime, forward positive phase shifts or delays were detected when cultures were transferred to LL (Fig. 26-B, C, E and F left). Whereas backward negative phase shifts or advances were found when cultures were transferred to DD (Fig. 26-B, C, E and F right). In addition, the phase delays in LL were more drastic for SD than LD entrained cultures although the advances in DD were more evident for LD than SD entrained cultures.

Constant dark or light as free-running conditions have been widely studied in nocturnal mammals (Bartoszewicz et al., 2010; Hundahl et al., 2012; Imai et al., 2020), plants (Edwards et al., 2010; Ohara et al., 2015) and other organisms (Biebach et al., 1991; Vatakis et al., 2018). The effect over the amplitude of biological rhythms has been previously observed at different molecular levels and is commonly associated with a loss of synchrony (Paajanen et al., 2021; Vatakis et al., 2018). Therefore, although *Ostreococcus* growth is dependent on photosynthesis and, thus, on light, the drastic reduction in amplitude detected under LL is possibly due to a decreased culture synchrony at the transcriptomic level. Individual cell transcriptional programs could be desynchronized by constant light, leading to largely out of phase individual gene expression profiles, resulting in damped average gene expression oscillations at the entire cell culture level (Fig. 27). Similar desynchronization effects at the single cell level have been reported in *Arabidopsis* leaves under constant light (Wenden et al., 2012; Yakir et al., 2011). Conversely, a slight increase in amplitude was observed under DD condition after SD entrainment, indicating a synchronization

tion increase between individual cell transcriptional programs. This supports the notion that LL has a stronger desynchronization effect than DD in *Ostreococcus* cultures, which has been already pointed in this work. The free-running rhythms observed in *Ostreococcus* could be possibly found in other photosynthetic organisms as well, but there is a huge lack of research on this topic since light is currently considered the primary transcriptional zeitgeber or synchronizing signal in plants (S. Wang et al., 2022; Wenden et al., 2012). Disregarding, thus, the relevance of dark periods in regulating diel rhythms, at least at the transcriptomic level.

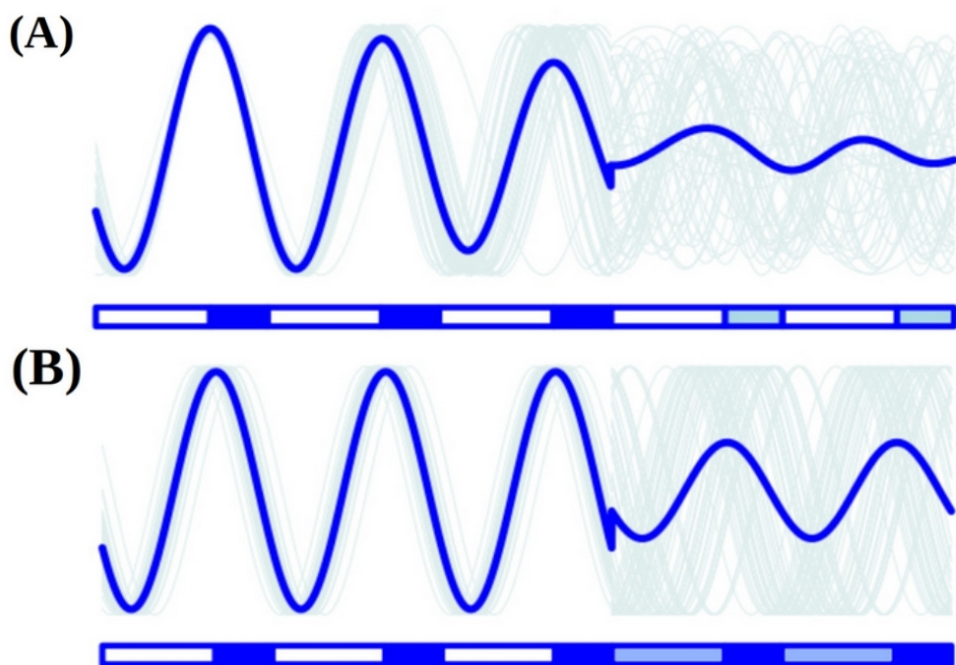


Figure 27: Reductions in amplitude under free running conditions can be explained by a decline in culture synchrony. Culture average gene expression profile under LD followed by LL (A) and DD (B) is represented by a thick blue line. Examples of individual cell gene expression profiles are represented by thin grey lines.

Moreover, analysis of the rhythmic patterns under free-running conditions unveiled typical responses of nocturnal character, such as backward and forward phase shifts under DD and LL, respectively, when compared to LD and SD. This has never been characterized in photosynthetic organisms before, but positive and negative phase shifts under LL and DD have been also observed in algae-coral symbiosis content in photosynthetic pigments (Sorek et al., 2013). However, Similar responses have been observed in behavioral traits in nocturnal animals, where DD condition have been extensively studied (Bartoszewicz et

al., 2010; Hundahl et al., 2012; Imai et al., 2020; Vatakis et al., 2018). In fact, constant light is commonly used as a activity circadian disruption model in those organisms. In this work, most transcripts peaked during the night or skotoperiod (Fig. 28-B), under both LD and SD, confirming this nocturnal transcriptomic character in this phytoplanktonic picoeukaryote. This results provide evidence of the importance of dark periods also in synchronizing diel cycles in photosynthetic organisms for the first time, possibly due to the predominant nocturnal character of *Ostreococcus* transcriptome.

Transcriptomic characterization of seasonal effects over gene expression profiles

Seasonal changes induce changes in amplitude and phase over gene expression profiles.

Specific differences in phase and amplitude between LD and SD rhythmic gene expression patterns were identified. A significant reduction in amplitude was observed in SD compared to LD entrained cultures, with a p-value of 1.16×10^{-111} (Fig. 28-A). Specifically, more than 2000 genes presented this effect. The reduction in amplitude could be attributed to an increased desynchronization of individual cells under SD when compared to LD condition, as discussed earlier (Fig. 28).

Negative phase shift or phase anticipation were also globally observed over the transcriptome of *Ostreococcus*. Whereas under LD entrainment, gene phases accumulate uniformly from the end of the day ZT12, to the end of the night ZT20, under SD entrainment gene phases are concentrated during the first half of the night from ZT8 to ZT16 (Fig. 28-B). Specifically, 3424 genes comprising 64.95% of the rhythmic genes exhibited a significantly anticipated phase under SD condition when compared to LD condition. In addition, only a low number of rhythmic genes exhibit their phase or maximum level of expression during the light period in LD and SD. This indicates that the main transcriptomic activity takes place during the night in *Ostreococcus*, which supports the nocturnal character of its transcriptome as described previously when analyzing the effects of free running conditions.

These transcriptomic seasonal responses to changes in photoperiod length were captured in a predictive model based on linear interpolations able to estimate the phase and amplitude of any gene expression profile over the year. Previously published microarray data,

generated under neutral day condition (12 h light : 12 h dark) (Monnier et al., 2010) were used to evaluate its predictive power. Model simulations showed that approximately two thirds of the rhythmic genes under both LD and SD conditions respond to seasonal changes in photoperiod length by gradually adjusting their phases in accordance with the increasing or decreasing length of the day over the year.

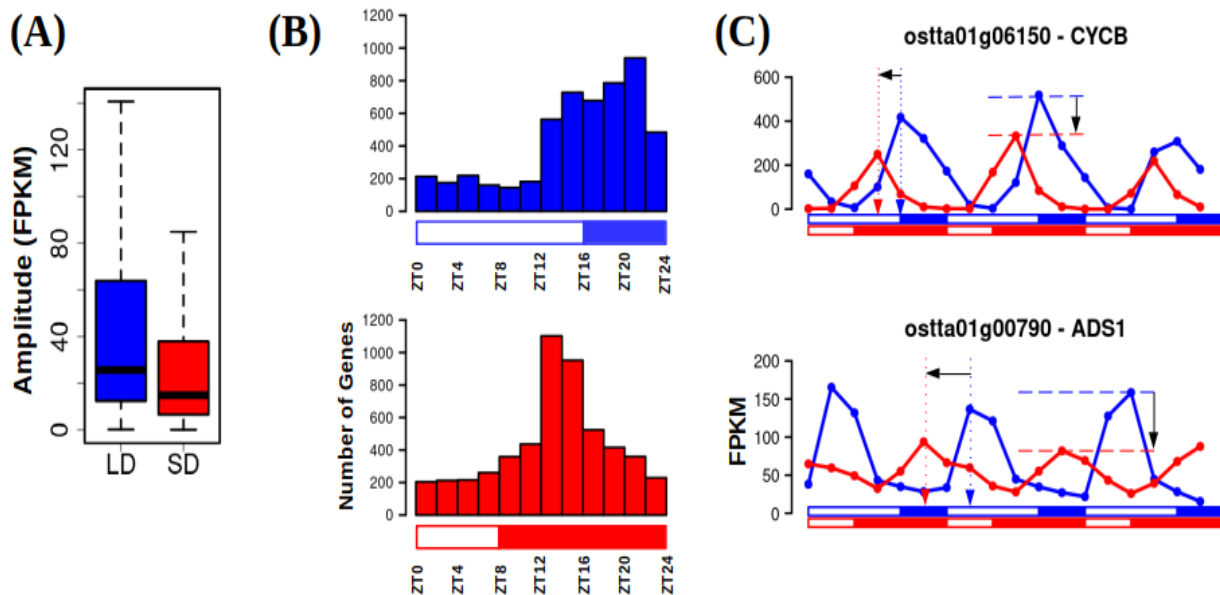


Figure 28: Photoperiod changes cause amplitude reductions and phase shifts over gene expression profiles. (A) Boxplot representing rhythmic genes amplitude or maximum expression level reached under LD and under SD. SD amplitudes are significantly reduced with respect to LD according to a p -value of 1.16×10^{-11} computed using Mann-Whitney-Wilcoxon test; (B) Histograms showing the distribution of the number of genes with phase or maximum expression level at specific time points during the day under LD condition (blue, top) and SD condition (red, bottom); (C) Gene expression profiles under LD (blue line) and SD (red line) of Cyclin B (*ostta01g06150*, CYCB, top) and Delta-9 acyl-lipid desaturase 1 (*ostta01g00790*, ADS1, bottom). Blue and red vertical dotted arrows mark LD and SD phases. Horizontal black arrow represents backward phase shifts under SD when compared to LD. Blue and red horizontal dashed lines mark LD and SD amplitudes. Vertical black arrows represent the reductions in amplitude under SD with respect to LD.

Photoperiodic dependent changes in amplitude and phase shifts in biological rhythms have been already described in mammals (Messenger et al., 2000; Sumová et al., 2003; Van Dongen et al., 1997; Wucher et al., 2022), as well as in plants and microalgae (Flis et al., 2016; Panter et al., 2019; Serrano et al., 2009). Depending on the organisms under study increments or decrements in amplitude as a response to shortening or lengthening photoperiods have been reported. Global phase shifts as an adaptation to changes in ph-

to period has been described in *Arabidopsis thaliana*, and changes amplitude were observed in individual genes in both *A. thaliana* and *Chlamydomonas*. For example, the rhythmic expression profile of the gene *CrCO* potential ortholog of the *CONSTANS* gene in *Arabidopsis thaliana* shows an increase in amplitude under SD condition as well as a negative (backward) phase shift (Flis et al., 2016; Serrano et al., 2009). Same effects linked to seasonal changes can be observed at the gene level in *Ostreococcus*. For example *Cyclin B* (ostta01g06150, CYCB) and *Delta-9 acyl-lipid desaturase 1* (ostta01g00790, ADS1) exhibit the described phase anticipation and amplitude reduction under SD condition when compared to LD condition (Fig. 28-C).

Seasonal changes promote the emergence of 12 h period cycles

When comparing SD and LD conditions, another phenomenon has been identified over the transcriptome of *Ostreococcus* emerging as a response to photoperiod shortening. Under LD condition, almost every rhythmic gene (5825 genes covering 75.97% of the entire genome) reached its maximum level of expression once a day, presenting one single peak every 24h in its expression profile (Fig. 29-A, B). However, more complex rhythmic expression profiles with two expression peaks per day (every 12 h) are found in a small number of genes, specifically 376 genes (Fig. 29-A, Appendix 12). Under SD condition the number of genes presenting one single expression peak per day decreases to 4249 (55.41% of the entire genome). This is coupled to an increasing number of genes, namely 1855 genes, presenting two expression peaks per day (Fig. 29-A, B, Appendix 13).

When re-analyzing a published microarray data set generated from cultures of *Ostreococcus tauri* under neutral day condition (12 h light:12 h dark) (Monnier et al., 2010), bimodal gene expression patterns were also found. Most of the rhythmic genes presented rhythmic expression profiles with a 24 hours period and, thus, a single expression peak. However, 1171 genes presented rhythmic expression pattern with an apparent period of 12 hours (two peaks of expression per day). This photoperiod can be considered an intermediate step between the two extreme photoperiods studied in this thesis (LD and SD). Indeed, the data show an intermediate number of genes with two peaks of expression per day between the ones identified in this thesis for LD and SD conditions (Fig. 29-A). Also, in agreement with our results, this bimodal rhythmic patterns can be found in data generated from other organisms like *Chlamydomonas* under neutral day (Zones et al. 2015). This

suggests that, at least in *Ostreococcus* (and possibly other microalgae), there is an increasing number of genes that present high levels of expression twice a day (every 12h) as the photoperiod get shorter although its biological role remains to be determined.

Tides take place following rhythms of approximately 12 h and can give rise to circatidal gene expression patterns which persist under free running conditions (Fauré-Fremiet, 1951; Rock et al., 2022). Biological rhythms with specifically 12 h periods are hypothesized to be a reminiscent of the ~ 12 h circatidal rhythms of coastal and estuarine organisms (Ballance & Zhu, 2021). The maintenance of these rhythms after evolving to live on land could provide an advantage in the adaptation to metabolic stress that peak at transition periods during diel cycles (Pan et al., 2020; B. Zhu et al., 2017). Indeed, bimodal rhythms presenting two peaks per day that are maintained under free running conditions have been observed in animals (Binkley & Mosher, 1985; Foà & Bertolucci, 2001; Kyorku & Brady, 1994; Prabhakaran & Sheeba, 2012; Watanabe et al., 2007), plants (Hayes et al., 2010; Van Gelderen, 2020) and some microalgae like Euglena (Mohabir & Edmunds, 1999). They have been described only for specific processes, genes or compounds, not as a global response in the transcriptome to external signals.

However, although tides play a central role in the dynamics of the natural environment of *Ostreococcus*, this hypothesis was discarded in this study since the observed 12 h period rhythmic gene expression profiles in *Ostreococcus* transcriptome are not maintained under free-running conditions. Instead, bimodality disappears and only one of the expression peaks is maintained under constant light whereas the other one persisted only under constant darkness (Fig. 29-C).

This observation suggest that the seasonal effect observed over the transcriptome of *Ostreococcus* is not a self-sustained 12 h rhythm, but a combination of two distinct rhythmic profiles: one dependent on the photoperiod or light periods (maintaining its rhythmicity only under LL) and another one sustained by the skotoperiod or dark periods (maintaining its rhythmicity only under DD). To support this hypothesis, a model capturing this response was developed. First, a decomposition was performed over the bimodal gene expression profiles present under SD conditions (based on Non Linear Squares tools (Baty et al., 2015)) into two co-sinusoidal single peak profiles, one peaking during the photoperiod and another one peaking during the skotoperiod (Fig. 29-C). Then, linear interpolation was

used to simulate phase shifts of these two unimodal profiles as a response to photoperiod shortening. As a validation of its predictive accuracy, this model predicted the emergence of bimodal rhythmic profiles under neutral conditions.

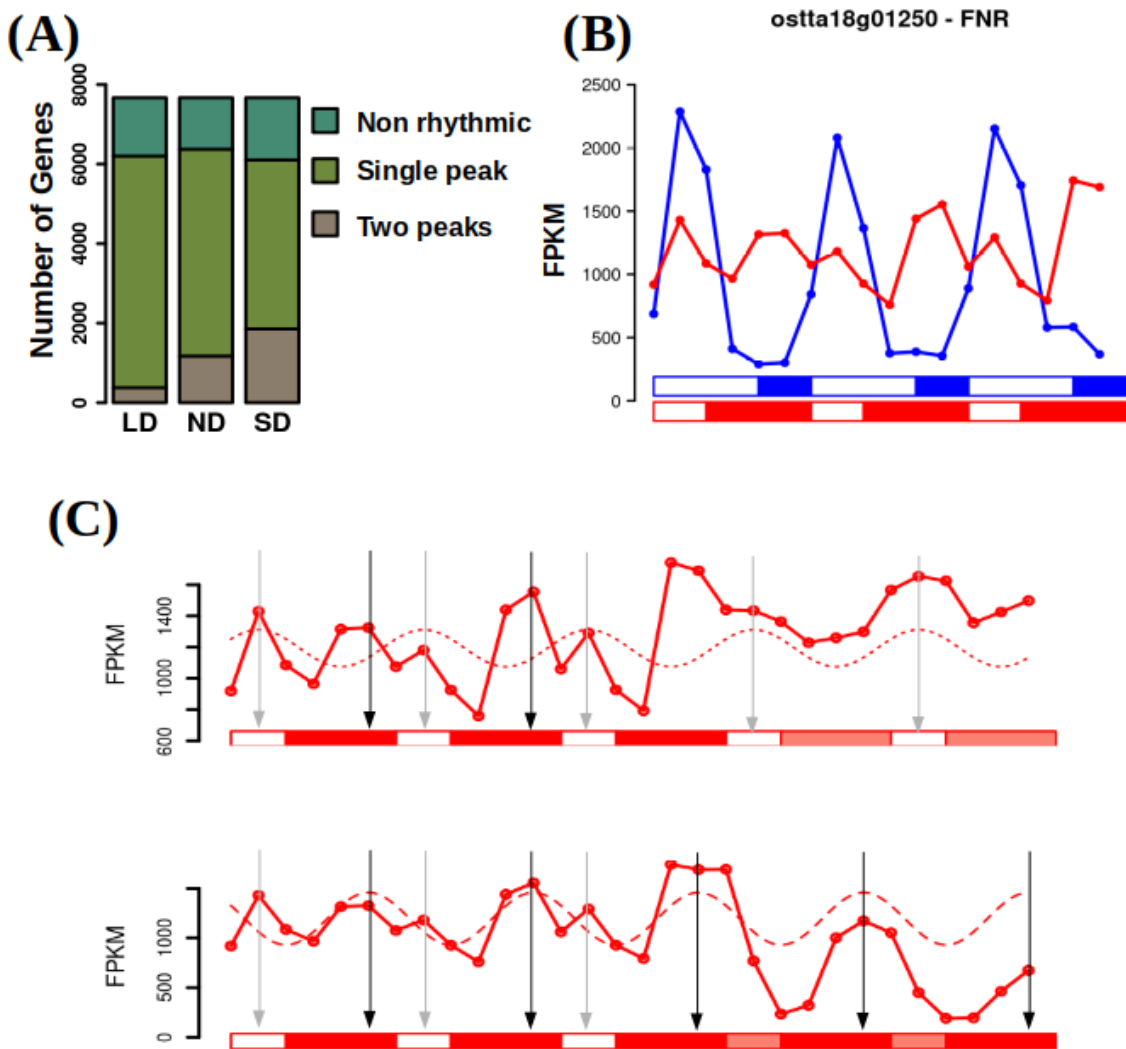


Figure 29: Emergence of 12 h period rhythmic expression profiles under SD. (A) Barplot representing in different green colors the number of non rhythmic, single peak rhythmic and two peaks rhythmic genes under LD, ND and SD conditions; (B) Gene expression profiles under LD (blue line) and SD (red line) of Ferredoxin-NADP⁺ reductase (*ostta18g01250*, FNR); (C) Gene expression profiles under SD and free running conditions consisting of constant light (LL) or constant dark (DD) of Ferredoxin-NADP⁺ reductase (*ostta18g01250*, FNR). The two unimodal profiles extracted from the real bimodal profile detected are represented: the one depending on the photoperiod as dotted line with phase marked with a grey vertical arrow maintaining its rhythmicity only under LL (top); and the one depending on the skotoperiod (dashed line) with phase marked with a black vertical arrow maintaining its rhythmicity only under DD (bottom).

As a result, model simulations showed how, under LD condition, the two distinct profiles regulated independently by the photoperiod and skotoperiod overlap in time, producing a single peak, while as the photoperiod shortens and the skotoperiod lengthens they become out of phase resulting in a bimodal profile under SD condition. Suggesting a joint but independent regulation exerted by the photoperiod and skotoperiod in the expression of this set of genes (Fig. 29-C).

Seasonal cycles induces distinct temporal transcriptional programs organizing biological processes during diel cycles

In order to determine the temporal organisation of the transcriptional program in *Ostreococcus* under summer LD and winter SD conditions, gene clusters (Appendix 14-25) were defined based on their phases (when their maximum level of expression is reached). Functional enrichment analyses of the resulting gene clusters revealed the cellular processes activated at the transcriptomic level in each temporal point (Fig. 30-31). Focusing on the most enriched processes in each time point, a transcriptional temporal map of *Ostreococcus* under each photoperiod is illustrated in Fig. 32.

Under long day condition (Fig. 30), *Ostreococcus* activates genes involved in RNA processing and ribosome biogenesis at dawn (ZT0). Examples for such genes are *U3 small nucleolar RNA-associated protein 14* (*ostta04g00770*, *Utp14*) and the *Ribosome Biogenesis Factor BMS1* (*ostta05g01080*, *BMS1*). During the first part of the morning (ZT4) *Ostreococcus* transcriptome is almost completely focused in genes involved in translation, such as *eukaryotic Initiation Factor 2* (*ostta03g02100*, *eIF2*) and *translation elongation factor P* (*ostta03g03015*, *YeIP*). The genes mainly involved in photosynthesis but also in carbohydrate metabolism reach their maximum expression level during midday, when irradiance is maximum (ZT8). Some of those genes are subunits of both photosystems: *ostta01g03170* (*PsbP*), *ostta02g00580* (*PsaL*), *ostta02g02560* (*PsbX*), *ostta02g03860* (*PsaE*), *ostta04g01790* (*PsaF*), *ostta05g04560* (*PsbR*), etc. During the afternoon (ZT12), the activation of genes involved in DNA replication takes place. Some minichromosome maintenance proteins *ostta01g02580* (*MCM6*) and *ostta05g01680* (*MCM9*) are found, as well as the *proliferating cell nuclear antigen* *ostta06g02890* (*PCNA*) which is central to the DNA replication process. Intracellular transport and cellular respiration are the two most promi-

inent biological processes whose genes reach their maximum expression level at dusk (ZT16) under LD condition. Genes like *lysophospholipases* *ostta01g04440* (*CLC*) or *nucleoporins* *ostta14g02210* (*Nup133*) are some examples for this time point. Finally, during midnight, *Ostreococcus* focuses on expressing genes involved mainly in cellular amino acid metabolic process, like *3-Deoxy-D-arabinoheptulosonate 7-phosphate () synthase* *ostta06g03270*, (*DAHP*) which encodes the first enzyme in the biosynthesis of the amino acids phenylalanine, tyrosine and tryptophan.

Under short day condition (Fig. 31), the most prominent biological process whose genes reach their maximum expression level at dawn (ZT0) is protein catabolism. Examples for such genes are *Signal transduction Histidine Kinase* *ostta09g02190* (*HK*), or *Ubiquitin Fusion Degradation protein* *ostta09g00750* (*UFD*). In agreement with what was observed in long day condition, genes having their peak of expression during midday (which in short day takes place at ZT4, maximum irradiance time) are involved in photosynthesis. Once again, genes encoding photosystems subunits are clustered in this time point. When the dusk comes at ZT8, genes involved in DNA replication show their maximum level of expression during this time point. The same genes used as an example in LD are found also in SD but anticipating their peak of expression 4h. Then, RNA processing and ribosome biogenesis are the two most prominent biological processes early during the night (ZT12), showing an anticipation of 12h compared with LD temporal program. In addition, genes involved in translation also show a 12h anticipation reaching its maximum expression level during midnight (ZT16) and genes involved in carbohydrate metabolism reach their maximum expression level after midnight at ZT20.

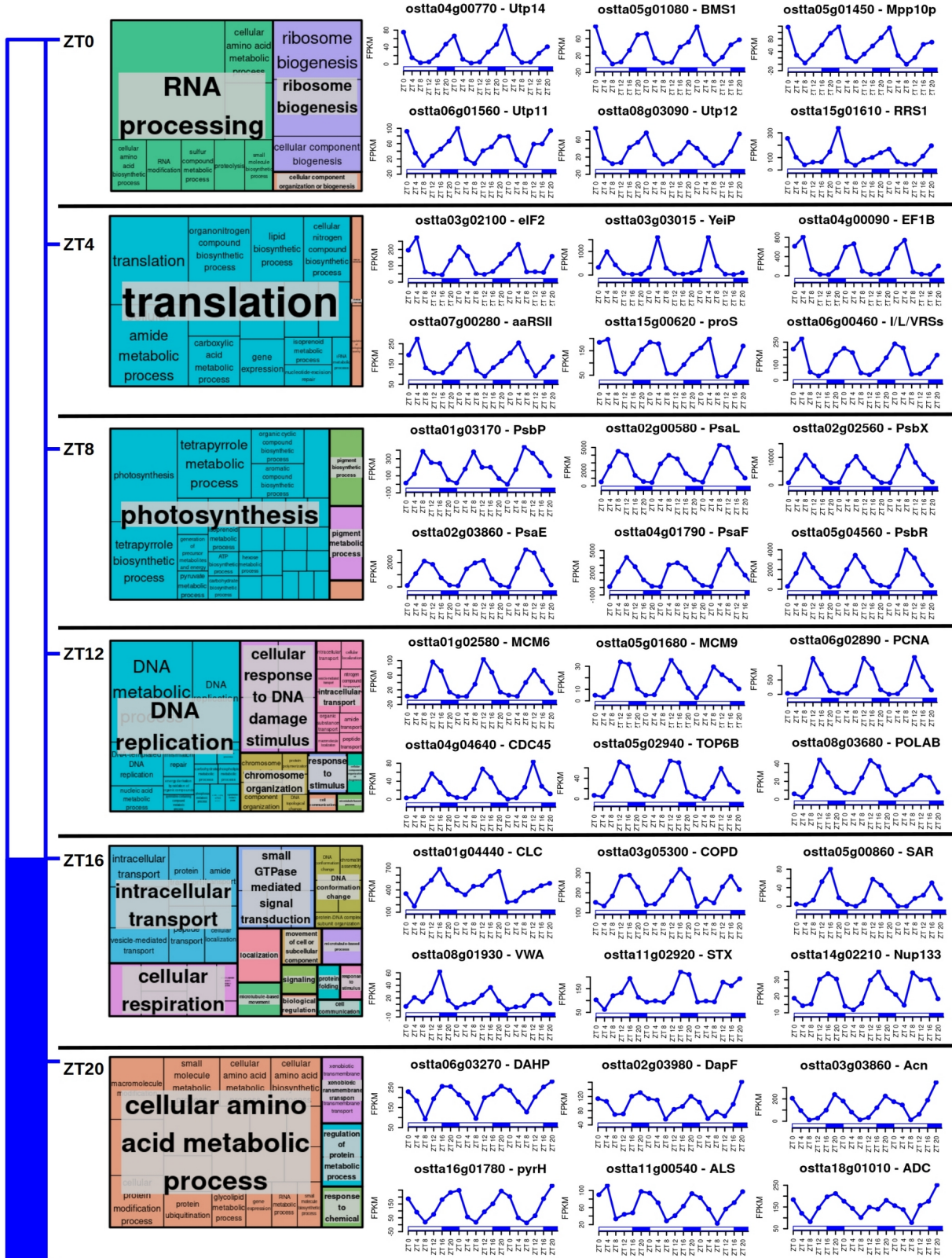


Figure 30: Cellular processes transcriptomically activated in each time point under LD condition. For each cluster of genes with phase in the different time points, there are: a treemap summarizing the biological processes significantly enriched and expression profiles representation of relevant genes.

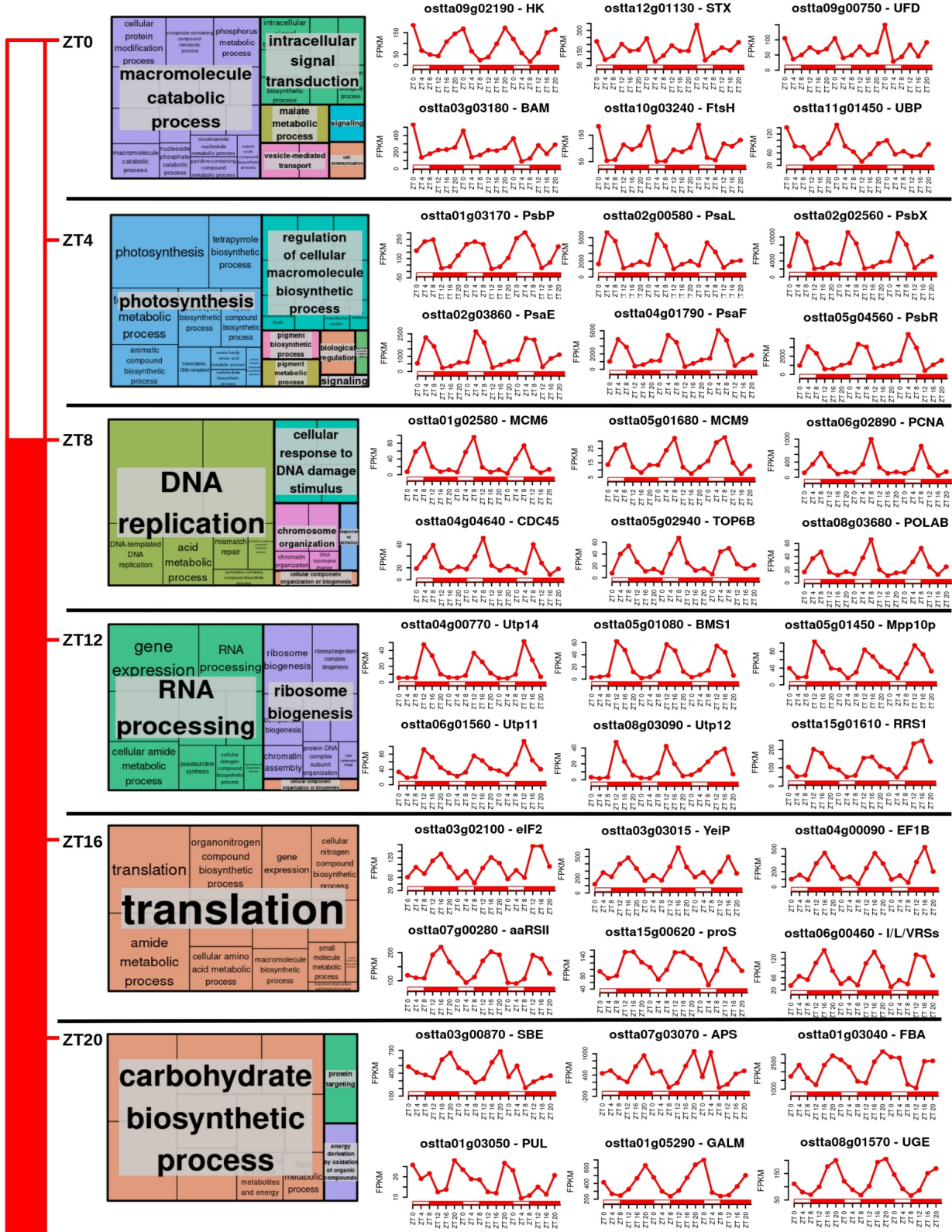


Figure 31: Cellular processes transcriptomically activated in each time point under SD condition. For each cluster of genes with phase in the different time points, there are: a treemap summarizing the biological processes significantly enriched and expression profiles representation of relevant genes.

These programs consisted of distinct times for the activation of biological processes produced by the previously mentioned gene phase backward shifts under SD with respect to LD.

Simple anticipation in time resulting in the same sequential order of activation but 4-12h earlier were found. For example, genes involved in photosynthesis peak at ZT8 under LD (Fig. 32-A) and at ZT4 under SD (Fig. 32-B), coinciding with the moment of maximal light irradiance in both cases. Similarly, genes involved in DNA replication reached their maximum expression level at the end of the day under LD, ZT12 (Fig. 32-A), and at dusk under SD, ZT8 (Fig. 32-B). These are clear examples of set of genes that present phase shifts caused by seasonal changes that simply adjust their phases in order to align with specific times of the day, like midday and evening times, in any photoperiod. However, they take place always in the same sequential order.

In addition, phase shifts rearrangements in the sequential order of activation of specific biological processes were also found. For instance, under LD conditions, genes involved in amino acid biosynthesis, ribosome biogenesis, and translation reached their full activation sequentially at ZT20, ZT0 and ZT4, respectively (Fig. 32-A). However, in SD entrained cultures, first ribosome biogenesis genes were fully activated at ZT12 and subsequently at the same time point (ZT16) amino acid biosynthesis and genes involved in translation reached their maximum expression level (Fig. 32-B). A re-arrangement in time is also observed for carbohydrate metabolism genes, which align with the activation times of photosynthesis genes in LD (both take place at midday) but reach their full activation 8 h before photosynthesis genes do in SD entrained cultures (Fig. 32).

This suggests that phase shifts globally observed over the transcriptome of *Ostreococcus tauri* as an adaptation to photoperiods, not only consist in anticipating processes but also in a re-arrangement of the complete diel gene activation programme.

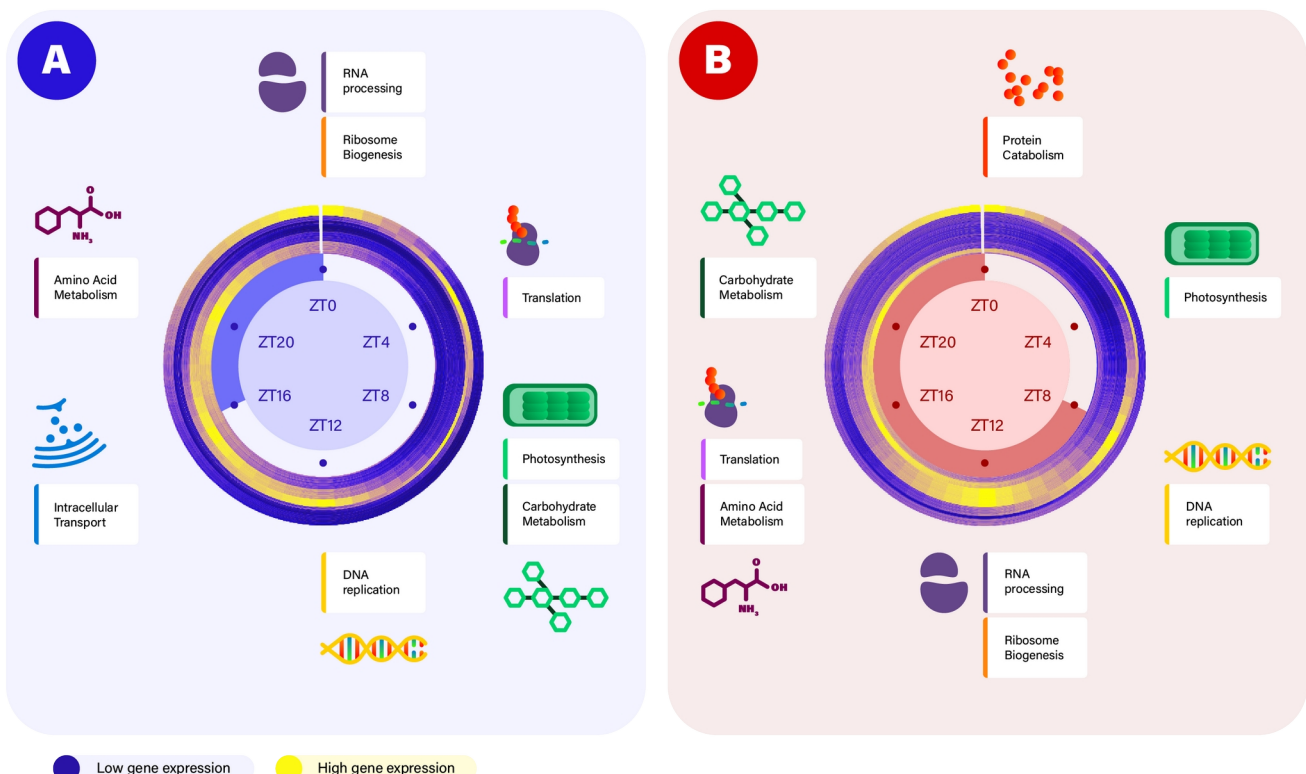


Figure 32: Summary of the transcriptional temporal program of *Ostreococcus tauri* under LD and SD conditions. Circular heatmap representing the temporal organization of gene expression profiles under LD condition (A) and SD condition (B). Dark blue stands for low expression whereas yellow represents high expression. Genes are clustered depending on their phase or time of maximum expression where genes with phase at ZT0 are located in the outer circle and genes with phase at subsequent ZTs are placed sequentially into inner circles. The most enriched processes in each gene cluster are illustrated capturing the diel gene activation program under LD and SD condition.

Chapter 3: Proteomic analysis of seasonal variations in diel cycles in *Ostreococcus tauri*

Proteins are the primary molecular entities that carry out the majority of biological processes in living cells. Therefore, proteomic analysis, which involves the identification and quantification of proteins, plays a crucial role in characterizing the responses of living organisms to diel cycles (Kay et al., 2021; Le Bihan et al., 2011). In this study, a total of 3,672 proteins were successfully identified and quantified under LD or SD conditions, accounting for approximately 48% of the *Ostreococcus* annotated proteome. In addition, the subcellular location of the detected proteins covered most cellular components or organelle (Fig. 33).

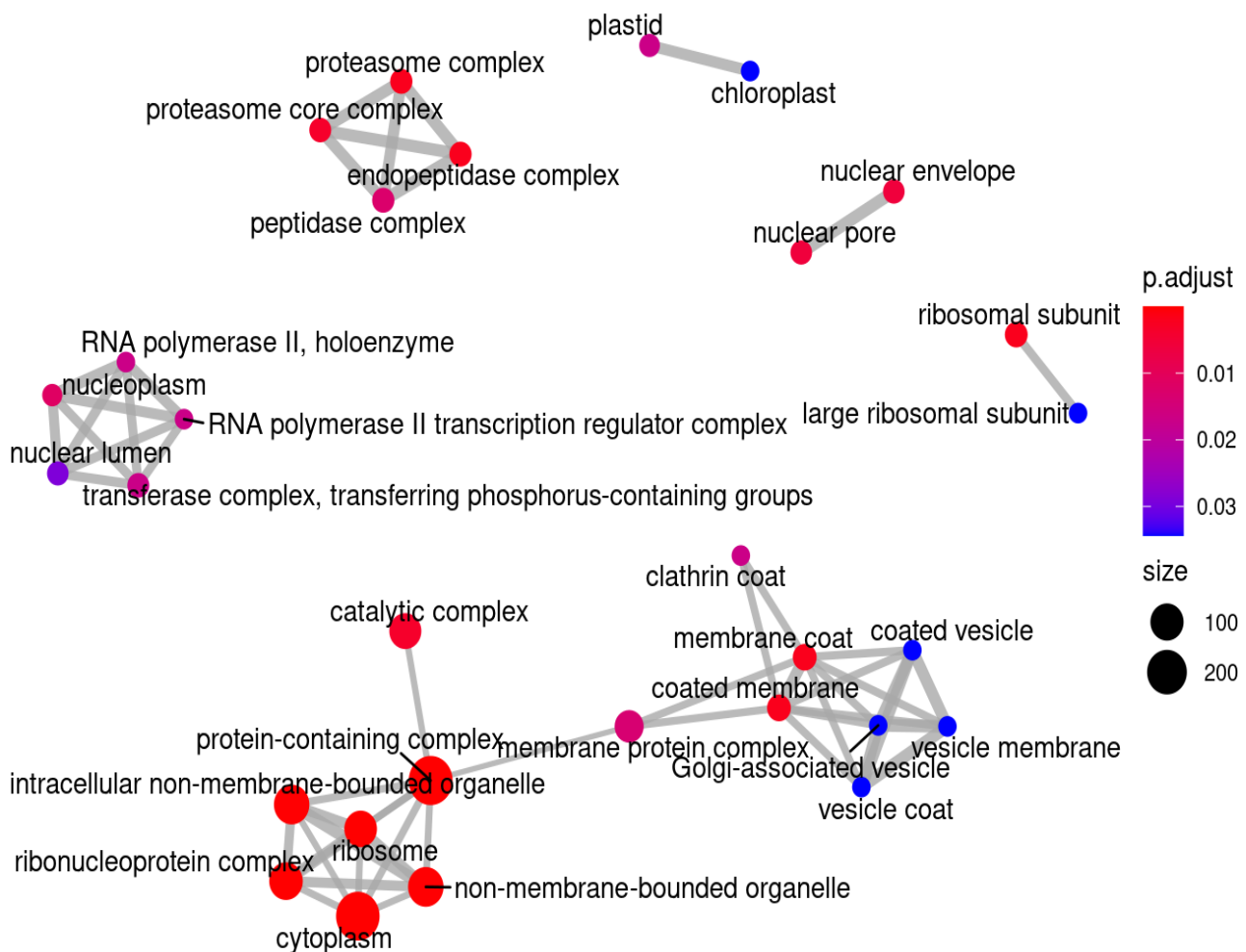


Figure 33: Enrichment map representing the cellular components or organelle significantly covered by the proteins detected. Dots or nodes sizes represent the number of proteins identified located in the corresponding organelle. A blue to red gradient is used to represent the level of significance. Lines or edges link dots or nodes representing related organelle.

Since our data is obtained from 3 technical replicates of each biological replicate (3 light/dark cycles), it can be observed that the global distribution of each group of 3 technical replicates is similar in the raw data (Fig. 34-A). The differences observed over the global distribution of different groups of technical replicates are solved with log2 quantile normalization of the data, ensuring data comparability (Fig. 34-B).

In order to obtain a deeper understanding of the underlying structure in the proteomic data, principal components analysis (PCA) is performed separately over the LD (Fig. 34-C) and SD (Fig. 34-D) rhythmic proteomes. Under LD condition, the biological replicates tightly cluster together globally constituting a circular structure (Fig. 34-C) similar to the one observed over the transcriptomic data (Fig. 19-B). Under SD condition more variability is observed, as it was also observed over the SD transcriptomic data (Fig. 20-C), but the circular structure is still maintained in this case (Fig. 34-D). Also, the high similarity between the transcriptomes corresponding to late-night and sunrise in SD conditions (Fig. 20-A), ZT0 and ZT20, is not present in proteomic data. This suggests that the anticipation to the light hours is present only at the transcriptomic level, activating during the late-night hours the transcription of genes that will be translated into proteins during the morning. As a result of this anticipation to the light period, there is a similar transcriptome under ZT20 (last time point of the night) and ZT0 (sunrise) but it is not reflected at the proteomic level, where this anticipation to the light hours don't seem to exist. In fact, a higher differentiation between the night samples and the light samples is observed in the proteomic data than in the transcriptomic data (Fig. 34-C,D).

In overall, these results support that our experimental design grants good quality data and a high level of synchronization in our rhythmic proteomic data allowing us to proceed to the identification and comparison of proteins under LD and SD condition.

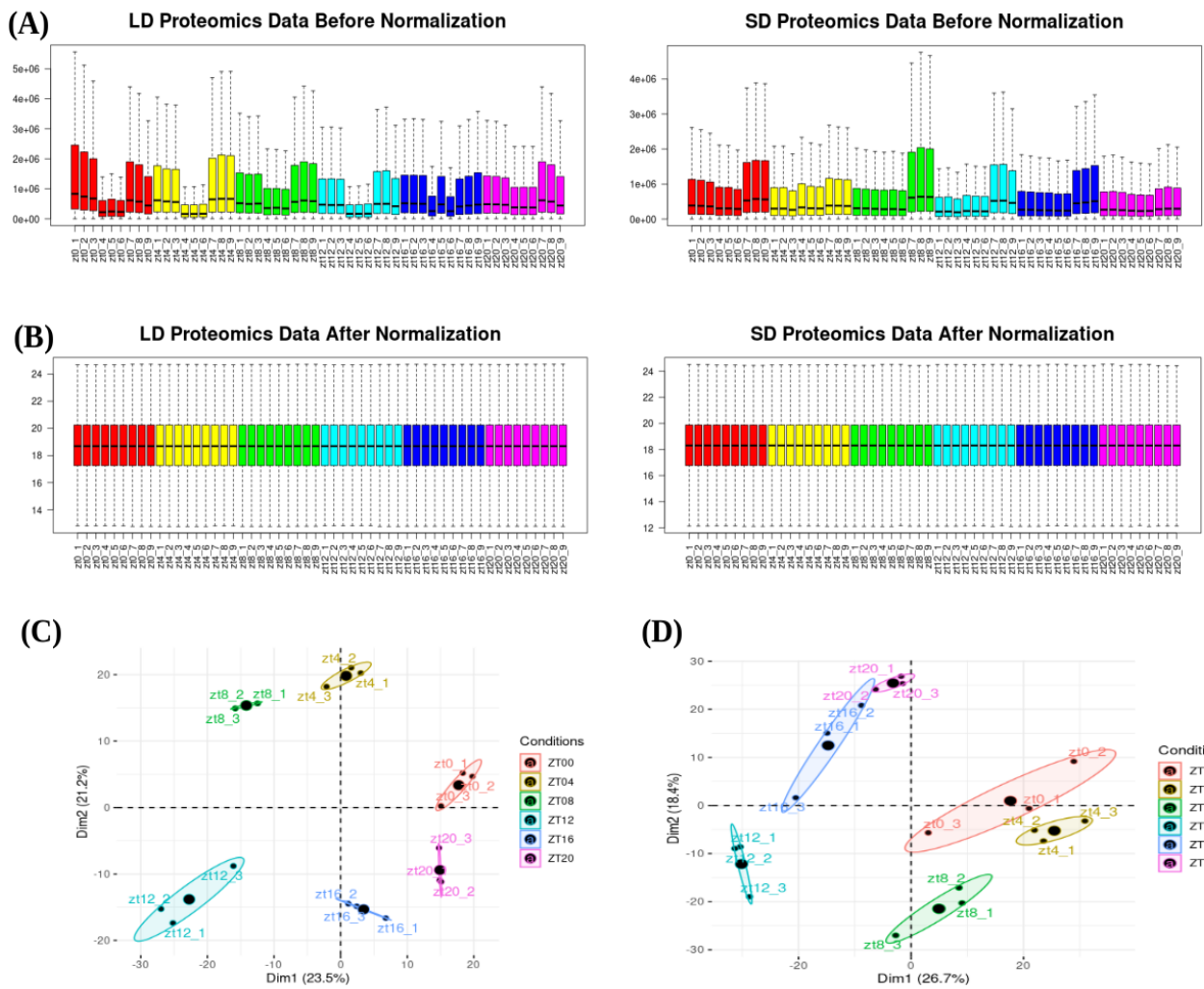


Figure 34: Proteomic data normalization and reliability. (A) Boxplots representing global distributions (before normalization) of protein abundances over the technical and biological replicates of long day condition on the left and short day condition on the right. Boxes corresponding to the replicates of the same time point are represented in the same color, as the legend in the bottom shows; (B) Boxplot representing global distributions after normalization; (C-D) Principal Component Analysis of the time point global rhythmic proteomes under LD and SD condition, respectively. Small dots correspond to the 2D projection of each time point global rhythmic proteome. Big dots correspond to the average of the three replicates 2D projections for each time point. Ellipses mark the 95% confidence regions corresponding to each time point global rhythmic proteome.

Proteomic characterization of diel rhythmic abundance profiles

Similarly to transcriptomic data analysis, the R packages RAIN and circacompare were used for proteomic data rhythmicity analysis. In LD entrained cultures, 928 proteins comprising approximately 32% of the total proteins detected presented diurnal rhythmic abundance profiles (Fig. 35-A, Appendix 26). An increase in rhythmicity was observed under SD conditions, detecting 1442 rhythmic proteins comprising 44% of the detected proteome (Fig. 35-B, Appendix 27). In contrast to the results on transcriptome rhythmicity, seasonality had a major effect over the identity of the rhythmic proteins: only 9% of the detected proteome presented rhythmicity under both conditions. In addition, the rhythmicity levels in the proteome were much lower than the ones observed in the transcriptome of *Ostreococcus tauri*, indicating a more dynamically cycling character in the transcriptome than in the proteome under diel cycles. The decrease in proteome rhythmicity has also been reported under ND conditions where 67% of the detected proteome presented rhythmic abundance profiles (Kay et al., 2021) where more than 80% of the transcriptome is known to be rhythmic under these conditions (Monnier et al., 2010). Therefore, transcripts rhythmic expression profiles do not seem to always lead to rhythmic protein abundance profiles. This phenomenon highlights the relevance of multiomics integration, since transcripts behavior cannot always be extrapolated to proteins or cellular processes, neither vice versa.

Rhythmic transcripts which encode for proteins that maintain their abundance levels constant over diurnal changes have been a paradox in chronobiology research. Protein degradation may account for differences between transcriptomic and proteomic data. This hypothesis suggests that rhythmic transcripts are needed to maintain a constant abundance level of the encoding protein when its degradation process is rhythmic (Lück et al., 2014). In that way, cells have to rhythmically supply new transcripts to balance protein synthesis/degradation ratio.

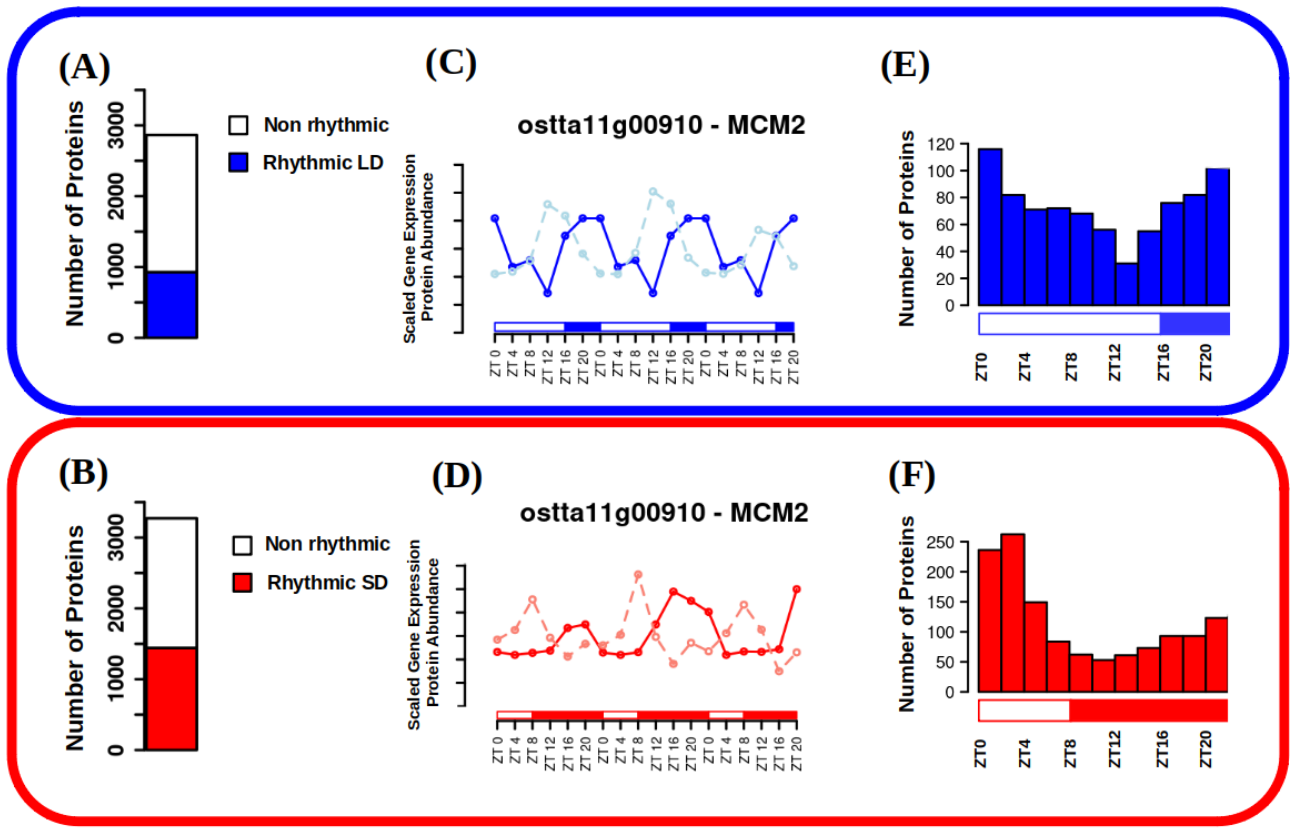


Figure 35: Proteome rhythmicity under alternating light/dark cycles. (A-B) Barplots representing the number of identified proteins under long day (A) and short day (B) conditions; (C-D) Protein abundance profiles under LD (C) and SD (D) conditions represented together with gene expression profiles under LD (light blue, dashed line) and SD (light red, dashed line) conditions for Minichromosome Maintenance 2 (*ostta11g00910*, *MCM2*); (E-F) Histograms showing the distribution of the number of proteins with phase or maximum abundance at specific time points under LD (E) and SD (F) conditions.

Rhythmic protein abundance profiles were compared to the corresponding rhythmic gene expression profiles detecting phase offsets between them (Fig. 35-C,D). It suggests that protein translation may takes place few hours after gene expression. In fact, while the majority of the transcripts have their maximum expression level during night hours in both photoperiods (Fig. 28-B), the majority of the rhythmic proteins present their maximum abundance level during light hours.

In addition, the phase shifts dependent on photoperiods that were found in the transcriptomic data don't seem to be apparent in the proteome. Under both conditions, rhythmic proteins reach their maximum abundance around ZT0-ZT4 (Fig. 35-E,F). Indeed, no coincidences between the corresponding rhythmic protein and transcript abundance profiles were observed, indicating a lack of global correlation between proteome and transcriptome

dynamics. (Fig. 36-A,B). This observations point to the decoupling of transcription and translation and the existence of a significant regulation over translation initiation.

However, when protein and transcript abundance profiles were aligned omitting transcript/protein offsets, a positive high correlation value of 0.84 is found (Fig. 36-A,C). This indicates that transcriptome and proteome dynamics are indeed linked but separated temporally. Similar temporal offsets between transcripts and proteins have been reported in other organisms, such as *Mus musculus* (Robles et al., 2014), where over 50% of transcript phases were found to precede their corresponding protein phases by more than 6 hours.

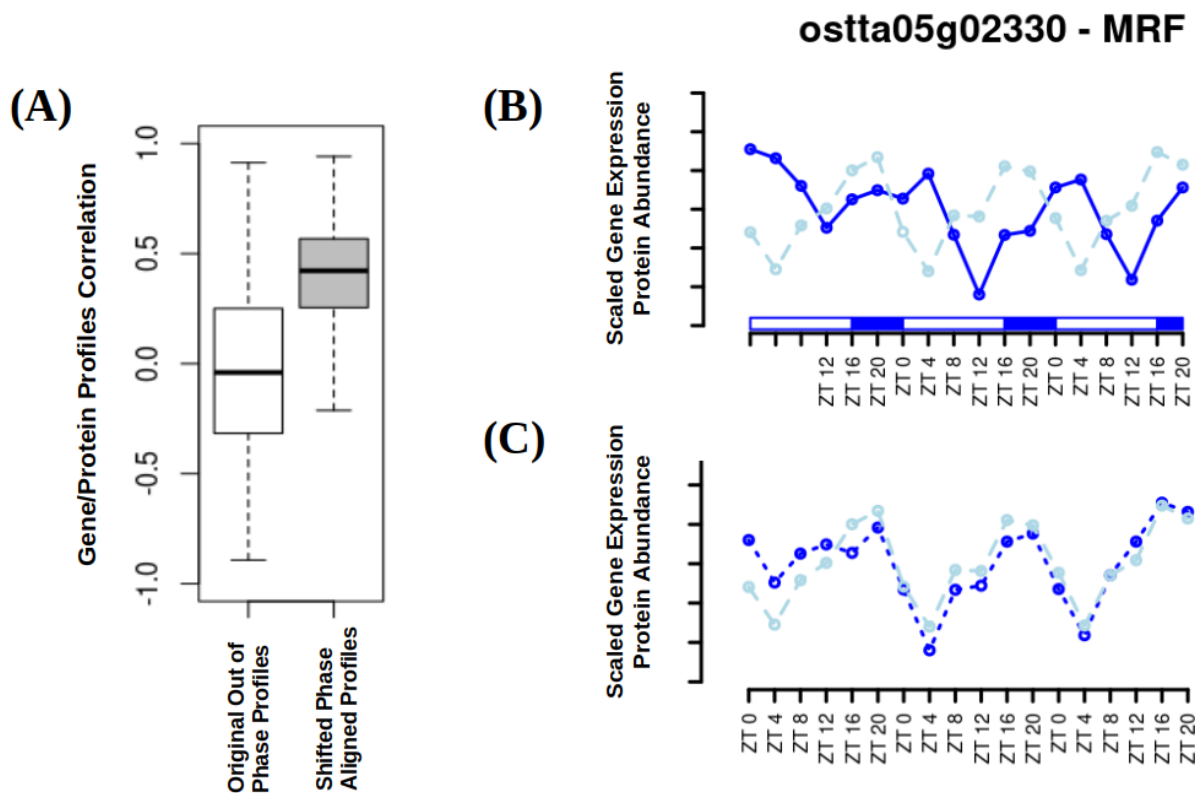


Figure 36: Protein/gene correlation analysis. (A) Boxplots representing the global distribution of the correlations between protein abundance and gene expression profiles (white box) and shifted aligned profiles with coincident phases (grey); (B) Protein abundance (continuous blue line) and gene expression (dashed light blue line) profiles under LD conditions for MA3 domain-containing translation Regulatory Factor (ostta05g02330, MRF); (C) Phase aligned protein abundance (dotted blue line) and gene expression (dashed light blue line) profiles.

Phase offsets between genes and proteins involved in the same biological process are adjusted by seasons

In order to obtain a deeper understanding of transcript/protein phase offsets, an extensive analysis of its correlation with different factors and protein properties was carried out.

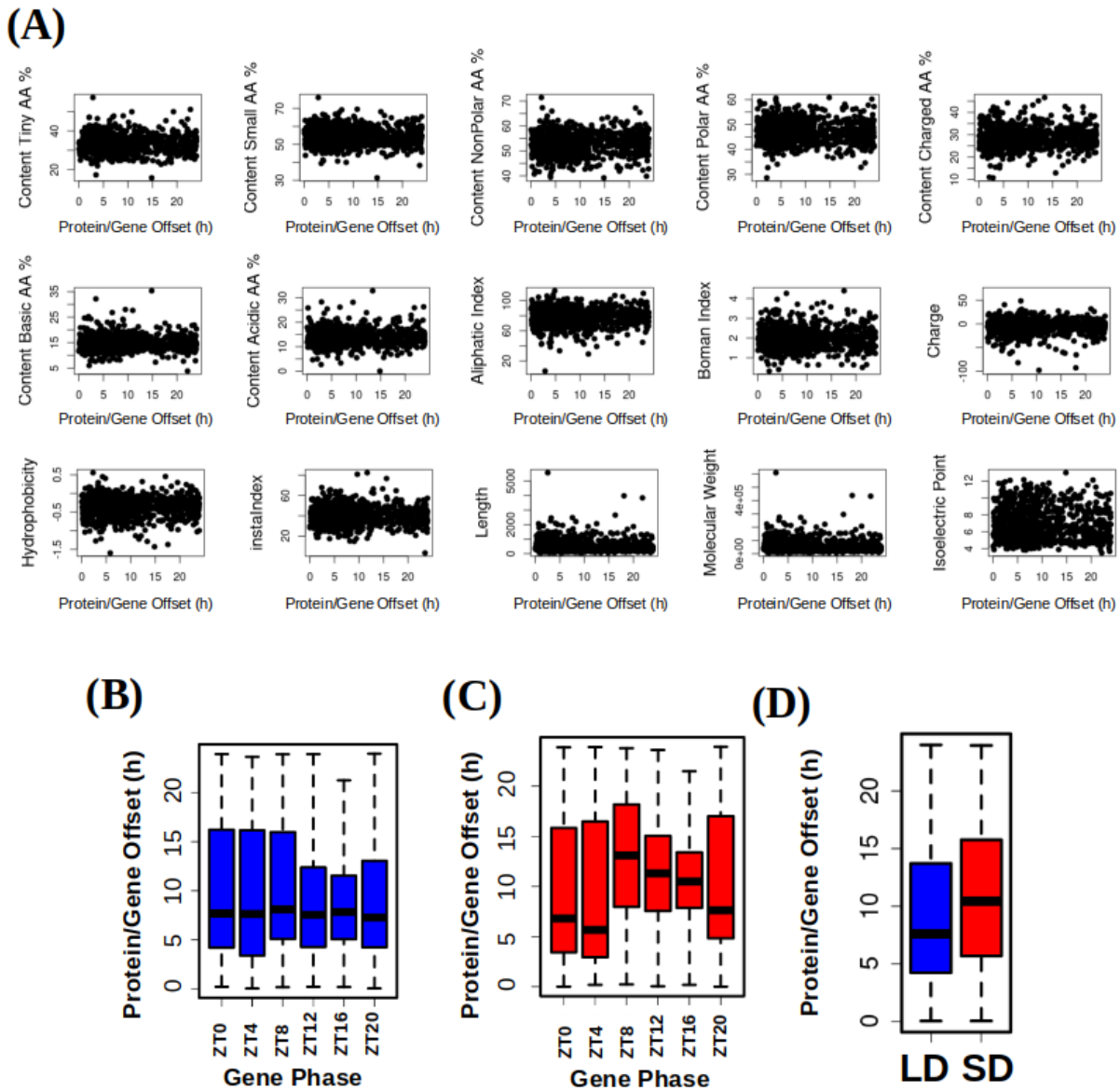


Figure 37: Analysis of transcript/protein offsets correlation with protein properties, gene phase and photoperiod of entrainment. (A) Scatter plots where each dot stands for a protein, x-coordinates represent protein/gene offsets and y-coordinates different protein indexes or properties computed from their sequences such as amino acid composition, charge and hydrophobicity; (B-C) Boxplot representing protein/gene offsets under LD (B) and SD (C) for different gene sets with specific phases or maximum expression time points; (D) Boxplot representing the offset in hours between protein abundance and gene expression phases under LD (blue) and SD (red) conditions.

One of the possible hypothesis was that transcript/protein offsets depended on common indexes or properties computed from protein sequences such as amino acid composition, charge or hydrophobicity. However, no relation is detected between any protein index and protein/gene offsets (Fig. 37-A).

Another of the possible hypothesis was that transcript/protein offsets depend on the time when the maximum gene expression level is reached (gene phase). For example, a gene that reaches its maximum level of expression during the morning could take less time to translate than a gene which peak of expression takes place in the middle of the night. However, under LD conditions, no significant differences are found when comparing transcript/protein offsets of different genes sets with specific phases (Fig. 37-B). Nonetheless, under SD condition transcript/protein offsets were significantly longer for transcripts peaking during the skotoperiod, ZT8, ZT12, ZT16 and ZT20, when compared to those genes with transcript phases during the photoperiod, ZT0 and ZT4 (Fig. 37-C). In addition, our analysis revealed that seasonal variations in photoperiod length affected transcript/protein offsets. In fact, global protein/gene offsets were significantly longer under SD conditions with respect to LD conditions according to a p-value of 1.2×10^{-9} computed using Mann-Whitney-Wilcoxon test (Fig. 37-D).

Nonetheless, the key factor associated to differences in transcript/protein offsets identified in our analysis was the specific biological process in which the corresponding protein is involved according to Gene Ontology annotation. In order to explore this, the average transcript/protein offset of each GO term is computed for both light/dark cycles of entrainment (Fig. 38-A). Specifically, the most representative biological processes with short offsets were DNA replication and photosynthesis both under LD and SD conditions (Fig. 38-B,D). Whereas, a process involved in translation was the most representative one exhibiting long transcript/protein offsets (Fig. 38-C,D). This finding could indicate the existence of a differential post-transcriptional regulation under diel cycles for each specific biological process.

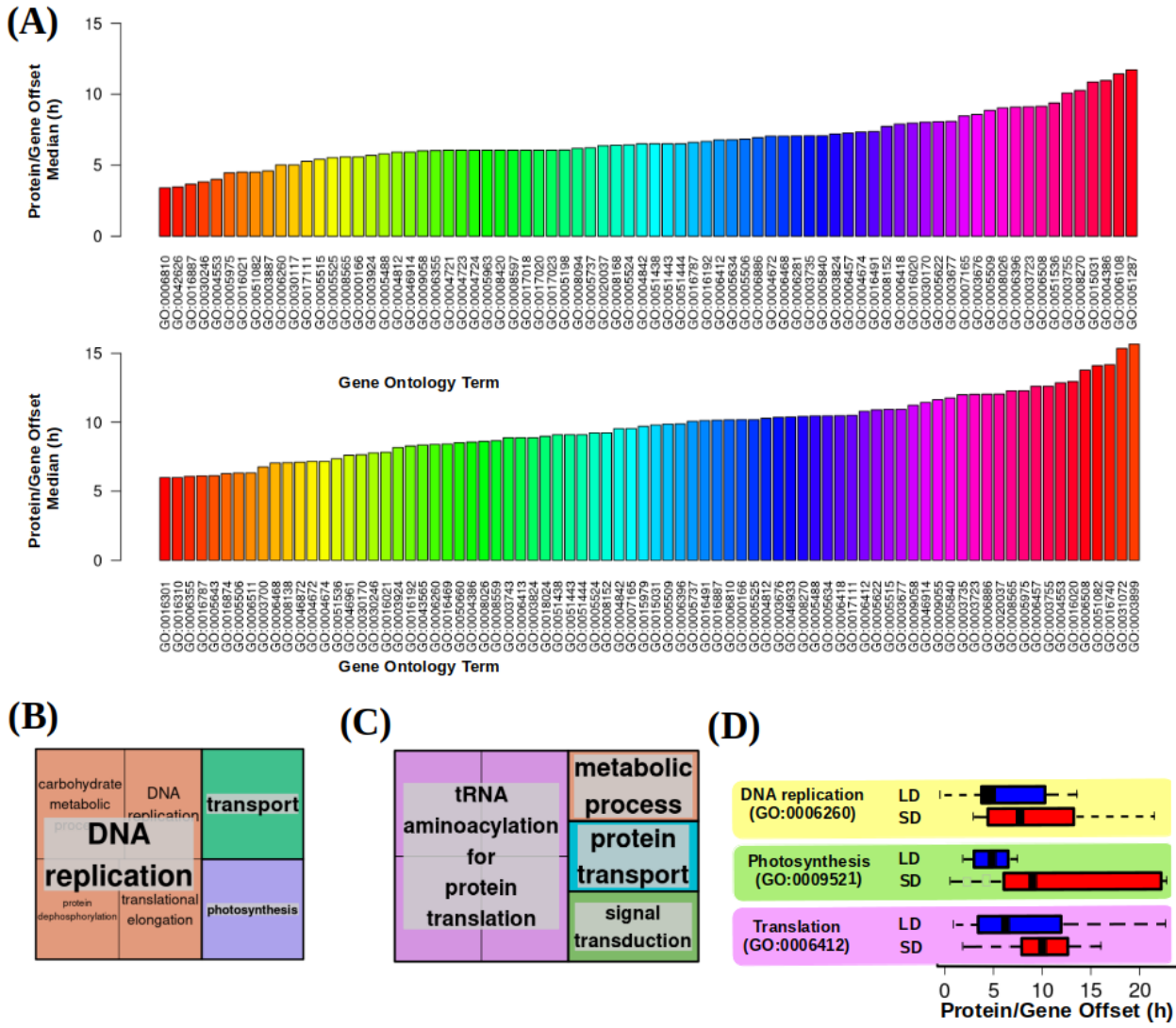


Figure 38: Analysis of transcript/protein offsets correlation with their biological function. (A) Median protein/gene offset for gene sets annotated with the same Gene Ontology (GO) term under LD condition (top) and SD condition (bottom). (B-C) Treemaps summarizing the biological processes with shortest protein/gene offsets: (B) and with longest protein/gene offsets (C); (D) Boxplot illustrating how genes involved in different biological processes according to their gene ontology (GO) annotation present distinct protein/gene offsets that are longer under SD (red) than LD (blue) conditions. DNA replication (GO:0006260), photosynthesis (GO:0009521) and translation (GO:0006412) are chosen as examples exhibiting short and long protein/gene offsets.

As it was discussed in the previous chapter, phase shifts globally observed over the transcriptome of *Ostreococcus tauri* as an adaptation to seasonal cycles, not only consist in anticipating processes but also in a re-arrangement in the sequential order of the diel gene activation program (Fig. 32). In fact, photosynthesis is simply anticipated when transferred to SD and amino acid biosynthesis, ribosome biogenesis and translation were complexly

re-arranged in time. Now, at the proteomic level it was observed that the different biological processes present distinct short or long offsets under both photoperiods (Fig 38-A).

One of the processes with the shortest transcript/protein offsets is, in fact, photosynthesis (Fig. 38-B,D). Some proteins involved in photosynthesis present a high turnover rate (Critchley & Russell, 1994; Nelson et al., 2014; Nelson & Millar, 2015), which can be preserved with short times between gene expression and translation. Genes involved in photosynthesis reach their maximum of expression during high irradiance hours, presenting a simple anticipation in time or phase shift between seasons (Fig. 32). The activation of this set of genes is strategically placed at that time of the day taking in count their short transcript/protein offset, so no further anticipation to the high irradiance hours is needed. In addition, translation is identified as one of the biological processes with larger transcript/protein offsets (Fig. 38-C,D). This process has been highlighted in the previous chapter for being one of the processes that are re-arranged in time over the diel gene activation program between seasons (Fig. 32), which could be linked to the long transcript/protein offset that it presents.

This two observations suggest that *Ostreococcus tauri* severely reorganize its transcriptional temporal program taking into account not only the current photoperiod but also the different transcript/proteins offsets that each biological function presents. In that way, every biological process is re-arranged in a certain time of the day ensuring that proteins will be ready in the exact time when they are needed, even compensating the long transcript/proteins offset.

Chapter 4: diel and seasonal multi-omic integration with physiological data.

In the last two chapters, an in-depth analysis and discussion have been carried out on biological rhythms described by proteins and mRNAs. Distinct behaviors between the proteome and the transcriptome, with evident time offsets and even instances of completely divergent patterns have been identified. These observations emphasize the significance of both transcriptional and post-translational regulation in governing biological rhythms. In order to attain a comprehensive understanding of how biological processes are regulated by diel and seasonal cycles, it is imperative to integrate not only the above mentioned multi-omic data but also the dynamics of physiological processes. Such integration serves not only as a biological validation of computational omics analysis but also as a crucial component in unraveling the intricate puzzle that biological systems present.

Cell Division Cycle (CDC) of *Ostreococcus tauri* under diel and seasonal cycles

The cell division cycle (CDC) is a highly regulated sequence of processes that govern cell proliferation, ranging from unicellular organisms to tissue renewal, and is conserved across eukaryotes. The impact of diel cycles on cell division has been studied in various phyla, including plants and microalgae such as *Chlamydomonas*, *Euglena* and *Gonyaulax* (Bruce, 1970; Edmunds & Laval-Martin, 2019; Fung-Uceda et al., 2018; Homma & Hastings, 1989) as well as in mice and humans (Fu et al., 2005; Matsuo et al., 2003).

Nevertheless, the confirmation that circadian regulation controls cell division has been a topic of controversy in some organisms, such as the common microalgae model organism, *Chlamydomonas reinhardtii*. While some studies have concluded that the cell division cycle of this microalgae is subject to circadian regulation (Bruce, 1970), others have proposed that the observed periodicity is linked to cyclic changes in energy status, resulting from circadian regulation of photosynthesis (Spudich & Sager, 1980).

Currently, it is widely accepted that this biological rhythm provides evidence of direct regulation by the circadian clock in nearly all organisms, including photosynthetic ones. It persists under free-running conditions and presents the ability to synchronize with different photoperiods (Roenneberg & Merrow, 2005), regardless of photosynthetic capacity. The

cell division cycle, therefore, possesses a complex regulatory mechanism comprising robust circadian clock regulation as well as light-dependence in photosynthetic organisms, since light serves as their primary energy source. (Goto & Johnson, 1995; Hagiwara et al., 2002; Moulager et al., 2007, 2010). In line with the results presented in Chapter 2, the expression patterns of DNA replication genes remained rhythmic under constant light , while rhythmicity was disrupted (Roenneberg & Merrow, 2005) under constant darkness (Fig. 23, Appendix 5-6). This observation supports the notion that a light stimulus is necessary to sustain rhythmicity under free-running conditions, which is in agreement with the complex regulatory mechanism that the cell division cycle (CDC) present in photosynthetic organisms.

The CDC of *Ostreococcus* follows the typical phases of a simple binary fission. Initially, there is a Gap 1 (G1) phase that is dependent on the light-energy status, during which the cell undergoes growth and commitment occurs (Moulager et al., 2007). In cell division cycle studies, the term commitment refers to the moment when the cell, taking into consideration its energy status, decides whether is ready or not to continue with the progression of the cell division cycle. Once cells are committed, cell division is not impaired by darkness. Consequently, if commitment is achieved, G1 phase is followed by the DNA Synthesis or S phase where DNA replication takes place. The initiation of the S phase is typically timed several hours after sunrise (Moulager et al., 2007, 2010). After DNA replication is completed, cells enter the final Gap 2 and Mitotic (G2|M) phase, where they prepare for cell division (G2) and undergo mitosis (M). These two phases are often considered together since they are the shortest and most challenging to distinguish using common techniques.

In all eukaryotes, the progression of cells through the cell division cycle is controlled by cyclins and cyclin-dependent kinases (CDKs). *Ostreococcus tauri* possesses an extremely limited set of cyclins and CDKs, with only a single copy of each gene (Robbens et al., 2005). Additionally, the genome of *Ostreococcus* contains a canonical cell division control protein 25 (CDC25), which is not present in plants (Khadaroo et al., 2004), and a plant-specific CDKB (Corellou et al., 2005).

In the preceding chapters, genes and proteins involved in DNA replication (S phase) have been highlighted several times. Now, in order to validate these observations, an estimation of the distribution of cells in each phase over diel cycles is conducted. This integration un-

veils the adaptation of the cell division cycle in *Ostreococcus* to different seasons and contributes to unraveling the molecular mechanisms of circadian regulation of cell division in microalgae.

Temporal program of cell division cycle under summer and winter photoperiod

The phases of the cell division cycle were determined by estimating the DNA content of cells through flow cytometry, and the division of chloroplasts was observed using fluorescence microscopy, as outlined in Materials and Methods section. The rhythmicity analysis was conducted using data obtained from three days in a row under light-dark cycles.

Table 8: Percentage of cells in G1, S and G2|M phases in each time point under LD conditions.
The p-values as a result of the significant rhythmicity analysis are included in the lowest row.

Time	% of cells			
	G1	S	G2 M	
1 st day	ZT00	69,6	7,03	18,6
	ZT04	73,4	5,62	16,4
	ZT08	82	4,1	11,2
	ZT12	78,4	10,7	10,6
	ZT16	58,5	18,2	21,7
	ZT20	56,4	17,4	22
2 nd day	ZT00	68,8	6,65	19,3
	ZT04	76,2	7,19	13,6
	ZT08	79,5	5,85	13,7
	ZT12	72,6	9,7	13,8
	ZT16	70	9,98	17,6
	ZT20	65,2	13,9	18,5
3 rd day	ZT00	70,5	5,67	21,5
	ZT04	73,1	5,75	18,8
	ZT08	76,1	3,75	19
	ZT12	73,6	7,01	16
	ZT16	64,8	10,4	19,1
	ZT20	67,2	12,6	17,8

Rhythmicity p-value 9,14x10⁻⁶ 4,45x10⁻⁵ 1,53x10⁻³

Table 9: Percentage of cells in G1, S and G2|M phases in each time point under SD conditions.
The p-values as a result of the significant rhythmicity analysis are included in the lowest row.

		% of cells		
Time		G1	S	G2 M
1 st day	ZT00	75,5	4,34	17,5
	ZT04	79,6	2,52	16,4
	ZT08	74	4,24	18,8
	ZT12	68,4	10,3	16,9
	ZT16	71,4	8,41	17,5
	ZT20	69,8	5,87	22,1
2 nd day	ZT00	71,9	5,31	20,2
	ZT04	75,1	6,54	16,2
	ZT08	76,3	5,05	14,5
	ZT12	68,5	10,7	17,4
	ZT16	67,2	8,72	21,4
	ZT20	71,1	9,85	14,7
3 rd day	ZT00	71,3	9,4	16,7
	ZT04	76,5	6,19	14,4
	ZT08	72,6	6,59	17,7
	ZT12	67,1	13,1	15,6
	ZT16	65,2	13,4	17,5
	ZT20	68,1	8,29	18,9
Rhythmicity p-value		9,07x10 ⁻⁶	8,69x10 ⁻⁴	6,42x10 ⁻²

During the summer photoperiod, the G1, S, and G2|M phases exhibit noteworthy rhythmic profiles, with p-values of $9,14 \times 10^{-6}$, $4,45 \times 10^{-5}$ and $1,53 \times 10^{-3}$, respectively (Table 8). Conversely, under the winter photoperiod, only the G1 and S phases demonstrate significant rhythmicity, with p-values of $9,07 \times 10^{-6}$ and $8,69 \times 10^{-4}$, respectively. Consistent with the findings from transcriptomic and proteomic analyses, a decline in synchronization, characterized by a reduction in amplitude, is evident under the winter photoperiod (Fig. 39-A). Notably, the reduction in amplitude is so substantial in the G2|M phase that the RAIN package used in the rhythmicity analysis fails to detect a rhythmic profile. These observations suggest that the cell division cycle of individual cells within the culture is more synchro-

nized during the summer photoperiod, which aligns with the higher synchronization during summer photoperiod that has been also found at the transcriptomic level in Chapter 2 (Fig. 28-A,C).

The few hours of light also seem to have a direct effect on the progression of the cell cycle, since a significant reduction of approximately 24% in the number of committed cells is observed under winter photoperiod. Additionally, significant backward shifts of approximately 4 hours were observed in the cell cycle phases under winter photoperiod (Fig. 39-A). These observations are consistent with the observed backward shifts in the time points when transcript abundances reach their maximum levels in response to photoperiod shortening (Fig. 28-C).

The mean percentage of cells involved in G1, S and G2|M phases was calculated for each time point, allowing the characterization of the temporal progression of the cell division cycle in *Ostreococcus* under different photoperiods (Fig. 39-B,C). Under summer photoperiod, G1 phase predominantly occurs during the light hours, with the maximum percentage of cells in this phase coinciding with the maximum irradiance hours (around ZT8). After commitment, the percentage of cells in G1 phase gradually decreases, while the percentage of cells in the S phase increases. The majority of cells are in the S phase around sunset and the first part of the night (ZT16-ZT20). Subsequently, the percentage of cells in the G2|M phase gradually rises as DNA duplication is successfully accomplished. The transition from the G2|M to G1 phase, which indicates the completion of cell division, takes place during the first part of the morning (ZT4). This indicates that cell division in *Ostreococcus* mainly takes place after sunrise in summer photoperiod (Fig. 39-B).

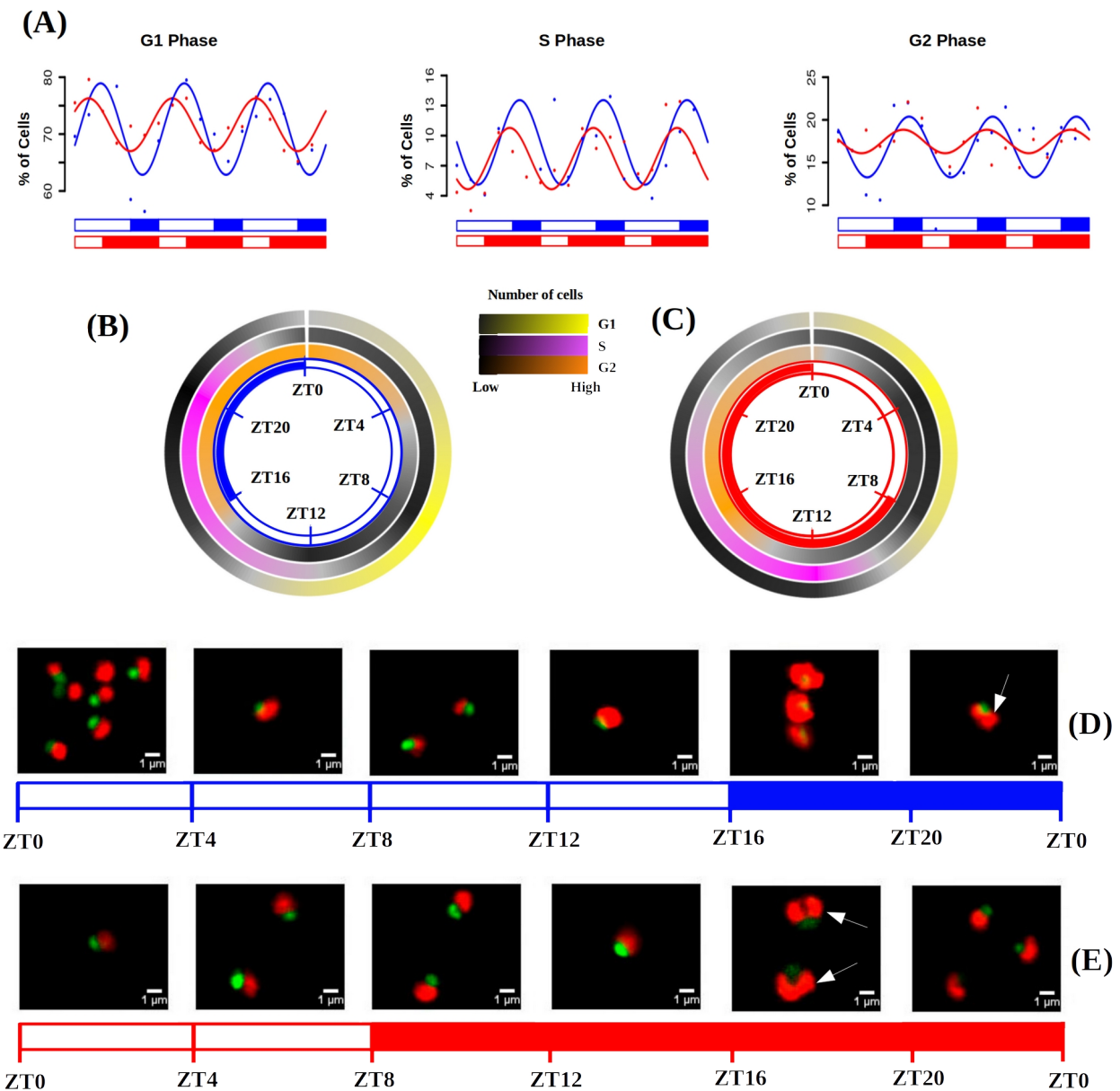


Figure 39: Cell division cycle (CDC) of *Ostreococcus tauri* under summer and winter photoperiod. (A) Percentage of cells in G1, S and G2|M phases during the three days of sampling. Points correspond to real data and lines represent waves approximations made by Circacompare during the rhythmicity analysis; (B-C) Circular heatmap representing mean percentage of cells in G1, S and G2|M phases during summer and winter photoperiod, respectively; (D-E) Photographs of cells under the fluorescence microscope. Each photograph correspond to a different time point of summer and winter photoperiod, respectively. Nucleus are dyed and they fluorescence in green, chloroplast in red. White arrows point cells that posses two chloroplasts due to chloroplast division prior to cell division.

During the winter photoperiod, consistent with the observations made in the summer photoperiod, the G1 phase coincides with maximum irradiance hours (ZT4 in winter photoperiod) and the S phase occurs 4 hours after sunset (around ZT8). However, the G2|M phase

not only adapts to the photoperiod but also undergoes a reorganization to anticipate the limited daylight hours ahead. In the winter photoperiod, the G2|M phase exclusively occurs during the night-time. As soon as the sun rises, cell division is completed, allowing cells to undergo growth in the morning. These findings suggest that the cell division cycle is strongly influenced by the circadian clock and can anticipate cyclic changes, such as the reduced duration of light during the winter photoperiod. To ensure this anticipation, the circadian clock ensures that all cells enter the G1 phase precisely at sunrise, maximizing the utilization of available daylight hours (Fig. 39-C).

This anticipation is also observed in chloroplast division. Under summer photoperiod, chloroplast duplication is achieved during the latter part of the night (ZT20) (Fig. 39-D), while under the winter photoperiod, it takes place at ZT16. Before sunrise, a substantial number of cells already possess only one chloroplast during the winter photoperiod (Fig.

Integration of CDC program with transcriptomic and proteomic data.

Ostreococcus tauri annotated genes involved in cell division cycle were organized in three different groups in order to mark in which phase of the cell cycle they are present, according to the current cell cycle model in plants (Carneiro et al., 2021).

Table 8: Proteins that are present during the G1 phase of the cell division cycle in *Ostreococcus* and the corresponding genes that encode them.

Gene IDs	Protein names
ostta18g01570	CYCD
ostta04g00110	CDKA
ostta04g01050	CDC6
ostta16g02100	Rb
ostta02g01950	E2F
ostta10g01190	Dp
ostta08g02940	DEL
ostta04g05220	ORC1
ostta15g02820	ORC2
ostta11g01820	ORC3
ostta03g02760	ORC5

Cyclin D and CDKA are present specifically during the first part of the G1 phase. Therefore, they are considered essential proteins associated with G1, facilitating the transition between G2|M to G1 phase and, thus, the progress of the cell cycle. Transcription factors like E2F and Dp as well as other proteins (Rb, cell division control protein 6 and ORCs) are also involved in G1 phase, playing a crucial role in the activation of genes associated with the S phase (Table 8). In order to start the S phase is required the presence of the Cyclin A (CYCA). Concurrently, there is a coordinated synthesis of polymerases and replication-related proteins (such as MCM complexes, replication factors, PCNA, primases, helicases, ligases, and others) that are essential for DNA replication (Table. 10). The onset of the G2|M phase is marked by the presence of Cyclin B (CYCB), along with subunits of the anaphase-promoting complex (APC) and cell division control proteins (CDC20 and CDC25) (Table. 9) (Carneiro et al., 2021; Moulager et al., 2007, 2010; Robbens et al., 2005).

Table 9: Proteins that are present during the G2|M phase of the cell division cycle in Ostreococcus and the corresponding genes that encode them.

Gene IDs	Protein names
ostta01g06150	CYCB
ostta15g00670	CDKB
ostta06g02700	APC1
ostta11g00730	APC2
ostta06g00360	APC3
ostta02g03470	APC4
ostta06g04290	APC5
ostta01g01000	APC6
ostta07g02520	APC8
ostta10g02910	APC10
ostta11g03040	APC11
ostta04g04580	Cdc20
ostta02g03080	Cdc25
ostta13g02370	CDH1
ostta08g02230	FTSZ1
ostta07g01610	FTSZ2

Table 10: Proteins that are present during the S phase of the cell division cycle in *Ostreococcus* and the corresponding genes that encode them.

Gene IDs	Protein names
ostta02g00150	CYCA
ostta11g00910	MCM2
ostta02g00690	MCM3
ostta14g01050	MCM4
ostta11g01760	MCM4-2
ostta04g00450	MCM5
ostta01g02580	MCM6
ostta02g02010	MCM7
ostta12g01020	MCM8
ostta14g01690	GINS1
ostta02g00490	PSF2
ostta16g02410	GINS3
ostta04g00390	SLD5
ostta02g00500	RFC1
ostta02g00555	RFC2
ostta09g00990	RFC4
ostta07g02710	RFA
ostta02g03430	DNA polymerase II
ostta05g00150	DNA polymerase III γ
ostta08g00710	DNA polymerase α
ostta11g01400	DNA polymerase α
ostta11g01400	DNA polymerase α
ostta07g02610	DNA polymerase δ
ostta08g03680	DNA polymerase α/ϵ
ostta12g00110	DNA polymerase α/ϵ
ostta11g01840	DNA polymerase ϵ
ostta06g02890	PCNA
ostta08g01110	DNA primase
ostta11g00940	DNA primase
ostta13g02040	DNA primare
ostta08g02290	XPG
ostta10g00340	DNA helicase
ostta10g00640	DNA ligase
ostta13g01140	RPA replication protein A
ostta10g00670	Wee1
ostta07g01870	Cks

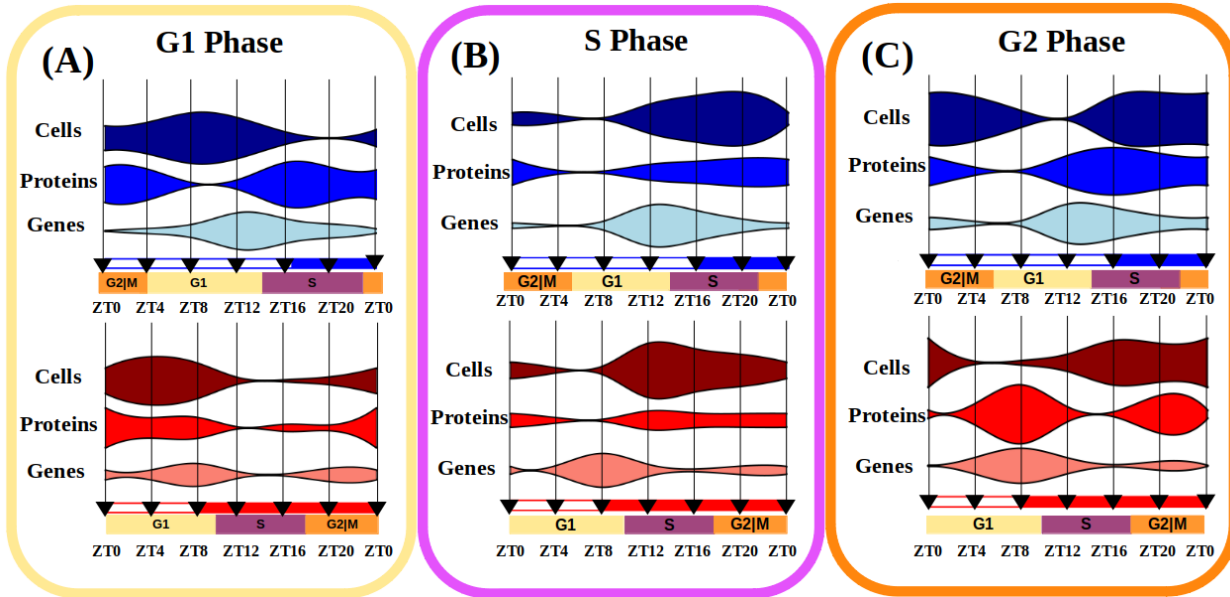


Figure 40: Integration of gene expression, protein abundance and cell population profiles for each phase of the cell cycle. Violin plots represent the three molecular levels studied: “Genes” for transcriptomic data, “Proteins” for proteomic data and “Cells” for DNA content estimation by flow cytometry. (A) Involves G1 phase related data, (B) S phase and (C) G2 phase.

The gene expression and protein abundance profiles are compared with the percentage of cells in the respective phase of the cell cycle in which these genes and proteins are present (Fig. 40). In addition to the globally observed gene-protein offset, an overall offset is also observed between protein abundance and the execution of their physiological role. Notably, this offset appears to be more pronounced in certain phases such as G1 or G2|M (Fig. 40-A,C). However, during the S phase, once the proteins are available, the corresponding biological processes are promptly executed, resulting in a shorter offset between protein and physiological execution (Fig. 40-B). It could be explained by the experimental design followed, since proteins included in the S phase set are directly involved in DNA replication and flow cytometry directly detect cell division phases based in the estimation of DNA content.

The transcriptomic and proteomic data for cyclins and CDKs found in *Ostreococcus* (Fig. 41) align with the current cell cycle model for plants (Carneiro et al., 2021). In both summer and winter photoperiods, the transcription of the CYCA, that will trigger the start of the S phase, occurs during the G1 phase and it is the first cyclin to be activated. It has been suggested that Cyclin A is predominantly regulated by the circadian clock, as it has been shown to be independent of metabolic status (Moulager et al., 2010). Consistent with

those findings and previous transcriptomic analyses (Carneiro et al., 2021; Moulager et al., 2007), the expression of Cyclin A (during G1 phase) present a strongly rhythmic expression profile that is followed by the expression of Cyclin B (during the S phase) (Fig 41-A).

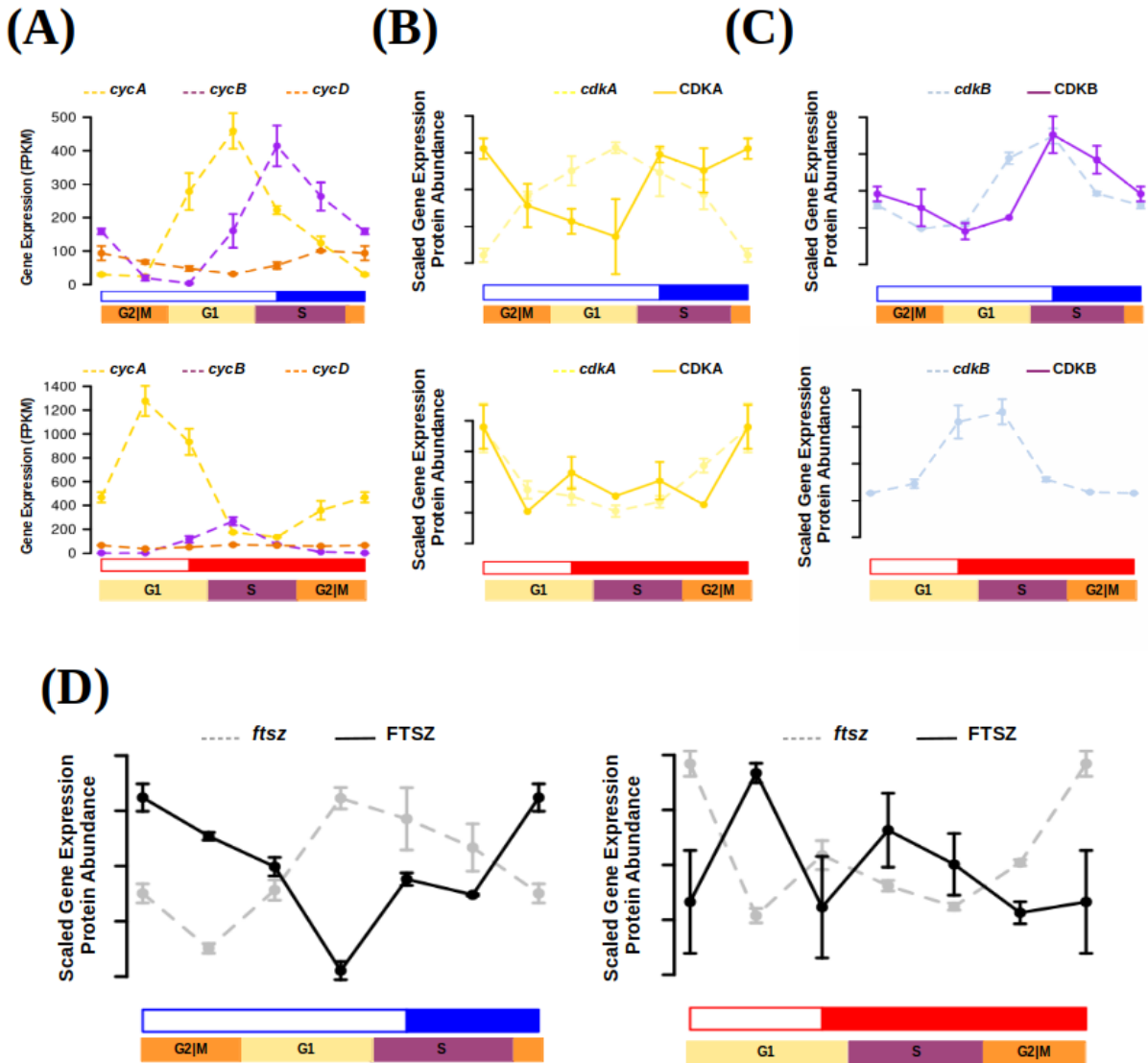


Figure 41: Transcript and protein abundance profiles of the main cell cycle proteins under summer and winter photoperiod in *Ostreococcus tauri*. (A) Expression level of cyclins A (yellow), B (purple) and D (orange) genes are represented with discontinued lines under summer (blue) and winter (red) photoperiods; (B-C-D) Transcript (discontinued line) and protein (solid line) abundances of CDKA are represented in yellow (B), CDKB in purple (C) and FTSZ in black (D).

Cyclin proteins were not detected in our proteomic analysis, but CDKA and CDKB protein abundance profiles are detected and their abundance profiles align with the proposed model (Carneiro et al., 2021). The expression of CDKA encoding gene reaches its maximum level during G1, preceding an increase in CDKA protein abundance during the latter

part of the G1 phase (Fig. 41-B). This increase, in conjunction with Cyclin A, facilitates the progression of the cell cycle into the S phase. During the S phase, the abundance of CDKB protein reaches its maximum level (Fig. 41-C), coinciding with Cyclin B transcript levels. The transcript levels of Cyclin D are relatively low under both photoperiods, but their peak of expression aligns with the G2|M phase (Fig. 35-A). Genes involved in chloroplast division, such as Filamentous Temperature-Sensitive Z (FtsZ, ostta07g01610), play central roles in the G2|M phase. It represents a crucial protein that has been conserved from its cyanobacterial ancestors (TerBush et al., 2013). FtsZ present protein peaks reached during the transition S/G2|M phase (at sunrise, ZT0, in summer photoperiod and during the night, ZT16, in winter photoperiod) (Fig. 41-D). Confocal microscopy images validated these findings by identifying cells with two chloroplasts as a result of recent divisions at ZT20 under LD condition and ZT16 under SD condition (Fig. 39-D,E).

Diel and seasonal rhythm of photosynthesis in *Ostreococcus tauri*

Photosynthesis constitutes a fundamental process for plants, wherein oxygen (O_2), adenosine triphosphate (ATP), and reduced nicotinamide adenine dinucleotide phosphate (NADPH) are generated from water (H_2O) and light. The generated oxygen is released into the atmosphere, while ATP serves as an essential energy source for cellular processes. Moreover, NADPH plays a crucial role as a reducing agent, facilitating assimilatory processes such as the Calvin cycle, which mediates the assimilation of atmospheric carbon dioxide (CO_2) into organic carbon compounds.

Within the genome of *Ostreococcus tauri*, all the indispensable proteins implicated in the electron transport chain of photosynthesis and carbon fixation are present. However, the number of copies in *Ostreococcus* appears to be lower when contrasted with plants and other microalgae. Notably, the composition of light-harvesting complexes in *Ostreococcus* exhibits distinct characteristics. While light-harvesting complex proteins associated with photosystem I (LHCI) are present, LHCII are lacking. Instead, specific chlorophyll-binding proteins unique in prasinophytes are identified in *Ostreococcus* (Blanc-Mathieu et al., 2014; Derelle et al., 2006). This observation suggests the presence of LHCI within the green lineage from an evolutionary stage prior to *Ostreococcus* ancestors (Six et al., 2005).

Understanding how photosynthesis is adapted to diel and seasonal cycles can contribute to develop systems enhancing plants productivity, which is a relevant topic in agriculture. The circadian regulation of photosynthesis was initially documented in marine algae, with the observation of circadian oscillations in oxygen production (Dodd et al., 2014; Sweeney & Haxo, 1961). After that discovery, circadian oscillations in various physiological phenomena associated with photosynthesis, including chloroplast ATP concentration, electron transport rate, starch content, and photosynthetic efficiency, have been observed in microalgae (Mackenzie & Morse, 2011; Ral et al., 2006; Sorek et al., 2013; Sweeney & Haxo, 1961). Furthermore, circadian oscillations in photosynthesis have also been documented in agriculturally relevant plant species (Feugier & Satake, 2013; Lonergan, 1981; Tucker et al., 2004). Nowadays, the application of omics techniques has enabled the elucidation of 24-hour rhythmic oscillations in genes involved in photosynthesis and carbon fixation in both microalgae and plants (Ferrari et al., 2019).

In addition, this thesis represents the first instance of describing the maintenance of rhythmic expression profiles of genes involved in photosynthesis and carbon assimilation under varying photoperiods and free-running conditions (constant light and constant darkness) in *Ostreococcus tauri*. The genes involved in photosynthesis have been described as *bona fide* circadian genes in Chapter 2 due to their sustained rhythmic expression profiles during both summer and winter photoperiods, as well as under free-running conditions (Fig. 25-C,B, Appendix 11). Additionally, in Chapter 3, it has been observed that photosynthesis exhibits one of the shortest offset between gene expression and translation in *Ostreococcus tauri* (Fig. 38-B). These findings, derived from multi-omics analyses, are now validated with photosynthetic efficiency measurements under winter and summer photoperiods. This integration sheds light on the adaptation of photosynthesis, as well as other interconnected processes such as carbon fixation and starch metabolism in *Ostreococcus*, to accommodate varying seasonal conditions. Furthermore, it provides valuable insights about the conserved mechanisms governing circadian regulation and ultimately influencing photosynthetic productivity within the green lineage.

Rhythmic oscillations of photosynthetic efficiency under summer and winter photoperiod

Photosynthesis efficiency has been calculated using Pulse-Amplitude-Modulation (PAM) by estimating maximum quantum efficiency (F_v/F_m), a widely accepted metric to assess

the overall integrity and efficiency of Photosystem II (PSII). To determine the rhythmicity of photosynthesis, Fv/Fm measurements were obtained from samples collected under 3 consecutive light-dark cycles. Detailed explanations of data generation and analysis are provided in the Materials and Methods section.

Table 13: Fv/Fm obtained at each time point under Long Day and Short Day conditions. The p-values as a result of the significant rhythmicity analysis are included in the lowest row, for rhythms with 24 h and 12 h periods.

Time		Fv/Fm	
		LD	SD
1 st day	ZT00	0,584	0,490
	ZT04	0,603	0,525
	ZT08	0,607	0,556
	ZT12	0,582	0,455
	ZT16	0,572	0,423
	ZT20	0,575	0,484
2 nd day	ZT00	0,587	0,491
	ZT04	0,611	0,511
	ZT08	0,609	0,556
	ZT12	0,569	0,453
	ZT16	0,561	0,462
	ZT20	0,569	0,484
3 rd day	ZT00	0,587	0,486
	ZT04	0,597	0,526
	ZT08	0,611	0,561
	ZT12	0,591	0,459
	ZT16	0,577	0,481
	ZT20	0,572	0,485
Rhythmicity p-value	24 h period	7,07x10 ⁻⁶	2,7x10 ⁻¹¹
	12 h period	1	1,5x10 ⁻²

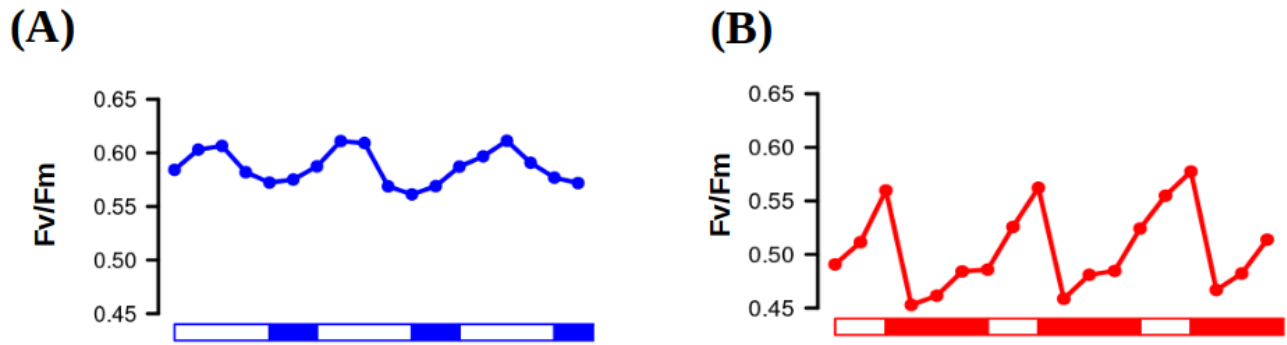


Figure 42. Photosynthetic efficiency rhythmic oscillations. Fv/Fm oscillating values used as an estimation of PSII performance and, thus, photosynthetic efficiency under three consecutive days of summer (A) and winter (B) photoperiods.

Under summer photoperiod, the Fv/Fm parameter exhibits an evident rhythmic profile with a 24 h period, displaying a significant p-value of 7.07×10^{-6} (Fig. 42-A). The maximum Fv/Fm value consistently occurs every 24 h during the maximum irradiance hours, around ZT8. This observation indicates that the photosystems operate at their highest efficiency during that specific time of the day, consequently enhancing photosynthetic efficiency. In contrast, the Fv/Fm profile under the winter photoperiod displays a rhythmic pattern with two peaks every 24 h (Fig. 42-B). Both peaks demonstrate significant periodicity every 12 hours, supported by a p-value of 1.5×10^{-2} . One of the peaks aligns with the Fv/Fm rhythmic profile observed under the summer photoperiod, occurring at ZT8 as well. Whereas the second peak represents a smaller increment in the Fv/Fm value, occurring more than 8 hours prior to sunrise. This finding suggests that the photosynthetic machinery in *Ostreococcus tauri* exhibits a circadian response, preparing itself in advance during the night to anticipate the limited daylight hours of the winter photoperiod. These outcomes underscore the ability of *Ostreococcus tauri* to anticipate cyclic variations in photoperiod, which is a widely accepted signal of robust circadian regulation (Roenneberg & Merrow, 2005).

Integration of photosynthesis efficiency rhythmic profile with multi-omics data

Photosynthesis is a complex process involving numerous proteins and different metabolic pathways strongly depend on its execution. It entails an electron transport chain consisting of three major protein complexes: Photosystem II, cytochrome b6f, and Photosystem I.

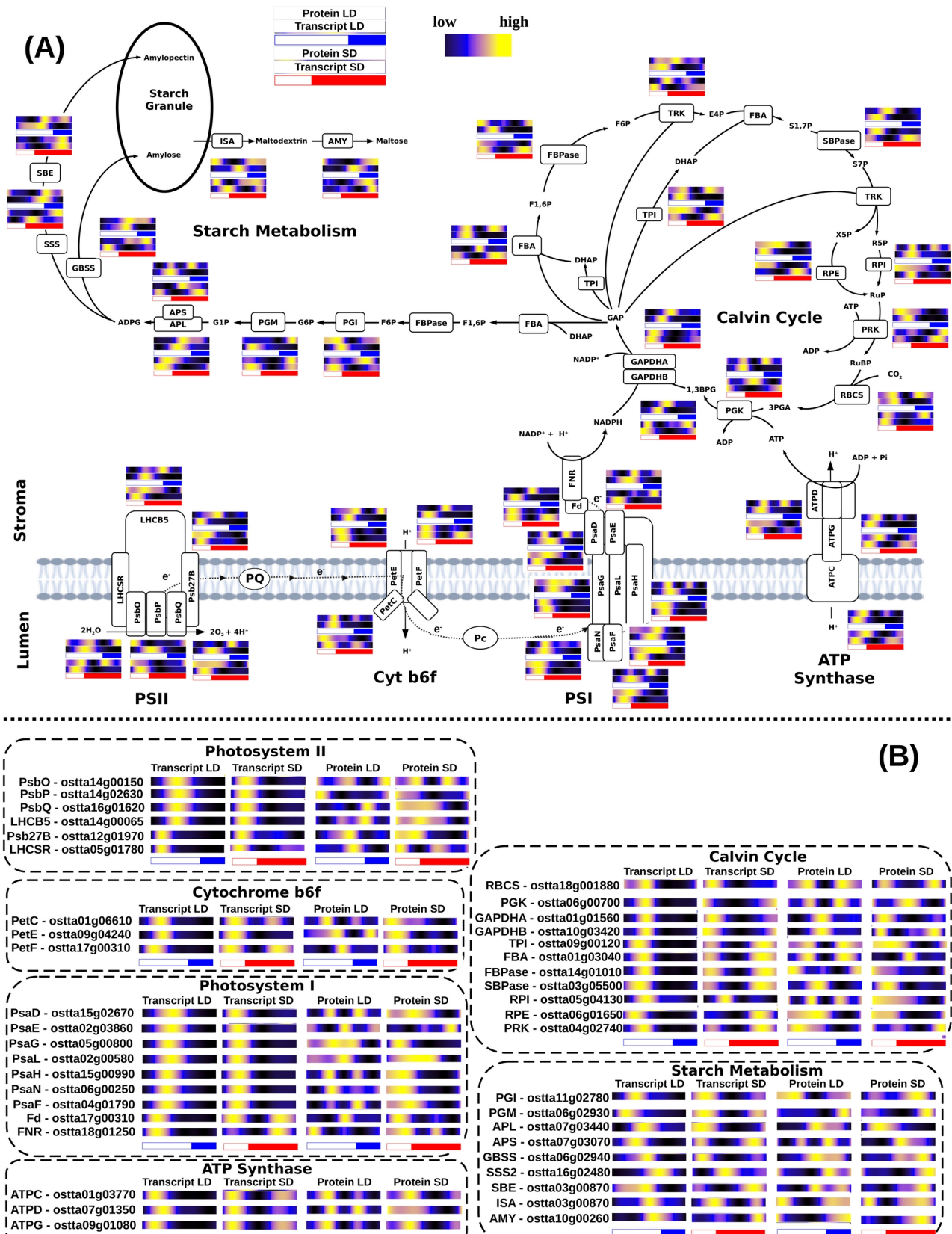


Figure 43: Integration of multi-omic data of enzymes and proteins involved in photosynthesis, Calvin cycle and starch biosynthesis. (A) Schematic representation of the mentioned metabolic pathways and (B) organized list of genes IDs involved in them, including protein abundance and gene expression profiles of each enzyme.

These complexes facilitate the transfer of electrons, generated through the cleavage of the water molecule to their final acceptor, NADP, generating the NADPH required for biosynthetic reactions. The energy derived from this transport enables the pumping of protons into the chloroplast lumen, ultimately leading to ATP synthesis as they return to the stroma via ATP synthase. NADPH and ATP are needed to fix CO₂ and generate carbon compounds within the Calvin cycle which can be stored as starch reserves (Fig. 43-A). In higher plants, the circadian clock participates in coordinating different physiological processes like photosynthesis, carbon fixation and starch biosynthesis (de los Reyes, Romero-Campero, Teresa Ruiz, et al., 2017; Farré & Weise, 2012; Graf et al., 2010). The Fv/Fm rhythmic profiles presented are now integrated with the proteomics and transcriptomics data of genes associated with the PSII, which are listed in Fig. 43-B. This integration provide a holistic understanding of how these processes respond to and anticipate to seasonal and diel cycles in *Ostreococcus tauri* (Fig. 43-44).

Under summer photoperiod, no temporal offsets were observed between the time points of maximum transcript and protein abundances and the highest Fv/Fm values (Fig. 44-A). The observations suggest that during the summer photoperiod, genes are promptly translated as soon as they are transcribed, leading to an increase in photosynthetic efficiency through *de-novo* protein synthesis. Conversely, during the winter photoperiod, as it was discussed in Chapter 3 (Fig. 38-D), there is a longer gene-protein temporal offset (Fig. 44-B). Consequently, the maximum photosynthetic efficiency occurs a few hours after the maximum gene expression level (Fig. 44-B). For example, the early increase in gene expression at the beginning of the night, observed in genes encoding components of the Oxygen Evolving Complex PSII subunits O, P and Q (PsbO, ostta14g00150; PsbP, ostta14g02630; PsbQ, ostta16g01620), among others, (Fig. 43-B) resulted in a corresponding increase in protein abundance and Fv/Fm values during the second half of the night with a ~4 h offset (Fig. 44-B).

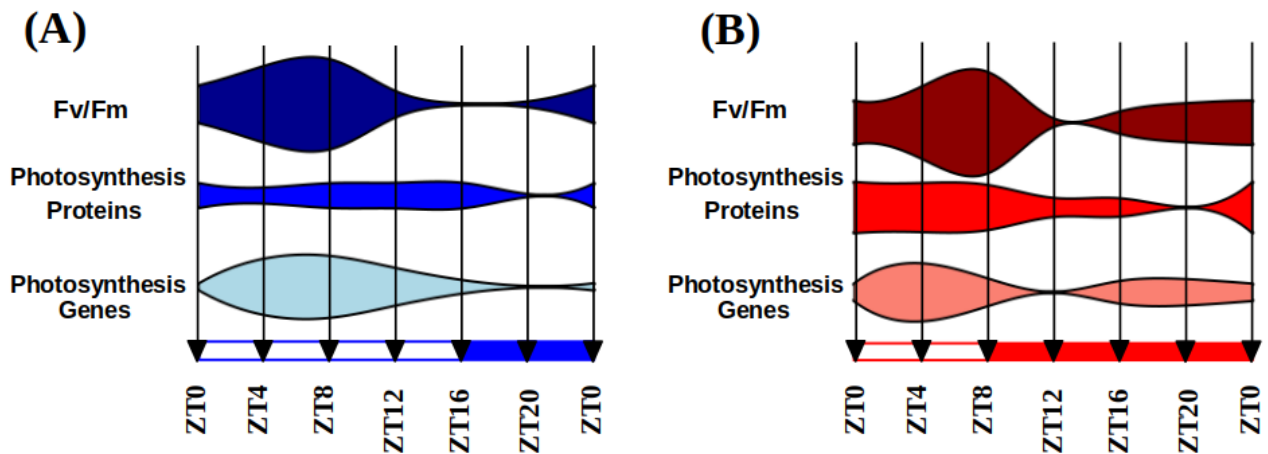


Figure 44: Integration of Fv/Fm oscillations with multi-omic data. Fv/Fm measurements are integrated with multi-omic data from proteins and genes related with photosynthetic efficiency under summer (A) and winter (B) photoperiod.

Rhythmic profiles with a 12-hour period (two peaks every 24 hours) are observed not only in Fv/Fm but also in the gene expression profiles under the winter photoperiod (Fig. 44-B). Profiles with two peaks under SD condition were found in genes such as Protein Electron Transfer C (PetC, ostta01g06610), Ferredoxin (Fd, ostta17g00310) and ATPase delta sub-unit (ATPD, ostta07g01350) coding for key components of Cytochrome b6f, Photosystem I and ATP Synthase (Fig. 43-B). These genes constitute examples of the emergence of two peaks under SD condition, one induced by the photoperiod maintained only under LL and the other one induced by the skotoperiod maintained only under DD (Fig. 29). Specifically in photosynthesis, one expression peak occurs during the early morning, enhancing photosynthetic efficiency during the hours of maximum irradiance. The second expression peak takes place during the night, inducing the anticipation of the photosynthetic machinery before sunrise. These findings suggest that the response of the photosynthetic machinery in anticipation to the photoperiod is transcriptionally regulated in *Ostreococcus tauri* and likely established since early in the green lineage.

In general, genes involved in photosynthesis electron transport chain and Calvin cycle are consistently expressed early in the morning, under both summer and winter photoperiods (Fig. 43-B). The expression of those genes seems to be unaffected by the photoperiod, since it has been also observed in *Ostreococcus* under a neutral photoperiod, consisting in 12h of light and 12h of dark cycles (Monnier et al., 2010). In fact, genes coding for key components on the Calvin Cycle such as Glyceraldehyde-3-phosphate dehydrogenase A

(GAPDHA, ostta01g01560) and Fructose-1,6-bisphosphate aldolase (FBA, ostta01g03040) are examples of *bona fide* circadian genes exhibiting rhythmicity under both summer and winter photoperiods, as well as free-running conditions of constant light and constant darkness (Appendix 11).

Not only the genes coding for PSI, PSII and antenna complexes exhibit 12 h period expression profiles during winter photoperiod. Numerous genes, involved in Calvin cycle and starch metabolism exhibit these expression profiles as well (Fig. 43-B). It suggests that the transcriptomically regulated anticipation to the short light hours during winter photoperiod is not limited to photosynthesis efficiency. Instead, it is found systematically in the complete metabolic interaction of all processes related with photosynthesis, including not only the electron transport chain but also the Calvin cycle and starch metabolism.

In addition, protein abundance rhythmic profiles with 12h period are observed under summer photoperiod systematically along numerous genes listed in Fig. 43-B. The secondary peaks observed in these proteins are not induced by an increment in the transcription level of their corresponding gene (Fig. 43-B). This phenomenon has been previously observed in RuBisCO small subunit (RBCS) protein abundance profile in plants during neutral photoperiod. Multi-omics integration of the results presented in this thesis shows that this phenomenon is present not only in RBCS but systematically all Calvin cycle enzymes, as well as some proteins from the photosynthetic electron transport chain (Fig. 43-B). These 12h period profiles are not transcriptomically regulated as the ones described in winter photoperiod, since its encoding transcripts describe one peak of expression per day (24 h period) (Fig. 43-B). The mRNA rhythmic profiles of enzymes from the Calvin cycle are in agreement with previously published data in plants, both showing a 24 h period (Pilgrim & McClung, 1993). It suggest that a strong post-translation regulatory mechanism is causing this 12h period profile in proteins involved in photosynthesis during long photoperiods (including summer and neutral ones) in both microalgae and plants.

Integration of starch content diel oscillations with multi-omic data

There exists an influx of carbon compounds, obtained from the Calvin cycle, to starch. The accumulation and degradation of starch have been described to be circadian regulated, since periodic oscillations of its content is observed in photosynthetic organisms as *Chlamydomonas* and *Arabidopsis*, as well as a rhythmic gene expression profile of the en-

zymes involved in the process (Flis et al., 2019; Geigenberger, 2011; Kötting et al., 2010; Ral et al., 2006; Smith et al., 2004; Sulpice et al., 2014). *Chlamydomonas* reaches its maximum starch content few hours after sunset (Ral et al., 2006), while *Arabidopsis* plants does it exactly at sunset (Feugier & Satake, 2013; Kötting et al., 2010). In both organisms, starch starts to accumulate during the light hours, until amylases (AMY) are activated and its degradation starts. Starch content is a result of a controlled balance between its degradation, by AMY, and its synthesis, ADP-glucose pyrophosphorylase with its small and large subunit genes (APS and APL) (Fig. 43-A).

Table 14: Starch content as percentage of Dry Weight under Long Day and Short Day conditions. The p-values as a result of the significant rhythmicity analysis are included in the lowest row.

		% DW	
Time		LD	SD
1 st day	ZT00	27,7	31,67
	ZT04	30,89	33,65
	ZT08	41,87	30,6
	ZT12	36,37	27,52
	ZT16	31,41	25,52
	ZT20	28,24	25,47
2 nd day	ZT00	29,96	30,34
	ZT04	36,22	33,11
	ZT08	40,46	29,12
	ZT12	34,66	27,8
	ZT16	34,37	27,52
	ZT20	29,24	26,14
Rhythmicity p-value		1,2x10 ⁻⁴	1,38x10 ⁻⁴

Starch content in *Ostreococcus tauri* under diel cycles is also rhythmic with a 24h period (Fig. 45-A) with a p-value < 0.05, which align with the periodic oscillations described in *Arabidopsis* and *Chlamydomonas*. However, *Ostreococcus* do not reach its maximum starch content around sunset as they do. Instead, the maximum starch content aligns with the high irradiance hours and it decreases gradually after that point, under both photoperi-

ods (Fig. 45-A). These results suggest that there is not a conserved starch content temporal program throughout the green lineage, since its degradation starts at different times of the day depending on the organism.

However, which seem to be conserved are the differences between photoperiods. In *Ostreococcus*, starch degradation during winter photoperiod seems to be executed more slowly than during summer photoperiod and a higher content in starch is reached during summer photoperiod, as it has been also described in plants (Feugier & Satake, 2013; Geigenberger, 2011; Kötting et al., 2010; Sulpice et al., 2014),

The starch temporal program observed in *Ostreococcus tauri* (Fig. 45-A) aligns with the transcriptomics and proteomics data generated and analyzed in this thesis. Under both summer and winter photoperiods, starch content reached its maximum at midday, despite the abundance of enzymes involved in starch biosynthesis, like APL (ostta07g03440), peaking several hours later, toward end of the day (Fig. 45-B). The halt in starch increase and the subsequent decrease in its content can be attributed instead to the activation of the genes encoding enzymes involved in starch catabolism or degradation, like AMY (ostta10g00260). The consequently increase in abundance of the corresponding proteins during the second half of the day under both photoperiod is, thus, coincident with the decrement in starch content (Fig. 45-B).

In Chapter 3, gene-protein offsets were hypothesized to be affected by the photoperiod of entrainment and the biological process where those proteins are involved (Fig. 37-38). Our findings show how temporal offsets of genes involved in the same biological process increase uniformly under short photoperiods, indicating a common regulation under seasonal cycles. In this metabolic pathway, offsets of APL (~4 h under both photoperiods) and AMY (8 h in summer and 12 h in winter) are different and they increment in a differently range under short photoperiod (Fig. 45-B). This support previous results in plants, that suggest the hypothesis that synthesis and degradation of starch are complex processes that are regulated by different mechanisms (Geigenberger, 2011; Hartman et al., 2023; Kötting et al., 2010). In addition, both APL and AMY protein abundance profiles are strongly coincident with their gene expression profile except for the described offset (Fig. 45-B), showing that at least transcriptomic regulation is one of the mechanisms that may contribute to starch synthesis-degradation balance in *Ostreococcus tauri* as it has been

observed previously with *Arabidopsis* and other plants as well (Finegan et al., 2022; Geigenberger, 2011; Kötting et al., 2010; Sorokina et al., 2011).

Other metabolic pathways of *Ostreococcus tauri* showing periodic oscillations under diel and seasonal cycles

Carotenoids biosynthesis in Ostreococcus tauri under diel and seasonal cycles

Carotenoid are a group of isoprenoid pigments that are widely distributed among various organisms, including microalgae and plants. Some of these pigments are associated with light-harvesting complexes and perform a crucial role in photosynthesis by efficiently absorbing light energy and transferring it to reaction centers. In addition, carotenoids exhibit antioxidant properties, safeguarding the organism against potential harm induced by excessive light exposure and environmental stress (García-Plazaola et al., 2017; T. Sun et al., 2022). Remarkably, the expression of genes associated with carotenoid biosynthesis is intricately regulated by the circadian clock in both plants and algae. This circadian regulation ensures that the production and accumulation of carotenoids aligns with the physiological demands and environmental conditions. Optimal timing of carotenoids production maximize their effectiveness in light absorption, energy transfer, and antioxidant protection. (Covington et al., 2008; García-Plazaola et al., 2017; Pan et al., 2009; T. H. Sun et al., 2010; Zhang et al., 2022).

In addition to their role in photosynthesis, carotenoids have considerable nutritional value for humans. Certain carotenoids, including β-carotene, possess the capacity to be converted into vitamin A, a vital nutrient essential for maintaining vision and bolstering the immune system. Furthermore, specific carotenoids, such as astaxanthin, have exhibited promising potential in promoting health, as they have been associated with reducing the risk of certain cancers and cardiovascular diseases. (Eggersdorfer & Wyss, 2018).

Microalgae have emerged as a promising source for large-scale production of carotenoids. However, the full potential of this technology has not been reached due to limited understanding of the molecular mechanisms underlying carotenoid biosynthesis. Over the past two decades, numerous research groups have been studying growth conditions, microalgae metabolism and optimizing photobioreactors design to maximize carotenoid produc-

tion while minimizing associated costs (Del Campo et al., 2004; Hoys et al., 2021; Sierra et al., 2008).

Industrial-scale cultivation of microalgae is predominantly achieved in outdoor settings. Therefore, comprehending the oscillation patterns of carotenoid biosynthesis under diel and seasonal cycles becomes crucial for ensuring the maximum carotenoid content at harvesting time, as well as identifying potential gene and protein targets for further optimization. To understand the adaptive nature of carotenoid content to seasonal variations in diel cycles and its implications for optimizing light energy capture, photoprotection and, thus, its possibilities of industrial optimization, we examined the transcript and protein abundance profiles of carotenoid biosynthesis genes in *Ostreococcus*. In addition, these profiles were integrated with carotenoid content profiles as biological validation of the results (Fig. 46).

Integration of multi-omics data with oscillations described by carotenoids content in *Ostreococcus tauri* under diel and seasonal cycles

Ostreococcus tauri is rich in widely distributed carotenoids like violaxanthin, antheraxanthin or zeaxanthin. Although specific carotenoids of Mamiellophyceae like micromonal, uriolide or prasinoxanthin are also found in this prasinophyte, being prasinoxanthin the most abundant one (Egeland et al., 1995; Guyon et al., 2018; Six et al., 2009). Its genome presents genes encoding for the Methylerythritol 4-phosphate (MEP) pathway (Derelle et al., 2006; L. Zhao et al., 2013), which derives pyruvate to the production of geranyl pyrophosphate (GPP), the main carotenoid precursor (Fig. 46-A). Most genes encoding enzymes involved in the MEP pathway peaked at sunrise under summer photoperiod and during the last part of the night under winter photoperiod, preceding the corresponding protein abundance peaks by 4 hours or less (Fig. 46-B). Similar patterns were observed in the first enzymes of the preceding carotenoid biosynthesis pathway or carotenogenesis. This pathway starts with the production of phytoene by the phytoene synthase (PSY), that will finally result in lycopene (Fig. 46-A). The progression of the MEP and carotenogenesis pathways allow the cell to produce the main precursors needed for carotenoids production and seems to be transcriptomically regulated in a similar way. In both pathways, enzymes are transcribed during the night under winter photoperiod ensuring the presence of its encoding proteins during the day (Fig. 46-B). From this point, the pathway diverges in two different branches, due to the Lycopene α/β cyclase (LCY α/β , ostta14g00700) that seems to be

regulated in specific ways depending of the biological function of the carotenoids produced: β -branch, including the xanthophylls cycle; and α -branch, including the main antenna carotenoids in prasinophyte (Fig. 46-A) which biosynthesis pathways are still unknown (Guyon et al., 2018; Six et al., 2009).

Carotenoids content during diel cycles under both summer and winter photoperiods have been estimated from HPLC profiles, as described in Materials and Methods.

Table 15: Carotenoid content (% of total carotenoids) in Long Day entrained cultures. The abbreviations used for each carotenoid are: AC for α -carotene; L for lutein, P for prasinoxanthin; DL for dihydrolutein; M for micromonal; U for Uriolide; BC for β -carotene; Z for zeaxanthin; A for antheraxanthin; V for violaxanthin and N for neoxanthin.

Time		% of total carotenoids										
		AC	L	P	DL	M	U	BC	Z	A	V	N
1 st day	ZT00	0,88	0	29,08	7,63	5,67	7,39	4,76	6,34	6,3	18,3	13,63
	ZT04	0,84	0	29,97	8,1	6	7,86	4,89	4,96	4,24	18,09	15,05
	ZT08	0,51	3,42	25,31	7,74	5,97	5,77	5,53	9,39	19,94	3,55	12,87
	ZT12	0,79	3,15	26,23	7,31	5,48	5,81	6,32	10,09	17,2	4,93	12,68
	ZT16	0,86	0	27,88	7,74	5,31	7,54	5,67	8,11	12,59	11,06	13,24
	ZT20	0,85	0	29,26	7,5	5,65	7,87	5,59	6,69	7,74	14,69	14,18
2 nd day	ZT00	0,74	0	29,29	7,33	5,71	7,92	4,71	5,99	4,91	18,02	15,38
	ZT04	0,78	2,07	26,41	8,42	5,28	7,22	5,4	6,7	18,17	6,1	13,45
	ZT08	0,84	3,1	25,95	7,06	5,18	6,63	5,38	10,47	20,18	3,23	11,98
	ZT12	0,69	2,66	27,34	6,13	4,82	7,5	5,64	11,44	17,45	4,72	11,6
	ZT16	0,82	0	29,18	7,19	5,14	7,5	5,34	8,42	11,11	12,41	12,87
	ZT20	1,22	0	30,69	7,39	5,58	7,59	5,7	7,39	6,77	14,67	12,99
3 rd day	ZT00	0,81	0	28,91	6,84	5,33	7,03	4,86	6,23	5,32	20,44	14,23
	ZT04	0,86	1,92	26,51	7,54	5,16	7,03	5,45	8,16	19,44	5,08	12,86
	ZT08	0,59	3,18	26,15	6,27	4,95	6,63	5,32	11,91	20,64	2,45	11,91
	ZT12	0,57	3,79	27,5	5,86	4,16	6,6	5,69	12,65	16,24	5,72	11,23
	ZT16	1,24	0	29,46	6,04	4,96	6,67	4,91	9,91	14,24	10,13	12,44
	ZT20	1,02	0	32,72	5,27	5,69	7,59	3,43	9,68	11,27	11,15	12,19

Table 16: Carotenoid content (% of total carotenoids) in Short Day entrained cultures. The abbreviations used for each carotenoid are: AC for α -carotene; L or luthein, P for prasinoxanthin; DL for dihydrolutein; M for micromonal; U for Uriolide; BC for β -carotene; Z for zeaxanthin; A for antheraxanthin; V for violaxanthin and N for neoxanthin.

		% of total carotenoids										
Time		AC	L	P	D	M	U	BC	Z	A	V	N
1 st day	ZT00	1,23	0	27,17	10,33	6,97	9,64	9,72	3,62	1,23	14,8	15,29
	ZT04	1,34	0	25,2	12,39	6,22	9,68	9,71	4,28	2,68	12,93	15,56
	ZT08	1,52	0	25,5	11,62	6,43	9,73	9,96	4,01	1,56	13,99	15,67
	ZT12	1,23	0	26,43	10,98	6,72	10,06	8,86	4,66	1,57	13,44	16,06
	ZT16	1,32	0	26,72	10,62	6,59	10,36	8,89	5	1,39	13,03	16,07
	ZT20	1,17	0	27,09	10,58	6,76	10,45	8,7	4,5	1,48	13,76	15,5
2 nd day	ZT00	1,26	0	25,93	10,33	6,71	10,47	9,68	3,64	1,43	15,14	15,42
	ZT04	1,57	0	24,46	12,41	6,34	9,71	10,07	4,26	2,47	13,59	15,12
	ZT08	1,4	0	25,66	11,72	6,68	10,57	9,83	4,2	1,85	12,72	15,35
	ZT12	1,1	0	26,15	10,93	6,66	9,97	8,76	4,58	1,56	14,37	15,92
	ZT16	1,36	0	25,74	10,45	6,55	10,63	8,67	4,87	1,75	13,86	16,12
	ZT20	1,15	0	26,19	10,86	6,89	10,31	8,89	4,66	1,65	14,18	15,23
3 rd day	ZT00	1,28	0	26,48	10,16	7,03	10,89	9,7	3,68	1,38	14,11	15,29
	ZT04	1,39	0	24,16	12,11	6,05	9,93	9,95	4,14	3,63	13,12	15,52
	ZT08	1,79	0	24,83	12,15	6,38	10,22	10,24	4,56	2,01	12,97	14,85
	ZT12	0,99	0	27,03	10,45	5,98	10,04	8,45	4,77	1,55	15,74	15,01
	ZT16	1,15	0	26,52	10,37	6,41	10,08	8,66	4,82	1,82	15,24	14,93
	ZT20	1,56	0	26,67	9,77	6,22	10,12	8,61	4,77	1,61	15,59	15,07

The rhythmicity analysis detected rhythmic abundance profiles with periods of 24h in all carotenoids under both photoperiods. With the exception of lutein and violaxanthin, that do not maintain their rhythmicity under winter photoperiod. In general, fluctuations on carotenoids content during winter photoperiod are less drastic, resulting in a lower wave amplitude. (Fig. 46-A).

Table 17: Results of the significant rhythmicity analysis for the carotenoids profiles in LD and SD conditions.

Carotenoid	P-value	
	LD	SD
α-carotene	4,98x10 ⁻²	3,00x10 ⁻³
Lutein	1,54x10 ⁻³	
Prasinoxanthin	1,48x10 ⁻⁶	7,37x10 ⁻⁴
Dihydrolutein	4,28x10 ⁻²	6,93x10 ⁻⁶
Micromonal	2,04x10 ⁻²	2,77x10 ⁻²
Uriolide	3,25x10 ⁻⁴	7,63x10 ⁻²
β-carotene	1,10x10 ⁻³	6,24x10 ⁻⁵
Zeaxanthin	8,75x10 ⁻⁶	2,28x10 ⁻⁷
Antheraxanthin	7,70x10 ⁻⁸	1,48x10 ⁻³
Violaxanthin	5,44x10 ⁻⁹	8,28x10 ⁻²
Neoxanthin	1,65x10 ⁻⁴	8,80x10 ⁻¹

The xanthophyll cycle, the interconversion between violaxanthin, antheraxanthin and zeaxanthin as a response to light intensity (CITA), was especially active under summer photoperiod, although its activity was also detected under winter photoperiod. The changes in these xanthophylls coincided with the accumulation of transcripts and proteins encoded by genes associated with the xanthophyll cycle, with short temporal offsets (Fig. 46-A). Under summer photoperiod, the maximum protein abundance of violaxanthin de-epoxidase (VDE, *ostta16g00660*) (Fig. 46-B) match the increasing zeaxanthin content during the light hours (Fig. 46-B) match the increasing content of violaxanthin during the dark hours (Fig. 46-C). These enzymes are transcribed sequentially with a clear temporal regulation. βCH gene is expressed early in the morning, sequentially followed by ZEP and VDE in that specific order under both photoperiods (Fig. 46-B). However, there is not a significant amount of zeaxanthin being accumulated during winter photoperiod. Instead, a high level of violaxanthin without drastic variations is maintained during diel cycles (Fig. 46-A). It suggests that xanthophylls cycle is not enhancing the production of zeaxanthin due to the limited day-

light hours during winter. There are some studies regarding irradiance stress in *Ostreococcus* and other prasinophytes that present variations in xanthophylls contents in a similar way to the ones observed in this thesis due to short light periods (Böhme et al., 2002; Guyon et al., 2018; Six et al., 2009).

In general, the enzymes of the β-branch pathway seem to present a strong transcriptomic regulation to sequentially achieve their roles at the right time. However, these transcriptomic regulation does not reach the physiological level under winter photoperiod (Fig. 46-A), where xanthophylls contents are similar to the ones observed in low irradiance stress experiments (Böhme et al., 2002; Guyon et al., 2018; Six et al., 2009). Suggesting that despite the strong temporal transcriptomic regulation that is also reflected in proteins abundance profile (Fig. 46-C), there are other regulatory pathways that balance xanthophylls production under certain conditions like winter photoperiod.

Regarding pigment of the α-branch biosynthesis pathway, a lack of lutein during winter photoperiod is observed (Fig. 46-A). However, during summer photoperiod lutein is accumulated during the light hours, which is followed by the increment of prasinoxanthin content after sunset (Fig. 46-C). Lutein and prasinoxanthin contents behavior under summer photoperiod are similar to the results obtained in irradiance stress experiments in other prasinophytes. For example, a *Mantoniella squamata* study linked the accumulation of lutein to irradiance stress and its following conversion to prasinoxanthin when the stress condition is over (Böhme et al., 2002).

Although the α-branch biosynthesis pathway is still unknown there are some hypothesis about the inter-conversion of lutein-prasinoxanthin (Egeland et al., 1997). This could supported by our results in *Ostreococcus* since the contents of lutein and prasinoxanthin seem to be linked, not only under irradiance stress as it has been described in previous published studies, but under different photoperiods as well. However, The enzymes involved in the interconversion of these carotenoids remain to be identified, and a comparison of their gene expression and protein accumulation was not feasible in this study.

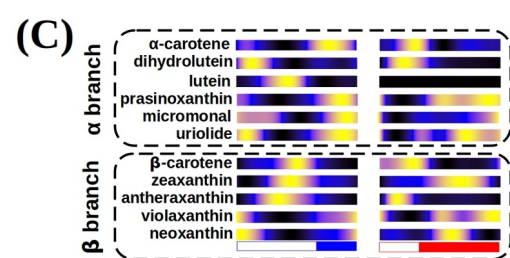
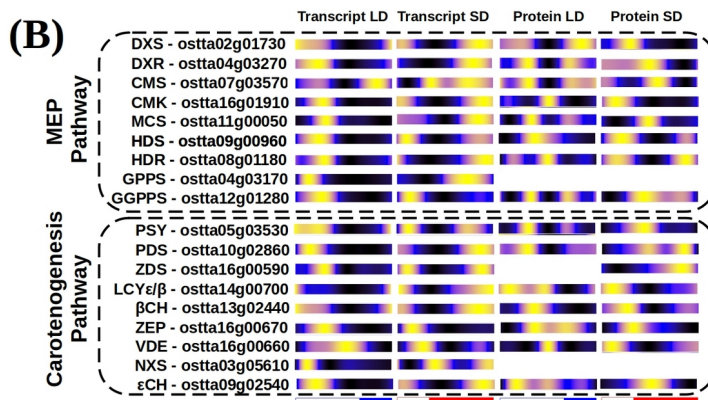
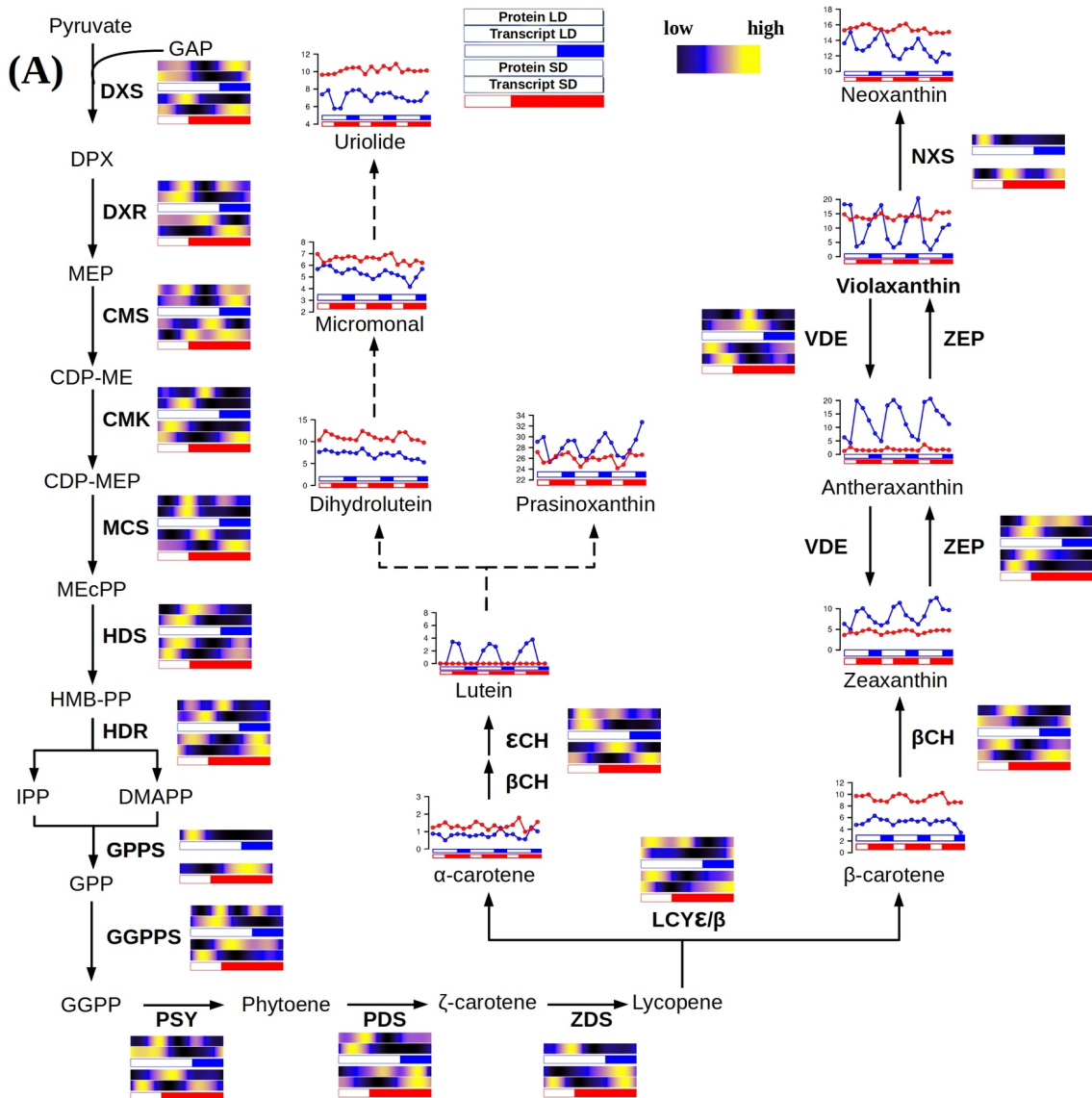


Figure 46: Integration of multi-omics data from the complete carotenoids biosynthesis pathway and carotenoids content of *Ostreococcus tauri*. (A) Schematic MEP pathway and carotenogenesis pathways; (B) Organized list of the gene IDs involved in these pathways including multi-omic data; (C) Organized visualization of content oscillations of each carotenoid from the β and α branch.

In summary, *Ostreococcus tauri* carotenogenesis present the common characteristics of a process regulated by the circadian clock, as being able to adapt to different photoperiods and presenting an anticipation to diel changes in the transcriptome encoding enzymes of starch metabolism provide evidence for both transcriptional and posttranscriptional regulation of starch metabolism in *Arabidopsis* leaves I cyclic changes. However, content in carotenoids seem to also depend on other regulatory pathways besides the circadian clock, as some of the changes observed under the photoperiods studied align with high and low irradiance experiment results.

Nitrate assimilation under diel and seasonal cycles in Ostreococcus tauri

The macroelement nitrogen is also an essential component in biomolecules of great importance for all living beings. In the atmosphere, N₂ is the most abundant form of nitrogen. This gas is dissolved in water ecosystems but is inaccessible for microalgae, it can only be used by fixing bacteria like *Synechococcus*. In fact, nitrogen is a major limiting nutrient of marine phytoplankton (Barros et al., 2005; Mittag, 2001; Sanz-Luque et al., 2015).

O. tauri have developed competitive mechanisms to ensure nitrogen assimilation in the marine ecosystem. It can grow on nitrate, ammonium, and urea, and complete sets of genes allowing transport and assimilation of these substrates have been identified in its genome (Blanc-Mathieu et al., 2014; Derelle et al., 2006). Specifically, in the growth media used during this work, nitrate was the main nitrogen source (Table 2). In the previous chapters of this thesis, nitrate assimilation has been identified as one of the biological processes which genes and proteins present significant rhythmic profiles under diel cycles, as well as one of the processes with larger offset between gene expression and translation. In this section, enzymatic activities of two of the main enzymes involved in the nitrate assimilation pathway are integrated with the transcript and protein abundance profiles of the complete pathway. This results give new insights on the adaptive response of this assimilation process to seasonal variations in diel cycles and its implications for optimizing nutrient uptake and metabolism.

Integration of key enzyme activities from nitrate assimilation pathway with multi-omic data

Nitrate is first transported into the cell by Nitrate Transporters 2 and 3 (NRT2, ostta10g00950 and NRT3, ostta10g00940), followed by its reduction to nitrite by Nitrate Reductase (NR, ostta10g00920). Nitrite is further reduced to ammonia by Nitrite Reductase (NIR, ostta10g00930). The central part of nitrate assimilation is played by the Glutamine Synthetase (GS, ostta01g05020) and Glutamine Oxoglutarate Aminotransferase (GOGAT, ostta14g01900) cycle, which converts inorganic nitrogen, ammonia, into glutamine and glutamate (Fig. 47), a central precursor for the biosynthesis of nitrogen-containing compounds such as amino acids and nucleotides. (Sanz-Luque et al., 2015).

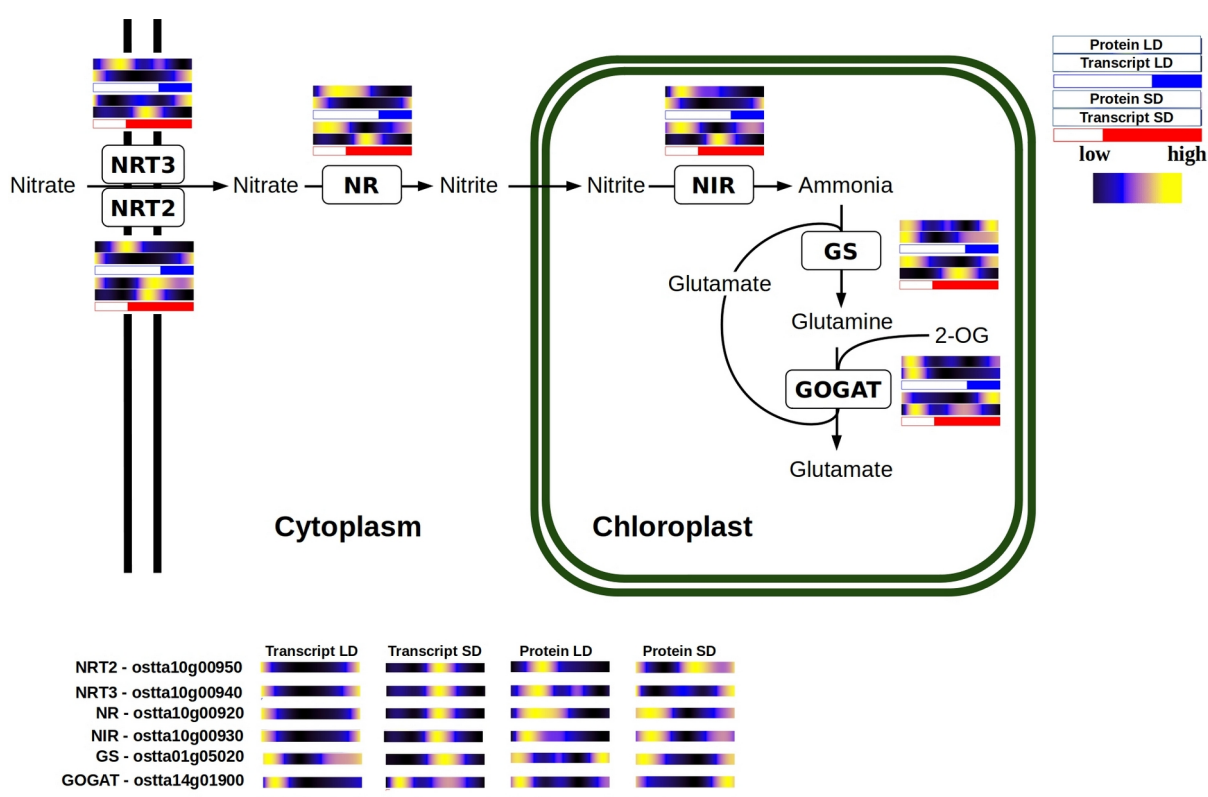


Figure 47: Multi-omics integration of nitrate assimilation pathway. Schematic nitrate assimilation pathway and list of the gene IDs involved including protein abundance and gene expression profiles of each enzyme.

During summer photoperiod, gene expression profiles of NRT2/3, NR and NIR reached their maximum at dawn (ZT0), while their protein abundances peaked 8 hours later at mid-day (ZT8), coinciding with the time point of maximum light irradiance. GS and GOGAT

gene expression and protein abundance profiles are almost coincident, reaching their maximum at the beginning of the day (ZT4) without noticeable temporal offsets between them. However, a slight increase in protein abundance was detected at the end of the day (ZT12) for both GS and GOGAT (Fig. 47).

In contrast, under winter photoperiod, all genes encoding the transporters and enzymes involved in nitrate assimilation showed their maximum expression level during the first part of the night (ZT12-ZT16), preceding their protein abundance peaks at dawn (ZT0) or mid-day (ZT4) by 8 hours or more. Notably, GOGAT gene expression displayed a bimodal pattern under SD condition, maintaining the peak observed under LD at ZT4 besides the new peak at ZT16. Therefore, GOGAT gene expression constitutes an example of the emergence of complex expression patterns under summer photoperiod consisting of two gene expression peaks per day (Fig. 47).

Circadian oscillations in expression and activity of the first enzyme of this pathway (NR) have been described in *Arabidopsis* and other crop plants as maize or tomato (Lillo et al., 2001; Lillo & Ruoff, 1989; Tucker et al., 2004; Z. Yang & Midmore, 2005). In fact, light is apparently an important factor for NR to maintain its rhythmic behavior. Rhythms in NR activity or NR gene expression profiles were shown to persist only in continuous light in plants (Lillo et al., 2001; Lillo & Ruoff, 1989). These results are in agreement with the transcriptomic data obtained in this work, where NR gene expression rhythmic profiles, as well as other enzymes involved in this pathway, are maintained only under light-dark cycles and constant light.

To validate these results, the enzymatic activities of NR and GS are measured throughout complete diel cycles under summer and winter photoperiods. These measurements presented a significant rhythmic profile with a p-value lower than 0.05 and an almost non-existent offset between their protein abundance profiles and their activity profiles was found (Fig. 48).

Table 17: Nitrate Reductase (NR) and Glutamine Synthetase (GS) enzymatic activities (U) for each time point in long day and short day entrained cultures. The p-values as a result of the significant rhythmicity analysis are included in the lowest row.

		LD		SD	
Time		NR (U)	GS (U)	NR (U)	GS (U)
1 st day	ZT00	1,13	0,06	2,76	0,16
	ZT04	1,14	0,07	2,96	0,22
	ZT08	1,26	0,04	3,28	0,16
	ZT12	1,07	0,07	2,38	0,17
	ZT16	0,93	0,04	2,04	0,17
	ZT20	0,85	0,03	2,77	0,16
2 nd day	ZT00	1,25	0,04	2,46	0,19
	ZT04	1,1	0,08	2,32	0,19
	ZT08	1,5	0,05	3,1	0,18
	ZT12	1,27	0,04	2,52	0,12
	ZT16	1,02	0,04	2,48	0,14
	ZT20	1,15	0,04	1,87	0,15
Rhythmicity p-value		2,35x10 ⁻²	4,53x10 ⁻²	3,24x10 ⁻²	2,04x10 ⁻²

The huge transcriptomic anticipation observed is adjusted by the clock taking in count the large offset between gene expression and translation described by the enzymes involved in this pathway. In fact, although genes are transcribed at different times under winter and summer photoperiod, proteins reach their maximum abundance level at a similar time of the day in both cases (Fig. 47, 48). This is a clear example of how *Ostreococcus* adjust its transcriptional program in order to ensure the presence of proteins at the exact right time, in spite of their specific translation offset.

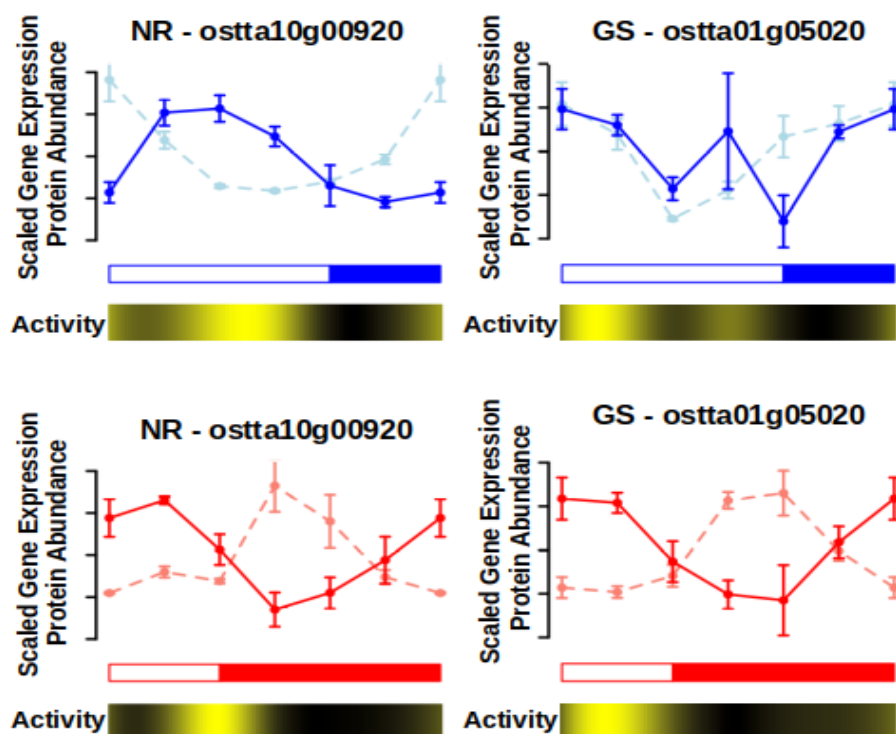


Figure 48: NR and GS rhythmic activity compared with its proteomic and transcriptomic data generated. Transcript (lighter color) and protein (darker color) abundance profiles for Nitrate reductase (NR, left) and Glutamine Synthetase (GS, right) under LD condition (top, blue) and SD condition (bottom, red). Heatmaps are incorporated below to represent the changes in enzymatic activity of these enzymes. Black represents low activity and white high activity.

Conclusions

- ¿Como puedo añadir algo sobre el chapter1? Copiado del chapter1: Since molecular systems biology has much to contribute to microalgae research, we hope that ALGAEFUN with MARACAS will reach the hands of many research groups and will be as useful to them as it has been to us. Editar y meter visitas.
- Around 80% of the *Ostreococcus* transcriptome present rhythmic expression patterns under diel cycles, but bona fide circadian genes represent only the 4% of the transcriptome.
- Although *Ostreococcus* is a photosynthetic organism, its transcriptome strongly depends on dark periods to maintain rhythmic expression patterns described under light-dark cycles. The effects of the free-running conditions observed over the transcriptome (greater desynchronization under LL, positive phase shifts under LL and negative phase shifts under DD) agree with the ones described in activity circadian records of nocturnal organisms.
- Seasonal cycles induced changes in gene expression profiles consisting of the emergence of 12 h period cycles, phase shifts and amplitude reductions.
- The 12 h period cycles (2 peaks every 24h) emerged under winter photoperiod are not a self-sustained rhythm, but a combination of two distinct rhythmic profiles: one depending on the photoperiod and another depending on the skotoperiod. These rhythmic profiles are coincident under long photoperiods, becoming out of phase as photoperiod gets shorter.
- Only 25% of the *Ostreococcus* proteome present rhythmic protein abundances under diel cycles.
- The transcriptome of *Ostreococcus tauri* present a nocturnal activity (the maximum expression levels take place during the night hours) while its proteome present a clear diel activity (the maximum protein abundance levels take place during the light hours).

- There exist a temporal offset between gene expression and translation. The rhythmic wave described by a gene expression level and its encoding protein abundance are almost identical, except for their phase offsets.
- The offset between gene expression and translation increases during winter photoperiod and its dependent on the physiological function in which they are involved. Therefore, *Ostreococcus tauri* severely reorganize its transcriptional temporal program taking in count not only the current photoperiod but also the different transcript/proteins offsets that each biological function presents.
- There exist a temporal offset between the proteome of *Ostreococcus tauri* and the execution of their physiological processes.
- Cell division cycle is strongly influenced by the circadian clock in *Ostreococcus*, it can anticipate cyclic changes like the short time of light in winter photoperiods. To anticipate it, the circadian clock ensures that all cells have completed the division phase before sunrise, so any hour of light is wasted. The cell cycle temporal program observed is in agreement with the transcriptomic and proteomic data generated.
- **Photosynthetic** efficiency rhythmic oscillations present a 12 h period cycles under winter photoperiod, which is again in agreement with the transcriptomic and proteomic data generated. Photosynthesis machinery anticipation to photoperiod is transcriptionally regulated in *Ostreococcus tauri* and, probably, since early in the green lineage.
- Starch content in *Ostreococcus tauri* present a rhythmic 24 h cycle, reaching its maximum starch content at the high irradiance hours under both summer and winter photoperiods. Both APL and AMY protein abundance profiles are strongly coincident with their gene expression profile with a ~4h offset, showing that starch circadian synthesis-degradation balance is possibly transcriptomically regulated.
- *Ostreococcus tauri* carotenogenesis and nitrate assimilation pathway present the common characteristics of processes regulated by the circadian clock (at a transcriptomic, proteomic and physiological level), as being able to adapt to different photoperiods and present an anticipation to diel cyclic changes.

Bibliography

- Abascal, F., Acosta, R., Addleman, N. J., Adrian, J., Afzal, V., Aken, B., Akiyama, J. A., Jammal, O. Al, Amrhein, H., Anderson, S. M., Andrews, G. R., Antoshechkin, I., Ardlie, K. G., Armstrong, J., Astley, M., Banerjee, B., Barkal, A. A., Barnes, I. H. A., Barozzi, I., ... Myers, R. M. (2020). Perspectives on ENCODE. In *Nature* (Vol. 583, Issue 7818). <https://doi.org/10.1038/s41586-020-2449-8>
- Abinandan, S., Subashchandrabose, S. R., Venkateswarlu, K., & Megharaj, M. (2018). Nutrient removal and biomass production: advances in microalgal biotechnology for wastewater treatment. *Critical Reviews in Biotechnology*, 38(8), 1244–1260. <https://doi.org/10.1080/07388551.2018.1472066>
- Ajjawi, I., Verruto, J., Aqui, M., Soriaga, L. B., Coppersmith, J., Kwok, K., Peach, L., Orchard, E., Kalb, R., Xu, W., Carlson, T. J., Francis, K., Konigsfeld, K., Bartalis, J., Schultz, A., Lambert, W., Schwartz, A. S., Brown, R., & Moellering, E. R. (2017). Lipid production in *Nannochloropsis gaditana* is doubled by decreasing expression of a single transcriptional regulator. *Nature Biotechnology*, 35, 647–652. <https://doi.org/10.1038/nbt.3865>
- Akhtar, R. A., Reddy, A. B., Maywood, E. S., Clayton, J. D., King, V. M., Smith, A. G., Gant, T. W., Hastings, M. H., & Kyriacou, C. P. (2002). Circadian cycling of the mouse liver transcriptome, as revealed by cDNA microarray, is driven by the suprachiasmatic nucleus. *Current Biology*, 12(7). [https://doi.org/10.1016/S0960-9822\(02\)00759-5](https://doi.org/10.1016/S0960-9822(02)00759-5)
- Andreatta, G., & Tessmar-Raible, K. (2020). The Still Dark Side of the Moon: Molecular Mechanisms of Lunar-Controlled Rhythms and Clocks. In *Journal of Molecular Biology* (Vol. 432, Issue 12). <https://doi.org/10.1016/j.jmb.2020.03.009>
- Ashburner, M., Ball, C. A., Blake, J. A., Botstein, D., Butler, H., Cherry, J. M., Davis, A. P., Dolinski, K., Dwight, S. S., Eppig, J. T., Harris, M. A., Hill, D. P., Issel-Tarver, L., Kasarskis, A., Lewis, S., Matese, J. C., Richardson, J. E., Ringwald, M., Rubin, G. M.,

- & Sherlock, G. (2000). Gene ontology: Tool for the unification of biology. *Nature Genetics*, 25, 25–29. <https://doi.org/10.1038/75556>
- Bachy, C., Wittmers, F., Muschiol, J., Hamilton, M., Henrissat, B., & Worden, A. Z. (2022). The Land-Sea Connection: Insights Into the Plant Lineage from a Green Algal Perspective. In *Annual Review of Plant Biology* (Vol. 73). <https://doi.org/10.1146/annurev-arplant-071921-100530>
- Ballance, H., & Zhu, B. (2021). Revealing the hidden reality of the mammalian 12-h ultradian rhythms. *Cellular and Molecular Life Sciences*, 78(7), 3127–3140. <https://doi.org/10.1007/s0018-020-03730-5>
- Barros, M. P., Pinto, E., Sigaud-Kutner, T. C. S., Cardozo, K. H. M., & Colepicolo, P. (2005). Rhythmicity and oxidative/nitrosative stress in algae. *Biological Rhythm Research*, 36(1–2). <https://doi.org/10.1080/09291010400028666>
- Bartoszewicz, R., Chmielewska, D., Domoń, M., & Barbacka-Surowiak, G. (2010). Influence of short-term constant light on phase shift of mouse circadian locomotor activity rhythm induced by agonist and antagonist of serotonin. *Biological Rhythm Research*, 41(4). <https://doi.org/10.1080/09291010903018016>
- Baty, F., Ritz, C., Charles, S., Brutsche, M., Flandrois, J. P., & Delignette-Muller, M. L. (2015). A toolbox for nonlinear regression in R: The package nlstools. *Journal of Statistical Software*, 66(5). <https://doi.org/10.18637/jss.v066.i05>
- Becker, B., & Marin, B. (2009). Streptophyte algae and the origin of embryophytes. *Annals of Botany*, 103(7), 999–1004. <https://doi.org/10.1093/aob/mcp044>
- Benites, L. F., Buccini, F., Sanchez-Brosseau, S., Grimsley, N., Vandepoele, K., & Piégneau, G. (2021). Evolutionary Genomics of Sex-Related Chromosomes at the Base of the Green Lineage. *Genome Biology and Evolution*, 13(10). <https://doi.org/10.1093/gbe/evab216>
- Berube, P. M., Biller, S. J., Hackl, T., Hogle, S. L., Satinsky, B. M., Becker, J. W., Braakman, R., Collins, S. B., Kelly, L., Berta-Thompson, J., Coe, A., Bergauer, K., Bouman, H. A., Browning, T. J., De Corte, D., Hassler, C., Hulata, Y., Jacquot, J. E., Maas, E. W., ... Chisholm, S. W. (2018). Data descriptor: Single cell genomes of Prochlorococcus, Synechococcus, and sympatric microbes from diverse marine environments. *Scientific Data*, 5. <https://doi.org/10.1038/sdata.2018.154>
- Biebach, H., Falk, H., & Krebs, J. R. (1991). The Effect of Constant Light and Phase Shifts on a Learned Time-Place Association in Garden Warblers (*Sylvia borin*): Hourglass or Circadian Clock? *Journal of Biological Rhythms*, 6(4). <https://doi.org/10.1177/074873049100600406>

- Binkley, S., & Mosher, K. (1985). Direct and circadian control of sparrow behavior by light and dark. *Physiology and Behavior*, 35(5). [https://doi.org/10.1016/0031-9384\(85\)90413-5](https://doi.org/10.1016/0031-9384(85)90413-5)
- Blaby, I. K., Blaby-Haas, C. E., Tourasse, N., Hom, E. F. Y., Lopez, D., Aksoy, M., Grossman, A., Umen, J., Dutcher, S., Porter, M., King, S., Witman, G. B., Stanke, M., Harris, E. H., Goodstein, D., Grimwood, J., Schmutz, J., Vallon, O., Merchant, S. S., & Prochnik, S. (2014). The Chlamydomonas genome project: A decade on. In *Trends in Plant Science* (Vol. 19, Issue 10). <https://doi.org/10.1016/j.tplants.2014.05.008>
- Blanc-Mathieu, R., Verhelst, B., Derelle, E., Rombauts, S., Bouget, F.-Y., Carré, I., Château, A., Eyre-Walker, A., Grimsley, N., Moreau, H., Piégu, B., Rivals, E., Schackwitz, W., Van de Peer, Y., & Piganeau, G. (2014). An improved genome of the model marine alga *Ostreococcus tauri* unfolds by assessing Illumina de novo assemblies. *BMC Genomics*, 15(1), 1103. <https://doi.org/10.1186/1471-2164-15-1103>
- Blanc, G., Agarkova, I., Grimwood, J., Kuo, A., Brueggeman, A., Dunigan, D. D., Gurnon, J., Ladunga, I., Lindquist, E., Lucas, S., Pangilinan, J., Pröschold, T., Salamov, A., Schmutz, J., Weeks, D., Yamada, T., Lomsadze, A., Borodovsky, M., Claverie, J. M., ... Van Etten, J. L. (2012). The genome of the polar eukaryotic microalga *Coccomyxa subellipsoidea* reveals traits of cold adaptation. *Genome Biology*, 13(5). <https://doi.org/10.1186/gb-2012-13-5-r39>
- Bläsing, O. E., Gibon, Y., Günther, M., Höhne, M., Morcuende, R., Osuna, D., Thimm, O., Usadel, B., Scheible, W. R., & Stitt, M. (2005). Sugars and circadian regulation make major contributions to the global regulation of diurnal gene expression in *Arabidopsis*. *Plant Cell*, 17(12). <https://doi.org/10.1105/tpc.105.035261>
- Böhme, K., Wilhelm, C., & Goss, R. (2002). Light regulation of carotenoid biosynthesis in the prasinophycean alga *Mantoniella squamata*. *Photochemical and Photobiological Sciences*, 1(8). <https://doi.org/10.1039/b204965c>
- Borowitzka, M. A. (2013). High-value products from microalgae-their development and commercialisation. *Journal of Applied Phycology*, 25(3), 743–756. <https://doi.org/10.1007/s10811-013-9983-9>
- Bowler, C., Allen, A. E., Badger, J. H., Grimwood, J., Jabbari, K., Kuo, A., Maheswari, U., Martens, C., Maumus, F., Otillar, R. P., Rayko, E., Salamov, A., Vandepoele, K., Beszteri, B., Gruber, A., Heijde, M., Katinka, M., Mock, T., Valentin, K., ... Grigoriev, I. V. (2008). The *Phaeodactylum* genome reveals the evolutionary history of diatom genomes. *Nature*, 456(7219). <https://doi.org/10.1038/nature07410>
- Brandoli, C., Petri, C., Egea-Cortines, M., & Weiss, J. (2020). Gigantea: Uncovering new functions in flower development. In *Genes* (Vol. 11, Issue 10, pp. 1–15). MDPI AG. <https://doi.org/10.3390/genes11101142>

- Bray, N. L., Pimentel, H., Melsted, P., & Pachter, L. (2016). Near-optimal probabilistic RNA-seq quantification. *Nature Biotechnology*, 34(5). <https://doi.org/10.1038/nbt.3519>
- Bruce, V. G. (1970). The biological clock in Chlamydomonas reinhardtii. *J Protozool*, 17, 328–334. [https://doi.org/https://doi.org/10.1111/j.1550-7408.1970.tb02380.x](https://doi.org/10.1111/j.1550-7408.1970.tb02380.x)
- Carbon, S., Douglass, E., Dunn, N., Good, B., Harris, N. L., Lewis, S. E., Mungall, C. J., Basu, S., Chisholm, R. L., Dodson, R. J., Hartline, E., Fey, P., Thomas, P. D., Albou, L. P., Ebert, D., Kesling, M. J., Mi, H., Muruganujan, A., Huang, X., ... Westerfield, M. (2019). The Gene Ontology Resource: 20 years and still GOing strong. *Nucleic Acids Research*, 47(D1), D330–D338. <https://doi.org/10.1093/nar/gky1055>
- Carbon, S., Ireland, A., Mungall, C. J., Shu, S., Marshall, B., Lewis, S., Lomax, J., Mungall, C., Hitz, B., Balakrishnan, R., Dolan, M., Wood, V., Hong, E., & Gaudet, P. (2009). AmiGO: Online access to ontology and annotation data. *Bioinformatics*, 25(2), 288–289. <https://doi.org/10.1093/bioinformatics/btn615>
- Carlson, M., & Pagès, H. (2019). *AnnotationForge: Tools for building SQLite-based annotation data packages* (1.26.0.).
- Carneiro, A. K., Montessoro, P. da F., Fusaro, A. F., Araújo, B. G., & Hemerly, A. S. (2021). Plant cdks—driving the cell cycle through climate change. In *Plants* (Vol. 10, Issue 9). <https://doi.org/10.3390/plants10091804>
- Chapman, R. L. (2013). Algae: The world's most important “plants”—an introduction. *Mitigation and Adaptation Strategies for Global Change*, 18(1). <https://doi.org/10.1007/s11027-010-9255-9>
- Chen, H., Li, T., & Wang, Q. (2019). Ten years of algal biofuel and bioproducts: gains and pains. *Planta*, 249(1), 195–219. <https://doi.org/10.1007/s00425-018-3066-8>
- Chen, M. X., Zhang, Y., Fernie, A. R., Liu, Y. G., & Zhu, F. Y. (2021). SWATH-MS-Based Proteomics: Strategies and Applications in Plants. In *Trends in Biotechnology* (Vol. 39, Issue 5, pp. 433–437). Elsevier Ltd. <https://doi.org/10.1016/j.tibtech.2020.09.002>
- Cheng, S., Xian, W., Fu, Y., Marin, B., Keller, J., Wu, T., Sun, W., Li, X., Xu, Y., Zhang, Y., Wittek, S., Reder, T., Günther, G., Gontcharov, A., Wang, S., Li, L., Liu, X., Wang, J., Yang, H., ... Melkonian, M. (2019). Genomes of Subaerial Zygnematophyceae Provide Insights into Land Plant Evolution. *Cell*, 179(5). <https://doi.org/10.1016/j.cell.2019.10.019>
- Cock, J. M., & Coelho, S. M. (2011). Algal models in plant biology. In *Journal of Experimental Botany* (Vol. 62, Issue 8). <https://doi.org/10.1093/jxb/err117>
- Coleto-Alcudia, V., & Vega-Rodríguez, M. A. (2020). Artificial Bee Colony algorithm based on Dominance (ABCD) for a hybrid gene selection method. *Knowledge-Based Systems*, 205. <https://doi.org/10.1016/j.knosys.2020.106323>

- Collado-Fabbri, S., Vaulot, D., & Ulloa, O. (2011). Structure and seasonal dynamics of the eukaryotic picophytoplankton community in a wind-driven coastal upwelling ecosystem. *Limnology and Oceanography*, 56(6). <https://doi.org/10.4319/lo.2011.56.6.2334>
- Corellou, F., Camasses, A., Ligat, L., Peaucellier, G., & Bouget, F. Y. (2005). Atypical regulation of a green lineage-specific B-type cyclin-dependent kinase. *Plant Physiology*, 138(3). <https://doi.org/10.1104/pp.105.059626>
- Correa, A., & Bell-Pedersen, D. (2002). Distinct signaling pathways from the circadian clock participate in regulation of rhythmic conidiospore development in *Neurospora crassa*. *Eukaryotic Cell*, 1(2). <https://doi.org/10.1128/EC.1.2.273-280.2002>
- Corteggiani Carpinelli, E., Telatin, A., Vitulo, N., Forcato, C., D'Angelo, M., Schiavon, R., Vezzi, A., Giacometti, G. M., Morosinotto, T., & Valle, G. (2014). Chromosome scale genome assembly and transcriptome profiling of *nannochloropsis gaditana* in nitrogen depletion. *Molecular Plant*, 7(2). <https://doi.org/10.1093/mp/sst120>
- Covington, M. F., Maloof, J. N., Straume, M., Kay, S. A., & Harmer, S. L. (2008). Global transcriptome analysis reveals circadian regulation of key pathways in plant growth and development. *Genome Biology*, 9(8). <https://doi.org/10.1186/gb-2008-9-8-r130>
- Craig, R. J., Hasan, A. R., Ness, R. W., & Keightley, P. D. (2021). Comparative genomics of Chlamydomonas. *Plant Cell*, 33(4). <https://doi.org/10.1093/plcell/koab026>
- Critchley, C., & Russell, A. W. (1994). Photoinhibition of photosynthesis in vivo: The role of protein turnover in photosystem II. In *Physiologia Plantarum* (Vol. 92, Issue 1). <https://doi.org/10.1111/j.1399-3054.1994.tb06670.x>
- Cui, Y., Thomas-Hall, S. R., & Schenk, P. M. (2019). *Phaeodactylum tricornutum* microalgae as a rich source of omega-3 oil: Progress in lipid induction techniques towards industry adoption. In *Food Chemistry* (Vol. 297). <https://doi.org/10.1016/j.foodchem.2019.06.004>
- Cumming, B. G., & Wagner, E. (1968). Rhythmic Processes in Plants. *Annual Review of Plant Physiology*, 19(1). <https://doi.org/10.1146/annurev.pp.19.060168.002121>
- De Candolle, M. (1832). *Physiologie végétale*. Bechet Jeune.
- De Keersmaecker, S. C. J., Thijs, I. M. V., Vanderleyden, J., & Marchal, K. (2006). Integration of omics data: How well does it work for bacteria? In *Molecular Microbiology* (Vol. 62, Issue 5). <https://doi.org/10.1111/j.1365-2958.2006.05453.x>
- de los Reyes, P., Romero-Campero, F. J., Ruiz, M. T., Romero, J. M., & Valverde, F. (2017). Evolution of Daily Gene Co-expression Patterns from Algae to Plants. *Frontiers in Plant Science*. <https://doi.org/10.3389/fpls.2017.01217>

- de los Reyes, P., Romero-Campero, F. J., Ruiz, M. T., Romero, J. M., Valverde, F., Teresa Ruiz, M., Romero, J. M., & Valverde, F. (2017). Evolution of daily gene co-expression patterns from algae to plants. *Frontiers in Plant Science*, 8(July), 1–22. <https://doi.org/10.3389/fpls.2017.01217>
- de los Reyes, P., Romero-Campero, F. J., Teresa Ruiz, M., Romero, J. M., & Valverde, F. (2017). Evolution of daily gene co-expression patterns from algae to plants. *Frontiers in Plant Science*, 8(July), 1–22. <https://doi.org/10.3389/fpls.2017.01217>
- De Mairan, J. J. . (1729). Observation Botanique. *Histoire de l'Academie Royale Des Sciences*.
- Del Campo, J. A., Rodríguez, H., Moreno, J., Vargas, M. Á., Rivas, J., & Guerrero, M. G. (2004). Accumulation of astaxanthin and lutein in Chlorella zofingiensis (Chlorophyta). *Applied Microbiology and Biotechnology*, 64(6). <https://doi.org/10.1007/s00253-003-1510-5>
- Demir-Hilton, E., Sudek, S., Cuvelier, M. L., Gentemann, C. L., Zehr, J. P., & Worden, A. Z. (2011). Global distribution patterns of distinct clades of the photosynthetic picoeukaryote Ostreococcus. *ISME Journal*, 5(7). <https://doi.org/10.1038/ismej.2010.209>
- Derelle, E., Ferraz, C., Rombauts, S., Rouze, P., Worden, A. Z., Robbens, S., Partensky, F., Degroeve, S., Echevynie, S., Cooke, R., Saeys, Y., Wuyts, J., Jabbari, K., Bowler, C., Panaud, O., Piegu, B., Ball, S. G., Ral, J.-P., Bouget, F.-Y., ... Moreau, H. (2006). Genome analysis of the smallest free-living eukaryote Ostreococcus tauri unveils many unique features. *Proceedings of the National Academy of Sciences*, 103(31), 11647–11652. <https://doi.org/10.1073/pnas.0604795103>
- Ditz, B., Boekhoudt, J. G., Aliee, H., Theis, F. J., Nawijn, M., Brandsma, C.-A., Hiemstra, P. S., Timens, W., Tew, G. W., Grimaldeston, M. A., Neighbors, M., Guryev, V., van den Berge, M., & Faiz, A. (2021). Comparison of genome-wide gene expression profiling by RNA Sequencing versus microarray in bronchial biopsies of COPD patients before and after inhaled corticosteroid treatment: does it provide new insights? *ERJ Open Research*, 7(2), 00104–02021. <https://doi.org/10.1183/23120541.00104-2021>
- Dodd, A. N., Kusakina, J., Hall, A., Gould, P. D., & Hanaoka, M. (2014). The circadian regulation of photosynthesis. In *Photosynthesis Research* (Vol. 119, Issues 1–2). <https://doi.org/10.1007/s11120-013-9811-8>
- Donnan, L., & John, P. C. L. (1983). Cell cycle control by timer and sizer in Chlamydomonas. *Nature*, 304(5927). <https://doi.org/10.1038/304630a0>
- Duhamel du Monceau, H. L. (1759). *La physique des arbres*. H. L. Guerin & L. F. Delatour.

- Edmunds, L. N. (1983). Chronobiology at the cellular and molecular levels: Models and mechanisms for circadian timekeeping. *American Journal of Anatomy*, 168(4). <https://doi.org/10.1002/aja.1001680404>
- Edmunds, L. N., & Laval-Martin, D. L. (2019). Cell Division Cycles And Circadian Oscillators In Euglena. In *Intracellular space as oligogenetic ecosystem. Proceedings*. <https://doi.org/10.1515/9783110841237-033>
- Edwards, K. D., Akman, O. E., Knox, K., Lumsden, P. J., Thomson, A. W., Brown, P. E., Pokhilko, A., Kozma-Bognar, L., Nagy, F., Rand, D. A., & Millar, A. J. (2010). Quantitative analysis of regulatory flexibility under changing environmental conditions. *Molecular Systems Biology*, 6. <https://doi.org/10.1038/msb.2010.81>
- Eelderink-Chen, Z., Bosman, J., Sartor, F., Dodd, A. N., Kovács, Á. T., & Merrow, M. (2021). A circadian clock in a nonphotosynthetic prokaryote. *Science Advances*, 7(2). <https://doi.org/10.1126/sciadv.abe2086>
- Egeland, E. S., Eikrem, W., Throndsen, J., Wilhelm, C., Zapata, M., & Liaaen-Jensen, S. (1995). Carotenoids from further prasinophytes. In *Biochemical Systematics and Ecology* (Vol. 23, Issues 7–8). [https://doi.org/10.1016/0305-1978\(95\)00075-5](https://doi.org/10.1016/0305-1978(95)00075-5)
- Egeland, E. S., Guillard, R. R. L., & Liaaen-Jensen, S. (1997). Additional carotenoid prototype representatives and a general chemosystematic evaluation of carotenoids in Prasinophyceae (Chlorophyta). *Phytochemistry*. [https://doi.org/10.1016/S0031-9422\(96\)00650-4](https://doi.org/10.1016/S0031-9422(96)00650-4)
- Eggersdorfer, M., & Wyss, A. (2018). Carotenoids in human nutrition and health. In *Archives of Biochemistry and Biophysics* (Vol. 652). <https://doi.org/10.1016/j.abb.2018.06.001>
- Eissenberg, J. C., & Elgin, S. C. R. (2006). Marking time. In *Nature Genetics* (Vol. 38, Issue 3). <https://doi.org/10.1038/ng0306-276>
- El Gamal, A. A. (2010). Biological importance of marine algae. *Saudi Pharmaceutical Journal*, 18(1), 1–25. <https://doi.org/10.1016/j.jps.2009.12.001>
- Engel, S. R., Dietrich, F. S., Fisk, D. G., Binkley, G., Balakrishnan, R., Costanzo, M. C., Dwight, S. S., Hitz, B. C., Karra, K., Nash, R. S., Weng, S., Wong, E. D., Lloyd, P., Skrzypek, M. S., Miyasato, S. R., Simison, M., & Cherry, J. M. (2014). The Reference Genome Sequence of *Saccharomyces cerevisiae*: Then and Now. *G3: Genes, Genomes, Genetics*, 4(3). <https://doi.org/10.1534/g3.113.008995>
- Evans, D. R. (1961). Biological Clocks. Volume XXV. Cold Spring Harbor Symposia on Quantitative Biology. . *The Quarterly Review of Biology*, 36(3). <https://doi.org/10.1086/403447>

- Farré, E. M., & Weise, S. E. (2012). The interactions between the circadian clock and primary metabolism. In *Current Opinion in Plant Biology* (Vol. 15, Issue 3). <https://doi.org/10.1016/j.pbi.2012.01.013>
- Fauré-Fremiet, E. (1951). The tidal rhythm of the diatom Hantzschia amphioxys. *Biological Bulletin*, 100(3), 173–177.
- Ferrari, C., Proost, S., Janowski, M., Becker, J., Nikoloski, Z., Bhattacharya, D., Price, D., Tohge, T., Bar-Even, A., Fernie, A., Stitt, M., & Mutwil, M. (2019). Kingdom-wide comparison reveals the evolution of diurnal gene expression in Archaeplastida. In *Nature Communications*. <https://doi.org/10.1038/s41467-019-08703-2>
- Feugier, F. G., & Satake, A. (2013). Dynamical feedback between circadian clock and sucrose availability explains adaptive response of starch metabolism to various photoperiods. *Frontiers in Plant Science*, 3(JAN). <https://doi.org/10.3389/fpls.2012.00305>
- Finegan, C., Boehlein, S. K., Leach, K. A., Madrid, G., Hannah, L. C., Koch, K. E., Tracy, W. F., & Resende, M. F. R. (2022). Genetic Perturbation of the Starch Biosynthesis in Maize Endosperm Reveals Sugar-Responsive Gene Networks. *Frontiers in Plant Science*, 12. <https://doi.org/10.3389/fpls.2021.800326>
- Flis, A., Mengin, V., Ivakov, A. A., Mugford, S. T., Hubberten, H. M., Encke, B., Krohn, N., Höhne, M., Feil, R., Hoefgen, R., Lunn, J. E., Millar, A. J., Smith, A. M., Sulpice, R., & Stitt, M. (2019). Multiple circadian clock outputs regulate diel turnover of carbon and nitrogen reserves. *Plant Cell and Environment*, 42(2). <https://doi.org/10.1111/pce.13440>
- Flis, A., Sulpice, R., Seaton, D. D., Ivakov, A. A., Liput, M., Abel, C., Millar, A. J., & Stitt, M. (2016). Photoperiod-dependent changes in the phase of core clock transcripts and global transcriptional outputs at dawn and dusk in Arabidopsis. *Plant Cell and Environment*, 39(9). <https://doi.org/10.1111/pce.12754>
- Foà, A., & Bertolucci, C. (2001). Temperature cycles induce a bimodal activity pattern in ruin lizards: Masking or clock-controlled event? A seasonal problem. *Journal of Biological Rhythms*, 16(6). <https://doi.org/10.1177/074873001129002268>
- Frazee, A. C., Pertea, G., Jaffe, A. E., Langmead, B., Salzberg, S. L., & Leek, J. T. (2015). Ballgown bridges the gap between transcriptome assembly and expression analysis. *Nature Biotechnology*, 33, 243. <https://doi.org/10.1038/nbt.3172>
- Fu, L., Patel, M. S., Bradley, A., Wagner, E. F., & Karsenty, G. (2005). The molecular clock mediates leptin-regulated bone formation. *Cell*, 122(5). <https://doi.org/10.1016/j.cell.2005.06.028>

- Fung-Uceda, J., Lee, K., Seo, P. J., Polyn, S., De Veylder, L., & Mas, P. (2018). The Circadian Clock Sets the Time of DNA Replication Licensing to Regulate Growth in *Arabidopsis*. *Developmental Cell*, 45(1). <https://doi.org/10.1016/j.devcel.2018.02.022>
- Galperin, M. Y., Wolf, Y. I., Makarova, K. S., Alvarez, R. V., Landsman, D., & Koonin, E. V. (2021). COG database update: Focus on microbial diversity, model organisms, and widespread pathogens. *Nucleic Acids Research*, 49(D1). <https://doi.org/10.1093/nar/gkaa1018>
- García-Cubero, R., Moreno-Fernández, J., & García-González, M. (2018). Potential of *Chlorella vulgaris* to Abate Flue Gas. *Waste and Biomass Valorization*, 9(11), 2015–2019. <https://doi.org/10.1007/s12649-017-9987-9>
- García-Domínguez, M., & Florencio, F. J. (1997). Nitrogen availability and electron transport control the expression of *glnB* gene (encoding PII protein) in the cyanobacterium *Synechocystis* sp. PCC 6803. *Plant Molecular Biology*, 35(6). <https://doi.org/10.1023/A:1005846626187>
- García-Plazaola, J. I., Fernández-Marín, B., Ferrio, J. P., Alday, J. G., Hoch, G., Landais, D., Milcu, A., Tissue, D. T., Voltas, J., Gessler, A., Roy, J., & Resco de Dios, V. (2017). Endogenous circadian rhythms in pigment composition induce changes in photochemical efficiency in plant canopies. *Plant Cell and Environment*, 40(7). <https://doi.org/10.1111/pce.12909>
- Gaspar, J. M. (2018). Improved peak-calling with MACS2. *BioRxiv*.
- Geigenberger, P. (2011). Regulation of starch biosynthesis in response to a fluctuating environment. *Plant Physiology*, 155(4). <https://doi.org/10.1104/pp.110.170399>
- Goodstein, D. M., Shu, S., Howson, R., Neupane, R., Hayes, R. D., Fazo, J., Mitros, T., Dirks, W., Hellsten, U., Putnam, N., & Rokhsar, D. S. (2012). Phytozome: A comparative platform for green plant genomics. *Nucleic Acids Research*, 40(D1), D1178–D1186. <https://doi.org/10.1093/nar/gkr944>
- Goto, K., & Johnson, C. H. (1995). Is the cell division cycle gated by a circadian clock? The case of *Chlamydomonas reinhardtii*. *Journal of Cell Biology*, 129(4). <https://doi.org/10.1083/jcb.129.4.1061>
- Graf, A., Schlereth, A., Stitt, M., & Smith, A. M. (2010). Circadian control of carbohydrate availability for growth in *Arabidopsis* plants at night. *Proceedings of the National Academy of Sciences*, 107(20), 9458–9463. <https://doi.org/10.1073/pnas.0914299107>
- Granados-Fuentes, D., Tseng, A., & Herzog, E. D. (2006). A circadian clock in the olfactory bulb controls olfactory responsiveness. *Journal of Neuroscience*, 26(47). <https://doi.org/10.1523/JNEUROSCI.3445-06.2006>

- Grigoriev, I. V., Hayes, R. D., Calhoun, S., Kamel, B., Wang, A., Ahrendt, S., Dusheyko, S., Nikitin, R., Mondo, S. J., Salamov, A., Shabalov, I., & Kuo, A. (2021). PhycoCosm, a comparative algal genomics resource. *Nucleic Acids Research*, 49(D1). <https://doi.org/10.1093/nar/gkaa898>
- Guyon, J.-B., Vergé, V., Schatt, P., Lozano, J.-C., Liennard, M., & Bouget, F.-Y. (2018). Comparative Analysis of Culture Conditions for the Optimization of Carotenoid Production in Several Strains of the Picoplanktonic Eukaryote *Ostreococcus*. *Marine Drugs*, 16(3). <https://doi.org/10.3390/md16030076>
- Hagiwara, S., Bolige, A., Zhang, Y., Takahashi, M., Yamagishi, A., & Goto, K. (2002). Circadian Gating of Photoinduction of Commitment to Cell-cycle Transitions in Relation to Photoperiodic Control of Cell Reproduction in *Euglena*. *Photochemistry and Photobiology*, 76(1). [https://doi.org/10.1562/0031-8655\(2002\)076<0105:cgpoc>2.0.co;2](https://doi.org/10.1562/0031-8655(2002)076<0105:cgpoc>2.0.co;2)
- Hartman, M. D., Rojas, B. E., Iglesias, A. A., & Figueroa, C. M. (2023). The involvement of allosteric effectors and post-translational modifications in the control of plant central carbon metabolism. *Plant Journal*, 114(5). <https://doi.org/10.1111/tpj.16215>
- Hastings, J. W., & Sweeney, B. M. (1957). The luminescent reaction in extracts of the marine dinoflagellate, *Gonyaulax polyedra*. *Journal of Cellular Physiology*, 49(2). <https://doi.org/10.1002/jcp.1030490205>
- Hayes, K. R., Beatty, M., Meng, X., Simmons, C. R., Habben, J. E., & Danilevskaya, O. N. (2010). Maize global transcriptomics reveals pervasive leaf diurnal rhythms but rhythms in developing ears are largely limited to the core oscillator. *PLoS ONE*, 5(9). <https://doi.org/10.1371/journal.pone.0012887>
- Henderson, G. P., Gan, L., & Jensen, G. J. (2012). 3-D Ultrastructure of *O. tauri*: Electron Cryotomography of an Entire Eukaryotic Cell. *PLoS ONE*, 2(1). <https://doi.org/10.1371/journal.pone.0000749>
- Homma, K., & Hastings, J. W. (1989). The S phase is discrete and is controlled by the circadian clock in the marine dinoflagellate *Gonyaulax polyedra*. *Experimental Cell Research*, 182(2). [https://doi.org/10.1016/0014-4827\(89\)90265-6](https://doi.org/10.1016/0014-4827(89)90265-6)
- Hoopes, G. M., Zarka, D., Feke, A., Acheson, K., Hamilton, J. P., Douches, D., Buell, C. R., & Farré, E. M. (2022). Keeping time in the dark: Potato diel and circadian rhythmic gene expression reveals tissue-specific circadian clocks. *Plant Direct*, 6(7). <https://doi.org/10.1002/pld3.425>
- Hori, K., Maruyama, F., Fujisawa, T., Togashi, T., Yamamoto, N., Seo, M., Sato, S., Yamada, T., Mori, H., Tajima, N., Moriyama, T., Ikeuchi, M., Watanabe, M., Wada, H., Kobayashi, K., Saito, M., Masuda, T., Sasaki-Sekimoto, Y., Mashiguchi, K., ... Ohta, H. (2014). *Klebsormidium flaccidum* genome reveals primary factors for plant terrestrial adaptation. *Nature Communications*, 5. <https://doi.org/10.1038/ncomms4978>

- Howe, K. L., Achuthan, P., Allen, J., Allen, J., Alvarez-Jarreta, J., Ridwan Amode, M., Armean, I. M., Azov, A. G., Bennett, R., Bhai, J., Billis, K., Boddu, S., Charkhchi, M., Cummins, C., da Rin Fioretto, L., Davidson, C., Dodiya, K., El Houdaigui, B., Fatima, R., ... Flieck, P. (2021). Ensembl 2021. *Nucleic Acids Research*, 49(D1). <https://doi.org/10.1093/nar/gkaa942>
- Hoys, C., Romero-Losada, A. B., del Río, E., Guerrero, M. G., Romero-Campero, F. J., & García-González, M. (2021). Unveiling the underlying molecular basis of astaxanthin accumulation in Haematococcus through integrative metabolomic-transcriptomic analysis. *Bioresource Technology*, 332. <https://doi.org/10.1016/j.biortech.2021.125150>
- Hundahl, C. A., Fahrenkrug, J., Hay-Schmidt, A., Georg, B., Faltoft, B., & Hannibal, J. (2012). Circadian behaviour in neuroglobin deficient mice. *PLoS ONE*, 7(4). <https://doi.org/10.1371/journal.pone.0034462>
- Ideker, T., Galitski, T., & Hood, L. (2001). A new approach to decoding life: Systems biology. In *Annual Review of Genomics and Human Genetics* (Vol. 2). <https://doi.org/10.1146/annurev.genom.2.1.343>
- Imai, R., Makino, H., Katoh, T., Kimura, T., Kurita, T., Hokamura, K., Umemura, K., & Nakajima, Y. (2020). Desflurane anesthesia shifts the circadian rhythm phase depending on the time of day of anesthesia. *Scientific Reports*, 10(1). <https://doi.org/10.1038/s41598-020-75434-6>
- Jamers, A., Blust, R., & De Coen, W. (2009). Omics in algae: Paving the way for a systems biological understanding of algal stress phenomena? In *Aquatic Toxicology* (Vol. 92, Issue 3). <https://doi.org/10.1016/j.aquatox.2009.02.012>
- Joyce, A. R., & Palsson, B. (2006). The model organism as a system: Integrating “omics” data sets. In *Nature Reviews Molecular Cell Biology* (Vol. 7, Issue 3). <https://doi.org/10.1038/nrm1857>
- Kanehisa, M., Sato, Y., Kawashima, M., Furumichi, M., & Tanabe, M. (2016). KEGG as a reference resource for gene and protein annotation. *Nucleic Acids Research*, 44(D1), D457–D462. <https://doi.org/10.1093/nar/gkv1070>
- Karahalil, B. (2016). Overview of Systems Biology and Omics Technologies. *Current Medicinal Chemistry*, 23(37), 4221–4230. <https://doi.org/10.2174/0929867323666160926150617>
- Kato, S., & Nam, H. G. (2021). The cell division cycle of euglena gracilis indicates that the level of circadian plasticity to the external light regime changes in prolonged-stationary cultures. *Plants*, 10(7). <https://doi.org/10.3390/plants10071475>
- Kay, H., Grünewald, E., Feord, H. K., Gil, S., Peak-Chew, S. Y., Stangerlin, A., O'Neill, J. S., & van Ooijen, G. (2021). Deep-coverage spatiotemporal proteome of the pi-

coeukaryote *Ostreococcus tauri* reveals differential effects of environmental and endogenous 24-hour rhythms. *Communications Biology*, 4(1), 1–11. <https://doi.org/10.1038/s42003-021-02680-3>

Kester, D. R., Duedall, I. W., Connors, D. N., & Pytkowicz, R. M. (1967). PREPARATION OF ARTIFICIAL SEAWATER. *Limnology and Oceanography*, 12(1), 176–179. <https://doi.org/10.4319/lo.1967.12.1.0176>

Khadaroo, B., Robbens, S., Ferraz, C., Derelle, E., Eychenié, S., Cooke, R., Peaucellier, G., Delseny, M., Demaille, J., Van De Peer, Y., Picard, A., & Moreau, H. (2004). The first green lineage cdc25 dual-specificity phosphatase. *Cell Cycle*, 3(4). <https://doi.org/10.4161/cc.3.4.815>

Kim, D., Langmead, B., & Salzberg, S. L. (2015). HISAT: A fast spliced aligner with low memory requirements. *Nature Methods*, 12, 357–360. <https://doi.org/10.1038/nmeth.3317>

Klante, G., & Steinlechner, S. (1994). Light Irradiance and Wavelength as Seasonal Cues for Djungarian Hamsters. *Biological Rhythm Research*, 25(4). <https://doi.org/10.1080/09291019409360310>

Konopka, R. J., & Benzer, S. (1971). Clock mutants of *Drosophila melanogaster*. *Proceedings of the National Academy of Sciences of the United States of America*, 68(9). <https://doi.org/10.1073/pnas.68.9.2112>

Kötting, O., Kossmann, J., Zeeman, S. C., & Lloyd, J. R. (2010). Regulation of starch metabolism: The age of enlightenment? In *Current Opinion in Plant Biology* (Vol. 13, Issue 3). <https://doi.org/10.1016/j.pbi.2010.01.003>

Krumholz, E. W., Yang, H., Weisenhorn, P., Henry, C. S., & Libourel, I. G. L. (2012). Genome-wide metabolic network reconstruction of the picoalga *Ostreococcus*. *Journal of Experimental Botany*, 63(6), 2353–2362. <https://doi.org/10.1093/jxb/err407>

Kuhlman, S. J., Craig, L. M., & Duffy, J. F. (2018). Introduction to chronobiology. *Cold Spring Harbor Perspectives in Biology*, 10(9). <https://doi.org/10.1101/cshperspect.a033613>

Kyorku, C., & Brady, J. (1994). A free-running bimodal circadian rhythm in the tsetse fly *Glossina longipennis*. *Journal of Insect Physiology*, 40(1). [https://doi.org/10.1016/0022-1910\(94\)90112-0](https://doi.org/10.1016/0022-1910(94)90112-0)

Laloum, D., & Robinson-Rechavi, M. (2020). Methods detecting rhythmic gene expression are biologically relevant only for strong signal. *PLoS Computational Biology*, 16(3). <https://doi.org/10.1371/journal.pcbi.1007666>

Lamesch, P., Berardini, T. Z., Li, D., Swarbreck, D., Wilks, C., Sasidharan, R., Muller, R., Dreher, K., Alexander, D. L., Garcia-Hernandez, M., Karthikeyan, A. S., Lee, C. H.,

- Nelson, W. D., Ploetz, L., Singh, S., Wensel, A., & Huala, E. (2012). The Arabidopsis Information Resource (TAIR): Improved gene annotation and new tools. *Nucleic Acids Research*, 40(D1). <https://doi.org/10.1093/nar/gkr1090>
- Langmead, B., & Salzberg, S. L. (2012). Fast gapped-read alignment with Bowtie 2. *Nature Methods*, 9(4). <https://doi.org/10.1038/nmeth.1923>
- Lawrence, M., Huber, W., Pagès, H., Aboyoun, P., Carlson, M., Gentleman, R., Morgan, M. T., & Carey, V. J. (2013). Software for Computing and Annotating Genomic Ranges. *PLoS Computational Biology*, 9(8). <https://doi.org/10.1371/journal.pcbi.1003118>
- Le Bihan, T., Martin, S. F., Chirnside, E. S., van Ooijen, G., Barrios-Llerena, M. E., O'Neill, J. S., Shliaha, P. V., Kerr, L. E., & Millar, A. J. (2011a). Shotgun proteomic analysis of the unicellular alga *Ostreococcus tauri*. *Journal of Proteomics*, 74(10). <https://doi.org/10.1016/j.jprot.2011.05.028>
- Le Bihan, T., Martin, S. F., Chirnside, E. S., van Ooijen, G., Barrios-Llerena, M. E., O'Neill, J. S., Shliaha, P. V., Kerr, L. E., & Millar, A. J. (2011b). Shotgun proteomic analysis of the unicellular alga *Ostreococcus tauri*. *Journal of Proteomics*, 74(10), 2060–2070. <https://doi.org/10.1016/j.jprot.2011.05.028>
- Le Bihan, T., Martin, S. F., Chirnside, E. S., van Ooijen, G., Barrios-Llerena, M. E., O'Neill, J. S., Shliaha, P. V., Kerr, L. E., & Millar, A. J. (2011c). Shotgun proteomic analysis of the unicellular alga *Ostreococcus tauri*. *Journal of Proteomics*, 74(10), 2060–2070. <https://doi.org/10.1016/j.jprot.2011.05.028>
- Lebert, M., Porst, M., & Häder, D. P. (1999). Circadian rhythm of gravitaxis in *Euglena gracilis*. *Journal of Plant Physiology*, 155(3). [https://doi.org/10.1016/S0176-1617\(99\)80115-1](https://doi.org/10.1016/S0176-1617(99)80115-1)
- Leconte, J., Benites, L. F., Vannier, T., Wincker, P., Piganeau, G., & Jaillon, O. (2020). Genome resolved biogeography of mamiellales. *Genes*, 11(1). <https://doi.org/10.3390/genes11010066>
- Lelandais, G., Scheiber, I., Paz-Yepes, J., Lozano, J.-C., Botebol, H., Pilátová, J., Žářský, V., Léger, T., Blaiseau, P.-L., Bowler, C., Bouget, F.-Y., Camadro, J.-M., Sutak, R., & Lesuisse, E. (2016). *Ostreococcus tauri* is a new model green alga for studying iron metabolism in eukaryotic phytoplankton. *BMC Genomics*, 17(1), 319. <https://doi.org/10.1186/s12864-016-2666-6>
- Leliaert, F., Smith, D. R., Moreau, H., Herron, M. D., Verbruggen, H., Delwiche, C. F., & De Clerck, O. (2012). Phylogeny and Molecular Evolution of the Green Algae. *Critical Reviews in Plant Sciences*, 31(1). <https://doi.org/10.1080/07352689.2011.615705>

- Leliaert, F., Verbruggen, H., & Zechman, F. W. (2011). Into the deep: New discoveries at the base of the green plant phylogeny. In *BioEssays* (Vol. 33, Issue 9). <https://doi.org/10.1002/bies.201100035>
- Lillo, C., Meyer, C., & Ruoff, P. (2001). The nitrate reductase circadian system. The central clock dogma contra multiple oscillatory feedback loops. In *Plant Physiology* (Vol. 125, Issue 4). <https://doi.org/10.1104/pp.125.4.1554>
- Lillo, C., & Ruoff, P. (1989). An unusually rapid light-induced nitrate reductase mRNA pulse and circadian oscillations. *Naturwissenschaften*, 76(11). <https://doi.org/10.1007/BF00374129>
- Lonergan, T. A. (1981). A Circadian Rhythm in the Rate of Light-Induced Electron Flow in Three Leguminous Species. *Plant Physiology*, 68(5). <https://doi.org/10.1104/pp.68.5.1041>
- López, D., Casero, D., Cookus, S. J., Merchant, S. S., & Pellegrini, M. (2011). Algal Functional Annotation Tool: A web-based analysis suite to functionally interpret large gene lists using integrated annotation and expression data. *BMC Bioinformatics*, 12, 282. <https://doi.org/10.1186/1471-2105-12-282>
- Lück, S., Thurley, K., Thaben, P. F., & Westermark, P. O. (2014). Rhythmic degradation explains and unifies circadian transcriptome and proteome data. *Cell Reports*, 9(2), 741–751. <https://doi.org/10.1016/j.celrep.2014.09.021>
- Ludwig, C., Gillet, L., Rosenberger, G., Amon, S., Collins, B. C., & Aebersold, R. (2018). Data-independent acquisition-based SWATH - MS for quantitative proteomics: a tutorial. *Molecular Systems Biology*, 14(8). <https://doi.org/10.15252/msb.20178126>
- Ma, D., Przybylski, D., Abruzzi, K. C., Schlichting, M., Li, Q., Long, X., & Rosbash, M. (2021). A transcriptomic taxonomy of drosophila circadian neurons around the clock. *eLife*, 10. <https://doi.org/10.7554/eLife.63056>
- Mack, G. A., & Wolfe, D. A. (1981). K-sample rank tests for umbrella alternatives. *Journal of the American Statistical Association*, 76(373). <https://doi.org/10.1080/01621459.1981.10477625>
- Mackenzie, T. D. B., & Morse, D. (2011). Circadian photosynthetic reductant flow in the dinoflagellate *Lingulodinium* is limited by carbon availability. *Plant, Cell and Environment*, 34(4). <https://doi.org/10.1111/j.1365-3040.2010.02271.x>
- Masseroli, M., Martucci, D., & Pincioli, F. (2004). GFINDer: Genome Function INtegrated Discoverer through dynamic annotation, statistical analysis, and mining. *Nucleic Acids Research*, 32(WEB SERVER ISS.). <https://doi.org/10.1093/nar/gkh432>

- Matsuo, T., Yamaguchi, S., Mitsui, S., Emi, A., Shimoda, F., & Okamura, H. (2003). Control mechanism of the circadian clock for timing of cell division in vivo. *Science*, 302(5643). <https://doi.org/10.1126/science.1086271>
- Mazzocchi, F. (2012). Complexity and the reductionism-holism debate in systems biology. *Wiley Interdisciplinary Reviews: Systems Biology and Medicine*, 4(5), 413–427. <https://doi.org/10.1002/wsbm.1181>
- Mazzoccoli, G., Vinciguerra, M., Carbone, A., & Relógio, A. (2020). The circadian clock, the immune system, and viral infections: The intricate relationship between biological time and host-virus interaction. In *Pathogens* (Vol. 9, Issue 2). <https://doi.org/10.3390/pathogens9020083>
- McClung, C. R. (2006). Plant circadian rhythms. In *Plant Cell* (Vol. 18, Issue 4). <https://doi.org/10.1105/tpc.106.040980>
- Merchant, S. S., Prochnik, S. E., Vallon, O., Harris, E. H., Karpowicz, S. J., Witman, G. B., Terry, A., Salamov, A., Fritz-Laylin, L. K., Maréchal-Drouard, L., Marshall, W. F., Qu, L. H., Nelson, D. R., Sanderfoot, A. A., Spalding, M. H., Kapitonov, V. V., Ren, Q., Ferris, P., Lindquist, E., ... Zhou, K. (2007). The Chlamydomonas genome reveals the evolution of key animal and plant functions. *Science*, 318(5848). <https://doi.org/10.1126/science.1143609>
- Merchante, C., Stepanova, A. N., & Alonso, J. M. (2017). Translation regulation in plants: an interesting past, an exciting present and a promising future. *Plant Journal*, 90(4). <https://doi.org/10.1111/tpj.13520>
- Mermet, J., Yeung, J., & Naef, F. (2017). Systems chronobiology: Global analysis of gene regulation in a 24-hour periodic world. *Cold Spring Harbor Perspectives in Biology*, 9(3). <https://doi.org/10.1101/cshperspect.a028720>
- Merrow, M., Spoelstra, K., & Roenneberg, T. (2005). The circadian cycle: Daily rhythms from behaviour to genes. In *EMBO Reports* (Vol. 6, Issue 10). <https://doi.org/10.1038/sj.embo.7400541>
- Messager, S., Hazlerigg, D. G., Mercer, J. G., & Morgan, P. J. (2000). Photoperiod differentially regulates the expression of Per1 and ICER in the pars tuberalis and the suprachiasmatic nucleus of the Siberian hamster. *European Journal of Neuroscience*, 12(8). <https://doi.org/10.1046/j.1460-9568.2000.00174.x>
- Mi, H., Ebert, D., Muruganujan, A., Mills, C., Albou, L. P., Mushayamaha, T., & Thomas, P. D. (2021). PANTHER version 16: A revised family classification, tree-based classification tool, enhancer regions and extensive API. *Nucleic Acids Research*, 49(D1). <https://doi.org/10.1093/nar/gkaa1106>

- Miller, B. H., McDearmon, E. L., Panda, S., Hayes, K. R., Zhang, J., Andrews, J. L., Antoch, M. P., Walker, J. R., Esser, K. A., Hogenesch, J. B., & Takahashi, J. S. (2007). Circadian and CLOCK-controlled regulation of the mouse transcriptome and cell proliferation. *Proceedings of the National Academy of Sciences of the United States of America*, 104(9). <https://doi.org/10.1073/pnas.0611724104>
- Mistry, J., Chuguransky, S., Williams, L., Qureshi, M., Salazar, G. A., Sonnhammer, E. L. L., Tosatto, S. C. E., Paladin, L., Raj, S., Richardson, L. J., Finn, R. D., & Bateman, A. (2021). Pfam: The protein families database in 2021. *Nucleic Acids Research*, 49(D1). <https://doi.org/10.1093/nar/gkaa913>
- Mitsui, A., Kumazawa, S., Takahashi, A., Ikemoto, H., Cao, S., & Arai, T. (1986). Strategy by which nitrogen-fixing unicellular cyanobacteria grow photoautotrophically. *Nature*, 323(6090). <https://doi.org/10.1038/323720a0>
- Mittag, M. (2001). Circadian rhythms in microalgae. *International Review of Cytology*, 206. [https://doi.org/10.1016/S0074-7696\(01\)06023-5](https://doi.org/10.1016/S0074-7696(01)06023-5)
- Mohabir, G., & Edmunds, L. N. (1999). Circadian clock regulation of the bimodal rhythm of cyclic AMP in wild-type Euglena. *Cellular Signalling*, 11(2). [https://doi.org/10.1016/S0898-6568\(98\)00046-1](https://doi.org/10.1016/S0898-6568(98)00046-1)
- Monnier, A., Liverani, S., Bouvet, R., Jesson, B., Smith, J. Q., Mosser, J., Corellou, F., & Bouget, F. Y. (2010). Orchestrated transcription of biological processes in the marine picoeukaryote Ostreococcus exposed to light/dark cycles. *BMC Genomics*, 11(1). <https://doi.org/10.1186/1471-2164-11-192>
- Moreau, H., Grimsley, N., Derelle, E., Ferraz, C., Escande, M.L., Eychenié, S., Cooke, R., Piganeau, G., Desdevives, Y., Bellec, L. (1995). A new marine picoeukaryote: *Ostreococcus tauri* gen. et sp. nov. (*Chlorophyta, Prasinophyceae*). 34(4), 285–292.
- Moreau, H., Verhelst, B., Couloux, A., Derelle, E., Rombauts, S., Grimsley, N., Van Bel, M., Poulain, J., Katinka, M., Hohmann-Marriott, M. F., Piganeau, G., Rouzé, P., Da Silva, C., Wincker, P., Van de Peer, Y., & Vandepoele, K. (2012). Gene functionalities and genome structure in Bathycoccus prasinos reflect cellular specializations at the base of the green lineage. *Genome Biology*, 13(8). <https://doi.org/10.1186/gb-2012-13-8-r74>
- Morimoto, D., Yoshida, T., & Sawayama, S. (2020). Draft Genome Sequence of the Astaxanthin-Producing Microalga Haematococcus lacustris Strain NIES-144. *Microbiology Resource Announcements*, 9(23). <https://doi.org/10.1128/mra.00128-20>
- Moriya, Y., Itoh, M., Okuda, S., Yoshizawa, A. C., & Kanehisa, M. (2007). KAAS: An automatic genome annotation and pathway reconstruction server. *Nucleic Acids Research*, 35(SUPPL.2), 182–185. <https://doi.org/10.1093/nar/gkm321>

- Morris, A. R., Stanton, D. L., Roman, D., & Liu, A. C. (2020). Systems Level Understanding of Circadian Integration with Cell Physiology. In *Journal of Molecular Biology* (Vol. 432, Issue 12). <https://doi.org/10.1016/j.jmb.2020.02.002>
- Moulager, M., Corellou, F., Vergé, V., Escande, M. L., & Bouget, F. Y. (2010). Integration of light signals by the retinoblastoma pathway in the control of S phase entry in the Pico-phytoplanktonic cell Ostreococcus. *PLoS Genetics*, 6(5), 11. <https://doi.org/10.1371/journal.pgen.1000957>
- Moulager, M., Monnier, A., Jesson, B., Bouvet, R., Mosser, J., Schwartz, C., Garnier, L., Corellou, F., & Bouget, F. Y. (2007). Light-dependent regulation of cell division in Ostreococcus: Evidence for a major transcriptional input. *Plant Physiology*, 144(3), 1360–1369. <https://doi.org/10.1104/pp.107.096149>
- Nelson, C. J., Alexova, R., Jacoby, R. P., & Harvey Millar, A. (2014). Proteins with high turnover rate in barley leaves estimated by proteome analysis combined with in planta isotope labeling. *Plant Physiology*, 166(1). <https://doi.org/10.1104/pp.114.243014>
- Nelson, C. J., & Millar, A. H. (2015). Protein turnover in plant biology. In *Nature Plants* (Vol. 1). <https://doi.org/10.1038/nplants.2015.17>
- Ngan, C. Y., Wong, C. H., Choi, C., Yoshinaga, Y., Louie, K., Jia, J., Chen, C., Bowen, B., Cheng, H., Leonelli, L., Kuo, R., Baran, R., Garcíá-Cerdán, J. G., Pratap, A., Wang, M., Lim, J., Tice, H., Daum, C., Xu, J., ... Wei, C. L. (2015). Lineage-specific chromatin signatures reveal a regulator of lipid metabolism in microalgae. *Nature Plants*, 1, 15107. <https://doi.org/10.1038/nplants.2015.107>
- Nishiwaki-Ohkawa, T., & Yoshimura, T. (2016). Molecular basis for regulating seasonal reproduction in vertebrates. In *Journal of Endocrinology* (Vol. 229, Issue 3). <https://doi.org/10.1530/JOE-16-0066>
- Noordally, Z. B., & Millar, A. J. (2015). Clocks in algae. *Biochemistry*, 54(2), 171–183. <https://doi.org/10.1021/bi501089x>
- Numata, H., Miyazaki, Y., & Ikeno, T. (2015). Common features in diverse insect clocks. *Zoological Letters*, 1(1). <https://doi.org/10.1186/s40851-014-0003-y>
- O'Kelly, C. J., Sieracki, M. E., Thier, E. C., & Hobson, I. C. (2003). A transient bloom of Ostreococcus (Chlorophyta, Prasinophyceae) in West Neck Bay, Long Island, New York. *Journal of Phycology*, 39(5). <https://doi.org/10.1046/j.1529-8817.2003.02201.x>
- Ogata, H., Goto, S., Sato, K., Fujibuchi, W., Bono, H., & Kanehisa, M. (1999). KEGG: Kyoto encyclopedia of genes and genomes. In *Nucleic Acids Research*. <https://doi.org/10.1093/nar/27.1.29>

- Ohara, T., Fukuda, H., & Tokuda, I. T. (2015). An extended mathematical model for reproducing the phase response of *Arabidopsis thaliana* under various light conditions. *Journal of Theoretical Biology*, 382. <https://doi.org/10.1016/j.jtbi.2015.07.016>
- Ottesen, E. A., Young, C. R., Eppley, J. M., Ryan, J. P., Chavez, F. P., Scholin, C. A., & DeLong, E. F. (2013). Pattern and synchrony of gene expression among sympatric marine microbial populations. *Proceedings of the National Academy of Sciences of the United States of America*, 110(6). <https://doi.org/10.1073/pnas.1222099110>
- Paajanen, P., Lane de Barros Dantas, L., & Dodd, A. N. (2021). Layers of crosstalk between circadian regulation and environmental signalling in plants. In *Current Biology* (Vol. 31, Issue 8). <https://doi.org/10.1016/j.cub.2021.03.046>
- Palenik, B., Brahamsha, B., Larimer, F. W., Land, M., Hauser, L., Chain, P., Lamerdin, J., Regala, W., Allen, E. E., McCarren, J., Paulsen, I., Dufresne, A., Partensky, F., Webb, E. A., & Waterbury, J. (2003). The genome of a motile marine *Synechococcus*. *Nature*, 424(6952). <https://doi.org/10.1038/nature01943>
- Palenik, B., Grimwood, J., Aerts, A., Rouzé, P., Salamov, A., Putnam, N., Dupont, C., Jorgensen, R., Derelle, E., Rombauts, S., Zhou, K., Ollilar, R., Merchant, S. S., Podell, S., Gaasterland, T., Napoli, C., Gendler, K., Manuell, A., Tai, V., ... Grigoriev, I. V. (2007). The tiny eukaryote *Ostreococcus* provides genomic insights into the paradox of plankton speciation. *Proceedings of the National Academy of Sciences of the United States of America*, 104(18). <https://doi.org/10.1073/pnas.0611046104>
- Pan, Y., Ballance, H., Meng, H., Gonzalez, N., Kim, S. M., Abdurehman, L., York, B., Chen, X., Schnytzer, Y., Levy, O., Dacso, C. C., McClung, C. A., O'Malley, B. W., Liu, S., & Zhu, B. (2020). 12-h clock regulation of genetic information flow by XBP1s. *PLoS Biology*, 18(1). <https://doi.org/10.1371/journal.pbio.3000580>
- Pan, Y., Michael, T. P., Hudson, M. E., Kay, S. A., Chory, J., & Schuler, M. A. (2009). Cytochrome P450 monooxygenases as reporters for circadian-regulated pathways. *Plant Physiology*, 150(2). <https://doi.org/10.1104/pp.108.130757>
- Panter, P. E., Muranaka, T., Cuitun-Coronado, D., Graham, C. A., Yochikawa, A., Kudoh, H., & Dodd, A. N. (2019). Circadian Regulation of the Plant Transcriptome Under Natural Conditions. In *Frontiers in Genetics* (Vol. 10). <https://doi.org/10.3389/fgene.2019.01239>
- Parsons, R., Parsons, R., Garner, N., Oster, H., & Rawashdeh, O. (2020). CircaCompare: A method to estimate and statistically support differences in mesor, amplitude and phase, between circadian rhythms. *Bioinformatics*, 36(4). <https://doi.org/10.1093/bioinformatics/btz730>
- Pereira, H., Sá, M., Maia, I., Rodrigues, A., Teles, I., Wijffels, R. H., Navalho, J., & Barbosa, M. (2021). Fucoxanthin production from *Tisochrysis lutea* and *Phaeodactylum*

tricornutum at industrial scale. *Algal Research*, 56. <https://doi.org/10.1016/j.algal.2021.102322>

Pertea, M., Kim, D., Pertea, G. M., Leek, J. T., & Salzberg, S. L. (2016). Transcript-level expression analysis of RNA-seq experiments with HISAT, StringTie and Ballgown. *Nature Protocols*, 11(9). <https://doi.org/10.1038/nprot.2016.095>

Pertea, M., Pertea, G. M., Antonescu, C. M., Chang, T. C., Mendell, J. T., & Salzberg, S. L. (2015). StringTie enables improved reconstruction of a transcriptome from RNA-seq reads. *Nature Biotechnology*, 33, 290–295. <https://doi.org/10.1038/nbt.3122>

Pfeuty, B., Thommen, Q., Corellou, F., Djouani-Tahri, E. B., Bouget, F. Y., & Lefranc, M. (2012). Circadian clocks in changing weather and seasons: Lessons from the picoalga *ostreococcus tauri*. *BioEssays*, 34(9), 781–790. <https://doi.org/10.1002/bies.201200012>

Pilgrim, M. L., & McClung, C. R. (1993). Differential involvement of the circadian clock in the expression of genes required for ribulose-1,5-bisphosphate carboxylase/oxygenase synthesis, assembly, and activation in *Arabidopsis thaliana*. *Plant Physiology*, 103(2), 553–564. <https://doi.org/10.1104/pp.103.2.553>

Pittendrigh, C. S. (1960). Circadian rhythms and the circadian organization of living systems. *Cold Spring Harbor Symposia on Quantitative Biology*, 25. <https://doi.org/10.1101/SQB.1960.025.01.015>

Polle, J. E. W., Barry, K., Cushman, J., Schmutz, J., Tran, D., Hathwaik, L. T., Yim, W. C., Jenkins, J., McKie-Krisberg, Z., Prochnik, S., Lindquist, E., Dockter, R. B., Adam, C., Molina, H., Bunkenborg, J., Jin, E. S., Buchheim, M., & Magnuson, J. (2017). Draft nuclear genome sequence of the halophilic and beta-carotene-accumulating green alga *Dunaliella salina* strain CCAP19/18. In *Genome Announcements* (Vol. 5, Issue 43). <https://doi.org/10.1128/genomeA.01105-17>

Potter, S. C., Luciani, A., Eddy, S. R., Park, Y., Lopez, R., & Finn, R. D. (2018). HMMER web server: 2018 update. *Nucleic Acids Research*, 46(W1). <https://doi.org/10.1093/nar/gky448>

Prabhakaran, P. M., & Sheeba, V. (2012). Sympatric drosophilid species *melanogaster* and *ananassae* differ in temporal patterns of activity. *Journal of Biological Rhythms*, 27(5). <https://doi.org/10.1177/0748730412458661>

Prendergast, S. C., Strobl, A. C., Cross, W., Pillay, N., Strauss, S. J., Ye, H., Lindsay, D., Tirabosco, R., Chalker, J., Mahamdallie, S. S., Sosinsky, A., Flanagan, A. M., & Amary, F. (2020). Sarcoma and the 100,000 Genomes Project: our experience and changes to practice. *Journal of Pathology: Clinical Research*, 6(4). <https://doi.org/10.1002/cjp2.174>

- Prochnik, S. E., Umen, J., Nedelcu, A. M., Hallmann, A., Miller, S. M., Nishii, I., Ferris, P., Kuo, A., Mitros, T., Fritz-Laylin, L. K., Hellsten, U., Chapman, J., Simakov, O., Rensing, S. A., Terry, A., Pangilinan, J., Kapitonov, V., Jurka, J., Salamov, A., ... Rokhsar, D. S. (2010). Genomic analysis of organismal complexity in the multicellular green alga *volvox carteri*. *Science*, 329(5988). <https://doi.org/10.1126/science.1188800>
- Radakovits, R., Jinkerson, R. E., Fuerstenberg, S. I., Tae, H., Settlage, R. E., Boore, J. L., & Posewitz, M. C. (2012). Draft genome sequence and genetic transformation of the oleaginous alga *Nannochloropsis gaditana*. *Nature Communications*, 3. <https://doi.org/10.1038/ncomms1688>
- Ral, J. P., Colleoni, C., Wattebled, F., Dauvillée, D., Nempong, C., Deschamps, P., Li, Z., Morell, M. K., Chibbar, R., Purton, S., D'Hulst, C., & Ball, S. G. (2006). Circadian clock regulation of starch metabolism establishes GBSSI as a major contributor to amylopectin synthesis in *Chlamydomonas reinhardtii*. *Plant Physiology*, 142(1). <https://doi.org/10.1104/pp.106.081885>
- Rayko, E., Maumus, F., Maheswari, U., Jabbari, K., & Bowler, C. (2010). Transcription factor families inferred from genome sequences of photosynthetic stramenopiles. *New Phytologist*, 188(1). <https://doi.org/10.1111/j.1469-8137.2010.03371.x>
- Richter, C. P. (1922). A behavioristic study of the activity of the rat. In *A behavioristic study of the activity of the rat*,. <https://doi.org/10.5962/bhl.title.151527>
- Ripperger, J. A., & Merrow, M. (2011). Perfect timing: Epigenetic regulation of the circadian clock. In *FEBS Letters* (Vol. 585, Issue 10). <https://doi.org/10.1016/j.febslet.2011.04.047>
- Ritchie, M. E., Phipson, B., Wu, D., Hu, Y., Law, C. W., Shi, W., & Smyth, G. K. (2015). limma powers differential expression analyses for RNA-sequencing and microarray studies. *Nucleic Acids Research*, 43(7), e47. <https://doi.org/10.1093/nar/gkv007>
- Robbens, S., Khadaroo, B., Camasses, A., Derelle, E., Ferraz, C., Inzé, D., Van De Peer, Y., & Moreau, H. (2005). Genome-wide analysis of core cell cycle genes in the unicellular green alga *Ostreococcus tauri*. *Molecular Biology and Evolution*, 22(3). <https://doi.org/10.1093/molbev/msi044>
- Robles, M. S., Cox, J., & Mann, M. (2014). In-Vivo Quantitative Proteomics Reveals a Key Contribution of Post-Transcriptional Mechanisms to the Circadian Regulation of Liver Metabolism. *PLoS Genetics*, 10(1). <https://doi.org/10.1371/journal.pgen.1004047>
- Rock, A., Wilcockson, D., & Last, K. S. (2022). Towards an Understanding of Circatidal Clocks. In *Frontiers in Physiology* (Vol. 13). <https://doi.org/10.3389/fphys.2022.830107>

- Roenneberg, T., Foster, R. G., & Klerman, E. B. (2022). The circadian system, sleep, and the health/disease balance: a conceptual review. *Journal of Sleep Research*, April, 1–14. <https://doi.org/10.1111/jsr.13621>
- Roenneberg, T., & Merrow, M. (2005). Circadian clocks - The fall and rise of physiology. In *Nature Reviews Molecular Cell Biology* (Vol. 6, Issue 12). <https://doi.org/10.1038/nrm1766>
- Roenneberg, T., & Merrow, M. (2016). The circadian clock and human health. In *Current Biology* (Vol. 26, Issue 10). <https://doi.org/10.1016/j.cub.2016.04.011>
- Roenneberg, T., Pilz, L. K., Zerbini, G., & Winnebeck, E. C. (2019). Chronotype and social jetlag: A (self-) critical review. In *Biology* (Vol. 8, Issue 3). <https://doi.org/10.3390/biology8030054>
- Romero-Campero, F. J., Perez-Hurtado, I., Lucas-Reina, E., Romero, J. M., & Valverde, F. (2016). ChlamyNET: A Chlamydomonas gene co-expression network reveals global properties of the transcriptome and the early setup of key co-expression patterns in the green lineage. *BMC Genomics*, 17, 227. <https://doi.org/10.1186/s12864-016-2564-y>
- Romero-Losada, A. B., Arvanitidou, C., de los Reyes, P., García-González, M., & Romero-Campero, F. J. (2022). ALGAEFUN with MARACAS, microALGAE FUNctional enrichment tool for MicroAlgae RnA-seq and Chip-seq Analysis. *BMC Bioinformatics*, 23(1). <https://doi.org/10.1186/s12859-022-04639-5>
- Roth, M. S., Cokus, S. J., Gallaher, S. D., Walter, A., Lopez, D., Erickson, E., Endelman, B., Westcott, D., Larabell, C. A., Merchant, S. S., Pellegrini, M., & Niyogi, K. K. (2017). Chromosome-level genome assembly and transcriptome of the green alga *Chromochloris zofingiensis* illuminates astaxanthin production. *Proceedings of the National Academy of Sciences of the United States of America*, 114(21), E4296–E4305. <https://doi.org/10.1073/pnas.1619928114>
- Rufty, T. W., & Huber, S. C. (1983). Changes in Starch Formation and Activities of Sucrose Phosphate Synthase and Cytoplasmic Fructose-1,6-bisphosphatase in Response to Source-Sink Alterations. *Plant Physiology*, 72(2). <https://doi.org/10.1104/pp.72.2.474>
- Sanz-Luque, E., Chamizo-Ampudia, A., Llamas, A., Galvan, A., & Fernandez, E. (2015). Understanding nitrate assimilation and its regulation in microalgae. In *Frontiers in Plant Science* (Vol. 6, Issue OCTOBER). <https://doi.org/10.3389/fpls.2015.00899>
- Sekimoto, H. (2017). Sexual reproduction and sex determination in green algae. *Journal of Plant Research*, 130(3). <https://doi.org/10.1007/s10265-017-0908-6>

- Serrano-Bueno, G., Romero-Campero, F. J., Lucas-Reina, E., Romero, J. M., & Valverde, F. (2017). Evolution of photoperiod sensing in plants and algae. *Current Opinion in Plant Biology*, 37, 10–17. <https://doi.org/10.1016/j.pbi.2017.03.007>
- Serrano-Pérez, E., Romero-Losada, A. B., Morales-Pineda, M., García-Gómez, M. E., Couso, I., García-González, M., & Romero-Campero, F. J. (2022). Transcriptomic and Metabolomic Response to High Light in the Charophyte Alga Klebsormidium nitens. *Frontiers in Plant Science*, 13. <https://doi.org/10.3389/fpls.2022.855243>
- Serrano, G., Herrera-Palau, R., Romero, J. M., Serrano, A., Coupland, G., & Valverde, F. (2009). Chlamydomonas CONSTANS and the Evolution of Plant Photoperiodic Signaling. *Current Biology*, 19(5). <https://doi.org/10.1016/j.cub.2009.01.044>
- Sharma, A., Tripathi, V., & Kumar, V. (2022). Control and adaptability of seasonal changes in behavior and physiology of latitudinal avian migrants: Insights from laboratory studies in Palearctic-Indian migratory buntings. *Journal of Experimental Zoology Part A: Ecological and Integrative Physiology*, 35677956. <https://doi.org/10.1002/jez.2631>
- Shen, M., Chang, Y. T., Wu, C. T., Parker, S. J., Saylor, G., Wang, Y., Yu, G., Van Eyk, J. E., Clarke, R., Herrington, D. M., & Wang, Y. (2022). Comparative assessment and novel strategy on methods for imputing proteomics data. *Scientific Reports*, 12(1). <https://doi.org/10.1038/s41598-022-04938-0>
- Sierra, E., Acién, F. G., Fernández, J. M., García, J. L., González, C., & Molina, E. (2008). Characterization of a flat plate photobioreactor for the production of microalgae. *Chemical Engineering Journal*, 138(1–3). <https://doi.org/10.1016/j.cej.2007.06.004>
- Six, C., Sherrard, R., Lionard, M., Roy, S., & Campbell, D. A. (2009). Photosystem II and Pigment Dynamics among ecotypes of the green alga Ostreococcus. *Plant Physiology*, 151(1). <https://doi.org/10.1104/pp.109.140566>
- Six, C., Worden, A. Z., Rodríguez, F., Moreau, H., & Partensky, F. (2005). New insights into the nature and phylogeny of prasinophyte antenna proteins: Ostreococcus tauri, a case study. *Molecular Biology and Evolution*, 22(11), 2217–2230. <https://doi.org/10.1093/molbev/msi220>
- Smith, S. M., Fulton, D. C., Chia, T., Thorneycroft, D., Chapple, A., Dunstan, H., Hylton, C., Zeeman, S. C., & Smith, A. M. (2004). Diurnal changes in the transcriptome encoding enzymes of starch metabolism provide evidence for both transcriptional and posttranscriptional regulation of starch metabolism in arabidopsis leaves. *Plant Physiology*, 136(1). <https://doi.org/10.1104/pp.104.044347>
- Somers, D. E., Webb, A. A. R., Pearson, M., & Kay, S. A. (1998). The short-period mutant, toc1-1, alters circadian clock regulation of multiple outputs throughout development in Arabidopsis thaliana. *Development*, 125(3). <https://doi.org/10.1242/dev.125.3.485>

- Sorek, M., Yacobi, Y. Z., Roopin, M., Berman-Frank, I., & Levy, O. (2013). Photosynthetic circadian rhythmicity patterns of Symbiodium, the coral endosymbiotic algae. *Proceedings of the Royal Society B: Biological Sciences*, 280(1759). <https://doi.org/10.1098/rspb.2012.2942>
- Sorokina, O., Corellou, F., Dauvillée, D., Sorokin, A., Goryanin, I., Ball, S., Bouget, F. Y., & Millar, A. J. (2011). Microarray data can predict diurnal changes of starch content in the picoalga Ostreococcus. *BMC Systems Biology*, 5(1), 36. <https://doi.org/10.1186/1752-0509-5-36>
- Spudich, J. L., & Sager, R. (1980). Regulation of the chlamydomonas cell cycle by light and dark. *Journal of Cell Biology*, 85(1). <https://doi.org/10.1083/jcb.85.1.136>
- Sterck, L., Billiau, K., Abeel, T., Rouzé, P., & Van de Peer, Y. (2012). ORCAE: online resource for community annotation of eukaryotes. *Nature Methods*. <https://doi.org/10.1038/nmeth.2242>
- Sulpice, R., Flis, A., Ivakov, A. A., Apelt, F., Krohn, N., Encke, B., Abel, C., Feil, R., Lunn, J. E., & Stitt, M. (2014). Arabidopsis coordinates the diurnal regulation of carbon allocation and growth across a wide range of Photoperiods. *Molecular Plant*, 7(1). <https://doi.org/10.1093/mp/sst127>
- Sumová, A., Jáč, M., Sládek, M., Šauman, I., & Illnerová, H. (2003). Clock gene daily profiles and their phase relationship in the rat suprachiasmatic nucleus are affected by photoperiod. *Journal of Biological Rhythms*, 18(2). <https://doi.org/10.1177/0748730403251801>
- Sun, T. H., Liu, C. Q., Hui, Y. Y., Wu, W. K., Zhou, Z. G., & Lu, S. (2010). Coordinated Regulation of Gene Expression for Carotenoid Metabolism in Chlamydomonas reinhardtii. *Journal of Integrative Plant Biology*, 52(10). <https://doi.org/10.1111/j.1744-7909.2010.00993.x>
- Sun, T., Rao, S., Zhou, X., & Li, L. (2022). Plant carotenoids: recent advances and future perspectives. *Molecular Horticulture*, 2(1). <https://doi.org/10.1186/s43897-022-00023-2>
- Swanson, W. J., Aagaard, J. E., Vacquier, V. D., Monné, M., Sadat Al Hosseini, H., & Jovine, L. (2011). The molecular basis of sex: Linking yeast to human. *Molecular Biology and Evolution*, 28(7). <https://doi.org/10.1093/molbev/msr026>
- Swarbreck, D., Wilks, C., Lamesch, P., Berardini, T. Z., Garcia-Hernandez, M., Foerster, H., Li, D., Meyer, T., Muller, R., Ploetz, L., Radenbaugh, A., Singh, S., Swing, V., Tissier, C., Zhang, P., & Huala, E. (2008). The Arabidopsis Information Resource (TAIR): Gene structure and function annotation. *Nucleic Acids Research*, 36(SUPPL. 1). <https://doi.org/10.1093/nar/gkm965>

- Sweeney, B. M., & Haxo, F. T. (1961). Persistence of a photosynthetic rhythm in enucleated Acetabularia. *Science*, 134(3487). <https://doi.org/10.1126/science.134.3487.1361>
- Takahashi, J. S. (2021). The 50th anniversary of the konopka and benzer 1971 paper in PNAS: "Clock mutants of drosophila melanogaster." In *Proceedings of the National Academy of Sciences of the United States of America* (Vol. 118, Issue 39). <https://doi.org/10.1073/pnas.2110171118>
- TerBush, A. D., Yoshida, Y., & Osteryoung, K. W. (2013). FtsZ in chloroplast division: Structure, function and evolution. In *Current Opinion in Cell Biology* (Vol. 25, Issue 4). <https://doi.org/10.1016/j.ceb.2013.04.006>
- Thaben, P. F., & Westermark, P. O. (2014). Detecting rhythms in time series with rain. *Journal of Biological Rhythms*, 29(6). <https://doi.org/10.1177/0748730414553029>
- Tian, T., Liu, Y., Yan, H., You, Q., Yi, X., Du, Z., Xu, W., & Su, Z. (2017). AgriGO v2.0: A GO analysis toolkit for the agricultural community, 2017 update. *Nucleic Acids Research*, 45(W1), W122–W129. <https://doi.org/10.1093/nar/gkx382>
- Tragin, M., & Vaulot, D. (2019). Novel diversity within marine Mamiellophyceae (Chlorophyta) unveiled by metabarcoding. *Scientific Reports*, 9(1). <https://doi.org/10.1038/s41598-019-41680-6>
- Tucker, D. E., Allen, D. J., & Ort, D. R. (2004). Control of nitrate reductase by circadian and diurnal rhythms in tomato. *Planta*, 219(2). <https://doi.org/10.1007/s00425-004-1213-x>
- Van Dongen, H. P. A., Kerkhof, G. A., & Klöppel, H. B. (1997). Seasonal covariation of the circadian phases of rectal temperature and slow wave sleep onset. *Journal of Sleep Research*, 6(1). <https://doi.org/10.1046/j.1365-2869.1997.00021.x>
- Van Gelderen, K. (2020). The rhythm of the light: How light and the clock drive cycling of transcript levels in barley. In *Plant Physiology* (Vol. 183, Issue 2). <https://doi.org/10.1104/pp.20.00360>
- Vatakis, A., Balci, F., Di Luca, M., & Correa, Á. (2018). Circadian Timing: From Genetics to Behavior. In *Timing and Time Perception: Procedures, Measures, & Applications*. https://doi.org/10.1163/9789004280205_002
- Veenstra, T. D. (2021). Omics in Systems Biology: Current Progress and Future Outlook. In *Proteomics* (Vol. 21, Issues 3–4). <https://doi.org/10.1002/pmic.202000235>
- Wang, S., Steed, G., & Webb, A. A. R. (2022). Circadian entrainment in Arabidopsis. *Plant Physiology*, 190(2). <https://doi.org/10.1093/plphys/kiac204>
- Wang, Z., Gerstein, M., & Snyder, M. (2009). RNA-Seq: A revolutionary tool for transcriptomics. In *Nature Reviews Genetics* (Vol. 10, Issue 1). <https://doi.org/10.1038/nrg2484>

- Watanabe, T., Naito, E., Nakao, N., Tei, H., Yoshimura, T., & Ebihara, S. (2007). Bimodal clock gene expression in mouse suprachiasmatic nucleus and peripheral tissues under a 7-hour light and 5-hour dark schedule. *Journal of Biological Rhythms*, 22(1). <https://doi.org/10.1177/0748730406295435>
- Watson, J. V., Chambers, S. H., & Smith, P. J. (1987). A pragmatic approach to the analysis of DNA histograms with a definable G1 peak. *Cytometry*, 8(1), 1–8. <https://doi.org/10.1002/CYTO.990080101>
- Weckwerth, W. (2011). Green systems biology - From single genomes, proteomes and metabolomes to ecosystems research and biotechnology. In *Journal of Proteomics* (Vol. 75, Issue 1). <https://doi.org/10.1016/j.jprot.2011.07.010>
- Wenden, B., Toner, D. L. K., Hodge, S. K., Grima, R., & Millar, A. J. (2012). Spontaneous spatiotemporal waves of gene expression from biological clocks in the leaf. *Proceedings of the National Academy of Sciences of the United States of America*, 109(17). <https://doi.org/10.1073/pnas.1118814109>
- Willforss, J., Chawade, A., & Levander, F. (2019). NormalizerDE: Online Tool for Improved Normalization of Omics Expression Data and High-Sensitivity Differential Expression Analysis. *Journal of Proteome Research*, 18(2). <https://doi.org/10.1021/acs.jproteome.8b00523>
- Worden, A. Z., Lee, J. H., Mock, T., Rouzé, P., Simmons, M. P., Aerts, A. L., Allen, A. E., Cuvelier, M. L., Derelle, E., Everett, M. V., Foulon, E., Grimwood, J., Gundlach, H., Henrissat, B., Napoli, C., McDonald, S. M., Parker, M. S., Rombauts, S., Salamov, A., ... Grigoriev, I. V. (2009). Green evolution and dynamic adaptations revealed by genomes of the marine picoeukaryotes micromonas. *Science*, 324(5924). <https://doi.org/10.1126/science.1167222>
- Worden, A. Z., Nolan, J. K., & Palenik, B. (2004). Assessing the dynamics and ecology of marine picophytoplankton: The importance of the eukaryotic component. *Limnology and Oceanography*, 49(1). <https://doi.org/10.4319/lo.2004.49.1.0168>
- Wu, T., Hu, E., Xu, S., Chen, M., Guo, P., Dai, Z., Feng, T., Zhou, L., Tang, W., Zhan, L., Fu, X., Liu, S., Bo, X., & Yu, G. (2021). clusterProfiler 4.0: A universal enrichment tool for interpreting omics data. *The Innovation*, 2(3). <https://doi.org/10.1016/j.xinn.2021.100141>
- Wucher, V., Sodaei, R., Amador, R., Irimia, M., & Guigó, R. (2022). Day-night and seasonal variation of human gene expression across tissues. *BioRxiv : The Preprint Server for Biology*. <https://doi.org/10.1101/2021.02.28.433266>
- Yakir, E., Hassidim, M., Melamed-Book, N., Hilman, D., Kron, I., & Green, R. M. (2011). Cell autonomous and cell-type specific circadian rhythms in Arabidopsis. *Plant Journal*, 68(3). <https://doi.org/10.1111/j.1365-313X.2011.04707.x>

- Yang, M., Lin, X., Liu, X., Zhang, J., & Ge, F. (2018). Genome Annotation of a Model Diatom *Phaeodactylum tricornutum* Using an Integrated Proteogenomic Pipeline. *Molecular Plant*, 11(10). <https://doi.org/10.1016/j.molp.2018.08.005>
- Yang, Z., & Midmore, D. J. (2005). A model for the circadian oscillations in expression and activity of nitrate reductase in higher plants. *Annals of Botany*, 96(6). <https://doi.org/10.1093/aob/mci254>
- Youthed, G. J., & Moran, V. C. (1969). The lunar-day activity rhythm of myrmeleontid larvae. *Journal of Insect Physiology*, 15(7). [https://doi.org/10.1016/0022-1910\(69\)90235-2](https://doi.org/10.1016/0022-1910(69)90235-2)
- Yu, G., Wang, L.-G., Han, Y., & He, Q.-Y. (2012). clusterProfiler: an R package for comparing biological themes among gene clusters. *Omics : A Journal of Integrative Biology*, 16(5). <https://doi.org/10.1089/omi.2011.0118>
- Yu, G., Wang, L. G., & He, Q. Y. (2015). ChIP seeker: An R/Bioconductor package for ChIP peak annotation, comparison and visualization. *Bioinformatics*, 31(14), 2382–2383. <https://doi.org/10.1093/bioinformatics/btv145>
- Zee, P. C., & Abbott, S. M. (2020). Circadian Rhythm Sleep-Wake Disorders. In *CONTINUUM Lifelong Learning in Neurology* (Vol. 26, Issue 4). <https://doi.org/10.1212/CON.0000000000000884>
- Zhang, Z., Han, T., Sui, J., & Wang, H. (2022). Cryptochrome-mediated blue-light signal contributes to carotenoids biosynthesis in microalgae. *Frontiers in Microbiology*, 13, 1083387. <https://doi.org/10.3389/fmicb.2022.1083387>
- Zhao, L., Chang, W., Xiao, Y., Liu, H., & Liu, P. (2013). Methylerythritol phosphate pathway of isoprenoid biosynthesis. *Annual Review of Biochemistry*, 82, 497–530. <https://doi.org/10.1146/annurev-biochem-052010-100934>
- Zhao, X., Rastogi, A., Deton Cabanillas, A. F., Ait Mohamed, O., Cantrel, C., Lombard, B., Murik, O., Genovesio, A., Bowler, C., Bouyer, D., Loew, D., Lin, X., Veluchamy, A., Vieira, F. R. J., & Tirichine, L. (2021). Genome wide natural variation of H3K27me3 selectively marks genes predicted to be important for cell differentiation in *Phaeodactylum tricornutum*. *New Phytologist*, 229(6). <https://doi.org/10.1111/nph.17129>
- Zheng, Y., Jiao, C., Sun, H., Rosli, H. G., Pombo, M. A., Zhang, P., Banf, M., Dai, X., Martin, G. B., Giovannoni, J. J., Zhao, P. X., Rhee, S. Y., & Fei, Z. (2016). iTAK: A Program for Genome-wide Prediction and Classification of Plant Transcription Factors, Transcriptional Regulators, and Protein Kinases. In *Molecular Plant* (Vol. 9, Issue 12). <https://doi.org/10.1016/j.molp.2016.09.014>
- Zhu, B., Zhang, Q., Pan, Y., Mace, E. M., York, B., Antoulas, A. C., Dacso, C. C., & O'Malley, B. W. (2017). A Cell-Autonomous Mammalian 12 hr Clock Coordinates Metabolic

and Stress Rhythms. *Cell Metabolism*, 25(6). <https://doi.org/10.1016/j.cmet.2017.05.004>

Zhu, L. J. (2013). Integrative analysis of ChIP-chip and ChIP-seq dataset. *Methods in Molecular Biology*, 1067. https://doi.org/10.1007/978-1-62703-607-8_8

Zones, J. M., Blaby, I. K., Merchant, S. S., & Umen, J. G. (2015). High-resolution profiling of a synchronized diurnal transcriptome from *Chlamydomonas reinhardtii* reveals continuous cell and metabolic differentiation. *Plant Cell*, 27(10). <https://doi.org/10.1105/tpc.15.00498>

Zurbriggen, M. D., Moor, A., & Weber, W. (2012). Plant and bacterial systems biology as platform for plant synthetic bio(techno)logy. *Journal of Biotechnology*, 160(1–2). <https://doi.org/10.1016/j.jbiotec.2012.01.014>